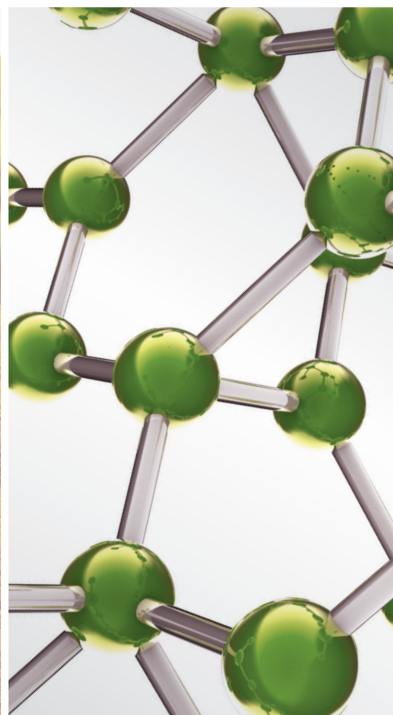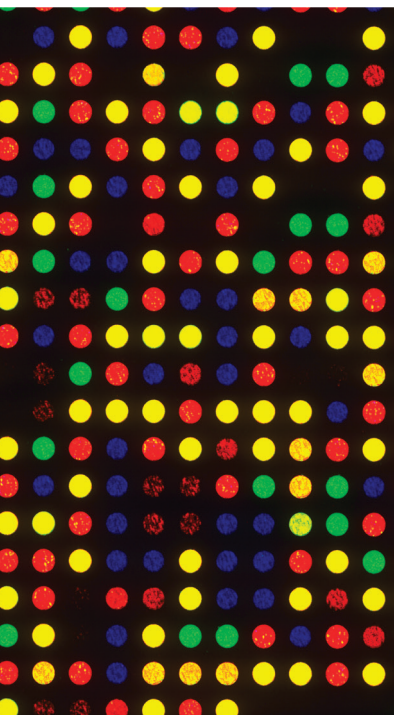# Sustainable Utilization of TCM Resources

Guest Editors: Shilin Chen, Yitao Wang, Zhongzhen Zhao, Christine J. Leon, and Robert J. Henry

Sustainable Utilization of TCM Resources

Sustainable Utilization of TCM Resources

Guest Editors: Shilin Chen, Yitao Wang, Zhongzhen Zhao, Christine J. Leon, and Robert J. Henry

ChunGuang Li, Australia
Xiu-Min Li, USA
Shao Li, China
Yong Hong Liao, China
Sabina Lim, Republic of Korea
Bi-Fong Lin, Taiwan
Wen Chuan Lin, China
Christopher G. Lis, USA
Gerhard Litscher, Austria
Ke Liu, China
I-Min Liu, Taiwan
Gaofeng Liu, China
Yijun Liu, USA
Cun-Zhi Liu, China
Gail B. Mahady, USA
Juraj Majtan, Slovakia
Subhash C. Mandal, India
Jeanine Marnewick, South Africa
Virginia S. Martino, Argentina
James H. McAuley, Australia
Karin Meissner, USA
Andreas Michalsen, Germany
David Mischoulon, USA
Syam Mohan, Malaysia
J. Molnar, Hungary
Valério Monteiro-Neto, Brazil
H.-I. Moon, Republic of Korea
Albert Moraska, USA
Mark Moss, UK
Yoshiharu Motoo, Japan
Frauke Musial, Germany
MinKyun Na, Republic of Korea
Richard L. Nahin, USA
Vitaly Napadow, USA
F. R. F. Nascimento, Brazil
S. Nayak, Trinidad And Tobago
Isabella Neri, Italy
Télesphore Nguelefack, Cameroon
Martin Offenbacher, Germany
Ki-Wan Oh, Republic of Korea
Y. Ohta, Japan
Olumayokun A. Olajide, UK
Thomas Ostermann, Germany
Stacey A. Page, Canada
Tai-Long Pan, Taiwan
Bhushan Patwardhan, India
Berit Smestad Paulsen, Norway

Andrea Pieroni, Italy
Richard Pietras, USA
Waris Qidwai, Pakistan
Xianqin Qu, Australia
Cassandra L. Quave, USA
Roja Rahimi, Iran
Khalid Rahman, UK
Cheppail Ramachandran, USA
Gamal Ramadan, Egypt
Ke Ren, USA
Man Hee Rhee, Republic of Korea
Mee-Ra Rhyu, Republic of Korea
José Luis Ríos, Spain
Paolo Roberti di Sarsina, Italy
Bashar Saad, Palestinian Authority
Sumaira Sahreen, Pakistan
Omar Said, Israel
Luis A. Salazar-Olivo, Mexico
Mohd. Zaki Salleh, Malaysia
Andreas Sandner-Kiesling, Austria
Adair Santos, Brazil
G. Schmeda-Hirschmann, Chile
Andrew Scholey, Australia
Veronique Seidel, UK
Senthamil R. Selvan, USA
Tuhinadri Sen, India
Hongcai Shang, China
Karen J. Sherman, USA
Ronald Sherman, USA
Kuniyoshi Shimizu, Japan
Kan Shimpo, Japan
B.-C. Shin, Republic of Korea
Yukihiro Shoyama, Japan
Chang G. Son, Republic of Korea
Rachid Soulimani, France
Didier Stien, France
Shan-Yu Su, Taiwan
Mohd Roslan Sulaiman, Malaysia
Venil N. Sumantran, India
John R. S. Tabuti, Uganda
Toku Takahashi, USA
Rabih Talhouk, Lebanon
Wen-Fu Tang, China
Yuping Tang, China
Lay Kek Teh, Malaysia
Mayank Thakur, India
Menaka C. Thounaojam, India

Mei Tian, China
Evelin Tiralongo, Australia
S. C. Tjen-A-Looi, USA
MichaThl Tomczyk, Poland
Yao Tong, Hong Kong
K. V. Trinh, Canada
Karl Wah-Keung Tsim, Hong Kong
Volkan Tugcu, Turkey
Yew-Min Tzeng, Taiwan
Dawn M. Upchurch, USA
Maryna Van de Venter, South Africa
Sandy van Vuuren, South Africa
Alfredo Vannacci, Italy
Mani Vasudevan, Malaysia
Carlo Ventura, Italy
Wagner Vilegas, Brazil
Pradeep Visen, Canada
Aristo Vojdani, USA
Y. Wang, USA
Shu-Ming Wang, USA
Chenchen Wang, USA
Chong-Zhi Wang, USA
Kenji Watanabe, Japan
Jintanaporn Wattanathorn, Thailand
Wolfgang Weidenhammer, Germany
Jenny M. Wilkinson, Australia
Darren Williams, Republic of Korea
Haruki Yamada, Japan
Nobuo Yamaguchi, Japan
Yong-Qing Yang, China
Junqing Yang, China
Ling Yang, China
Eun Jin Yang, Republic of Korea
Xiufen Yang, China
Ken Yasukawa, Japan
Min H. Ye, China
M. Yoon, Republic of Korea
Jie Yu, China
Jin-Lan Zhang, China
Zunjian Zhang, China
Wei-bo Zhang, China
Hong Q. Zhang, Hong Kong
Boli Zhang, China
Ruixin Zhang, USA
Hong Zhang, Sweden
Haibo Zhu, China

Contents

Editorial
Sustainable Utilization of TCM Resources

Shilin Chen,[1] Yitao Wang,[2] Zhongzhen Zhao,[3] Christine J. Leon,[4] and Robert J. Henry[5]

[1]*Institute of Chinese Materia Medica, China Academy of Chinese Medical Sciences, Beijing 100700, China*
[2]*Institute of Chinese Medical Sciences, University of Macau, Macau*
[3]*School of Chinese Medicine, Hong Kong Baptist University, Kowloon Tong 999077, Hong Kong*
[4]*Royal Botanic Gardens, Kew, Richmond, Surrey TW9 3AB, UK*
[5]*Queensland Alliance for Agriculture and Food Innovation, University of Queensland, Brisbane, QLD 4027, Australia*

Correspondence should be addressed to Shilin Chen; slchen@implad.ac.cn

Sustainable development aims to maintain utilization of finite resources without exhausting them and meet the demand of present and future generations [1]. Sustainability can only be achieved by balancing production and consumption in a reasonable dimension. It offers a vision of progress that integrates immediate and longer-term objectives. However, the nature of our current resource use endangers their future survival. Moreover, the consequences of our resource use in terms of impacts on the environment may induce serious damage to the environment. Sustainable utilization of natural resources should combine market demand of raw materials, ecological stability, and social benefits [2] and regard them as inseparable and interdependent components in the whole progress of industrial production.

Traditional Chinese Medicine (TCM) has a long history of application and has attracted more and more world-wide attention for its significant effect in prevention and treatment of diseases. Wild medicinal resource is the basis of TCM and accounts for nearly 80% of all the sources of Chinese herbs. With the development of the modern TCM industry and gradual degradation of the natural environment, natural reserves of medicinal resources face a tremendous amount of pressure. Many medicinal plants are at risk of extinction and some adulterants have appeared on the market bringing to attention the need to ensure sustainable utilization of medicinal resources. More and more measures have been taken to guarantee the supply [3] and identification [4–6] as well as quality control [7, 8] and new drug development [9].

In this special issue, a total of 15 papers have been devoted to sustainable utilization of TCM resources. Identification

of Radix Astragali using DNA barcoding, DNA barcode-based PCR-RFLP, and diagnostic PCR for authentication of Jinqian Baihua She (*Bungarus Parvus*), using ITS2 to identify *Ferula* species and indirubin-containing medicinal plants, are included. Rapid identification of plants in the Asteraceae with improved RBF-ANN classification models based on MOS-sensor E-nose is also provided.

Introduction and cultivation can supply raw medicinal materials in short supply and play an important role in the sustainable utilization of TCM. Prevention and cure of diseases and insect pests and characteristics of soil microbial community in ginseng cultivation are offered. A systematic review on the production mode of Chinese herbal medicines is also presented. This special issue also reports natural resource monitoring of *Rheum tanguticum* by multilevel remote sensing. Traceability based on chemical two-dimensional barcode for controlling quality in the whole process of the industrial chain of TCM is included. Finally, measuring Agarwood formation ratio quantitatively by fluorescence spectral imaging technique and determining oleanolic and ursolic acids using hyphenated ultrasound-assisted supercritical carbon dioxide extraction and chromatography are introduced.

Readers of this special issue will find not only different identification methods and updated reviews on cultivation, but also some important issues influencing quality control. The industrial chain of TCM, from the production of raw materials to the sale of the finished products, is a complicated multilink process. There are still some key questions to be resolved in the whole process including but not limited to

breeding, prevention and cure of diseases and insect pests, quality traceability, exploiting new medicinal resources, and the mechanism of drug metabolism.

Shilin Chen
Yitao Wang
Zhongzhen Zhao
Christine J. Leon
Robert J. Henry

References

[1] N. Zhao-Seiler, "Sustainability of Chinese medicinal herbs: a discussion," *Journal of Chinese Medicine*, no. 101, pp. 52–56, 2013.

[2] S. L. Chen, G. Q. Su, J. Q. Zou, L. F. Huang, B. L. Guo, and P. G. Xiao, "The sustainable development framework of national Chinese medicine resources," *Zhongguo Zhongyao Zazhi*, vol. 30, no. 15, pp. 1141–1146, 2005.

[3] X. Li, J. Song, J. Wei, Z. Hu, C. Xie, and G. Luo, "Natural Fostering in *Fritillaria cirrhosa*: integrating herbal medicine production with biodiversity conservation," *Acta Pharmaceutica Sinica B*, vol. 2, no. 1, pp. 77–82, 2012.

[4] C. J. Nock, D. L. E. Waters, M. A. Edwards et al., "Chloroplast genome sequences from total DNA for plant identification," *Plant Biotechnology Journal*, vol. 9, no. 3, pp. 328–333, 2011.

[5] M. H. Wu, W. Zhang, P. Guo, and Z. Z. Zhao, "Identification of seven Zingiberaceous species based on comparative anatomy of microscopic characteristics of seeds," *Chinese Medicine*, vol. 9, no. 1, pp. 10–16, 2014.

[6] X. W. Li, Y. Yang, R. J. Henry, M. Rossetto, Y. Wang, and S. L. Chen, "Plant DNA barcoding: from gene to genome," *Biological Reviews*, vol. 90, no. 1, pp. 157–166, 2015.

[7] L. Liang, Z. Z. Zhao, and T. G. Kang, "Application of microscopy technique and high performance liquid chromatography for quality assessment of *Polygonum multiflorum*Thunb. (Heshouwu)," *Pharmacognosy Magazine*, vol. 10, no. 40, p. 415, 2014.

[8] Y. L. Song, W. H. Jing, G. Du, F. Q. Yang, R. Yan, and Y. T. Wang, "Qualitative analysis and enantiospecific determination of angular-type pyranocoumarins in Peucedani Radix using achiral and chiral liquid chromatography coupled with tandem mass spectrometry," *Journal of Chromatography A*, vol. 1338, pp. 24–37, 2014.

[9] W.-Y. Wu, J.-J. Hou, H.-L. Long, W.-Z. Yang, J. Liang, and D.-A. Guo, "TCM-based new drug discovery and development in China," *Chinese Journal of Natural Medicines*, vol. 12, no. 4, pp. 241–250, 2014.

Research Article

DNA Barcode-Based PCR-RFLP and Diagnostic PCR for Authentication of Jinqian Baihua She (Bungarus Parvus)

Xiaolei Li,[1] Weiping Zeng,[1] Jing Liao,[1,2] Zhenbiao Liang,[1,3] Shuhua Huang,[1] and Zhi Chao[1]

[1]*School of Traditional Chinese Medicine, Southern Medical University, Guangzhou 510515, China*
[2]*Beijing Royal Intergrative Medicine Hospital, Beijing 102209, China*
[3]*Department of Pharmacy, Zhongshan People's Hospital, Zhongshan 528403, China*

Correspondence should be addressed to Zhi Chao; chaozhi@smu.edu.cn

We established polymerase chain reaction-restriction fragment length polymorphism (PCR-RFLP) and diagnostic PCR based on cytochrome C oxidase subunit I (COI) barcodes of *Bungarus multicinctus*, genuine Jinqian Baihua She (JBS), and adulterant snake species. The PCR-RFLP system utilizes the specific restriction sites of *Spe*I and *Bst*EII in the COI sequence of *B. multicinctus* to allow its cleavage into 3 fragments (120 bp, 230 bp, and 340 bp); the COI sequences of the adulterants do not contain these restriction sites and therefore remained intact after digestion with *Spe*I and *Bst*EII (except for that of *Zaocys dhumnades*, which could be cleaved into a 120 bp and a 570 bp fragment). For diagnostic PCR, a pair of species-specific primers (COI37 and COI337) was designed to amplify a specific 300 bp amplicon from the genomic DNA of *B. multicinctus*; no such amplicons were found in other allied species. We tested the two methods using 11 commercial JBS samples, and the results demonstrated that barcode-based PCR-RFLP and diagnostic PCR both allowed effective and accurate authentication of JBS.

1. Introduction

Jinqian Baihua She (JBS) (coin-like white-banded snake, Bungarus Parvus) is a widely used high-value traditional Chinese drug recorded in Chinese Pharmacopoeia (ChP, Vol.1, 2010 Edition). It derives from the dried body of infant *Bungarus multicinctus* Blyth and is effective in dispelling the wind, removing obstruction of the collaterals, and relieving spasm [1]. As attempts of domestication and breeding of *B. multicinctus* remain unsuccessful so far, the supply of JBS has to rely entirely on the gradually diminishing wild resource. The shortage in JBS supply results in its high price in market and also in the emergence of its adulterants using other snake species such as baby *Dinodon rufozonatum* and *B. fasciatus*. By now nine snake species have been found for sale under the name of JBS [2, 3], and according to our previous study, the adulterants accounted for about 50% of JBS crude drug market [4]. The conventional approach to JBS authentication depends solely on the macroscopic characters, which can be

rather confusing even for experienced professionals [5, 6]. A convenient and accurate means for distinguishing genuine JBS from its adulterants is therefore urgently needed to ensure the safety and effectiveness of the drug use.

Recent developments in biological techniques and molecular genetic markers make JBS identification possible at the molecular level using species-specific DNA sequences. We previously demonstrated the efficiency of cytochrome C oxidase subunit I (COI) barcodes for identification of JBS against its adulterants [4]. However, sequence splicing and analysis involved in DNA barcoding requires knowledge in specific specialties, and sequence identification based on BLAST might result in hit of several species with a high sequence homology; in such cases, choosing an appropriate threshold for a decision becomes difficult. In addition, because conventional DNA sequencing is time-consuming and expensive, DNA barcoding technique has only limited application in routine practice of drug control, especially in elementary institutions in remote or underdeveloped areas.

TABLE 1: Samples used in this study.

Sample	Species	Collecting site	GenBankID	BINs
BM1	*Bungarus multicinctus*	Zhongshan, Guangdong	JN833585	AAF9297
BM2	*B. multicinctus*	Taishan, Guangdong	JN833594	AAF9297
BM3	*B. multicinctus*	Conghua, Guangdong	JN833596	AAF9297
BM4	*B. multicinctus*	Maoming, Guangdong	JN860064	AAF9297
BF	*B. fasciatus*	Guangxi	JN833615	AAI8427
DA	*Deinagkistrodon acutus*	Jiangxi	JQ658431	ACC5654
DR1	*Dinodon rufozonatum*	Zhongshan, Guangdong	JN833598	AAD0172
DR2	*Di. rufozonatum*	Hunan	JN833601	AAD0172
DF	*Di. flavozonatum*	Shaoguan, Guangdong	JX233649	
OM	*Orthriophis moellendorffi* (*Elaphe moellendorffi*)	Guangxi	JN833617	ABA1479
EP	*Enhydris plumbea*	Zhongshan, Guangdong	JN833609	AAJ0753
NJ	*Naja atra*	Taishan, Guangdong	JN833602	AAF7608
SA	*Sinonatrix annularis*	Zhongshan, Guangdong	JN833613	ABA1332
XF	*Xenochrophis flavipunctatus*	Zhongshan, Guangdong	JN833606	AAH9231
ZY	*Zaocys dhumnades*	Conghua, Guangdong	JX233651	

Diagnostic polymerase chain reaction (PCR) (also called highly specific PCR) and polymerase chain reaction-restriction fragment length polymorphism (PCR-RFLP) were recently recorded in ChP for identification of several traditional Chinese drugs. In diagnostic PCR, a pair of primers is designed based on a specific gene fragment of the target species to amplify a species-specific DNA segment. In PCR-RFLP, the restriction sites are identified in a specific gene fragment of the target species, and with appropriate restriction enzymes, the gene fragment only of the target species is cleaved into 2 or more segments. These two methods, relatively simple and time-saving, can yield reliable results and meet the needs in practice of drug quality control [7–13]. In 2010, ChP recorded, for the first time, protocols of diagnostic PCR identification of Zaocys and Agkistrodon (derived from the snake species *Zaocys dhumnades* and *Deinagkistrodon acutus*, resp.) [1] and PCR-RFLP identification of Fritillariae Cirrhosae Bulbus [14]. As for JBS, reports have been available describing Cytb sequence-based identification of *B. multicinctus* against some adulterant snake species using species-specific primers and diagnostic PCR [15–17].

Our previous work has proved the feasibility and efficiency of COI barcodes in JBS authentication [4]. In the present study, we further established diagnostic PCR and PCR-RFLP systems based on the barcode sequences for differentiation of JBS from its adulterants. This is the first report describing COI barcode-based diagnostic PCR and PCR-RFLP for crude drug identification. Together with DNA barcodes system we previously reported and macroscopic identification, they compose an integrated system of JBS authentication.

2. Materials and Methods

2.1. Materials. Fifteen specimens of 11 snake species (including *B. multicinctus* and its adulterants) were obtained from

different locations in Guangdong Province, Jiangxi Province, Hunan Province, and Guangxi Zhuang Autonomous Region in China (Table 1). Vouchers were deposited in School of Traditional Chinese Medicine, Southern Medical University, and all the specimens were preserved in 75% ethanol. Eleven samples of JBS crude drug were purchased from the local drug stores or crude drug market in Guangzhou, Guangdong Province (Table 2). All the snake specimens and crude drug samples were identified by Dr. Zhang Liang, South China Institute of Endangered Animals.

2.2. DNA Extraction. Tissue samples were dissected from the dorsal muscle of the snake. The total DNA was extracted using TIANamp Genomic DNA kit (Tiangen Biotech Co., Ltd., Beijing) following the manufacturer's instructions, dissolved in 100 μL TE buffer, and stored at -20°C.

2.3. COI Barcode Amplification. The universal primers LCO1490 (5$'$-GGTCAACAAATCATAAAGATATTGG-3$'$) and HCO2198 (5$'$-TAAACTTCAGGGTGACCAAAAAAT-CA-3$'$) [18] were used to amplify the COI barcode region. A pair of primers designed for Viperidae snakes, DK1-CO1 (5$'$-CAACTAACCACAAAGACATCGG-3$'$) and DK1-CO2 (5$'$-CTTCTGGGTGGCCGAAAAACA-3$'$) [19], was used when the universal primers failed to obtain the target amplicon.

PCR reactions were carried out with an Applied Biosystems 2720 Thermal Cycler (Applied Biosystems, Carlsbad CA, USA), in a total volume of 25 μL containing 12.5 μL of 2 × Taq PCR MasterMix (Tiangen), 1 μL of each primer, 1 μL of genomic DNA, and 9.5 μL of ddH$_2$O. Thermal cycling was performed with an initial denaturing at 93°C for 5 min and annealing at 55°C for 2 min, followed by 35 cycles of 93°C for 30 s, 55°C for 45 s, and 70°C for 45 s, with a final extension at 70°C for 5 min and chilling to 4°C. The PCR products (5

TABLE 2: Identification results of JBS crude drug samples.

Samples	Commodity name	Producing area	Macroscopical inspection	PCR-RFLP	Diagnostic PCR	DNA barcoding	Sequence similarity
D1	Xiao Baihua She	Guangxi	*B. multicinctus*	+	+	*B. multicinctus*	100%
D2	Xiao Baihua She	Guangxi	*B. multicinctus*	+	+	*B. multicinctus*	100%
D3	Da Baihua She	Guangxi	*B. multicinctus*	+	+	*B. multicinctus*	100%
D4	Xiao Baihua She	Hunan	*B. multicinctus*	+	+	*B. multicinctus*	99.85%
D5	Jinqian Baihua She	Guangdong	*B. multicinctus*	+	+	*B. multicinctus*	100%
D6	Baihua She	Guangdong	*Di. rufozonatum*	−	−	*Di. rufozonatum*	99.85%
D7	Baihua She	Unknown	*Di. rufozonatum*	−	−	*Di. rufozonatum*	99.69%
D8	Baihua She	Unknown	*S. annularis*	−	−	*S. annularis*	99.24%
D9	Baihua She	Unknown	*En. chinensis*	−	−	*En. chinensis*	98%
D10	Baihua She	Unknown	*Di. rufozonatum*	−	−	*Di. rufozonatum*	99.54%
D11	Xiao Baihua She	Guangxi	Colubridae sp.	−	−	*Di. rufozonatum*	99.24%

+: Jinqian Baihua She; −: adulterant.

μL) were subjected to 1.2% agarose gel electrophoresis and visualized with ethidium bromide (EB) staining under UV.

PCR products were purified using Universal DNA Purification Kit (Tiangen Biotech Co., Ltd., Beijing) following the manufacturer's instructions and were in a final DNA concentration of 100 ng/μL~500 ng/μL.

2.4. Restriction Analysis of the PCR Products. COI barcode sequences of 15 specimens representing 11 snake species obtained in our previous studies were downloaded from BOLD system and GenBank. Restriction mapping of the COI sequences was carried out using the Nebcutter V2.0 [20]. Based on the restriction maps, *Spe*I and *Bst*EII were selected as candidate restriction endonucleases for discrimination between *B. multicinctus* and other snakes. Digestions with *Spe*I and *Bst*EII (Takara) were performed in a total volume of 20 μL containing 2 μL PCR products, 0.8 μL enzymes, 14.4 μL ddH$_2$O, and 2 μL 10 × digestion buffer at 37°C for 1 h as recommended by the manufacturer. The DNAs were fractionated by 2.0% agarose gel electrophoresis and visualized by EB staining under UV.

2.5. Species-Specific Primer Design and Diagnostic PCR. Fifteen COI sequences of 11 snake species were aligned with ClustalX and analyzed with Mega5.0 software. A pair of species-specific primers for *B. multicinctus* was designed based on COI sequences with the software Primer-Premier 5.0 and synthesized by Invitrogen Biotechnology (Shanghai) Co., Ltd. The reaction systems of diagnostic PCR are the same as those described in Section 2.3 except for the primers. Thermal cycling was performed with an initial step at 94°C for 5 min and 65°C for 2 min, followed by 25 cycles of 94°C for 30 s, 65°C for 50 s, and 72°C for 30 s, with a final extension at 72°C for 5 min and chilling to 4°C. The DNAs were fractionated by 2% agarose gel electrophoresis and visualized by EB staining under UV.

2.6. Identification of JBS Samples. Eleven JBS crude drug samples purchased were authenticated with the established

PCR-RFLP and diagnostic PCR systems following the protocols described above. These samples were also identified by DNA barcoding; that is, the COI barcode region of these 11 samples were sequenced and analyzed with the identification engine provided by BOLD; the retrieved results were used to validate the established methods.

3. Results

3.1. COI Region Amplification. Using the primer pairs LCO1490 and HCO2198, or DK1-CO1 and DK1-CO2, a single PCR product about 700 bp was amplified (Figure 1). The amplification results of the DNA templates from the original animals and from snake crude drugs were identical.

3.2. Restriction Analysis. Analysis of the restriction maps revealed two restriction sites of endonucleases *Spe*I (A▼CTAGT) and *Bst*EII (G▼GTAACC) in the COI sequence of *B. multicinctus*, while that of *Z. dhumnades* had the restriction site of *Spe*I only; the other species contained neither *Spe*I nor *Bst*EII restriction site (Table 3). Thus, the COI region of *B. multicinctus* could be cleaved by *Spe*I and *Bst*EII into 3 fragments of 120 bp, 230 bp, and 340 bp. Because of the single *Spe*I restriction site in the COI region, the PCR product of *Z. dhumnades* was cleaved into only two fragments (120 bp and 570 bp) in the double endonuclease system. The PCR products of the other species could not be cleaved by the two endonucleases for the absence of restriction sites in the COI region (Figure 2).

3.3. Diagnostic PCR with Species-Specific Primers. The designed species-specific primers for identification of *B. multicinctus* COI37 (5′-AATCGGAGCCTGTCTAAG-3′) and COI337 (5′-GACTGTTCAACCTGTGCC-3′) are shown in Table 4. The forward and reverse primers are fully paired with the sequences of the COI region of *B. multicinctus*. The PCR conditions, especially the annealing temperature, were optimized. When the annealing temperature was raised to 65°C, only the template DNA of *B. multicinctus* could

(a)

(b)
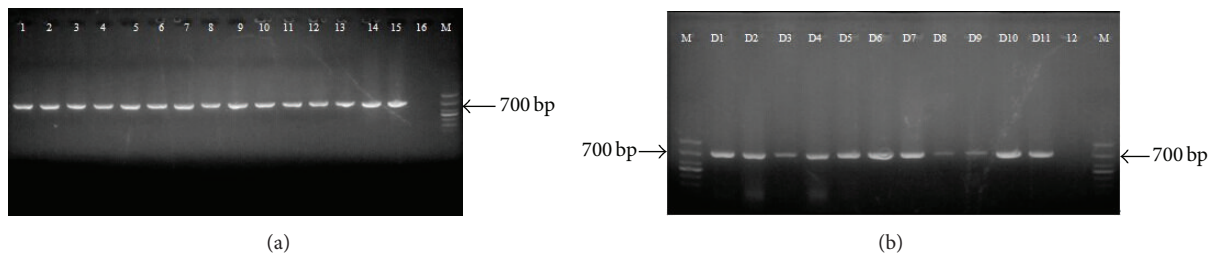
FIGURE 1: (a) Agarose gel electrophoresis of PCR results from BM1 (1), BM2 (2), BM3 (3), BM4 (4), BF (5), NJ (6), DR1 (7), DR2 (8), OM (9), EP (10), SA (11), DA (12), DF (13), ZY (14), XF (15), negative control (16) (water was used as sample), and DNA marker (M) in bp was indicated. (b) PCR products of the COI regions from JBS samples (D1–D11) and negative control (12) (water was used as sample) and DNA marker (M) in bp were indicated.
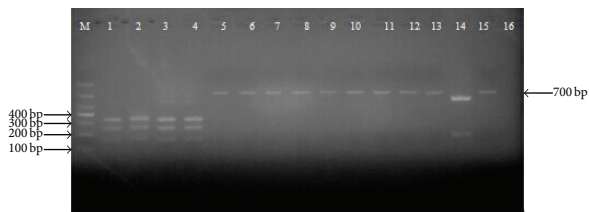
FIGURE 2: PCR-RFLP patterns of COI region digested with *Spe*I and *Bst*EII. BM1 (1), BM2 (2), BM3 (3), BM4 (4), BF (5), NJ (6), DR1 (7), DR2 (8), OM (9), EP (10), SA (11), DA (12), DF (13), ZY (14), XF (15), negative control (16) (water was used as sample), and DNA marker (M) in bp were indicated.
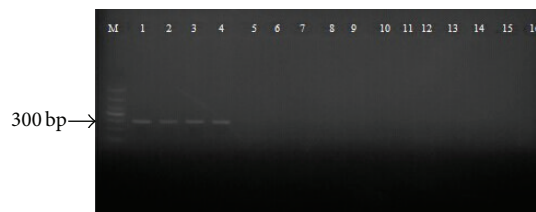
FIGURE 3: Diagnostic PCR for *B. multicinctus* and its adulterants. BM1 (1), BM2 (2), BM3 (3), BM4 (4), BF (5), NJ (6), DR1 (7), DR2 (8), OM (9), EP (10), SA (11), DA (12), DF (13), ZY (14), XF (15), negative control (16) (water was used as sample), and DNA marker (M) in bp were indicated.

TABLE 3: Two restriction endonucleases selected for the identification of *B. multicinctus* based on COI sequences among eleven species.

| | *Spe*I | *Bst*EII |
	121	353
BM	A▼CTAGT ············· G▼GTAACC	
DR	T CTAGT ············· G GAAACC	
NJ	A CTTGT ············· G GAAACC	
XF	A TTGAT ············· G GTAACT	
EP	C CTAGT ············· G GAAACC	
SA	C CTAGT ············· G GAAACC	
BF	G TTAGT ············· G GTAACT′	
OM	T CTGGT ············· G GAAATC	
DA	C CTAGT ············· G GAAACC	
ZY	A▼CTAGT ············· G GAAACC	
DF	T CTAGT ············· G GAAACC	

be amplified whereas the diagnostic PCRs yielded negative results for the other species. Under the optimized conditions, a single, distinct, and brightly resolved band of 300 bp was obtained only for *B. multicinctus*, while no amplification product was obtained for the others (Figure 3).

3.4. Commercial JBS Sample Identification. We tested 11 commercial JBS crude drug samples from the local market with the PCR-RFLP and diagnostic PCR. The universal primers

LCO1490 and HCO2198, or the specifically designed primers DK1-CO1 and DK1-CO2, were used to amplify COI regions from the crude drug samples, and a single PCR product about 700 bp was observed (Figure 1).

PCR-RFLP analysis of the 11 commercial JBS samples was carried out using the double endonuclease system with *Spe*I and *Bst*EII. The PCR products (COI barcode region) of samples D1 to D5 could be digested into 3 fragments (120 bp, 230 bp, and 340 bp); these results were successfully repeated, indicating that these samples were authentic JBS. The COI fragments from the other 6 samples (D6–D11) could not be digested, indicating their identity as JBS adulterants (Figure 4).

Diagnostic PCRs of the 11 commercial JBS samples yielded a single, distinct, and bright band of 300 bp for samples D1–D5; no amplification product was obtained for the other samples. These results suggested that samples D1–D5 were from *B. multicinctus* (Figure 5).

Macroscopical inspection and DNA barcoding confirmed the results of PCR-RFLP and diagnostic PCR that samples 1–5 were derived from *B. multicinctus*. The identities of samples 6–11 determined by macroscopical inspection and DNA barcoding were listed in Table 2.

4. Discussion

B. multicinctus, the highly venomous many-banded krait, has long been used as a folk medicine in South China, especially in the tropical and subtropical mountainous regions around

TABLE 4: Primer sites of species-specific primers COI37 and COI337 designed for the identification of *B. multicinctus* based on COI sequences among 11 species.

	37																	54
BM	A	A	T	C	G	G	A	G	C	C	T	G	T	C	T	A	A	G
DR	.	.	.	.	.	.	G	.	.	T	.	.	C	.	.	T	.	.
NJ	.	.	.	.	.	.	G	.	.	.	.	.	C	.	.	.	.	.
XF	.	.	.	T	.	.	.	.	.	T	.	.	C	.	.	.	.	.
EP	.	.	.	.	.	.	C	.	.	.	.	.	C	.	.	.	.	.
SA	.	.	.	.	.	.	.	.	.	.	.	.	C	.	.	.	.	.
BF	.	.	.	.	.	.	.	.	.	.	.	.	C	.	.	.	.	.
OM	.	.	.	T	.	.	G	.	.	T	A	.	.	.	.	.	.	.
DA	T	.	.	A	.	.	.	.	.	.	.	.	C	.	.	.	.	.
ZY	.	.	.	.	.	G	.	.	A	.	.	C	.	.	.	.	.	.
DF	T	.	.	.	.	.	.	.	.	T	.	.	C	.	.	T	.	.

	320																	337
BM	G	G	C	A	C	A	G	G	T	T	G	A	A	C	A	G	T	C
DR	.	.	.	.	.	.	.	.	G	.	.	.	.	.	A	.	.	.
NJ	.	.	T	.	.	C	.	C	.	.	.	.	.	.	.	.	.	.
XF	.	.	.	.	.	C	.	C	.	.	.	.	.	.	.	.	.	G
EP	.	.	.	.	.	.	.	A	.	.	.	.	.	.	.	.	.	A
SA	.	.	.	.	.	C	.	G	.	.	.	.	.	.	.	.	.	G
BF	.	.	.	.	.	.	.	C	.	.	.	.	.	.	.	.	.	T
OM	.	.	.	.	.	.	.	G	.	.	.	.	.	.	.	.	C	.
DA	.	.	A	.	.	.	.	.	.	.	.	.	.	.	C	.	.	.
ZY	.	.	.	.	.	T	.	G	.	.	.	.	.	.	.	.	.	A
DF	.	.	T	.	.	.	.	A	.	.	.	.	.	.	C	.	.	A
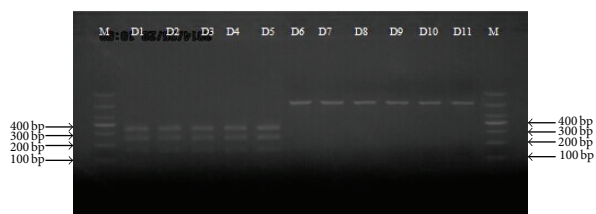
FIGURE 4: PCR-RFLP patterns of COI region from JBS samples (D1–D11) digested with *Spe*I and *Bst*EII, DNA marker (M) in bp were indicated.
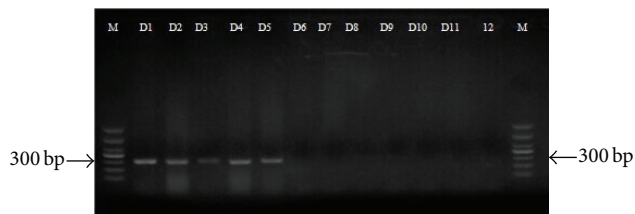
FIGURE 5: Diagnostic PCR products generated by primers (COI37 and COI337) using template DNA of JBS samples (D1–D11), negative control (12) (water was used as sample), and DNA marker (M) in bp were indicated.

Nanling Mountains, that is, Guangdong, Guangxi, Hunan, Jiangxi, and so forth. Due to the hot summer and cold winter and high humidity almost all through the year, the residents in these areas often suffer from bone pain, arthritis, rheumatism, and even paralysis. To relieve or prevent these ailments, they preserved the snake in strong alcoholic drinks for months to allow the pharmaceutically active ingredients to be slowly released and regularly take the drinks. The effectiveness of such remedies has now been acknowledged in ChP, and the dried infant snakes (JBS) are thought to have stronger pharmacological actions.

However, artificial breeding of *B. multicinctus* remains unsuccessful, and JBS supply depends entirely on wild resources. The increasing demand of *B. multicinctus* in recent decades has drastically diminished their wild population and

it is now listed in China Red Data Book of Endangered Animals [21] and IUCN Red List of Threatened Species 2012. As a result, the price of JBS increases considerably.

The high price of JBS gives rise to various versions of adulterants. The common practice of adulteration is decoloring the body bands of other snakes with decolorants, coloring the bands into white with paint, or even painting the bands on a snake without bands [22]. Such tricks were encountered in this study, as in JBS crude drug samples number 9 and number 11. Another practice faking JBS is splitting the body of large genuine snakes into small strips and assembling them with the heads of other snake species [22]. The differentiation of these adulterants from genuine JBS merely by their morphological characters is rather difficult

because of their high resemblance in appearance, especially for the young snakes.

The development of molecular biological techniques provides a new solution for the identification of traditional Chinese medicinal materials [23, 24]. In 2010, PCR-RFLP and diagnostic PCR were officially adopted in ChP, and DNA barcoding would be included in the coming edition. Our previous studies indicated that COI barcodes had great advantages in the identification of JBS [4, 19, 25]. Compared with DNA barcoding technique, DNA barcode-based PCR-RFLP and diagnostic PCR are more convenient and efficient to distinguish JBS from its adulterants with reliable results; they can be complementary to DNA barcoding and macro-scopical identification.

In PCR-RFLP, we initially considered single endonuclease digestion. *Spe*I, whose restriction site was located at bases 121 through 126 in the COI barcode region of *B. multicinctus*, allows restriction digestion of the sequence between bases 121 and 122. The barcode sequences of 9 reported JBS adulterants did not contain a *Spe*I restriction site, but when we expanded the investigation to more snake species, we found *Z. dhumnades* had the same sequences at bases 121 to 126 as *B. multicinctus*. *Bst*EII is another endonuclease specific to *B. multicinctus* and recognizes nucleotides at positions 353 to 359 to result in cleavage at position 353, yielding two fragments of 353 bp and 345 bp in length that can not be separated by electrophoresis. Single endonuclease digestion with either *Spe*I or *Bst*EII did not produce optimal results. But when combined, these 2 endonucleases cut COI amplicons of *B. multicinctus* into 3 fragments (340 bp, 230 bp, and 120 bp in length) and that of *Z. dhumnades* into 2 fragments (580 bp and 120 bp) without causing cleavage of the amplicons of other species (700 bp), thus allowing authentication of JBS crude drug samples. In addition, partial digestion did not occur with these 2 endonucleases as shown in previous studies [13].

Diagnostic PCR using primers specific to Cytb sequences had been applied in authenticating JBS [15–17]. In this study, for the first time, we successfully discriminated JBS from its adulterants with diagnostic PCR using species-specific primers based on COI barcode sequences. The primer pair COI37 and COI337 we used had a theoretical T_m value higher than 80°C to allow a high annealing temperature in PCR, which is an important factor for diagnostic PCR to improve the specificity. At the annealing temperature 55°C, the diagnostic PCR system amplified a DNA segment about 300 bp from the 4 template DNAs of *B. multicinctus*, *O. moellendorffi*, *Di. flavozonatum*, and *B. fasciatus*; at 60°C, the template DNA was amplified only from *B. multicinctus* and *B. fasciatus* of the same genus with only a 3-base difference in their primer sites. At an even higher annealing temperature of 65°C, the fragment was amplified only from *B. multicinctus* but not from other species or negative control. Under the optimized condition, the diagnostic PCR system could also distinguish *B. multicinctus* from other snake species such as *Ptyas mucosus*, *Lycodon ruhstrati*, and *Enhydris chinensis* (data not shown).

We tested 11 commercial JBS crude drugs with the established PCR-RFLP and diagnostic PCR systems. By both methods, samples D1–D5 were recognized as genuine JBS and samples D6–D11 as fake ones. Morphological identification and DNA barcodes analysis also indicated that samples D1–D5 were derived from *B. multicinctus*, whereas samples D6–D11 were not, suggesting the validity of these two methods in JBS authentication.

Molecular identification also has inherent limitations, such as its inability to determine whether the crude drug is derived from adult or juvenile snakes. Of the 11 commercial JBS samples we tested, sample D3 (Da Baihua She) was identified as genuine JBS of *B. multicinctus* origin by PCR-RFLP, diagnostic PCR, and DNA barcoding as well; but morphologically, it was a part of dried body of an adult *B. multicinctus* individual, which did not match the description of "dried body of infant snakes" in ChP. In such case, macro-scopical inspection serves as a complementary means for molecular markers-based identification. On the other hand, molecular identification makes up for the inadequacy of identification based on morphological characters. The sample D11 could not be identified for origin through its appearance, but both PCR-RFLP and diagnostic PCR clearly suggested adulteration, and DNA barcoding further identified it as *Di. rufozonatum*.

The PCR-RFLP and diagnostic PCR systems we estab-lished, combined with macroscopical identification and DNA barcoding, constitute a comprehensive approach to JBS iden-tification. These methods can be used independently or in different combinations according to the objective of the work, laboratory conditions, and the advantages and disadvantages of each method. For the purpose of authentication only without considering the zoological origin, either PCR-RFLP or diagnostic PCR will suffice because both of them are rapid, simple, cost-effective, and time-saving. Further investigation of the zoological origin of an adulterant requires the use of DNA barcoding for a conclusive result.

5. Conclusions

We for the first time established COI barcode-based PCR-RFLP and diagnostic PCR systems for effective authentication of JBS. These two methods can be integrated with macro-scopical identification and DNA barcoding technique to constitute a comprehensive authentication and identification system for JBS.

Conflict of Interests

The authors declare that there is no conflict of interests regarding the publication of this paper.

Acknowledgment

References

[1] State Pharmacopoeia Committee, *Pharmacopoeia of the People's Republic of China*, vol. 1, Chemical Industry Press, Beijing, China, 2010.

[2] R. A. Weng and L. R. Li, "Study on feature of Bungarus Parvus and its confused species," *Hunan Guiding Journal of TCMP*, vol. 8, no. 5, p. 292, 2002.

[3] C. Y. Huang, "Survey of studies on identification of Bungarus multicinctus multicinctus," *Chinese Traditional and Herbal Drugs*, vol. 33, no. 4, p. 382, 2002.

[4] Z. Chao, J. Liao, Z. B. Liang, S. H. Huang, L. Zhang, and Z. D. Li, "Cytochrome C oxidase subunit I barcodes provide an efficient tool for Jinqian Baihua She (*Bungarus parvus*) authentication," *Pharmacognosy Magazine*, vol. 10, no. 40, pp. 449–457, 2014.

[5] Y. J. Qu, Y. G. Kang, X. H. Feng, and S. W. Liang, "Study on microscopic feature of *Bungarus parvus* and its confused species," *China Journal of Chinese Materia Medica*, vol. 23, no. 2, pp. 71–73, 1998.

[6] J. Sun, J. Jia, and R. J. Zhang, "Identification of Jinqian Baihua She (Bungarus Parvus) and its confused species," *Medical Information*, vol. 1, no. 6, p. 1523, 2010.

[7] X. H. Liu, Y. Q. Wang, K. Y. Zhou, Z. Q. Liu, and L. Cao, "Study on allele-specific diagnostic PCR of the traditional Chinese medicines of the deers," *Acta Pharmaceutica Sinica*, vol. 36, no. 8, pp. 634–635, 2001.

[8] Z. Liu, Y. Q. Wang, K. Zhou, D. Han, X. Yang, and X. Liu, "Authentication of Chinese crude drug, Gecko, by allele-specific diagnostic PCR," *Planta Medica*, vol. 67, no. 4, pp. 385–387, 2001.

[9] X. Y. Ding, Z. T. Wang, K. Y. Zhou, L. Xu, H. Xu, and Y. Wang, "Allele-specific primers for diagnostic PCR authentication of Dendrobium officinale," *Planta Medica*, vol. 69, no. 6, pp. 587–588, 2003.

[10] Y. Ying, H. Xu, and Z. T. Wang, "Allele-specific diagnostic PCR authentication of *Dendrobium thyrsiflorum*," *Acta Pharmaceutica Sinica*, vol. 42, no. 1, pp. 98–103, 2007.

[11] J. Y. Um, H. S. Chung, M. S. Kim et al., "Molecular authentication of Panax ginseng species by RAPD analysis and PCR-RFLP," *Biological and Pharmaceutical Bulletin*, vol. 24, no. 8, pp. 872–875, 2001.

[12] C. Z. Wang, P. Li, J. Y. Ding, G. Q. Jin, and C. S. Yuan, "Identification of *Fritillaria pallidiflora* using diagnostic PCR and PCR-RFLP based on nuclear ribosomal DNA internal transcribed spacer sequences," *Planta Medica*, vol. 71, no. 4, pp. 384–386, 2005.

[13] C. Z. Wang, P. Li, J. Y. Ding, X. Peng, and C. S. Yuan, "Simultaneous identification of *Bulbus Fritillariae cirrhosae* using PCR-RFLP analysis," *Phytomedicine*, vol. 14, no. 9, pp. 628–632, 2007.

[14] State Pharmacopoeia Committee, *The First Expanded Edition of Pharmacopoeia of the People's Republic of China*, China Medical Science Press, Beijing, China, 2012.

[15] Y. Q. Wang, K. Y. Zhou, L. S. Xu, and G. J. Xu, "Authentication of Bungarus Parvus and its adulterants by DNA molecular method using diagnostic primer," *Journal of Chinese Pharmaceutical Sciences*, vol. 9, no. 2, pp. 61–66, 2000.

[16] C. Q. Feng, X. J. Tang, L. Q. Huang, Z. Z. Qian, J. Zhang, and G. H. Cui, "High specific PCR identification of *Bungarus multicinctus* and its adulterants," *China Journal of Chinese Materia Medica*, vol. 31, no. 13, pp. 1050–1053, 2006.

[17] J. X. Zhao, G. H. Cui, M. T. Xin, and S. H. Tang, "The establishment of PCR system to identify *Bungarus multicinctus*

rapidly," *Acta Pharmaceutica Sinica*, vol. 45, no. 10, pp. 1327–1332, 2010.

[18] O. Folmer, M. Black, W. Hoeh, R. Lutz, and R. Vrijenhoek, "DNA primers for amplification of mitochondrial cytochrome c oxidase subunit I from diverse metazoan invertebrates," *Molecular Marine Biology and Biotechnology*, vol. 3, no. 5, pp. 294–299, 1994.

[19] J. Liao, Z. B. Liang, L. Zhang, J. D. Li, and Z. Chao, "DNA barcoding of common medicinal snakes in China," *Chinese Pharmaceutical Journal*, vol. 48, no. 15, pp. 1255–1260, 2013.

[20] T. Vincze, J. Posfai, and R. J. Roberts, "NEBcutter: a program to cleave DNA with restriction enzymes," *Nucleic Acids Research*, vol. 31, no. 13, pp. 3688–3691, 2003.

[21] E. M. Zhao, *China Red Data Book of Endangered Animals: Amphibia and Reptilia*, Science Press, Beijing, China, 1998.

[22] B. Z. Lu, Q. Wang, X. B. He, and Y. M. Wu, "Identification of *Bungarus parvus* and its adulterants," *Strait Pharmaceutical Journal*, vol. 17, no. 2, pp. 91–92, 2005.

[23] P. D. N. Hebert, A. Cywinska, S. L. Ball, and J. R. DeWaard, "Biological identifications through DNA barcodes," *Proceedings of the Royal Society B: Biological Sciences*, vol. 270, no. 1512, pp. 313–321, 2003.

[24] P. D. N. Hebert, S. Ratnasingham, and J. R. DeWaard, "Barcoding animal life: cytochrome c oxidase subunit 1 divergences among closely related species," *Proceedings of the Royal Society B: Biological Sciences*, vol. 270, supplement 1, pp. S96–S99, 2003.

[25] J. Liao, Z. Chao, and L. Zhang, "Identification of common medicinal snakes in medicated liquor of Guangdong by COI barcode sequence," *Journal of Chinese Medicinal Materials*, vol. 36, no. 11, pp. 1740–1742, 2013.

Research Article

Endangered Uyghur Medicinal Plant *Ferula* Identification through the Second Internal Transcribed Spacer

Congzhao Fan,[1] Xiaojin Li,[1] Jun Zhu,[1] Jingyuan Song,[2,3] and Hui Yao[2]

[1] *Xinjiang Institute of Chinese Materia Medica and Ethnical Materia, 9 Xinming Road, Urumqi, Xinjiang 830002, China*
[2] *The National Engineering Laboratory for Breeding of Endangered Medicinal Materials, Institute of Medicinal Plant Development, Chinese Academy of Medical Sciences and Peking Union Medical College, Beijing 100193, China*
[3] *Chongqing Institute of Medicinal Plant Cultivation, Chongqing 408335, China*

Correspondence should be addressed to Xiaojin Li; xjlxj@126.com

The medicinal plant *Ferula* has been widely used in Asian medicine, especially in Uyghur medicine in Xinjiang, China. Given that various substitutes and closely related species have similar morphological characteristics, *Ferula* is difficult to distinguish based on morphology alone, thereby causing confusion and threatening the safe use of *Ferula*. In this study, internal transcribed spacer 2 (ITS2) sequences were analyzed and assessed for the accurate identification of two salable *Ferula* species (*Ferula sinkiangensis* and *Ferula fukangensis*) and eight substitutes or closely related species. Results showed that the sequence length of ITS2 ranged from 451 bp to 45 bp, whereas guanine and cytosine contents (GC) were from 53.6% to 56.2%. A total of 77 variation sites were detected, including 63 base mutations and 14 insertion/deletion mutations. The ITS2 sequence correctly identified 100% of the samples at the species level using the basic local alignment search tool 1 and nearest-distance method. Furthermore, neighbor-joining tree successfully identified the genuine plants *F. sinkiangensis* and *F. fukangensis* from their succedaneum and closely related species. These results indicated that ITS2 sequence could be used as a valuable barcode to distinguish Uyghur medicine *Ferula* from counterfeits and closely related species. This study may broaden DNA barcoding application in the Uyghur medicinal plant field.

1. Introduction

The endangered Uyghur medicinal herb *Ferula* has a long history of application in China. It was first utilized in the *Tang Materia Medica* during the Tang Dynasty (AD 659) because of its effectiveness in removing food residues, as well as its dispersed stuffiness and chlordime form [1]. To date, *Ferula* is traditionally employed for treating different diseases such as asthma, epilepsy, stomach ache, flatulence, intestinal parasites, weak digestion, and influenza in many countries [2, 3]. Pharmacological and biological studies have shown that *Ferula* has antioxidant [4], antiviral [5], antifungal [6], cancer chemopreventive [7], antidiabetic [8], antispasmodic [6], hypotensive [9], and molluscicidal effects [10]. *Ferula* is now included in the Uyghur Medicine Criteria [11] and calendar version of the Chinese Pharmacopoeia [12]. The original plants for this medicine are *Ferula sinkiangensis* and *Ferula fukangensis*. In addition to a close relationship with

traditional Chinese medicine, Uyghur medicine has absorbed the essences of Indian, Arabian, Iran, and ancient Greek medicine, thereby forming a complete system of medicine with distinctive ethnic characteristics. However, its medicinal parts and functions are not precisely the same. For instance, traditional Chinese medicine utilizes *Ferula* resin, whereas Uyghur medicineutilizes *Ferula* resin, roots, and seeds [13] as clinical parts.

In China, the *Ferula* genus is mostly distributed in Xinjiang, but has been destroyed in this area as a result of excessive collection. In addition to seed plant breeding, change in reclamation, irrigation, road building, and deterioration of the original habitat contribute to the annual shrinking of *Ferula* resources. Currently, *F. fukangensis* is on the verge of extinction, and *F. sinkiangensis* is listed as a class 3 endangered plant and class 2 protected wild medicinal species. Given its high cost and scarce resources, various substitutes and adulterants have emerged. *F. sinkiangensis* and *F. fukangensis*

have been misused and substituted by other species such as *F. ferulaeoides* Korov [14]. Furthermore, numerous species from the *Ferula* genus have been utilized as traditional Chinese medicines and ethical materials. For example, *F. soongarica* has been utilized by Kazakhs in treating headaches, colds, and stomach aches; *F. caspica* in treating nervous breakdown; and *F. lehmannii* in treating parasitic malnutrition and cold pain in the heart and abdomen [15]. When mixed with substitutes, adulterants, and closely related species, the original medicinal plant could not be traced to the medicinal herb market. A famous line that is widely circulated in the herbal medicine field is "there is no false *Scutellaria*, no true *Ferula*." Thus, investigating the authenticity of the Uyghur medicinal herb *Ferula* is urgently required.

The *Ferula* genus is usually recognized as monophyletic; the delimitation of species requires examination of complete specimens with roots, stem bases, basal leaves, inflorescence, flowers, and ripe fruits based on the observations of living plants [16]. Given that members are similar in habit and morphology, flowers, inflorescences, and fruit anatomy are often hardly discernible taxa [17, 18]. Thus, the infrageneric classification method of the Uyghur medicinal herb *Ferula* urgently requires a solution. To address this problem, microscopic identification and powder identification techniques have been utilized for *F. sinkiangensis* and its closely related species [19–21]. However, these techniques could not solve the problem of authenticating the Uyghur medicinal herbs *F. sinkiangensis* and *F. fukangensis* from other traditional medicinal herbs and closely related *Ferula* species. By comparison, DNA barcoding employs a short DNA sequence from a standard locus as a species identification tool [22], which has been widely applied in forage identification [23] and animal genetic relationship identification [24]. The internal transcribed spacer (ITS) region of this barcode, which comprises ITS1, 5.8S, and ITS2, has been widely utilized as a core DNA barcode to identify different herbal medicinal materials [25]. Researchers have proposed ITS2 as a standard DNA barcode for medicinal plant authentication [26, 27]. However, molecular identification of *F. sinkiangensis* and *F. fukangensis* from their closely related species utilizing the ITS2 sequence has not been reported. In the present study, DNA barcoding technology was applied for the first time to distinguish *F. sinkiangensis* and *F. fukangensis* from their succedaneum and other closely related species. The application of DNA barcoding in trade and market management could ensure the safe use of the pharmacopoeia herb *Ferula*.

2. Samples and Methods

2.1. Materials and Methods for Sampling of Plant Materials. Seventy-three leaves and root samples, which represented 10 *Ferula* species, were collected from different locations. Nine *Ferula* species were acquired from Xinjiang and one species of *Ferula litwinowiana* was obtained from Kazakhstan. The 10 species were given specimen collection numbers (Table S1) (see Supplementary Material available online at http://dx.doi.org/10.1155/2014/479879)and authenticated by Researcher Guanmian Shen (Xinjiang Institute of Ecology and Geography, Chinese Academy of Sciences) and Associate

Fellow Guoping Wang (Xinjiang Institute of Chinese Traditional Medical and Ethical Materia Medica). All corresponding voucher samples were deposited in the herbarium of the Xinjiang Institute of Chinese Traditional Medical and Ethical Materia Medica. In addition, one published sequence was downloaded from GenBank for analysis (Table S1).

2.2. DNA Extraction, Amplification, and Sequencing. Genomic DNA was isolated from 30 mg of leaves or roots according to the protocol of the Plant Genomic DNA Kit (Tiangen Biotech Co., China). Specific regions of the ITS2 sequences were amplified from dried leaves and root extracts; universal primer and PCR conditions for ITS2 were obtained from previous studies [28]. The purified PCR products were sequenced using a 3730XL sequencer (Applied Biosystems, Foster City, CA, USA).

2.3. Sequence Alignment and Analysis. The CodonCode Aligner v 4.0.4 was utilized to edit the sequences and assemble the contigs and shear sequence using universal primers (5′-3′: ATTCACACCAAGTATCGCAT and 3′-5′: ATTGTAGTCTGGAGAAGCGTC). The ITS2 core region could be obtained using the HMMer annotation method based on the hidden Markov model (HMM) to remove the 5.8S and 28S sections at both ends of the sequences [29]. The interspecific/intraspecific variation of the samples was calculated according to Kress et al. [22]. A phylogenetic tree was constructed utilizing MEGA 5.0. Neighbor-joining algorithm (NJ tree) was used to evaluate the capability of the ITS2 sequence to authenticate the studied species. Bootstrap tests were conducted utilizing 1,000 resampling to assess the confidence of the phylogenetic relationships using employed MEGA 5.0 [30, 31]. BLAST1 and nearest-distance methods were performed to identify species, as previously described [32, 33].

3. Results

3.1. Universality and Sequence Characteristics. DNA was successfully extracted from 73 samples. Gel electrophoretic analysis revealed that all sample extractions emitted bright bands. ITS2 sequences were successfully amplified and sequenced; high-quality bidirectional sequences were obtained. The ITS2 sequence, including partial the 5.8S, ITS2 region, and partial 28S, ranged from 451 bp to 455 bp, and GC contents were 53.6% to 56.2%. The partial 5.8S length was 84 bp; the GC contents ranged from 57.1% to 58.3%. The length of the ITS2 region was 226 bp to 230 bp; the GC contents ranged from 53.0% to 56.8%. The partial 28S was 141 bp and the GC contents ranged from 51.8% to 53.9%.

3.2. Intraspecific/Interspecific Variations. Sequence length, variable sites, and average interspecific K2P distance of ITS2 regions were analyzed and summarized (Table 1). Most of the 10 *Ferula* species in this study were represented by severalsamples because they were collected from different localities. *F. sinkiangensis* was represented by 13 samples (Table S1), *F. fukanensis* by 6 samples, *F. ferulaeoides* by 14

```
                                   1111111111111111111111111111111122222222222222222222222222222333334444444
                                   5990000000011111122222233466677788889990223344445555556666677778899990001924444445
                                   4370124689013567037893943572683561286452568901245712789014589057923457 2127895
Ferula fukanensis KF793024         TGCCTGCAACATCTCTGATCCTGTGTTCCCAGACTTGAGTTTTATGC--GCTTCA-GCACGCAAGTGATCTAGTACT
Ferula lehmannii KF793028          ..................................C..........--......-.....................
Ferula caspica KF793015            ...........T.T.....T.....C.T..............--..C...-.....................
Ferula ferulaeoides KF793002       ....C.......T.T.......-..............--..C...-.....................
Ferula soongarica KF792996         ....C.......T.T.......-..............--..C...-.............T.......
Ferula dubjanskyi KJ804107         ....C-......T.T.A.........T.....T.....A.....--A.C.A.A...........C.......
Ferula syreitschikowi KJ804110     ....CA.....AT.T....................--..C...-A..T.............C...
Ferula sinkiangensis KF792984      ....C.......T........C...A.........A.........--..C-----...................
Ferula akitschkensis KJ804122      CC.ACAACCTCAACTGATGAA..AAC.T.GCT-.CC..-C.CCGAATGT.TCAG.-.GCTAGCCC---C.CGT.CTC
Ferula litwinowiana KF793035       ..T.................................C......C..--......-.....................
```

FIGURE 1: Variable sites in the haplotypes of the 10 *Ferula* species.

samples, *F. soongarica* by 6 samples, *F. caspica* by 11 samples, and so on (Table 1). The results showed that each *Ferula* species only possesses a haplotype, and their intraspecific distances were all zero.

Among the 74 ITS2 sequences, a total of 77 variation sites were detected in the region, including 63 base mutations and 14 insertion/deletion mutations. The following contents were detected among the 63 base mutation sites: C/T (26), C/G (5), A/C (12), G/A (10), T/A (5), T/G (4), C/G/A (1), and C/T/A (4) substitutions. A total of 76 distinctive variable sites were discovered among the 77 variation sites, which could precisely authenticate different *Ferula* species (Figure 1). For instance, the C–T transition at site 133 and the A–G transition at site 206 could distinguish *F. sinkiangensis* from the othernine *Ferula* species. The C–T transition at the 397 bp site could distinguish *F. soongarica* and the C–T transition at site 176 could individually classify *F. caspica*. The interspecific divergence calculated utilizing the K2P model indicated that the ITS2 sequences of *F. sinkiangensis* possessed an average interspecific distance of 0.030; *F. fukanensis* possessed an average intraspecific distance of 0.027 (Table 1).

3.3. Species Identification Capability of ITS2 Barcode and NJ Tree Analysis. BLAST1, nearest distance, and tree-based methods were utilized to determine whether the certified medicinal herb *Ferula* could be identified by ITS2 sequences. The results indicated that ITS2 correctly identified 100% of the samples at the species level through the BLAST1 method. The nearest genetic distance method also resulted in 100% success rate of identification.

Up to 74 ITS2 sequences of *Ferula* species were chosen to build the trees. NJ trees (Figure 2) were constructed based on the ITS2 sequences. The results showed that the Uyghur medicinal herbs *F. fukangensis* and *F. sinkiangensis* presented good monophyly; they could be correctly distinguished from their succedaneum *F. ferulaeoides* and other closely related species. Furthermore, the remaining *Ferula* species could

be distinguished from one another. Thus, the ITS2 barcode could correctly identify two Uyghur medicinal herb plants from their adulterants and closely related species.

4. Discussion

4.1. ITS2 Region Is a Useful DNA Barcode to Differentiate 10 Ferula Species. The genus *Ferula* is an important ephemeral plant that possesses highly ecological and medicinal values. Our results emphasized the advantages of using the ITS2 region as a DNA barcode, including high interspecific divergence but small intraspecific variation, favorable universality, and short length, which lead to easy amplification and sequencing efficiency. Given that pharmacologists often traded *Ferula* genus plants internationally for their medicinal values, our research provides a convenient tool for validating the quality products of *Ferula*. In a previous study [18], 83 accessions (74 species) of *Ferula* were used to ascertain the phylogenetic position of the genus within the family. Most species had one sample; hence, the intraspecific divergence could not be determined. The ITS1 and ITS2 regions are separately amplified, and then assembled to successfully redress several misplaced *Ferula* genus plants. Phylogenetic analyses of tree-based method successfully corrected the three accessions of misplaced *Ferula* species. In our study, 74 ITS2 sequences of 10 *Ferula* species were used to authenticate *F. sinkiangensis and F. ferulaeoides* from their succedaneum and closely related species, most of which were newly reported sequences and each species was represented by two or more samples. Therefore, intraspecific variation was clearly displayed.

Morphological characteristics are an important basis for identifying the original *Ferula* plants. However, morphological identification often relies on abundant experience, which could be easily affected by biocoenosis and geographical environment [17]. As a result, identification of traditional Chinese medicine *Ferula* has been limited. Genomic sequence is not
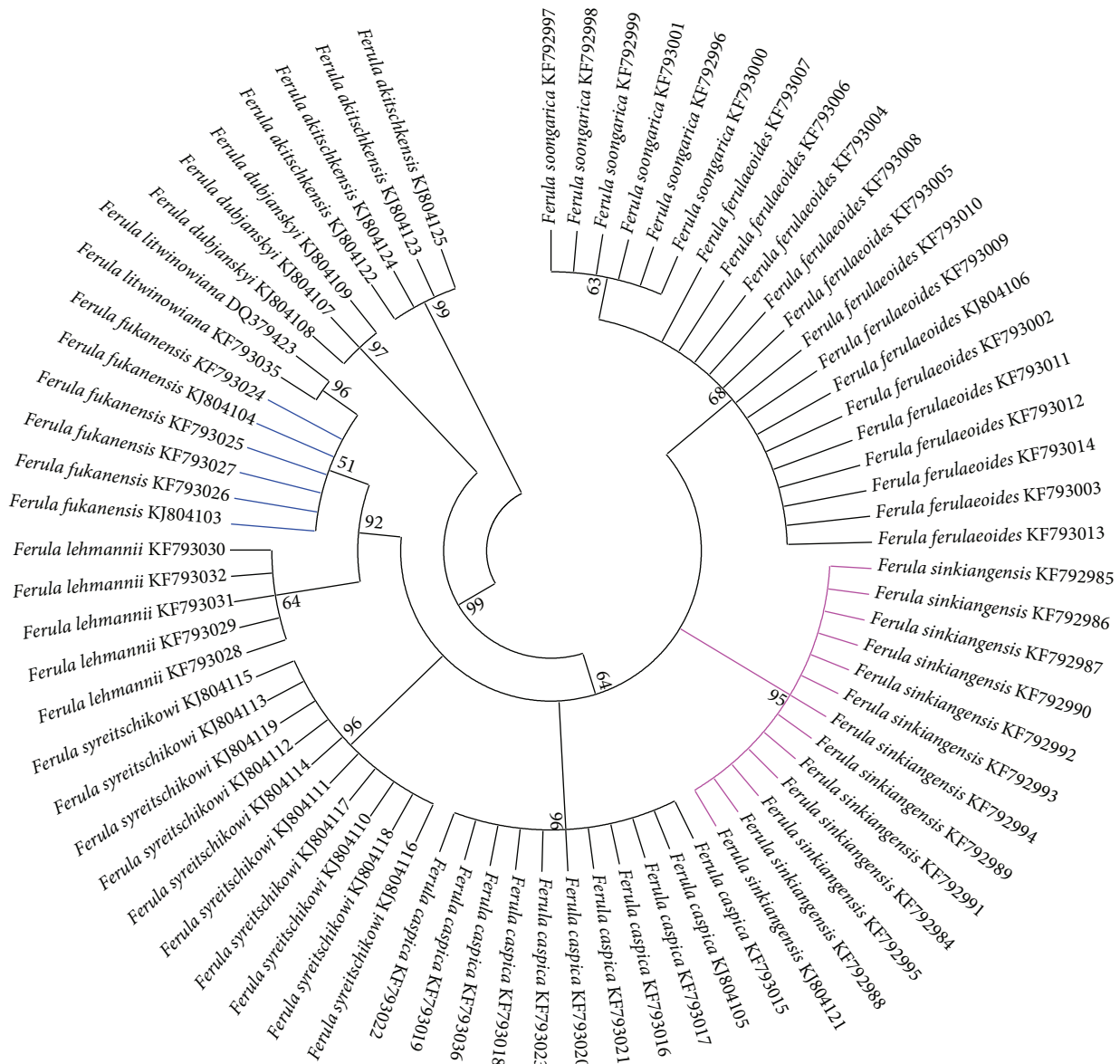
FIGURE 2: NJ tree of *F. sinkiangensis and F. fukangensis* and their closely related species constructed with the ITS2 sequence. The bootstrap scores (1,000 replicates) are shown (≥50%) for each branch.

TABLE 1: ITS2 sequence characteristics and K2P distances of *Ferula* used in this research.

Species	Sample number	GC content (%)	Sequence length (bp)	Distinctive variable site	Interspecific K2P distance (mean)
F. sinkiangensis	13	55.0	451	7	0.009–0.163 (0.030)
F. fukanensis	6	54.7	455	0	0.002–0.161 (0.027)
F. ferulaeoides	14	54.6	454	0	0.002–0.150 (0.023)
F. soongarica	6	54.4	454	1	0.002–0.154 (0.025)
F. caspica	11	54.3	455	3	0.009–0.161 (0.030)
F. lehmannii	5	54.9	455	0	0.002–0.157 (0.028)
F. syreitschikowi	10	54.3	455	3	0.007–0.145 (0.028)
F. akitschkensis	4	56.2	452	53	0.145–0.170 (0.156)
F. dubjanskyi	3	53.6	455	5	0.016–0.151 (0.035)
F. litwinowiana	2	54.9	455	4	0.007–0.170 (0.033)

influenced by individual characteristics and developmental stages; therefore, DNA barcode technology has been widely used in recent years [34]. DNA barcoding is an effective supplement to traditional morphological methods, and, in our study, the phylogenetic tree (Figure 2) demonstrated that the ITS2 region has an effective role in authenticating the Uyghur medicinal herb *Ferula* and differentiating 10 *Ferula* species from each other.

4.2. Identification of Uyghur Medicine Utilizing ITS2 Sequence. According to the records, Uyghur medicine includes 1,000 types of herbal medicines and up to 450 types are frequently utilized. Nevertheless, limited by rare resources and confusing plant origins, only about 200 species of Uyghur medicinal herbs have been formulated based on national and local criteria. Aside from the Uyghur medicinal herb *Ferula*, numerous other Uyghur medicinal herbs, such as *Cichorium intybus* L. and *Cichorium glandulosum* Boiss. et Huet, are facing the same dilemma [14]. These situations are significant obstacles to the standardization and industrialization of Uyghur medicine. Although morphological examination and chemical analysis are routine practices in identifying Uyghur medicinal herbs, these methods are influenced by biological and physical factors [35]. DNA barcoding and forensically informative nucleotide sequencing are less affected by these elements. The ITS2 barcode has been proposed as a universal DNA barcode for medicinal herb and animal identification [26, 27, 36, 37]. Thus, based on this study, DNA barcoding would have a broad prospect in authenticating more Uyghur medicinal herbs, which provides a new method for the Food and Drug Administration to control Uyghur medicine and ensure its safe and efficient use and has a considerable role in developing the Uyghur medicine industry.

4.3. Significance of DNA Barcode in Food Safety Control. Although several *Ferula* genus plant roots are used traditional medicine or folk medicine in Xinjiang, few *Ferula* species are edible. Starch extracted from *F. ferulaeoides and F. dubjanskyi* could be made into food [2]. The tender leaves of *F. lehmannii* could be used as wild herbs to make cold dishes and dumplings [38]. DNA barcoding has been used for food safety control [39–41]. The NJ tree demonstrated that the ITS2 barcode could accurately perform food safety control. Sequencing the ITS2 DNA barcode region represents a new technique that guarantees food and drug safety in *Ferula* species. This technology is easy to learn and utilized by food managers [42].

Conflict of Interests

The authors declare that there is no conflict of interests regarding the publication of this paper.

Acknowledgments

References

[1] E. P. Korovin, "*Ferula L.*," in *Flora Uzbekistana*, vol. 4, pp. 399–438, 1959.

[2] M. Iranshahy and M. Iranshahi, "Traditional uses, phytochemistry and pharmacology of asafoetida (*Ferula assa-foetida* oleo-gum-resin)—a review," *Journal of Ethnopharmacology*, vol. 134, no. 1, pp. 1–10, 2011.

[3] P. Mahendra and S. Bisht, "*Ferula asafoetida*: traditional uses and pharmacological activity," *Pharmacognosy Reviews*, vol. 6, no. 12, pp. 141–146, 2012.

[4] S. Ben Salem, A. Jabrane, F. Harzallah-Skhiri, and H. Ben Jannet, "New bioactive dihydrofuranocoumarins from the roots of the Tunisian *Ferula lutea* (Poir.) Maire," *Bioorganic and Medicinal Chemistry Letters*, vol. 23, no. 14, pp. 4248–4252, 2013.

[5] Z. E. Nazari and M. Iranshahi, "Biologically active sesquiterpene coumarins from *Ferula* species," *Phytotherapy Research*, vol. 25, no. 3, pp. 315–323, 2011.

[6] G. Kavoosi, A. Tafsiry, A. A. Ebdam, and V. Rowshan, "Evaluation of antioxidant and antimicrobial activities of essential oils from *Carum copticum* Seed and *Ferula assafoetida* latex," *Journal of Food Science*, vol. 78, no. 2, pp. T356–T361, 2013.

[7] M. Iranshahi, A. Sahebkar, S. T. Hosseini, M. Takasaki, T. Konoshima, and H. Tokuda, "Cancer chemopreventive activity of diversin from *Ferula diversivittata* in vitro and in vivo," *Phytomedicine*, vol. 17, no. 3-4, pp. 269–273, 2010.

[8] A. S. Abu-Zaiton, "Anti-diabetic activity of *Ferula assafoetida* extract in normal and alloxan-induced diabetic rats," *Pakistan Journal of Biological Sciences*, vol. 13, no. 2, pp. 97–100, 2010.

[9] M. Fatehi, F. Farifteh, and Z. Fatehi-Hassanabad, "Antispasmodic and hypotensive effects of *Ferula* asafoetida gum extract," *Journal of Ethnopharmacology*, vol. 91, no. 2-3, pp. 321–324, 2004.

[10] S. Kumar, D. K. Singh, and V. K. Singh, "Tertiary combination of freeze-dried urine of Indian breeds of cow with plant products against snail *Lymnaea acuminata*," *Pakistan Journal of Biological Sciences*, vol. 15, no. 20, pp. 992–996, 2012.

[11] Xinjiang Food and Drug Administration, *The Xinjiang Uygur Autonomous Region Traditional Chinese Medicine and Uygur Medicine Pieces Concoct Standard*, Xinjiang People's Saitary Press, 2010.

[12] Chinese Pharmacopoeia Commission, *Chinese Pharmacopoeia*, vol. 1, Chinese Medicine Science and Technology Press, 2010.

[13] Chinese Materia Medica Editorial Committee, *The Chinese Materia Medica (Uyghur Volume)*, Shanghai Science and Technology Press, 2005.

[14] C. Liu, W. J. Yang, Z. Y. Gu et al., "Research progress of Uygur medicine easy mixed species arrangement and the application of molecular biology," *Northwest Pharmaceutical Journa*, vol. 28, no. 4, pp. 440–442, 2013.

[15] D. Bandyopadhyay, B. Basak, A. Chatterjee et al., "Saradaferin, a new sesquiterpenoid coumarin from *Ferula assafoetida*," *Natural Product Research*, vol. 20, no. 10, pp. 961–965, 2006.

[16] E. P. Korovin, *Generis Ferula (Tourn.) L. Monographia illustra*, Academiae Scientiarum UzRSS, Taschkent, Uzbekistan, 1947.

[17] Y. Ajani, A. Ajani, J. M. Cordes, M. F. Watson, and S. R. Downie, "Phylogenetic analysis of nrDNA ITS sequences reveals relationships within five groups of Iranian *Apiaceae* subfamily Apioideae," *Taxon*, vol. 57, no. 2, pp. 383–401, 2008.

[18] R. Kurzyna-Młynik, A. A. Oskolski, S. R. Downie, R. Kopacz, A. Wojewódzka, and K. Spalik, "Phylogenetic position of the genus *Ferula* (Apiaceae) and its placement in tribe Scandiceae as inferred from nrDNA ITS sequence variation," *Plant Systematics and Evolution*, vol. 274, no. 1-2, pp. 47–66, 2008.

[19] Y. Tan, T.-T. Gao, Y. Ma, X. Ding, and Y.-H. Cheng, "Pharmacognostic identification of *Ferula syreitschikowii*," *Journal of Chinese Medicinal Materials*, vol. 34, no. 11, pp. 1694–1696, 2011.

[20] H. Y. Han, J. M. Xu, G. Y. Li et al., "Microscopic identification of *Ferula dissecta* (Ledeb.) Ledeb," *Modern Chinese Medicine*, vol. 12, no. 12, pp. 17–19, 2010.

[21] X. Ding, Y. Tan, Y. Zhang et al., "Pharmacognostic identification of *Ferula sinkiangensis*," *China Pharmacy*, vol. 35, pp. 3307–3309, 2011.

[22] W. J. Kress, K. J. Wurdack, E. A. Zimmer, L. A. Weigt, and D. H. Janzen, "Use of DNA barcodes to identify flowering plants," *Proceedings of the National Academy of Sciences of the United States of America*, vol. 102, no. 23, pp. 8369–8374, 2005.

[23] I. Ganopoulos, P. Madesis, and A. Tsaftaris, "Universal ITS2 barcoding DNA region coupled with High-Resolution Melting (HRM) analysis for seed authentication and adulteration testing in Leguminous forage and pasture species," *Plant Molecular Biology Reporter*, vol. 30, no. 6, pp. 1322–1328, 2012.

[24] R. Zomuanpuii, L. Ringngheti, S. Brindha, G. Gurusubramanian, and N. Senthil Kumar, "ITS2 characterization and *Anopheles* species identification of the subgenus *Cellia*," *Acta Tropica*, vol. 125, no. 3, pp. 309–319, 2013.

[25] M. Li, H. Cao, P. P. H. But, and P. C. Shaw, "Identification of herbal medicinal materials using DNA barcodes," *Journal of Systematics and Evolution*, vol. 49, no. 3, pp. 271–283, 2011.

[26] S. Chen, H. Yao, J. Han et al., "Validation of the ITS2 region as a novel DNA barcode for identifying medicinal plant species," *PLoS ONE*, vol. 5, no. 1, Article ID e8613, 2010.

[27] H. Yao, J. Song, C. Liu et al., "Use of ITS2 region as the universal DNA barcode for plants and animals," *PLoS ONE*, vol. 5, no. 10, Article ID e13102, 2010.

[28] Z. Sun and S. Chen, "Identification of cortex herbs using the DNA barcode nrITS2," *Journal of Natural Medicines*, vol. 67, no. 2, pp. 296–302, 2013.

[29] A. Keller, T. Schleicher, J. Schultz, T. Müller, T. Dandekar, and M. Wolf, "5.8S-28S rRNA interaction and HMM-based ITS2 annotation," *Gene*, vol. 430, no. 1-2, pp. 50–57, 2009.

[30] C. Koetschan, T. Hackl, T. Müller, M. Wolf, F. Förster, and J. Schultz, "ITS2 Database IV: interactive taxon sampling for internal transcribed spacer 2 based phylogenies," *Molecular Phylogenetics and Evolution*, vol. 63, no. 3, pp. 585–588, 2012.

[31] K. Tamura, D. Peterson, N. Peterson, G. Stecher, M. Nei, and S. Kumar, "MEGA5: molecular evolutionary genetics analysis using maximum likelihood, evolutionary distance, and maximum parsimony methods," *Molecular Biology and Evolution*, vol. 28, no. 10, pp. 2731–2739, 2011.

[32] L. Xiang, J. Song, T. Xin et al., "DNA barcoding the commercial Chinese caterpillar fungus," *FEMS Microbiology Letters*, vol. 347, no. 2, pp. 156–162, 2013.

[33] H. A. Ross, S. Murugan, and W. L. S. Li, "Testing the reliability of genetic methods of species identification via simulation," *Systematic Biology*, vol. 57, no. 2, pp. 216–230, 2008.

[34] C. Liu, D. Liang, T. Gao et al., "PTIGS-IdIt, a system for species identification by DNA sequences of the psbA-trnH intergenic spacer region," *BMC Bioinformatics*, vol. 12, no. 13, article S4, 2011.

[35] P. C. Shaw, F. N. Ngan, and P. P. H. But, *Authentication of Chinese Medicinal Materials by DNA Technology*, World Scientific Publishing, Singapore, 2002.

[36] P. D. N. Hebert, S. Ratnasingham, and J. R. DeWaard, "Barcoding animal life: cytochrome c oxidase subunit 1 divergences among closely related species," *Proceedings of the Royal Society B: Biological Sciences*, vol. 270, supplement 1, pp. S96–S99, 2003.

[37] M. Li, P. P. H. But, and P. C. Shaw, "Molecular identification of traditional medicinal materials," in *Molecular Pharmacognosy*, pp. 45–66, Springer, Dordrecht, The Netherlands, 2013.

[38] China Flora Editorial Board of Cas, *Flora China*, vol. 14, Sciences Press, Beijing, China, 1992.

[39] L. Jaakola, M. Suokas, and H. Häggman, "Novel approaches based on DNA barcoding and high-resolution melting of amplicons for authenticity analyses of berry species," *Food Chemistry*, vol. 123, no. 2, pp. 494–500, 2010.

[40] M. Á. Pavón, I. González, R. Martín, and T. G. Lacarra, "ITS-based detection and quantification of *Alternaria* spp. in raw and processed vegetables by real-time quantitative PCR," *Food Microbiology*, vol. 32, no. 1, pp. 165–171, 2012.

[41] T. Xin, H. Yao, H. Gao et al., "Super food *Lycium barbarum* (Solanaceae) traceability via an internal transcribed spacer 2 barcode," *Food Research International*, vol. 54, no. 2, pp. 1699–1704, 2013.

[42] M. Y. Stoeckle, C. C. Gamble, R. Kirpekar, G. Young, S. Ahmed, and D. P. Little, "Commercial teas highlight plant DNA barcode identification successes and obstacles," *Scientific Reports*, vol. 1, article 42, 2011.

Research Article

The Modified JiuWei QiangHuo Decoction Alleviated Severe Lung Injury Induced by H1N1 Influenza Virus by Regulating the NF-κB Pathway in Mice

Lijuan Chen,[1] Xin Yan,[2] Qianlin Yan,[1] Jiajun Fan,[3] Hai Huang,[3] Xunlong Shi,[3] Lei Han,[3] Tianxiong Han,[1] and Haiyan Zhu[3]

[1] *Department of Chinese Medicine, Shanghai Tenth People's Hospital, Tongji University School of Medicine, Shanghai 200092, China*
[2] *Institute of Chinese Medicine, Tongji University School of Medicine, Shanghai 200092, China*
[3] *Department of Biosynthesis, School of Pharmacy, Fudan University, 826 Zhangheng Road, Shanghai 201203, China*

Correspondence should be addressed to Haiyan Zhu; hyzhu@mail.shcnc.ac.cn

A new approach to treat infections of highly pathogenic influenza virus is to inhibit excessive innate immune response. JiuWei QiangHuo decoction has been used for centuries for the treatment of pulmonary disorders in China. In this study, we evaluated the anti-inflammatory activities of the modified JiuWei QiangHuo (MJWQH) decoction in the treatment of influenza A (H1N1) virus-induced severe pneumonia in mice. The results showed that MJWQH significantly increased the survival rate of H1N1-infected mice and suppressed the production of TNF-α, IL-1, IL-6, MCP-1, RANTES, and IFN-α on day 4 after infection. Moreover, oral administration of MJWQH efficiently inhibited virus replication and alleviated the severity of lung injuries. The results also showed that MJWQH may have potential therapeutic effect on severe lung injury induced by H1N1 virus by regulating the NF-κB pathway. Our study suggested that MJWQH might be an alternative therapy for the treatment of viral pneumonia.

1. Introduction

Influenza A (H1N1) virus can cause severe respiratory diseases and lead to pandemic outbreaks in humans. Some severe patients may develop acute lung injury and even acute respiratory distress syndrome, which are the most common causes of death in these H1N1-infected patients [1]. However, influenza continues to evolve and antiviral drugs are usually not given in the early stage of virus infection, thus rendering the antiviral therapy ineffective. It is suggested that modulation of the host immune response has the potential advantage of exerting less-selective pressure on viral populations [2]. Many traditional Chinese medicines (TCM) and herbs have been shown to have immunomodulatory, anti-inflammatory, antiviral, and antioxidant activities [3–5]. There are a number of clinical trials evaluating the potential benefit of TCM in the treatment of H1N1-induced pneumonia [6]. It seems to be a promising approach to extract effective ingredients from

TCM for the treatment of influenza virus-induced severe pneumonia.

The recruitment of innate immune cells into the lung and excessive proinflammatory cytokines and chemokines are hallmarks of influenza virus infection [7]. It has been shown that early recruitment of inflammatory leukocytes to the lung, followed by excessive early cytokine responses, is the key contributor to the morbidity and mortality of H1N1 virus infections [8, 9]. Toll-like receptors (TLRs) are the main intracellular/extracellular immune cell receptors that recognize pathogen-associated molecular patterns of the microbes and foreign particles, including viruses, to induce several immune cell functions ranging from migration and phagocytosis to inflammatory cytokine expression [10–13]. TLR7 is located in the membranes of the endosomal compartment and can recognize viral single-stranded RNA (ssRNA) [14]. TLR7 expression is upregulated in pulmonary epithelial cells and macrophages after virus infection. Upon

TABLE 1: Composition of MJWQH.

Chinese name	Latin name	Amount (g)	Place of origin
Qiang Huo	Rhizoma et Radix Notopterygii	5	Inner Mongolia, China
Cang Zhu	Rhizoma Atractylodis	10	Sichuan, China
Pu Gong Yin	Herba Taraxaci	20	Jiangsu, China
Huang Qin	Radix Scutellariae	10	Inner Mongolia, China
Huang Qi	Radix Astragali	20	Gansu, China
Fang Feng	Radix Saposhnikoviae	5	Hebei, China
Yu Xing Cao	Herba Houttuyniae	10	Gansu, China
Tian Hua Fen	Radix Trichosanthis	15	Henan, China

stimulation, cells recognize viral ssRNA via TLR7 and activate downstream signaling molecules through a MyD88 dependent pathway, causing subsequent cytokine storm and triggering inflammatory lung injury [15, 16].

JiuWei QiangHuo (JWQH) decoction was first introduced in the monograph *Cishinanzhi* written by an influential TCM physician Zhang Yuansu of Jin Dynasty (1151–1234). It has been used for over 900 years for the treatment of pulmonary disorders, such as common cold, bronchial infections, and pneumonia. This decoction has recently been modified by Dr. Yan Dexin, a Grandmaster of Chinese Medicine granted by the Ministry of Health of China, which consists of eight herbs including *Rhizoma et Radix Notopterygii, Herba Taraxaci, Radix Scutellariae, Radix Astragali, Rhizoma Atractylodis, Radix Saposhnikoviae, Herba Houttuyniae,* and *Radix Trichosanthis.* The modified JWQH (MJWQH) has been shown to be effective in patients with severe pneumonia induced by influenza virus. It may reverse H1N1-induced pneumonia in mice by regulating the metabolism of arachidonic acid, fatty acid, and amino acid and is thus involved in anti-inflammatory activity and cell protection [17]. Based on previous research findings and the pathogenesis of H1N1-induced pneumonia, we hypothesize that MJWQH has an immunoregulatory effect in the early stages of the disease by inhibiting excessive immune response, thus inhibiting virus replication, lung inflammation, and severe lung injury.

2. Materials and Methods

2.1. Preparation of MJWQH. MJWQH was prepared from eight dried raw materials (Table 1) purchased from Shanghai Shuguang Hospital (Shanghai, China) and authenticated by a physician in Fudan University. Voucher specimens were deposited in the Herbarium Center of the Department of Pharmacognosy, School of Pharmacy, Fudan University. All raw materials were extracted by boiling in distilled water (about 6-fold the weight of the mixture) at $100°C$ for 20 min and then filtered. The filtrates from two decoctions were combined, and the decoction was dried in vacuo at $70°C$ and ground into powder for use. The yield of the extraction was 24%. The extracts were stored in an airtight container at $-80°C$ until further analysis.

2.2. Chromatographic Analysis of MJWQH. MJWQH was dissolved in pyrogen-free isotonic saline and filtered through
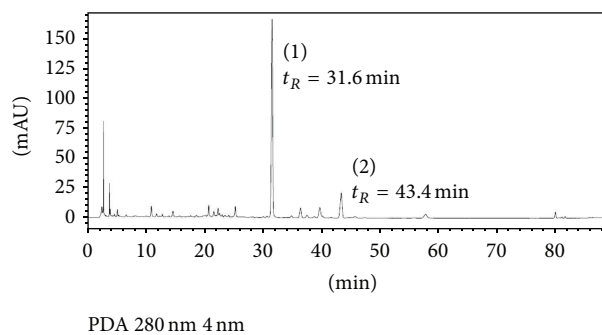

FIGURE 1: HPLC chromatogram of MJWQH (280 nm). Calycosin-7-O-β-D-glucopyranoside (1) and baicalin (2) were separated from MJWQH at a retention time of 31.6 and 43.4 min, respectively.

a 0.2 mm filter (Microgen, Laguna Hills, CA, USA) before high performance liquid chromatography (HPLC) analysis (Figure 1). HPLC analysis was performed on an Agilent series 1100 HPLC system (Agilent, Waldbronn, Germany) equipped with quaternary pump, diode-array detector, autosampler, and column compartment. Calycosin-7-O-β-D-glucopyranoside and baicalin purchased from the National Institute for the Control of Pharmaceutical and Biological Products (Beijing, China) were used as the external standards in HPLC. Chromatographic separation was performed on a Zorbax XDB-C18 column (5 μm, φ 4.6 × 250 mm, Agilent Technologies, USA). The mobile phase consisted of acetonitrile (A) and water containing 0.2% acetic acid (B), and the following gradient program was used: 5% A in the first 10 min, then a linear gradient to 36% A over 60 min, and then a linear gradient to 85% A over 30 min. The mobile phase flow rate was 0.8 mL/min, the detector was monitored at 280 nm, the spectral data for all peaks were accumulated in the range of 190–400 nm, and the column temperature was set at $25°C$.

2.3. Mice and Virus. Male BALB/c mice, 5 to 6 weeks old, were purchased from Shanghai SLAC Laboratory Animal Co. Ltd. (Certificate number 2007000548167, SCXK (Hu) 2012-0002; Shanghai, China) and bred and maintained in a closed breeding facility at the Animal Center of Fudan University. All animal experiments were performed in accordance with the guidelines of the Ethics Committee for Animal Use of Fudan University. The mouse adapted influenza A/FM/1/47
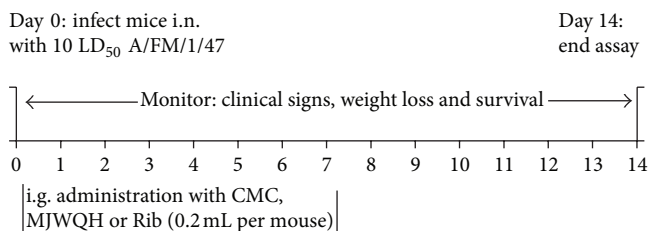
Day 0: infect mice i.n.
with 10 LD_{50} A/FM/1/47

Day 14:
end assay

←——— Monitor: clinical signs, weight loss and survival ———→

0 1 2 3 4 5 6 7 8 9 10 11 12 13 14

i.g. administration with CMC,
MJWQH or Rib (0.2 mL per mouse)

Figure 2: Experimental protocol. All BALB/c mice except the NC ones were challenged intranasally with influenza A/FM/1/47 (H1N1) virus (10 LD_{50} per mouse) and then treated with 0.5% CMC solution (model control, MC), MJWQH, or Rib one hour later for 2, 4, or 7 days, respectively.

(H1N1) virus was provided by the Institute of Medicinal Biotechnology, Chinese Academy of Medical Sciences (Beijing, China), and stored at −80°C until use. Mice were infected intranasally (i.n.) with 10 LD_{50} doses of H1N1 virus in 1640 culture medium.

2.4. Experimental Design. The BALB/c mice were randomly divided into four groups: normal control (NC); model control (MC); MJWQH; and ribavirin (Rib). The ribavirin was supplied by Star Lake Bioscience Co., Inc. (Guangdong, China). Figure 2 illustrates our initial protocol. On day 0, BALB/c mice (except for the NC) were anesthetized with isoflurane and infected i.n. with 10 LD_{50} doses of influenza A/FM/1/47 H1N1 virus in a volume of 30 μL. One hour later, the MJWQH and Rib mice were intragastrically (i.g.) administered with MJWQH (1.8 g/kg/d) or ribavirin (100 mg/kg/d dissolved in 0.5% carboxyl methyl cellulose (CMC) solution). The NC and MC mice were treated with the same volume of 0.5% CMC solution. All mice were monitored daily for clinical symptoms, body weight, and survival for 14 consecutive days [2]. Mice showing more than 25% of body weight loss were considered to have reached the experimental endpoint and were then humanely euthanized by CO_2 asphyxiation.

2.5. Pathological Examination and Immunohistochemistry. Lungs were removed on day 4 after infection, weighed, and then inflated with 10% phosphate-buffered formalin to their normal volume. The lung index (ratio of lung weight to body weight) was calculated as a parameter of lung edema. The left lobes were paraffin embedded and cut into 5 μm thick sections, and one section from each tissue sample was stained using a standard haematoxylin-and-eosin (HE) procedure. Lung sections were examined to determine the extent of pneumonia in a blinded fashion as previously described [18]: 0 = no pneumonia; 1 = mild interstitial pneumonia (<25% of the lung); 2 = moderate interstitial pneumonia (25–50% of the lung); and 3 = severe interstitial pneumonia (>50% of the lung). The scores of the individual samples were summed up to yield a composite score.

The tissue sections were immunostained using the streptavidin-biotin-horseradish peroxidase method. The sections were deparaffinized and rehydrated through a graded series of alcohols and then microwaved in EDTA buffer (pH 8.0) at 97°C for 12 min to unmask antigen epitopes. The sections were treated with 3% hydrogen peroxide methanol solution for 10 min to block endogenous peroxidase, washed in PBS, and incubated with rabbit anti-NF-κB p65 antibody (Assay Biotech, USA) at 1 : 200 dilution. They were washed again in PBS and incubated with avidin-biotin complex-horseradish peroxidase for 1 h at room temperature. The sections were incubated with chromogen-fast diaminobenzidine (DAB) for 1–5 min, after which they were counterstained in haematoxylin and mounted on aqueous mounting medium.

2.6. Hemagglutination (HA) Test. Lung tissues pooled from all mice in each group were homogenized in 1 mL of sterilized PBS. The homogenates were centrifuged at 10000 ×g for 10 min, and the resulting supernatant was analyzed by HA assay. Serial 2-fold dilutions of each viral preparation were made in PBS (pH 7.15) in 96-well V-bottomed microplates, and 25 μL of 0.5% suspension of chicken red blood cells (RBCs) was added to each well. The contents in plates were mixed and incubated at room temperature (22–25°C) until complete agglutination of erythrocytes. The HA titer was the reciprocal of the dilution of virus in the last well with complete hemagglutination.

2.7. ELISA. Lungs were homogenized in PBS and the supernatants were collected. The inflammatory cytokines (IL-1, IL-6, TNF-α, and IFN-α) and chemokines (MCP-1, RANTES, MIP-1, and IP-10) in the supernatants of each group were tested by ELISA kits (Abcam, England) supplied by Jinma Laboratory Equipment Co., Ltd. (Lot number: 201303; Shanghai, China), which was performed according to the manufacturer's instructions. ELISAs were read on a 96-well plate reader and concentrations were determined using Revelation software (BioTek Epoch, USA).

2.8. Western Blotting. Lung protein extracts were prepared using the Nuclear Extract Kit (BestBio, China) following the manufacturer's instruction. Equal amounts of protein were separated by SDS-PAGE and subsequently blotted on polyvinylidene fluoride membranes (220 mA, 65 min). Blots were blocked in TBS solution containing 0.1% Tween 20 and 5% nonfat dry milk overnight at 4°C. The following antibodies and dilutions were used: TLR7 (Catalog number 2633, Cell Signaling Technology; 1 : 1000); MyD88 (D80F5) (Catalog number 4283, Cell Signaling Technology; 1 : 1000); TRAF6 (Catalog number 04-451, Millipore, USA; 1 : 1000); IκB-α (c-21) (sc-371, Santa Cruz Biotechnology, 1 : 200); p-IKKα/β (Ser 176) (sc-21661, Santa Cruz Biotechnology, 1 : 200); NF-κB p65 (sc-109, Santa Cruz Biotechnology, 1 : 200); p-NF-κB p65 (Ser 276) (sc-101749, Santa Cruz Biotechnology, 1 : 200); and GAPDH (14C10) (Catalog number 2118, Cell Signaling Technology; 1 : 1000). The membranes were blotted with appropriate secondary antibodies (Immunology Consultants Laboratory, Inc., USA; 1 : 5000), and the blotted proteins were visualized by enhanced chemiluminescence using a commercially available kit (Millipore, USA).

TABLE 2: RT-PCR primer sequence.

Gene	Sequence
Influenza A virus M	
Forward	5′-GACCGATCCTGTCACCTCTGAC-3′
Reverse	5′-AGGGCATTCTGGACAAAGCGTCTA-3′
GAPDH	
Forward	5′-ACCACCATGGAGAAGGCTGG-3′
Reverse	5′-CTCAGTGTAGCCCAGGATGC-3′
TLR7	
Forward	5′-GGTGGCAAAATTGGAAGATCC-3′
Reverse	5′-AGCTGTATGCTCTGGGAAAGGTT-3′
MyD88	
Forward	5′-CCAGAGTGGAAAGCAGTGTC-3′
Reverse	5′-GTCCTTCTTCATCGCCTTGT-3′
TRIF	
Forward	5′-CCACGTCCTACACGGAAGAT-3′
Reverse	5′-AACAGCATCTGCAGCTACCA-3′
NF-κB P65	
Forward	5′-ATGTGCATCGGCAAGTGG-3′
Reverse	5′-CAGAAGTTGAGTTTCGGGTAG-3′

2.9. Real-Time Reverse Transcription-PCR. Lungs were homogenized with a homogenizer to prepare the suspension, which was serially diluted in Trizol reagent (1 mL of Trizol for 100 mg tissue). Total RNA was prepared using the RNA fast isolation kit (Shanghai Generay Biotech Co., Ltd., Shanghai, China). For first-strand cDNA synthesis, $1\,\mu$g of total RNA was primed with random primers by reverse transcriptase (Promega, USA), and then 1/20 volume of cDNA was amplified on a StepOne Plus instrument using SYBR Green Real-Time PCR Master Mix Reagent (Toyobo, Japan). The PCR was performed at 95°C for 10 min, followed by 35 cycles of 95°C for 10 s, 58°C for 15 s, and 72°C for 30 s. Amplification was followed by melting curve analysis. The primers were designed with Beacon Designer 7 software (Table 2). The level of gene transcription was determined by comparing with the NC group.

2.10. Statistical Analyses. All statistical analyses were performed using GraphPad Prism 5.0 software (GraphPad Software, Inc., CA, USA). Survival curves were estimated by the Kaplan-Meier method and their homogeneity was estimated by the log-rank test. Multiple group comparisons were performed using one-way analysis of variance (ANOVA), followed by Dunnett's test to determine significant differences from the control. A P value less than 0.05 was considered significant for all tests.

3. Results

3.1. MJWQH Increased the Survival Rate of the H1N1-Infected Mice. Mice receiving 0.5% CMC developed the most severe symptoms, that is, lethargy, ruffled fur, hunched posture,

piloerection, rapid shallow breathing, and audible rattling, whereas some MJWQH and Rib treated mice presented such symptoms over the 14 days of treatment. The CMC-treated mice showed a progressive weight loss from day 3 after infection onward (Figure 3(a)), while the MJWQH and Rib treated mice showed a comparable weight loss from day 3 through day 6 after infection, but followed by a steady weight gain. The survival curves further confirmed the efficacy of MJWQH against the lethal influenza infection (Figure 3(b)). It showed that all MC mice died by day 10 after infection; the MJWQH treatment significantly increased the survival of H1N1-infected mice (42%; $P < 0.01$ versus the MC group), and the Rib treatment further increased the survival rate up to 83% ($P < 0.01$ versus the MC group). The survival curves were ended on day 14 after infection as no further mortality occurred after this time point.

3.2. MJWQH Alleviated the Severity of Lung Injuries. Lungs were removed on day 4 after infection for gross observation and histopathological examination. Edema, consolidation, and profuse hemorrhage were observed in the MC mice, whereas significantly less lung damage was observed in the Rib or MJWQH treated mice (Figure 4(a)). Histopathological analysis also revealed a significant reduction in the thickness and congestion of alveolar walls, intra-alveolar edema, and infiltrated neutrophils in lung tissues of mice treated with Rib and MJWQH (Figure 4(b)). In agreement with these histopathological findings, the Rib and MJWQH treated mice had significantly lower pathological scores (Figure 4(c)) and lung index (Figure 4(d)) than the MC group on day 4 after infection. In summary, MJWQH treated mice had a reduced lung injury after a lethal inoculum of pandemic H1N1 influenza virus.

3.3. MJWQH Inhibited Influenza Virus Replication In Vivo. The antiviral effect of MJWQH was determined by HA titers and the relative quantitation (RQ) of influenza virus replication in the lungs. By day 4 after infection, the viral titer was increased in all infected mice as compared to the NC group (Figure 5(a)). However, MJWQH or Rib significantly inhibited virus replication, as evidenced by a significant reduction in HA titer ($P < 0.01$ versus the MC group, Figure 5(a)) and the RQ of influenza A virus in the lungs ($P < 0.05$ versus the MC group, Figure 5(b)), indicating that both of them were effective in decreasing the viral load in mice infected by H1N1.

3.4. MJWQH Suppressed the Secretion of Cytokine/Chemokine Induced by H1N1 Influenza Virus. Early dysregulated innate immune responses in the lung are associated with morbidity and mortality during infection with highly pathogenic strains of influenza virus [8, 19]. Robust innate proinflammatory cytokine expression is believed to cause direct tissue insult and to recruit potentially tissue destructive inflammatory cells. The results showed significant reductions in TNF-α, IL-1, IL-6, MCP-1, RANTES, and IFN-α in the MJWQH treated mice on day 4 after infection. However, in comparison to the Rib treatment, MJWQH failed to suppress MIP-1 and IP-10
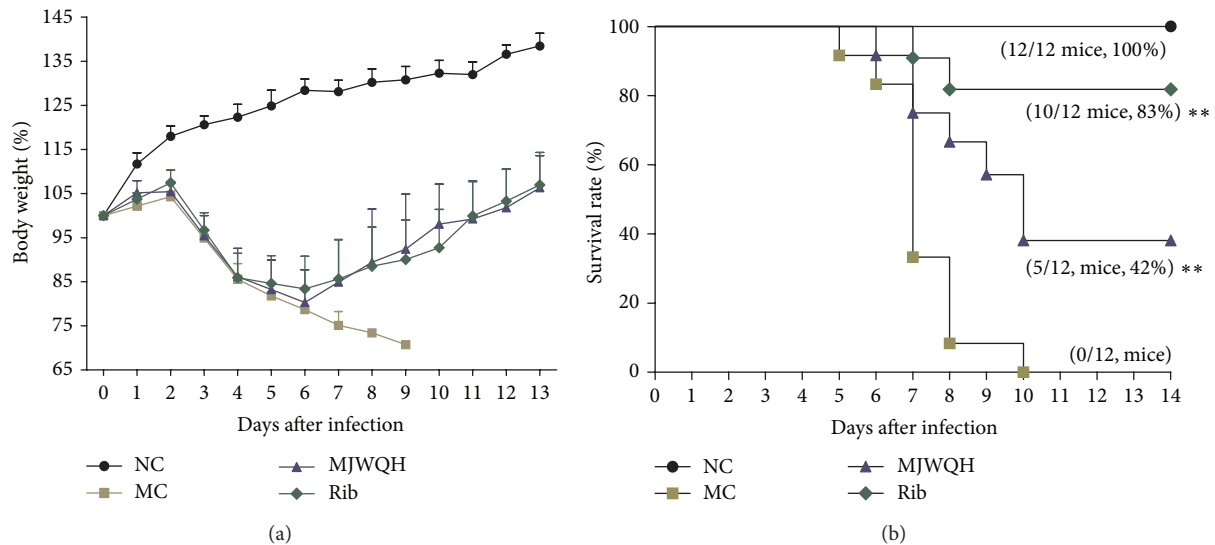
FIGURE 3: MJWQH treatment protected mice from lethal influenza challenge. BALB/c mice ($n = 12$ mice/group) were treated as described in Figure 2 for 7 days and monitored daily for signs and symptoms, body weight, and survival for 14 consecutive days. (a) Body weight (means ± SEM); (b) survival (number of survivors/total number of mice). $^{**}P < 0.01$ versus the MC group.

on day 4 after infection (Figures 6(a)–6(c)). All these results indicated that MJWQH suppressed cytokine production in severe pneumonia.

3.5. MJWQH Downregulated TLR7-MyD88-Dependent NF-κB Signaling Pathway.

NF-κB is an important transcription factor for the induction of various inflammation-associated genes, including cytokines and chemokines. To better understand the therapeutic mechanism of MJWQH in mice infected with H1N1 virus, we measured the expressions of TLR7, MyD88, TRAF6, p65, p-p65, IκB-α, and p-IKKα/β in lung tissues on days 2 and 4 after infection by using Western blot analysis. Figure 7 showed that influenza H1N1 infection significantly increased the protein expressions of TLR7, MyD88, and TRAF6 on days 2 and 4 after infection, which could be downregulated by the Rib or MJWQH treatment. We then examined whether MJWQH regulated the nuclear translocation of NF-κB as well as the phosphorylation and proteolytic degradation of IκB-α. No effect was observed on the NF-κB signaling pathway on day 2 after infection. However, NF-κB subunit p65 and p-p65 proteins in nucleus were significantly increased in virus-infected mice on 4 day after infection, but this increase could be suppressed by the MJWQH or Rib treatment. MJWQH also significantly inhibited the proteolytic degradation of IκB-α in mice. IKKα/β was expected to make an essential contribution to IκB phosphorylation, so we examined the p-IKKα/β level. The results showed that MJWQH significantly inhibited p-IKKα/β. These results together suggested that MJWQH inhibited H1N1 infection by inhibiting NF-κB signaling pathway on day 4 after infection.

To further demonstrate that MJWQH inhibited the NF-κB signaling pathway in the RNA level, we quantified the mRNA levels of TLR7, MyD88, and p65 in lung tissues on

day 4 after infection. Figure 8 showed that all of them were significantly reduced in the Rib and MJWQH treated mice.

Finally, we examined NF-κB signaling in lungs of H1N1-infected mice using immunohistochemistry with antibodies against p65 on day 4 after infection. Figure 9 showed that p65 could be hardly detected in the NC mice but it was abundant in the lungs of MC mice. However, there was a significant lower expression of p65 in the lungs of the Rib and MJWQH treated mice.

All these results clearly demonstrated that MJWQH blocked influenza virus infection by inhibiting the activation of TLR7/MyD88/TRAF6/IKKα/β/NF-κB signaling pathway.

4. Discussion

MJWQH is composed of eight herbs, each having specific antiviral, anti-inflammatory, or antioxidant activities. *Radix Scutellariae* has inhibitory effects on the influenza virus, hepatitis B virus, and human immunodeficiency virus [20–22]; *Radix Notopterygii* has antioxidant and anti-inflammatory activities [23]; *Herba Taraxaci* has antiviral, antiseptic, and anti-inflammatory activities [24]; *Radix Astragali* has antioxidant, immunopotentiating, and antistress activities [25, 26]; *Radix Saposhnikoviae* has immunoregulatory and antioxidant activities [27]; *Rhizoma Atractylodis* has potent antiviral and antioxidant activities [28]; *Herba Houttuyniae* has inhibitory effects on acute inflammation [29, 30]; and *Radix Trichosanthis* has antiviral activities and inhibits the replication of human immunodeficiency virus type 1 (HIV-1) [31, 32]. These biological activities would be helpful for severe pneumonia induced by influenza virus. However, the mechanism of their combined actions has not yet been verified.

A/FM/1/47 is a mouse-adapted influenza virus which exhibits high virulence and can induce strong immune responses and inflammation in the murine lung [33]. The
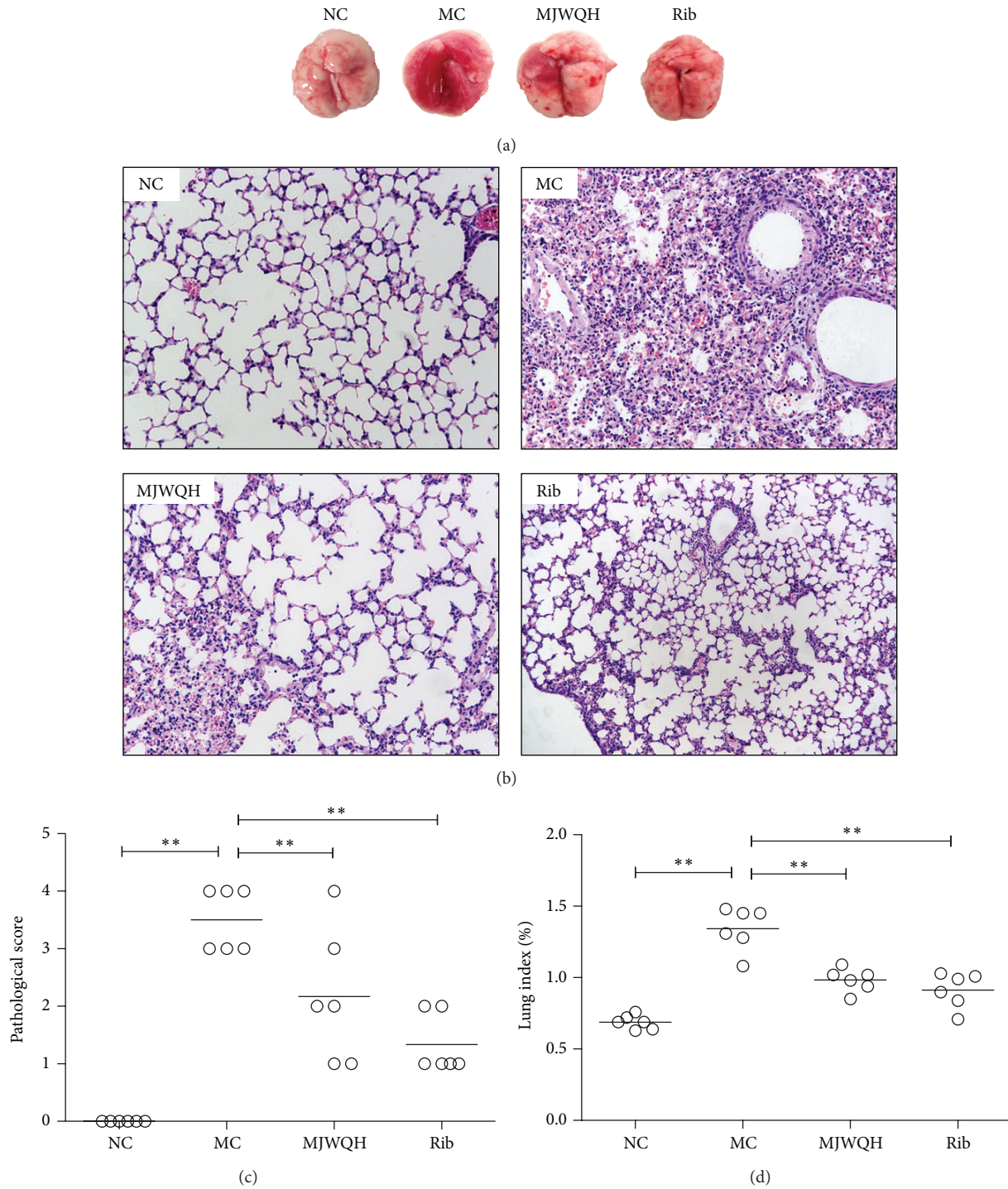
(a)

(b)

(c)

(d)

Figure 4: MJWQH alleviated the severity of H1N1-induced lung injuries. BALB/c mice ($n = 6$ mice/group) were treated as described in Figure 2 for 4 days. (a) Macroscopic appearance of lungs; (b) pathological changes of lung tissues (HE, ×200); (c) pathological scores; and (d) lung index. Data were presented as mean ± SD. **$P < 0.01$ versus the MC group.

effect of MJWQH on the H1N1-induced severe pneumonia was evaluated in a murine acute lung injury model in this study. The results showed that MJWQH significantly relieved the signs and symptoms, reduced body weight loss, and improved the survival rate of H1N1-infected mice. It also significantly inhibited virus replication, as evidenced by a significant reduction in HA titer and the relative quantitation of influenza A virus in the lungs. Altogether, these results suggested that MJWQH had potent antiviral activity against H1N1 influenza A virus infection in mice. Our previous studies showed that there was no reduction in the virus titer in the A549 cells infected by influenza A virus at 24 hours
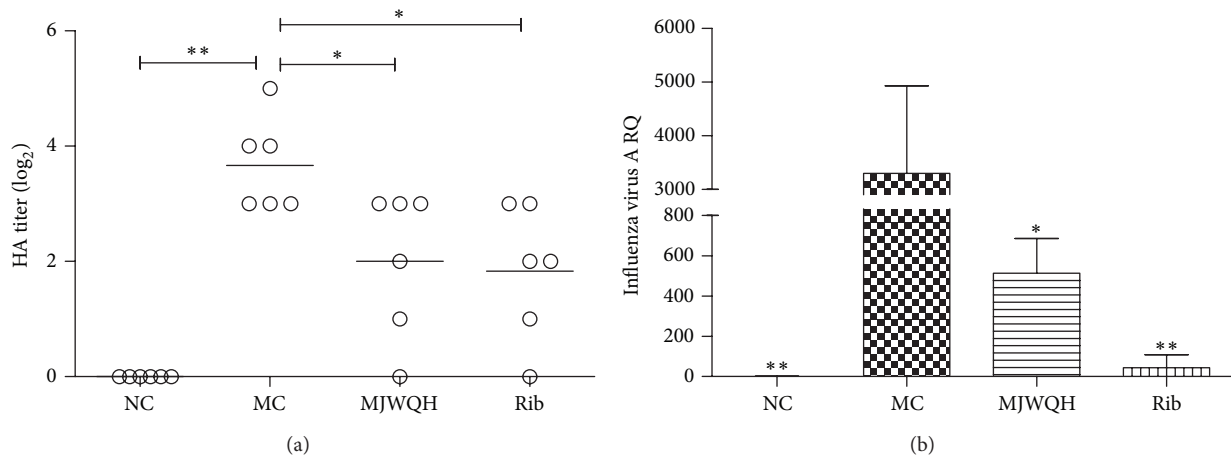
(a)

(b)

FIGURE 5: MJWQH inhibited virus replication. BALB/c mice ($n = 6$ mice/group) were treated as described in Figure 2 for 4 days. (a) HA titers of lung homogenates; (b) relative quantitation of influenza A virus. Data were presented as mean ± SD. $^*P < 0.05$; $^{**}P < 0.01$ versus the MC group.
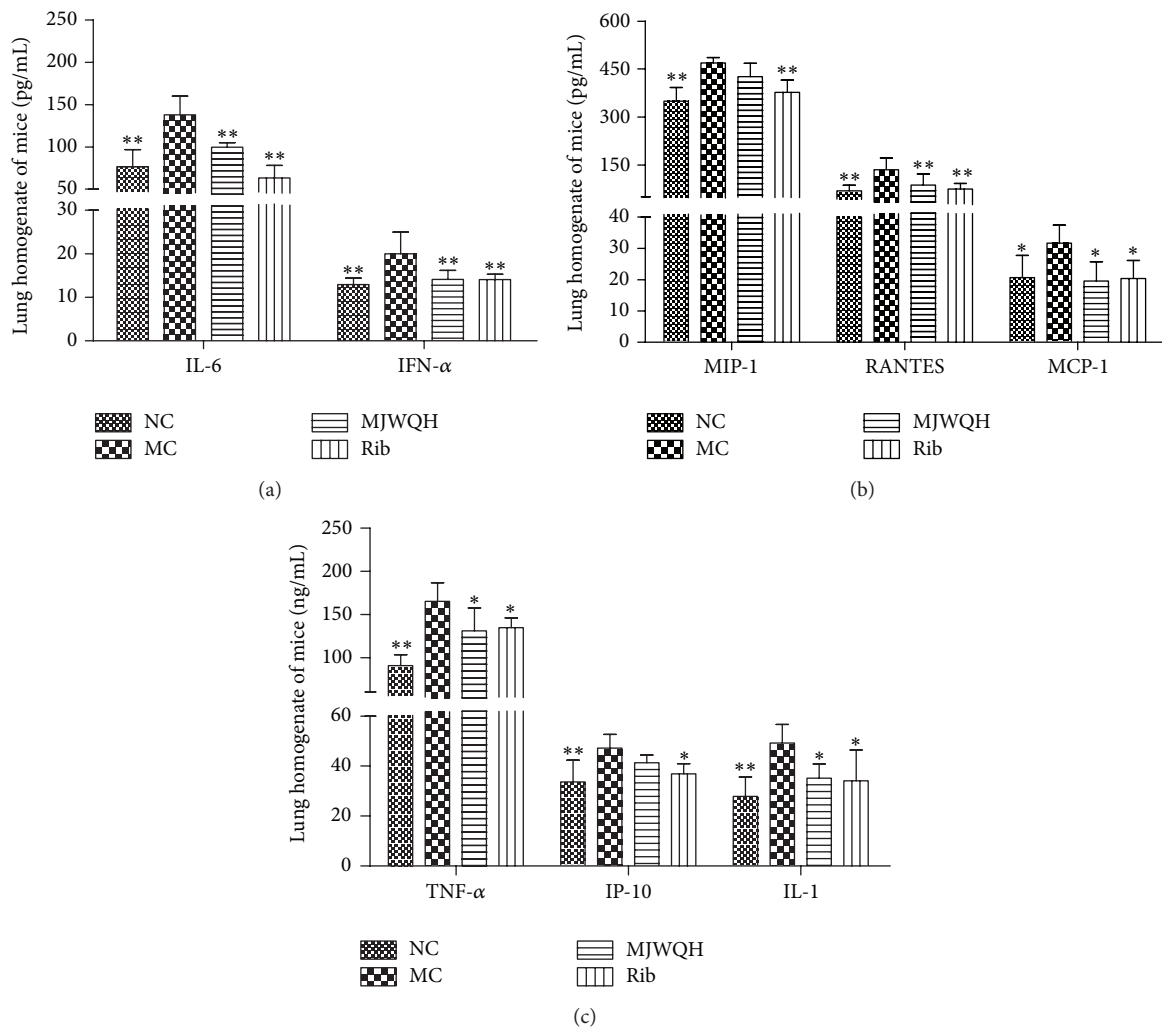

(a)

(b)

(c)

FIGURE 6: MJWQH suppressed innate immune responses. Proinflammatory cytokine and chemokine levels were analyzed in lung homogenates of mice on day 4 after infection by ELISA. Data were presented as mean ± SD. $^*P < 0.05$; $^{**}P < 0.01$ versus the MC group.
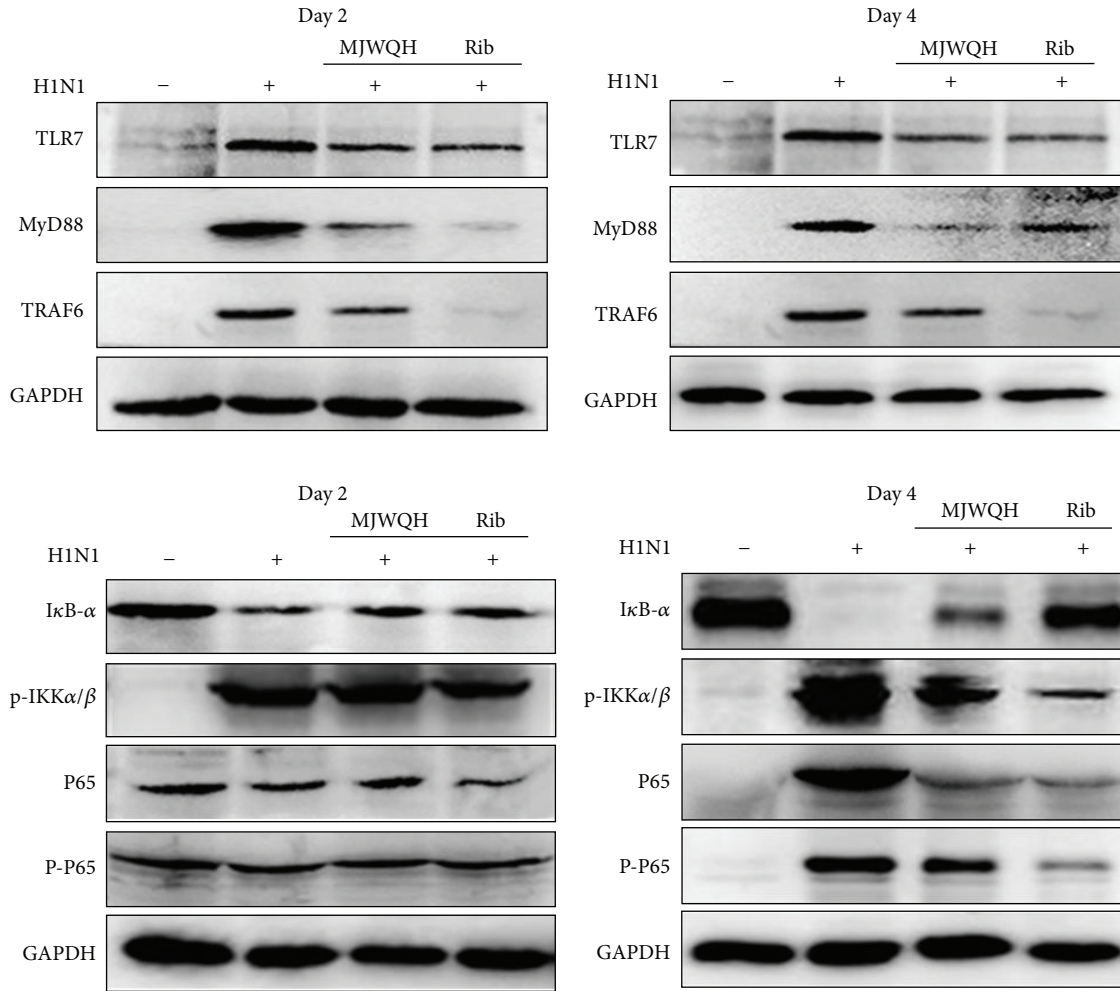
FIGURE 7: MJWQH inhibited the NF-κB signaling pathway. BALB/c mice ($n = 6$ mice/group) were treated as described in Figure 2 and killed on day 2 or 4 after infection. Cytosolic fractions and nuclear extracts were prepared from lung homogenates. NF-κB p65, IκB-α, TLR7, MyD88, and TRAF6 levels were detected by specific antibodies in cytosolic fractions using Western blot analysis. Phosphorylation of IKKα/β and p65 was determined in the nuclear extracts. GAPDH protein was used as a loading control.

after infection (data not shown here). However, in this study, we found that the MJWQH treatment significantly reduced lung HA titers. Therefore, we speculated that the antiviral activity of MJWQH was accomplished by inhibiting the early recruitment of inflammatory leukocytes to the lungs and suppressing excessive innate inflammatory responses.

Highly pathogenic flu can trigger excessive immune response or cytokine storm, which in turn leads to immune damage to the lung. In the case of infection, inflammation begins when the cells of the innate immune system recognize a pathogen-associated molecular pattern; then, certain host cells begin to secrete chemokines. Chemokines are small proteins (<10 kDa) that can activate and mediate the migration of leukocytes to the site of infection or inflammation [34]. Cytokines can be secreted by a variety of cells, including phagocytic cells such as macrophages and neutrophils, despite the fact that the endothelial cells are responsible for over half of all produced various cytokines and chemokines during inflammatory processes. [35]. The

early induction of cytokines and chemokines is associated with symptom formation in humans [36–38]. IFN-α activates inflammatory cells and stimulates expression of multiple cytokines and chemokines [39–41]. TNF-α, IL-1, and IL-6 have multifunctional activities and are associated with morbidity during influenza virus infection. Chemokines such as MCP-1, MIP-1, RANTES, and IP-10 induce the recruitment of innate immune cells into the lung, which can release more cytokines exacerbating cytokine storm and further damage the lung [42–44]. Therefore, balancing the inflammatory network may represent an effective treatment for influenza virus infection. We demonstrated in this study that the production of proinflammatory cytokines and chemokines from lung tissues following influenza infection was regulated by MJWQH. Thus, the efficacy of MJWQH is likely due to its ability to inhibit excessive innate immune response and immune-mediated pulmonary tissue injury.

TLRs are key receptors in innate immune recognition and play an important role in the initiation of acquired immune
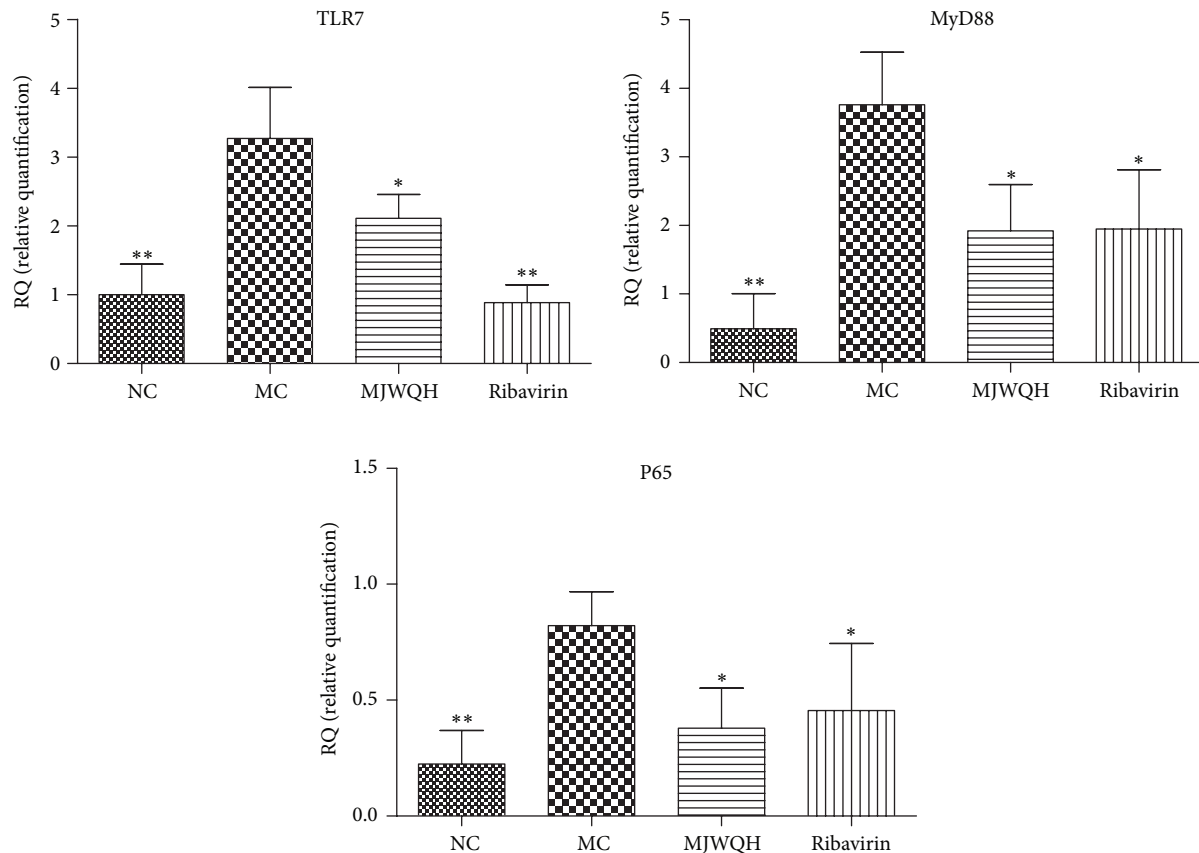
FIGURE 8: MJWQH inhibited the NF-κB signaling pathway. BALB/c mice (n = 6 mice/group) were treated as described in Figure 2 and killed on day 4 after infection. Lungs were processed for total RNA and subjected to real-time PCR for detection of TLR7, MyD88, and NF-κB p65 gene expressions, using GAPDH as a housekeeping gene. Data were presented as mean ± SD. $^*P < 0.05$; $^{**}P < 0.01$ versus the MC group.

response [45]. TLR7 has been demonstrated to be an intracellular receptor that recognizes ssRNA after the ribonucleoprotein complex has been degraded inside acidified endosomes [46, 47] and triggers cytokine secretion through the adapter MyD88, which recruits signaling mediators that activate NF-κB [48]. NF-κB could regulate the gene transcription of growth factors, transcription factors, cytokines, chemokines, and interferons [49]. Recognition and rapid clearance of pathogens by the innate immune system provide the first line of defense against infection. Overexpression of cytokines and chemokines induced by influenza virus infection is dependent on NF-κB signaling pathway. It has been well documented that inhibition of NF-κB or proteasome leads to IκB accumulation and inhibits influenza virus replication *in vitro* and *in vivo* [50–52]. The signaling cascade of all activated TLRs starts with the activation of MyD88, which activates TRAF6 and eventually leads to the activation of NF-κB [53]. MyD88 is a crucial adaptor protein downstream of TLRs, whereas TRAF6 is a signal transducer in the NF-κB pathway, both of which are essential for the production of inflammatory cytokines [54–56]. IKK stimulates NF-κB activity by causing phosphorylation and degradation of IκB proteins, the cytoplasmic inhibitors of NF-κB [57]. Activated IKK promotes the dissociation of the cytosolic inactive NF-κB-IκB complexes via the serine phosphorylation and

degradation of IκB, leading to NF-κB translocation to the nucleus and transcriptional upregulation of inflammatory genes [58]. The inhibitory effect of MJWQH on the NF-κB signaling pathway could be associated with the inhibition of IKK activation. We found that IκB and p65 levels were not affected on day 2 after infection; but p65 and p-p65 expressions were significantly increased on day 4 after infection. The real time-PCR and immunohistochemistry analysis revealed similar results. Therefore, it can be concluded that MJWQH modulates the immune response by inhibiting the TLR7-MyD88-dependent NF-κB signaling pathway. The antiviral effects of MJWQH might relate to the inhibition of TLR7/MyD88/TRAF6/IKKα/β NF-κB signaling pathway. However, as MJWQH contains numerous compounds with various pharmacological activities, it is not clear which compounds are responsible for the immune regulation. This underscores the need to further determine whether MJWQH directly blocks the combination of virus and TLR7 and what the active components are and how they work.

Taken together, the present study showed that early MJWQH treatment contributed to recovery from severe pneumonia due to its anti-inflammatory activity through regulating TLR7/MyD88/NF-κB signaling pathway. The results presented in this study may provide compelling evidence for the therapeutic potential of MJWQH as an alternative therapy
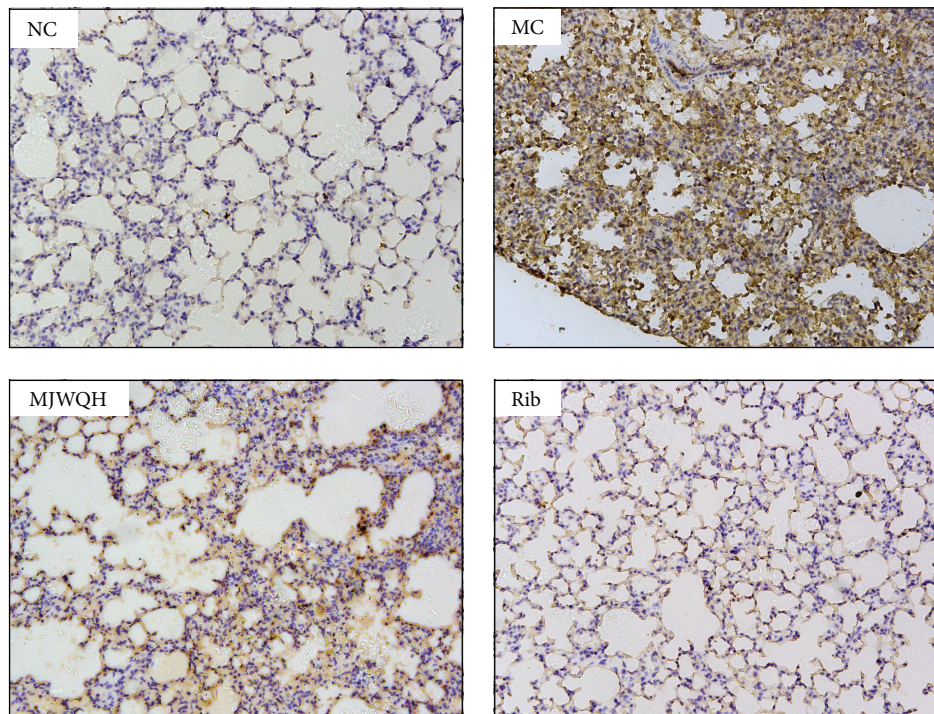
FIGURE 9: MJWQH inhibited the NF-κB expression in lung tissue ($\times$200). BALB/c mice ($n = 6$ mice/group) were treated as described in Figure 2 and killed on day 4 after infection. Lung sections were stained with rabbit anti-p65 (brown) and counterstained with hematoxylin.

to the western medicine in the treatment of influenza virus infections.

Abbreviations

BALF: Bronchoalveolar lavage fluid
IFN: Interferon
IL: Interleukin
TNF: Tumor necrosis factor
MCP-1: Macrophage chemotactic protein-1
RANTES: Regulated upon activation normal T cell expressed and presumably secreted
MIP-1:   Macrophage inflammatory protein-1
IP-10:   IFN-γ-inducible protein-10
NF-κB: Nuclear factor kappa-light-chain-enhancer of activated B cells
TLR: Toll-like receptor
MyD88: Myeloid differentiation factor 88
TRAF6: Tumor necrosis factor receptor-associated factor 6
IκB: Inhibitor of NF-κB
IKK: IκB kinase.

Conflict of Interests

The authors declare that there is no conflict of interests regarding the publication of this paper.

References

[1] J. K. Louie, M. Acosta, K. Winter et al., "Factors associated with death or hospitalization due to pandemic 2009 influenza A(H1N1) infection in California," *The Journal of the American Medical Association*, vol. 302, no. 17, pp. 1896–1902, 2009.

[2] K. A. Shirey, W. Lai, A. J. Scott et al., "The TLR4 antagonist Eritoran protects mice from lethal influenza infection," *Nature*, vol. 497, no. 7450, pp. 498–502, 2013.

[3] D. Wang, Y. Hu, J. Sun, X. Kong, B. Zhang, and J. Liu, "Comparative study on adjuvanticity of compound Chinese herbal medicinal ingredients," *Vaccine*, vol. 23, no. 28, pp. 3704–3708, 2005.

[4] C.-C. Yeh, C.-C. Lin, S.-D. Wang et al., "Protective and immunomodulatory effect of Gingyo-san in a murine model of acute lung inflammation," *Journal of Ethnopharmacology*, vol. 111, no. 2, pp. 418–426, 2007.

[5] C.-H. Hsu, K.-C. Hwang, C.-L. Chao et al., "An evaluation of the additive effect of natural herbal medicine on SARS or SARS-like infectious diseases in 2003: a randomized, double-blind, and controlled pilot study," *Evidence-Based Complementary and Alternative Medicine*, vol. 5, no. 3, pp. 355–362, 2008.

[6] W. Chen, C. E. D. Lim, H.-J. Kang, and J. Liu, "Chinese herbal medicines for the treatment of type A H1N1 influenza: a

systematic review of randomized controlled trials," *PLoS ONE*, vol. 6, no. 12, Article ID e28093, 2011.

[7] N. L. la Gruta, K. Kedzierska, J. Stambas, and P. C. Doherty, "A question of self-preservation: immunopathology in influenza virus infection," *Immunology and Cell Biology*, vol. 85, no. 2, pp. 85–92, 2007.

[8] D. Kobasa, S. M. Jones, K. Shinya et al., "Aberrant innate immune response in lethal infection of macaques with the 1918 influenza virus," *Nature*, vol. 445, no. 7125, pp. 319–323, 2007.

[9] D. M. Tscherne and A. García-Sastre, "Virulence determinants of pandemic influenza viruses," *The Journal of Clinical Investigation*, vol. 121, no. 1, pp. 6–13, 2011.

[10] T.-N. Nguyen-Pham, M.-S. Lim, T. A. T. Nguyen et al., "Type I and II interferons enhance dendritic cell maturation and migration capacity by regulating CD38 and CD74 that have synergistic effects with TLR agonists," *Cellular & Molecular Immunology*, vol. 8, no. 4, pp. 341–347, 2011.

[11] Y. S. Bae, J. H. Lee, S. H. Choi et al., "Macrophages generate reactive oxygen species in response to minimally oxidized low-density lipoprotein: toll-like receptor 4- and spleen tyrosine kinase-dependent activation of NADPH oxidase 2," *Circulation Research*, vol. 104, no. 2, pp. 210–218, 2009.

[12] T. Hirayama, Y. Tamaki, Y. Takakubo et al., "Toll-like receptors and their adaptors are regulated in macrophages after phagocytosis of lipopolysaccharide-coated titanium particles," *Journal of Orthopaedic Research*, vol. 29, no. 7, pp. 984–992, 2011.

[13] A. A. I. Fooladi, S. F. Mousavi, S. Seghatoleslami, S. Yazdani, and M. R. Nourani, "Toll-like receptors: role in inflammation and commensal bacteria," *Inflammation & Allergy-Drug Targets*, vol. 10, no. 3, pp. 198–207, 2011.

[14] K. Takeda and S. Akira, "Toll-like receptors in innate immunity," *International Immunology*, vol. 17, no. 1, pp. 1–14, 2005.

[15] S. Akira and K. Takeda, "Toll-like receptor signalling," *Nature Reviews Immunology*, vol. 4, no. 7, pp. 499–511, 2004.

[16] W. Barchet, A. Krug, M. Cella et al., "Dendritic cells respond to influenza virus through TLR7- and PKR-independent pathways," *European Journal of Immunology*, vol. 35, no. 1, pp. 236–242, 2005.

[17] L. Chen, J. Fan, Y. Li et al., "Modified Jiu Wei Qiang Huo decoction improves dysfunctional metabolomics in influenza A pneumonia-infected mice," *Biomedical Chromatography*, vol. 28, no. 4, pp. 468–474, 2014.

[18] M.-H. Ji, G.-M. Li, M. Jia et al., "Valproic acid attenuates lipopolysaccharide-induced acute lung injury in mice," *Inflammation*, vol. 36, no. 6, pp. 1453–1459, 2013.

[19] C. Cillóniz, K. Shinya, X. Peng et al., "Lethal influenza virus infection in macaques is associated with early dysregulation of inflammatory related genes," *PLoS Pathogens*, vol. 5, no. 10, 2009.

[20] Y. P. Tseng, Y. C. Wu, Y. L. Leu, S. F. Yeh, and C. K. Chou, "*Scutellariae radix* suppresses hepatitis B virus production in human hepatoma cells," *Frontiers in Bioscience*, vol. 2, no. 4, pp. 1538–1547, 2010.

[21] J. Dou, L. Chen, G. Xu et al., "Effects of baicalein on Sendai virus in vivo are linked to serum baicalin and its inhibition of hemagglutinin-neuraminidase," *Archives of Virology*, vol. 156, no. 5, pp. 793–801, 2011.

[22] Q. Zhang, B. Yang, N. Wang, L. Duan, S. He, and J. Sun, "Effect of total flavonoids of *Scutellaria baicalensis* Georgi on expression of influenza A virus nucleoprotein in HeLa cells," *Nan Fang Yi Ke Da Xue Xue Bao*, vol. 32, no. 7, pp. 966–969, 2012.

[23] X.-W. Yang, Z.-M. Gu, B.-X. Wang, M. Hattori, and T. Namba, "Comparison of anti-lipid peroxidative effects of the underground parts of *Notopterygium incisum* and N. forbesii in mice," *Planta Medica*, vol. 57, no. 5, pp. 399–402, 1991.

[24] M. Zheng, "Experimental study of 472 herbs with antiviral action against the herpes simplex virus," *Chinese Journal of Modern Developments in Traditional Medicine*, vol. 10, no. 1, pp. 39–41, 1990.

[25] G. Ye, Y.-H. Tang, G.-X. Xia, Z.-L. Sun, Z.-X. Li, and C.-G. Huang, "Characterization of anti-Coxsackie virus B3 constituents of Radix Astragali by high-performance liquid chromatography coupled with electrospray ionization tandem mass spectrometry," *Biomedical Chromatography*, vol. 24, no. 11, pp. 1147–1151, 2010.

[26] S. Wang, J. Li, H. Huang et al., "Anti-hepatitis B virus activities of astragaloside IV isolated from *Radix Astragali*," *Biological and Pharmaceutical Bulletin*, vol. 32, no. 1, pp. 132–135, 2009.

[27] Z. Q. Zhang, Y. J. Tian, and J. Zhang, "Studies on the antioxidative activity of polysaccharides from radix Saposhnikoviae," *Zhong Yao Cai*, vol. 31, no. 2, pp. 268–272, 2008.

[28] N. Inagaki, Y. Komatsu, H. Sasaki et al., "Acidic polysaccharides from rhizomes of Atractylodes lancea as protective principle in *Candida*-infected mice," *Planta Medica*, vol. 67, no. 5, pp. 428–431, 2001.

[29] K. Taguchi, Y. Hagiwara, K. Kajiyama, and Y. Suzuki, "Pharmacological studies of Houttuyniae Herba: the anti-inflammatory effect of quercitrin," *Yakugaku Zasshi*, vol. 113, no. 4, pp. 327–333, 1993.

[30] S. Li, R. Wang, Y. Zhang et al., "Symptom combinations associated with outcome and therapeutic effects in a cohort of cases with SARS," *American Journal of Chinese Medicine*, vol. 34, no. 6, pp. 937–947, 2006.

[31] J.-H. Wang, H.-L. Nie, S.-C. Tam, H. Huang, and Y.-T. Zheng, "Anti-HIV-1 property of trichosanthin correlates with its ribosome inactivating activity," *FEBS Letters*, vol. 531, no. 2, pp. 295–298, 2002.

[32] J.-H. Wang, H.-L. Nie, H. Huang, S.-C. Tam, and Y.-T. Zheng, "Independency of anti-HIV-1 activity from ribosome-inactivating activity of trichosanthin," *Biochemical and Biophysical Research Communications*, vol. 302, no. 1, pp. 89–94, 2003.

[33] L. Xu, L. Bao, F. Li et al., "Adaption of seasonal H1N1 influenza virus in mice," *PLoS ONE*, vol. 6, no. 12, Article ID e28901, 2011.

[34] C. L. Speyer and P. A. Ward, "Role of endothelial chemokines and their receptors during inflammation," *Journal of Investigative Surgery*, vol. 24, no. 1, pp. 18–27, 2011.

[35] R. V. D'elia, K. Harrison, P. C. Oyston, R. A. Lukaszewski, and G. C. Clark, "Targeting the "cytokine storm" for therapeutic benefit," *Clinical and Vaccine Immunology*, vol. 20, no. 3, pp. 319–327, 2013.

[36] S. Matsukura, F. Kokubu, H. Kubo et al., "Expression of RANTES by normal airway epithelial cells after influenza virus A infection," *American Journal of Respiratory Cell and Molecular Biology*, vol. 18, no. 2, pp. 255–264, 1998.

[37] F. G. Hayden, R. S. Fritz, M. C. Lobo, W. G. Alvord, W. Strober, and S. E. Straus, "Local and systemic cytokine responses during experimental human influenza A virus infection. Relation to symptom formation and host defense," *The Journal of Clinical Investigation*, vol. 101, no. 3, pp. 643–649, 1998.

[38] L. Kaiser, R. S. Fritz, S. E. Straus, L. Gubareva, and F. G. Hayden, "Symptom pathogenesis during acute influenza: interleukin-6 and other cytokine responses," *Journal of Medical Virology*, vol. 64, no. 3, pp. 262–268, 2001.

[39] J. Sirén, T. Sareneva, J. Pirhonen et al., "Cytokine and contact-dependent activation of natural killer cells by influenza A or Sendai virus-infected macrophages," *Journal of General Virology*, vol. 85, no. 8, pp. 2357–2364, 2004.

[40] C. L. Galligan, T. T. Murooka, R. Rahbar, E. Baig, B. Majchrzak-Kita, and E. N. Fish, "Interferons and viruses: signaling for supremacy," *Immunologic Research*, vol. 35, no. 1-2, pp. 27–40, 2006.

[41] A. Billiau, H. Heremans, K. Vermiere, and P. Matthys, "Immunomodulatory properties of interferon-γ. An update," *Annals of the New York Academy of Sciences*, vol. 856, pp. 22–32, 1998.

[42] J. R. Teijaro, K. B. Walsh, S. Cahalan et al., "Endothelial cells are central orchestrators of cytokine amplification during influenza virus infection," *Cell*, vol. 146, no. 6, pp. 980–991, 2011.

[43] H. Sprenger, R. G. Meyer, A. Kaufmann, D. Bussfeld, E. Rischkowsky, and D. Gemsa, "Selective induction of monocyte and not neutrophil-attracting chemokines after influenza A virus infection," *Journal of Experimental Medicine*, vol. 184, no. 3, pp. 1191–1196, 1996.

[44] V. A. Arankalle, K. S. Lole, R. P. Arya et al., "Role of host immune response and viral load in the differential outcome of pandemic H1N1 (2009) influenza virus infection in indian patients," *PLoS ONE*, vol. 5, no. 10, Article ID e13099, 2010.

[45] H. Hemmi, T. Kaisho, O. Takeuchi et al., "Small-antiviral compounds activate immune cells via the TLR7 MyD88-dependent signaling pathway," *Nature Immunology*, vol. 3, no. 2, pp. 196–200, 2002.

[46] J. M. Lund, L. Alexopoulou, A. Sato et al., "Recognition of single-stranded RNA viruses by Toll-like receptor 7," *Proceedings of the National Academy of Sciences of the United States of America*, vol. 101, no. 15, pp. 5598–5603, 2004.

[47] S. S. Diebold, T. Kaisho, H. Hemmi, S. Akira, and C. R. e Sousa, "Innate antiviral responses by means of TLR7-mediated recognition of single-stranded RNA," *Science*, vol. 303, no. 5663, pp. 1529–1531, 2004.

[48] K. Takeda and S. Akira, "TLR signaling pathways," *Seminars in Immunology*, vol. 16, no. 1, pp. 3–9, 2004.

[49] H. L. Pahl, "Activators and target genes of Rel/NF-κB transcription factors," *Oncogene*, vol. 18, no. 49, pp. 6853–6866, 1999.

[50] S. E. Dudek, C. Luig, E.-K. Pauli, U. Schubert, and S. Ludwig, "The clinically approved proteasome inhibitor PS-341 efficiently blocks influenza A virus and vesicular stomatitis virus propagation by establishing an antiviral state," *Journal of Virology*, vol. 84, no. 18, pp. 9439–9451, 2010.

[51] E. Haasbach, E.-K. Pauli, R. Spranger et al., "Antiviral activity of the proteasome inhibitor VL-01 against influenza A viruses," *Antiviral Research*, vol. 91, no. 3, pp. 304–313, 2011.

[52] I. Mazur, W. J. Wurzer, C. Ehrhardt et al., "Acetylsalicylic acid (ASA) blocks influenza virus propagation via its NF-κB-inhibiting activity," *Cellular Microbiology*, vol. 9, no. 7, pp. 1683–1694, 2007.

[53] C. E. van der Sandt, J. H. C. M. Kreijtz, and G. F. Rimmelzwaan, "Evasion of influenza A viruses from innate and adaptive immune responses," *Viruses*, vol. 4, no. 9, pp. 1438–1476, 2012.

[54] Z. Cao, J. Xiong, M. Takeuchi, T. Kurama, and D. V. Goeddel, "TRAF6 is a signal transducer for interleukin-1," *Nature*, vol. 383, no. 6599, pp. 443–446, 1996.

[55] E. Kopp and R. Medzhitov, "Recognition of microbial infection by Toll-like receptors," *Current Opinion in Immunology*, vol. 15, no. 4, pp. 396–401, 2003.

[56] S. Akira and S. Sato, "Toll-like receptors and their signaling mechanisms," *Scandinavian Journal of Infectious Diseases*, vol. 35, no. 9, pp. 555–562, 2003.

[57] E. Zandi, D. M. Rothwarf, M. Delhase, M. Hayakawa, and M. Karin, "The IκB kinase complex (IKK) contains two kinase subunits, IKKα and IKKβ, necessary for Iκb phosphorylation and NF-κB activation," *Cell*, vol. 91, no. 2, pp. 243–252, 1997.

[58] S. S. Makarov, "NF-KB in rheumatoid arthritis: a pivotal regulator of inflammation, hyperplasia, and tissue destruction," *Arthritis Research*, vol. 3, no. 4, pp. 200–206, 2001.

Research Article

Determination of Oleanolic and Ursolic Acids in *Hedyotis diffusa* Using Hyphenated Ultrasound-Assisted Supercritical Carbon Dioxide Extraction and Chromatography

Ming-Chi Wei,[1] Yu-Chiao Yang,[2] and Show-Jen Hong[2]

[1]*Department of Environmental Engineering & Science, Chia Nan University of Pharmacy and Science, Tainan 71710, Taiwan*
[2]*Department and Graduate Institute of Pharmacology, Kaohsiung Medical University, Kaohsiung 80708, Taiwan*

Correspondence should be addressed to Yu-Chiao Yang; ycyang230@gmail.com

Oleanolic acid (OA) and ursolic acid (UA) were extracted from *Hedyotis diffusa* using a hyphenated procedure of ultrasound-assisted and supercritical carbon dioxide (HSC–CO_2) extraction at different temperatures, pressures, cosolvent percentages, and SC–CO_2 flow rates. The results indicated that these parameters significantly affected the extraction yield. The maximal yields of OA (0.917 mg/g of dry plant) and UA (3.540 mg/g of dry plant) were obtained at a dynamic extraction time of 110 min, a static extraction time of 15 min, 28.2 MPa, and 56°C with a 12.5% (v/v) cosolvent (ethanol/water = 82/18, v/v) and SC–CO_2 flowing at 2.3 mL/min (STP). The extracted yields were then analyzed by high performance liquid chromatography (HPLC) to quantify the OA and UA. The present findings revealed that *H. diffusa* is a potential source of OA and UA. In addition, using the hyphenated procedure for extraction is a promising and alternative process for recovering OA and UA from *H. diffusa* at high concentrations.

1. Introduction

Historically, herbal medicines derived from plant extracts have been used to treat human diseases or maintain health. In recent years, plant research has received increasing amounts of attention worldwide; numerous studies describing the therapeutic properties of extracts from the plants used in traditional medicine have been developed, revealing the immense potential of medicinal plants. *Hedyotis diffusa* Willd, which belongs to the family Rubiaceae, is locally known as "Peh-Hue-Juwa-Chi-Cao" and is commonly known as Chinese tea [1, 2]. In traditional Chinese medicine, this plant is used extensively to treat hepatitis, tonsillitis, sore throat, appendicitis, urethral infection, and malignant tumors in the liver, lung, and stomach [3–7]. Recently, this herb has gained increasing amounts of attention regarding its usage as an antitumor herb in the liver, lungs, colon, brain, and pancreas [3, 4, 8, 9]. Ursolic acid (UA) and oleanolic acid (OA) are bioactive compounds that have been isolated from this herb and might be responsible for its therapeutic effectiveness. Both OA and UA have many important

pharmacological activities including anticancer, chemopreventive, hepatoprotective, antiviral, antibacterial, antidiabetic, antioxidant, anti-inflammatory, and gastroprotective effects; these compounds display similar activities because their chemical structures are similar. Furthermore, OA and UA have a wide variety of antitumor activities, inhibiting hepatocellular carcinoma, prostate carcinoma, colorectal cancer, acute myelogenous leukemia, skin tumorigenesis, cervical carcinoma, and lung carcinoma [10]. These findings have made UA and OA attractive dietary supplements in the expanding health food market. Therefore, finding an effective and optimal method for isolating UA and OA from *H. diffusa* has become highly important.

Because plant extracts are composed of a complex mixture of phytochemical constituents that can cause interference within a sample and that can contain compounds similar to the bioactive analytes of interest, a strong matrix effect is often observed. Furthermore, the simultaneous quantification of OA and UA in plant extracts is difficult due to their structural similarities [11]. Therefore, selecting an effective chromatographic method for determining the target

compounds is a key for the qualitative and quantitative analysis of the chemical constituents present in medical plants. Some studies have found that HPLC is the most convenient and comprehensive technique for separating triterpenic acids in plant extracts [12]. One goal of this work was to apply the HPLC method to determine the OA and UA contents of *H. diffusa*.

Traditionally, target compounds could be procured from herbs using organic solvent extraction along with maceration, heat-flux, and Soxhlet extraction techniques. However, a low selectivity or extraction yield, in addition to the long extraction times, toxic solvent residues, and degradation of temperature-sensitive compounds, may occur when using these techniques [12]. These issues are important for food, cosmetic, and medicinal extracts. Supercritical carbon dioxide (SC–CO$_2$) extraction technology may be a viable alternative for solvent extraction methods. SC–CO$_2$ is pushed beyond its critical point (7.38 MPa and 31.1°C) and has been recognized as an ideal extraction solvent. The most important advantages of this novel extraction method include the safe extraction of thermally labile compounds, shortened extraction times, the tunable selectivity, and solvent removal from the extracted materials [13, 14]. The extraction of OA and UA from various raw materials using SC–CO$_2$ had been studied by Domingues et al. [15], Patinha et al. [16], and Yang et al. [10]. Furthermore, SC–CO$_2$ was recently used as an attractive alternative extraction method for conventional liquid extraction in numerous areas including the food, pharmaceutical, and environmental engineering industries [17, 18].

Despite the above-mentioned advantages of SC–CO$_2$ extraction, high-pressure equipment exhibits serious drawbacks when compared to traditional atmospheric pressure extraction techniques. Owing to its high pressure operating conditions, SC–CO$_2$ extraction method is not only a high capital investment, but also a mechanical stirring difficult to be applied, resulting in a decrease in extraction kinetics. This limitation is often overcome by proper pretreatment of the sample, such as sonication to the entrainer prior to the extraction. Therefore, the use of combinatory and hyphenated SC–CO$_2$ with other techniques can achieve good extraction efficiency with required selectivity in the same or shorter duration using milder conditions than that of solely SC–CO$_2$ extraction. Recently, several studies investigating the combination application of SC–CO$_2$ extraction and ultrasound-assisted extraction of target compounds from raw matrices have been published [14]. In this study, a hyphenated process (HSC–CO$_2$) consisting of ultrasound-assisted static stage, followed by SC–CO$_2$ dynamic extraction (without ultrasound), was used for the simultaneous separation of OA and UA from *H. diffusa*. In addition, the effects of the HSC–CO$_2$ extraction parameters such as the pressure, temperature, cosolvent percentage, SC–CO$_2$ flow rate, and dynamic extraction time were evaluated to obtain the highest extraction yield, and the precision of the method was examined. The analyses of the extracts were performed using high performance liquid chromatography (HPLC) with ultraviolet/visible (UV/vis) multiwavelength detection. The results were compared with those obtained using conventional extraction techniques. The aim of this study was to develop a simpler and more environmentally friendly technique with high efficiency, low toxicity, and high selectivity for natural products.

2. Materials and Methods

2.1. Plant Materials. The dried whole-plant materials from *H. diffusa* (samples HD1 to HD3) were kindly provided by Chuang Song Zong Pharmaceutical Co. Ltd. (Kaohsiung, Taiwan). The air-dried whole plants were pulverized in a knife mill, and the plant particles were sieved to produce samples with sizes of 0.925, 0.725, 0.550, 0.355, and 0.210 mm (mean diameter). These fractions were subsequently packed in plastic bags and stored at 4°C for later use. The moisture contents (% of dry weight basis) were determined by drying at 105°C to a constant mass and were 11.32%, 10.41%, and 11.25%. All of the yields and compositions were calculated based on moisture-free conditions and represent the mean values of at least six experiments.

2.2. Chemicals and Reagents. Both OA and UA were purchased as HPLC reference standards from Sigma Chemical Co. (St. Louis, MO, USA). The methanol, ethanol, acetone, acetonitrile, ethyl acetate, *n*-hexane, and 85% phosphoric acid were purchased from Merck Co. (Darmstadt, Germany). Carbon dioxide was purchased from Yun-Shan Gas Co. Ltd. (Tainan, Taiwan) and was used during the SC–CO$_2$ extraction.

2.3. Hyphenated Procedure of Ultrasound-Assisted and Supercritical Carbon Dioxide (HSC–CO$_2$) Extraction. As shown in Figure 1, the HSC–CO$_2$ extraction apparatus was a semicontinuous flow, high-pressure system. The major parts of the apparatus were a CO$_2$ cylinder, two syringe pumps (ISCO 260D; 100DX, Lincoln, NE, USA), and a controller (ISCO SFX 200, Lincoln, NE, USA). The herb sample (10.0 g) was thoroughly mixed with 2 mm stainless steel balls before being placed into the 43 mL extraction vessel. The extraction vessel was then immersed in an ultrasonic bath with a working frequency of 40 kHz and 185 W of power (Branson B-33810E-DTH, USA), which was controlled by an electrical heater (Thermo Haake, model DC10, USA) to within ±0.1°C, and the system was brought to the desired temperature. The extraction system was operated with a static period of 15 min (with ultrasound-assisted) under working conditions to allow contact between the samples and the supercritical solvent, which was followed by dynamic extraction for 20–160 min (without ultrasound-assisted). More details regarding the equipment and its operation can be found in a previous work [13]. To ensure the accuracy of the experimental data, this extraction process was repeated six times for each sample. The data are presented as the means ± standard deviation (SD).

2.4. Heat-Reflux Extraction. Heat-reflux extraction (HRE) was also investigated and compared to the HSC–CO$_2$ extraction process and has already been described in detail [19–21].
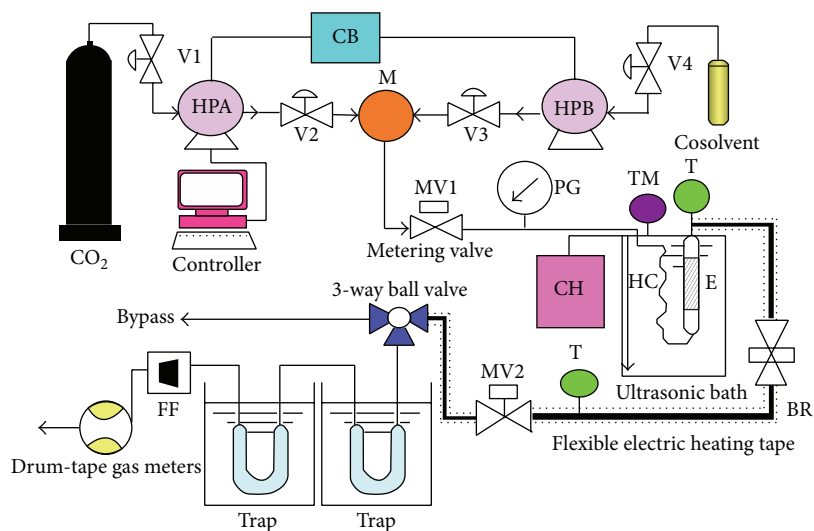
FIGURE 1: Schematic diagram of the HSC–CO$_2$ extraction apparatus. V1, V2, V3, and V4: stopping valve (on-off valve); HPA, HPB: syringe pump; M: mixer; CB: circulation bath; CH: circulating heater; MV1, MV2: micrometering valve; HC: heating coil; E: extraction vessel; PG: pressure gauge; BR: backpressure regulator; FF: float flowmeter T: thermocouple; and TM: mercury-in-glass thermometer.

2.5. HPLC Analysis. A double-beam U-300 UV/vis spectrophotometer (Hitachi, Japan) was originally used to determine the maximum absorbance wavelength for each analyte [12]. The HPLC analysis of OA and UA was carried out on a Jasco HPLC system (Jasco, Tokyo, Japan) with a LiChrospher C-18 analytical column (250 mm × 4 mm i.d., 5 μm particle size; Merck, Darmstadt, Germany). The mobile phase was composed of acetonitrile (solvent A) and water containing 0.1% phosphoric acid (solvent B) and was used under the following gradient conditions: 0–25 min at 22-23% (solvent A) and 1.0–1.5 mL/min, 25–40 min at 23% (solvent A) and 1.5–1.0 mL/min, and 40–60 min at 23–90% (solvent A) and 1.0 mL/min. The column was maintained at 40°C and the effluent was monitored at 210 nm with an intelligent UV/vis multiwavelength detector (Jasco MD-910, Jasco, Tokyo, Japan). The peaks for the target compounds within the extracts were identified based on the retention time and chromatographic behavior versus the authentic standards. The quantity of the target compounds was calculated by comparing their peak area to that of the standards.

2.6. Statistical Analysis. All of the yields and composition analyses were calculated on a moisture-free basis. The mean value and SD were calculated based on six experiments. The results are expressed as the means ± SD. An analysis of variance (ANOVA) was carried out using Tukey's method with a significance level of $P < 0.05$ using Microsoft Office Excel 2010 (Microsoft CO., USA) and Origin software version 6.1 (Origin Lab CO., Northampton, MA, USA).

3. Results and Discussion

3.1. Qualitative and Quantification Analysis of the Extracts by HPLC. The HPLC profiles are reported in Figure 2, which illustrates the separation of OA and UA. Figure 2(a) shows that the standard substances have retention times of 50.44 ±

0.06 min and 56.62 ± 0.08 min for OA and UA, respectively. The HPLC chromatograms of the *H. diffusa* extracts using HRE and HSC–CO$_2$ with aqueous ethanol as the cosolvent are also shown in Figures 2(b) and 2(c), respectively. Many other peaks appear in the HPLC chromatograms of the *H. diffusa* extracts. However, Figures 2(b) and 2(c) revealed that no interference peaks from the endogenous constituents of the HRE and HSC–CO$_2$ extracts were found in the region containing the investigated compounds; therefore, good separation could be obtained, and the OA and UA were assigned the retention times of 50.44 ± 0.06 min and 56.62 ± 0.08 min, respectively. The chromatographic peaks of OA and UA were confirmed by comparing their retention time and their spectral characteristics against those of the authentic standards. Furthermore, the contents of the analyzed compounds from the crude extracts of *H. diffusa* were quantitated based on the calibration curves for the standard compounds.

3.2. Heat-Flux Extraction. The type of solvent affects the extraction efficiency. First, to determine the effect of the solvent type on the yield of the studied compounds, two nonpolar solvents (chloroform and *n*-hexane) and two polar solvents (ethanol and water) under HRE were tested. The other parameters including the 60 min extraction time, temperature of 75°C, solvent-to-raw material ratio of 16 mL/g, mean particle size of 0.355 mm, and stirring rate of 300 rpm remained constant throughout the study. The solvents differ in polarity; therefore, they should alter the extraction performance. After comparing the tested extraction solvents, the highest amounts of target compounds were obtained when chloroform and ethanol were used; the two triterpenic acids are insoluble in water and in hexane (Table 1). The polarity of chloroform and ethanol relative to the discussed compounds explains these results. Additionally, due to the medium polarity OA and UA, the nonpolar hexane and polar water were not efficient for extraction. However, chloroform
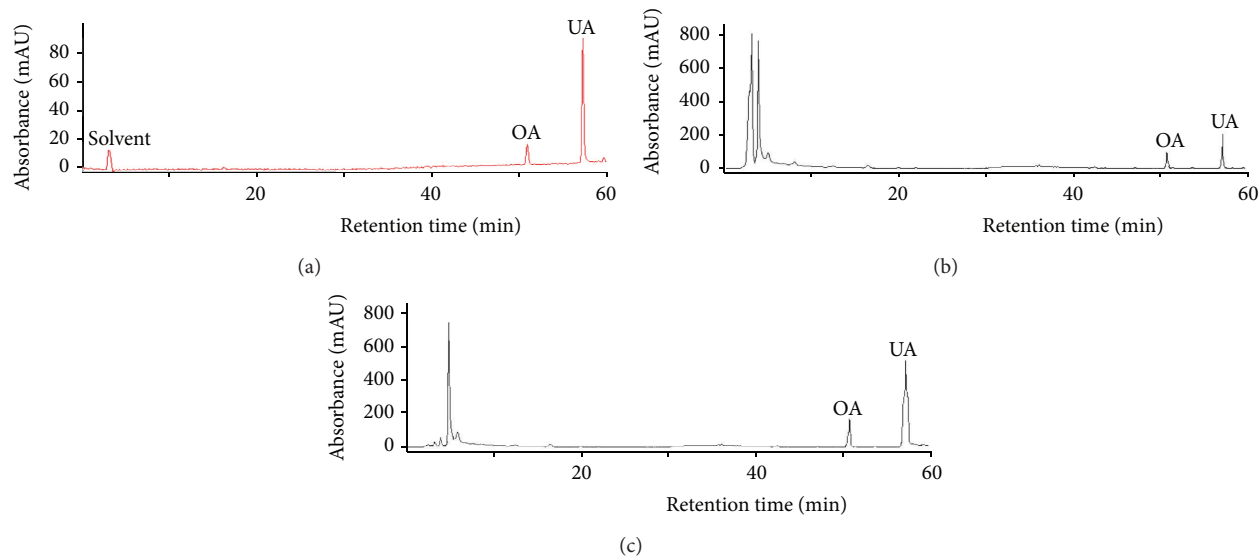
Figure 2: HPLC chromatograms of the standard solution (a), an extract obtained using HRE (b), and an extract obtained using HSC–CO$_2$ extraction (c).

Table 1: Yields of the investigated components obtained through the heat-reflux extraction (HRE) method with various solvents (one extraction cycle) and the pure SC–CO$_2$ extraction method.

Methods/solvents	Extraction yield (mg/g)[a]	
	OA	UA
HRE[b]		
Nonpolar		
Chloroform	0.582 ± 0.023	2.580 ± 0.105
n-Hexane	Not detected	Not detected
polar		
0% Ethanol (water)	Not detected	Not detected
10% Ethanol	Not detected	Not detected
20% Ethanol	Not detected	Not detected
30% Ethanol	Not detected	Not detected
40% Ethanol	Not detected	Not detected
50% Ethanol	Not detected	Not detected
60% Ethanol	0.544 ± 0.021	1.171 ± 0.045
70% Ethanol	0.661 ± 0.025	1.674 ± 0.060
80% Ethanol	0.650 ± 0.024	2.283 ± 0.082
90% Ethanol	0.629 ± 0.022	2.601 ± 0.093
95% Ethanol	0.623 ± 0.025	2.340 ± 0.092
99.5% Ethanol	0.599 ± 0.024	2.211 ± 0.081
Pure SC–CO$_2$[c]	Not detected	Not detected

[a]Values are mean ± SD of six replications and are calculated on plant dry weight basis (HD3).
[b]The experimental conditions are described in the experimental section.
[c]Pure SC–CO$_2$ conditions: extraction pressure at 10.4–30.0 MPa, extraction temperature at 40–70°C, a static extraction time of 30 min, a dynamic extraction time of 10–180 min, mean particle size at 0.096–0.925 mm, and CO$_2$ flow rate at 0.6–2.5 mL/min (STP).

is a toxic solvent; therefore, it is not suitable for use in the food, pharmaceutical, and cosmetic industries. However, the most commonly used extraction agent is ethanol due to its low toxicity, making it acceptable for practical use in the food, cosmetic, and pharmaceutical industries. Additionally, ethanol can be mixed with water in different ratios, and it was consequently chosen as the extraction solvent for the OA and UA from *H. diffusa*.

The influence of the aqueous ethanol concentration on the yields of OA and UA is shown in Table 1. The data indicate that 70% and 90% ethanol in water were the best solvent composition for extracting OA and UA selectively, respectively. Therefore, ethanol diluted with water increased the yield versus pure ethanol or water because the lower water content increased the swelling effect of the plant tissue matrix, decreased the viscosity of solvent, and improved the mass transport from the material, facilitating the extraction of the OA and UA. However, utilizing more than 50% water in aqueous ethanol increased the polarity of the mixed solvent beyond the point at which it was suitable for extracting OA and UA; therefore, the yield decreased. Similar outcomes were observed during the UAE of OA and UA from *Scutellaria barbata* D. Don [20], schisandrin B from *Schisandra chinensis* (Turcz.) Baill seeds [22], and cepharanthine from *Stephania rotunda* Lour [23].

3.3. Extraction with Carbon Dioxide. One of our objectives was to compare the HRE and SC–CO$_2$ extractions while using both nonpolar and polar solvents. During our study, pure SC–CO$_2$ was initially used to investigate the extraction of OA and UA from *H. diffusa*. To achieve the highest extraction efficiencies, several factors were investigated such as the extraction pressure (10.4–30.0 MPa), extraction temperature (40–70°C), static extraction time (10–30 min), dynamic extraction time (10–180 min), mean particle size (0.925–0.210 mm), and SC–CO$_2$ flow rate (0.6–2.5 mL/min (STP)). However, SC–CO$_2$ without a cosolvent was not selective for OA and UA, even under different extraction pressures and temperatures. OA and UA were not detected under any conditions analyzed
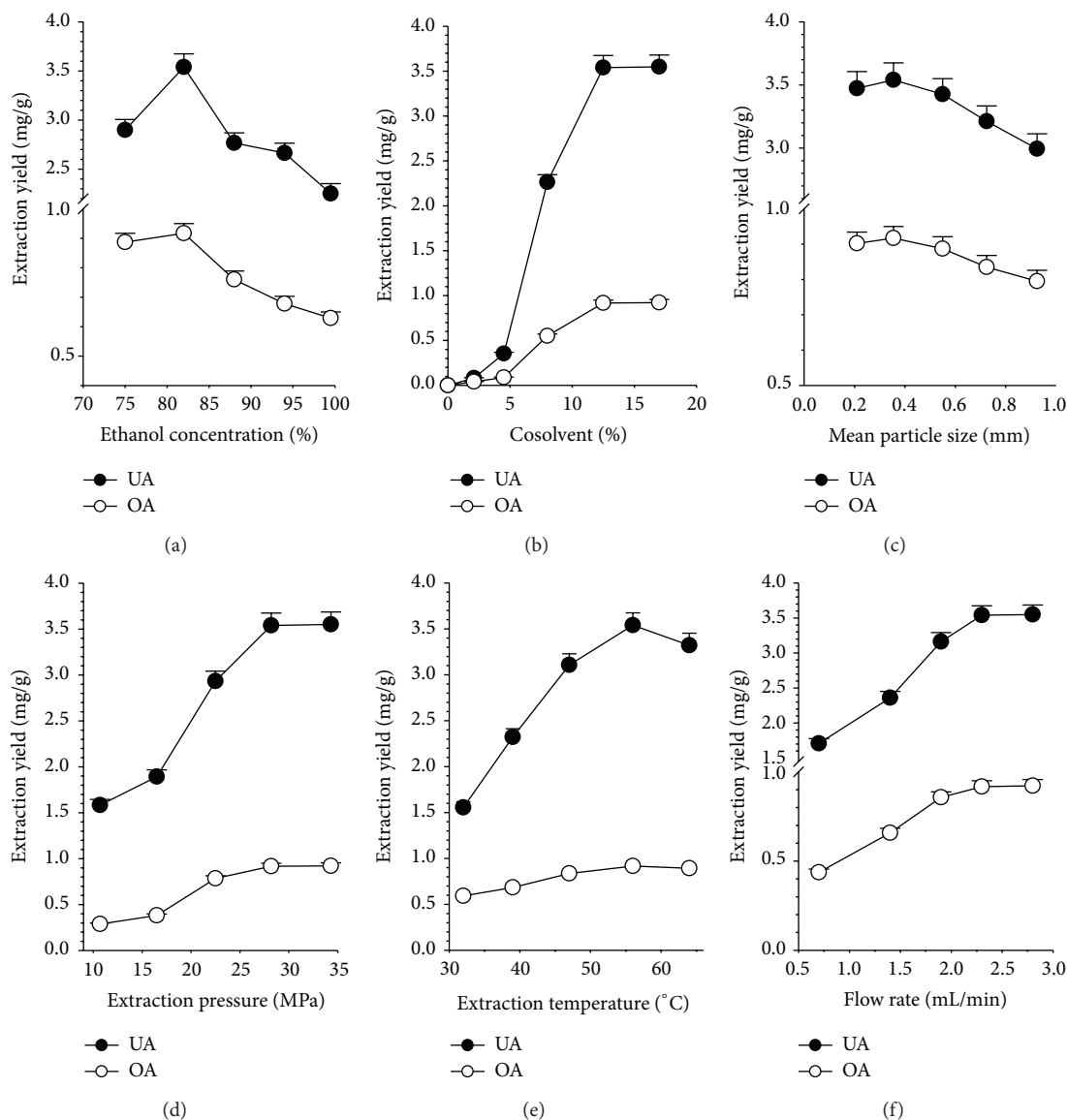
FIGURE 3: Effects of cosolvent contents (a), co-solvent percentage (b), mean particle size (c), extraction pressure (d), extraction temperature (e), and SC–CO$_2$ flow rate (f) on the extraction yields of OA and UA from *H. diffusa* using HSC–CO$_2$ extraction.

at different extraction pressures (10.4–30.0 MPa) and temperatures (40–70°C). The extraction using pure SC–CO$_2$ generated yields similar to those obtained when *n*-hexane was used as a solvent during HRE (Table 1).

3.4. Extraction with Carbon Dioxide: Aqueous Ethanol Mixtures. As mentioned above, OA and UA are polar compounds, rendering extractions using only SC–CO$_2$ ineffectively (Table 1). Consequently, a polar cosolvent should be used to enhance the selectivity and to increase the extraction efficiency for the selected components. Based on the preliminary experiments, adding a small amount of aqueous ethanol to the SC–CO$_2$ can significantly enhance the extraction efficiency and, consequently, increase the extraction yield. This method was used to improve the yields of OA and UA from *S. barbata* D. Don [10]. During this study, the

mean particle size, water content in the ethanol cosolvent, percent ratio of the cosolvent (aqueous ethanol) in the mixed fluid, and the extraction conditions including the SC–CO$_2$ flow rate, extraction time, temperature, and pressure are the significant variables when extracting OA and UA from *H. diffusa*.

3.4.1. Effect of the Cosolvent Contents. The effect of the water content of the ethanol cosolvent (water/ethanol = 0, 6/94, 12/88, 18/82, and 25/75, v/v) on the extraction yield was examined at a mean particle size of 0.355 mm, a temperature of 56°C, a pressure of 28.2 MPa, a static time of 15 min (with ultrasound-assisted), a dynamic time of 110 min, and a CO$_2$ flow rate of 2.3 mL/min while using 12.5% cosolvent (aqueous ethanol); the results are shown in Figure 3(a). Adding an aqueous ethanol cosolvent can greatly improve the extraction

efficiency due to the enhanced solubility of OA and UA after increasing the polarity of the $SC–CO_2$. Moreover, aqueous ethanol cosolvent accelerates the desorption process by reducing the interactions between the solutes and the sample matrix, competing with the solutes for active binding site and disrupting the matrix structure. As observed in Figure 3(a), the yield of OA and UA increased significantly when the water (v/v) content of the aqueous ethanol increased from 0 to 18% (v/v). After 110 min, a slight decrease was observed in the yield of the OA and UA when the water (v/v) content of the aqueous ethanol was 25% throughout the extraction period because the higher water content increases the polarity of the cosolvent, facilitating the extraction of OA and UA. Consequently, when the polarity of cosolvent is too high (25%), the capability for extracting the studied components will decrease. Similar results were also observed during $SC–CO_2$ extraction of OA and UA from *S. barbata* D. Don [10] and of flavonoids from hops (*Humulus lupulus* L.) [24]. Therefore, the best cosolvent composition for OA and UA extraction from *H. diffusa* was 82% ethanol.

3.4.2. Effect of Modifier (82% Aqueous Ethanol) Percentage. The major limitation of utilizing $SC–CO_2$ is its inability to dissolve polar analytes, even at very high densities. The most effective way to eliminate this limitation is to add a polar solvent to the $SC–CO_2$, increasing its polarity while decreasing the strength of the interaction between the analyte and the matrix; this method also efficiently displaces the polar analytes from the matrix. However, the percent ratio of the modifier in a mixed fluid ($SC–CO_2$ + modifier) is an important parameter. To test the effects of the modifier percentages on the extraction efficiency, the modifier (82% ethanol) content was explored while maintaining the following conditions: the mean particle size, dynamic time, CO_2 flow rate, pressure, and temperature of 0.355 mm, 110 min, 2.3 mL/min, 28.2 MPa, and 56°C, respectively. Various percent ratios of the modifier (82% ethanol) in a mixed fluid (4.5, 8.0, 12.5, and 17% (v/v)) were utilized during the HSC–CO_2 extraction of OA and UA from *H. diffusa*. Different extraction results could be expected when manipulating the ratios of the liquid cosolvent, and the effects of the cosolvent percentage on the extraction efficiency of OA and UA using HSC–CO_2 are shown in Figure 3(b). The amount of OA and UA extracted per gram of *H. diffusa* increases when increasing the cosolvent content to certain level (12.5%) before leveling off at higher percentages (17%). Similarly, Içen and Gürü reported that the yields significantly increased when increasing the ratio of alcohol/CO_2 to 5.2% but did not vary when increasing the ratio further during an extraction using ethanol with supercritical carbon dioxide for caffeine from tea stalk and fiber waste [25]. The various percentages of the cosolvent exhibited different effects when changing the polarity of the $SC–CO_2$; therefore, diverse effects were observed when enhancing the solubility of the polar analytes. The best extraction yield is obtained when the polarity of the mixed fluid ($SC–CO_2$ + cosolvent) and polar analytes are coincident. In this study, the results indicated that the best cosolvent (82% ethanol, v/v) percentage for extracting OA and UA was 12.5% (v/v). Moreover, adding 12.5% aqueous ethanol (82% ethanol, v/v) as the cosolvent increases the yields of OA and UA, indicating that the cosolvent percentage could affect the destruction of the cellular walls and improve the mass transfer from inside the cells. Therefore, 12.5% aqueous ethanol (82% ethanol, v/v) was the best cosolvent system because it produced higher yields of OA and UA.

3.4.3. Effect of the Mean Particle Size. The HSC–CO_2 extraction yields of OA and UA from *H. diffusa* samples with different particle sizes (0.925, 0.725, 0.550, 0.355, and ≤0.210 mm) at 56°C, 28.2 MPa, a static time of 15 min (with ultrasound-assisted), a dynamic time of 110 min, a CO_2 flow rate of 2.3 mL/min, and a cosolvent (82% ethanol, v/v) percentage of 12.5% are shown in Figure 3(c). As expected, the yields of the OA and UA increased significantly when the particle size of *H. diffusa* decreased from 0.925 to 0.355 mm. This increase occurred because the smaller particle size shortens the diffusion paths in solid matrix decreasing the intraparticle resistance toward diffusion while exposing more cells to the supercritical solvent; therefore, these extraction yields for the OA and UA were higher than those for the larger sample diameters. However, a slight decrease in the yields of the OA and UA was observed for the 0.210 mm particles throughout the extraction period because the small particles aggregated during extraction, causing the fluid to channel or short circuit. Moreover, the small particle size was implicated in the readsorption of extracted solutes onto the matrix surface, which may also be responsible for the effect of the particle sizes on the yield of OA and UA. Similar variations were also obtained during the UAE of antioxidants from pomegranate marc [26] and during the ultrasound-assisted SC–CO_2 extraction of oils from *Syzygium aromaticum* flower buds (clove) [14]. Therefore, the best mean particle size was 0.355 mm, which was adopted for the subsequent experiments.

3.4.4. Effect of the Extraction Pressure. The effects of the extraction pressure on the yields of OA and UA when the mean particle size was 0.355 mm, the temperature was 56°C, the static time was 15 min (with ultrasound-assisted), the dynamic time was 110 min, the CO_2 flow rate was 2.3 mL/min and the cosolvent (82% ethanol, v/v) percentage was 12.5% are shown in Figure 3(d). Notably, the yields of OA and UA increased when increasing the pressure from 10.7 to 28.2 MPa due to the increased density of SC–CO_2; modulating the density of the $SC–CO_2$ alters the solubility of the solute, enhancing the extraction efficiency. However, the yields of OA and UA plateaued when the pressure was raised from 28.2 to 34.3 MPa. The pressure can change the density, viscosity, and diffusion characteristics of the SC–CO_2. Theoretically, the higher the pressure, the larger the density of SC–CO_2; however the diffusivity of the fluid may decrease, lowering the extraction yield because the interaction between SC–CO_2 and solid matrix is decreased. Moreover, increasing the extraction pressure packs the solid matrix more tightly while decreasing the void fraction, further reducing the penetration of SC–CO_2 into the solid matrix and decreasing the extraction efficiency. Therefore, this study reveals the predominant effect of pressure on the amount of OA and UA extracted

by SC–CO_2; for pressures ranging from 10.7 to 28.2 MPa, increasing the density of SC–CO_2 is presumably the primary mechanism for increasing the yields of the triterpenic acids. However, the decreased effective diffusivity and mass transfer coefficient should affect the yields of OA and UA at 34.3 MPa more than the increased density. Similar results were reported by Içen and Gürü; their caffeine extraction yield increased considerably with increasing pressure up to 250 bar but did not vary significantly at higher pressures [25]. Similar findings were also obtained during the extraction of nobiletin and tangeretin from *Citrus depressa* Hayata [27]. However, using a higher pressure is not cost-effective due to the high operating costs and energy consumption. Therefore, a pressure of 28.2 MPa is appropriate for increasing the efficiency of the OA and UA extraction from *H. diffusa* in SC–CO_2.

3.4.5. Effect of the Extraction Temperature. To examine the effect of varying the temperature (32, 39, 47, 56, and 64°C), HSC–CO_2 extraction experiments were carried out at a pressure of 28.2 MPa, a static time of 15 min (with ultrasound-assisted), a dynamic time of 110 min, a CO_2 flow rate of 2.3 mL/min, and a cosolvent (82% ethanol, v/v) percentage of 12.5% while using sample HD3 with a mean particle size of 0.355 mm and a moisture content of 11.25%. As shown in Figure 3(e), when the temperature increases from 32 to 56°C, the yield of OA and UA increases from 0.592 to 0.917 mg/g dry plant and from 1.555 to 3.540 mg/g dry plant, respectively; if the extraction temperature is increased to 64°C, the yields decrease. Increasing the temperature at the given pressure decreases the density of the SC–CO_2 density, while the volatile properties of the analytes and the desorption of the substances from the matrix increase. Therefore, this study speculated that, from 32 to 56°C, the influence of the temperature on the yield is predominated by the solid vapor pressure and desorption effects more than the variations in the SC–CO_2 density; at temperatures above 56°C, the effects of the density predominate. These results agree with the SC–CO_2 extraction of Amaranth seed oil by Westerman et al. [28] and of andrographolide from *Andrographis paniculata* by Kumoro and Hasan [29]. Therefore, a lower extraction temperature (56°C) is recommendable to maximize the economy and yield of the process.

3.4.6. Effect of the SC–CO_2 Flow Rate. Another major parameter affecting the efficiency and overall economy of HSC–CO_2 extraction is the CO_2 flow rate. If the extractions in the experiments were performed at a constant temperature and pressure, a low CO_2 flow rate resulted in a longer residence time and vice versa. A critical analysis of the literature reveals that a longer residence time allows the SC–CO_2 to remain in the extraction vessel longer, allowing it to remain in contact with and diffuse through the pores of the raw materials while increasing the extraction yields [30]. SC–CO_2 flow rates too low to generate a sufficient amount of SC–CO_2 to extract the target compounds lower the extraction yields [31]. Increasing the CO_2 flow rate not only lowered the residence time but also increased the number of SC–CO_2 molecules in contact with the solute, increasing intermolecular interactions between

the SC–CO_2 and the solute and enhancing the dissolution of the solute. However, when the SC–CO_2 flow rate increased, it flows through the raw materials at high velocities instead of diffusing through the sample matrix, flowing around the raw materials through channels and consequently limiting the contact necessary for extracting the target compounds [30, 32]. Therefore, characterizing the kinetics and optimal CO_2 flow rates of the extraction process is critical to attain a complete extraction while accounting for the efficiency and cost of the extraction.

To minimize the extraction time and the related costs of the HSC–CO_2 extraction procedure, four flow rates (0.7, 1.4, 1.9, 2.3, and 2.8 mL/min (STP)) were carried out while assessing the yields of the OA and UA; these experiments were the same as those previously mentioned, except that the CO_2 flow rate was varied. Figure 3(f) reveals that when the flow rate was increased from 0.7 to 2.3 mL/min, the extraction rate of OA and UA increased but did not vary significantly above that range (2.8 mL/min). Similar phenomena were also reported for the extraction of nimbin from neem seeds using SC–CO_2 [33]. Therefore, 2.3 mL/min CO_2 value was selected as the flow rate for the following experiments.

3.4.7. Effect of the Extraction Time. To achieve high extraction efficiencies, a primary extraction step in static mode (with ultrasound-assisted for 15 min and without ultrasound-assisted for 25 min) was performed, allowing the SC–CO_2 to penetrate the matrix more thoroughly than in dynamic mode. This step was followed by a dynamic extraction to enhance the solubility of OA and UA in the SC–CO_2. Figure 4 shows the effects of the dynamic extraction time on the yields of OA and UA when the mean particle size was 0.355 mm, the temperature was 56°C, the pressure was 28.2 MPa, and the CO_2 flow rate was 2.3 mL/min while 12.5% cosolvent (82% ethanol, v/v) was used. The experimental results revealed that the dynamic time strongly affected the HSC–CO_2 extraction yields for OA and UA. Figure 4 shows that when the dynamic extraction time is increased from 20 to 110 min, the balance of the extraction shifted to favor the extraction of OA and UA. However, further increases in the dynamic extraction time (120–150 min) did not affect the yield of target compounds significantly; therefore, 110 min was selected for the extraction time. Özkal et al. [34] observed similar behavior during the supercritical extraction of hazelnut oil at 30–60 MPa and 40–60°C with 2 mL/min SC–CO_2.

The experimental conditions of conventional SC–CO_2 extraction were the same as those aforementioned HSC–CO_2 extraction except that the static extraction time of 25 min was without ultrasound-assisted. According to the result obtained (Figure 4), extraction yield was enhanced by increasing the dynamic extraction time (20–140 min). However, since the difference between the extraction yields obtained for 140 and 160 min was not significantly different, 140 min is a reasonable time to use for the conventional SC–CO_2 extraction. The results shown in Figure 4 indicate that HSC–CO_2 extraction time of 110 min was sufficient to obtain the maximum yield, while 140 min was required for conventional SC–CO_2 extraction to reach the maximum yield. Furthermore, HSC–CO_2 extraction significantly improved the extraction yield,

TABLE 2: Comparison of extraction yields and extraction conditions obtained by the HRE, SC–CO_2 and HSC–CO_2 methods.

Extraction parameters	Extraction mode		
	HRE	SC–CO_2	HSC–CO_2
Herbal sample	HD3	HD3	HD3
Mean particle size (mm)	0.355	0.355	0.355
Plant weight (g)	5	5	10
Stirring rate (rpm)	300	—	—
Static extraction time (min)	—	25	15
Ultrasonic frequency (kHz)	—	—	40
Duty cycle (%)	—	—	79
Dynamic time (min)	—	140	110
Extraction time (min)	60×4 (4 cycles)	165	125
Extraction temperature (°C)	75 (Boiling point)	56	56
Extraction pressure (MPa)	—	28.2	28.2
Liquid/solid ratio (mL/g)	16	64.4	50.6
CO_2 flow rate (mL/min)	—	2.3	2.3
Extraction cycles	4	—	—
Cosolvent (v/v%)	—	82% ethanol	82% ethanol
Percentage of cosolvent (82% ethanol) in SC–CO_2	—	12.5%	12.5%
OA:			
Yield (mg/g)[a]	0.762 ± 0.030	0.824 ± 0.032	0.917 ± 0.033
Ethanol (v/v%)[b]	70%	—	—
RSD (%)[c]	3.94	3.88	3.696
UA:			
Yield (mg/g)[a]	2.964 ± 0.094	3.175 ± 0.114	3.540 ± 0.135
Ethanol (v/v%)[b]	90%	—	—
RSD (%)[c]	3.17	3.59	3.825

[a]Values are written as the mean ± SD of six replications and are calculated based on plant dry weight basis.
[b]Ethanol concentration in water (v/v%).
[c]RSD (%) = (SD/mean) × 100.

compared to conventional SC–CO_2 extraction. Since swelling and hydration could be accelerated by ultrasonic in static stage, this results in a probable enlargement in the pores of the cell walls, leading to a better mass transfer of intracellular products into SC–CO_2. In addition, the rupture of cell walls by microjet may also cause an increased penetration rate of SC–CO_2 into tissue. Therefore, HSC–CO_2 extraction technique allowed the discussed compounds to dissolve in SC–CO_2 at a higher rate, thereby boosting yield in a relevant shorter time.

3.5. Comparison of the Different Extraction Methods. To evaluate the extraction efficiency of the HSC–CO_2, a HRE was also used to extract the OA and UA from *H. diffusa*. The extraction yields for the individual techniques are compared in Table 2. The two triterpenic acids are insoluble in water and nonpolar solvents such as hexane and pure SC–CO_2 but are freely soluble in alcoholic solvents. Furthermore, the HSC–CO_2 and HRE results revealed that the extraction conditions for OA were close to those of UA. This result is supported by the similarity of the chemical structures of OA and UA.

The best extraction conditions for HRE were as follows: 70% ethanol for OA or 90% ethanol for UA, a 1 : 16 ratio of material to liquid, a particle size of 0.355 mm, and an extraction time of 60 min at 75°C. Under the best HRE conditions, the yields of OA and UA were 0.762 ± 0.030 and 2.964 ± 0.094 mg/g (4 extraction cycles), respectively. Concurrently, the highest OA (0.917 mg/g dry plant) and UA yields (3.540 mg/g dry plant) of HSC–CO_2 extraction were obtained at 56°C, 28.2 MPa, 2.3 mL/min CO_2, a particle size of 0.355 mm, and a cosolvent (ethanol/water = 82/18, v/v) percentage of 12.5%. The yields of OA and UA from the HSC–CO_2 extraction were significantly higher than the yields from HRE. Compared to conventional HR, HSC–CO_2 extractions can also shorten the extraction time (125 versus 240 min), lower the extraction temperature (56°C versus 75°C), and decrease the amount of solvent consumed. These improvements might be very interesting for industrial processes because HSC–CO_2 extraction would improve both process rates and yields, consequently reducing the processing times and costs. Additionally, the HPLC results (Figure 2) revealed that the extracts obtained using HSC–CO_2 contained lower levels of impurities compared
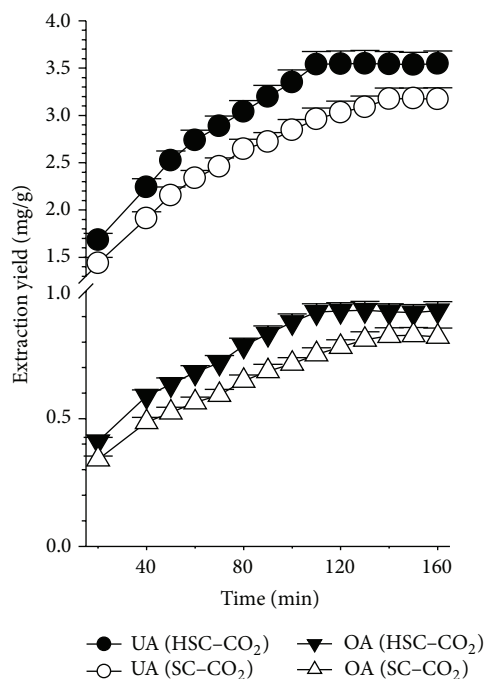
FIGURE 4: Effect of dynamic extraction time on the extraction yields of OA and UA from *H. diffusa* using HSC–CO$_2$ and SC–CO$_2$ extractions. Conditions: 0.355 mm, 56°C, 28.2 MPa, 2.3 mL/min, and 12.5% cosolvent (82% aqueous ethanol).

to the extracts obtained through the classical extraction procedure; therefore, SC–CO$_2$ extraction is more selective for OA and UA, generating better quality extracts. This improvement may be attributed to the fact that the lower HSC–CO$_2$ extraction temperature decreases the impurity contents while increasing the overall purity. This proposed behavior was supported by the increased extractability of OA and UA from the plants when using the HSC–CO$_2$ extraction process versus the classical extraction. Therefore, using HSC–CO$_2$ with aqueous ethanol as the cosolvent to extract OA and UA from *H. diffusa* was preferable and was considered the most environmentally friendly extraction method.

4. Conclusions

A hyphened ultrasound-assisted SC–CO$_2$ was used to extract OA and UA from *H. diffusa*. The extraction conditions were evaluated, and the yields of OA and UA reached 0.917 and 3.540 mg/g of dry material, respectively. The HSC–CO$_2$ extraction generated higher yields of OA and UA than the other conventional extraction methods while saving time and organic solvent. Furthermore, an HPLC analysis revealed that the purity of the OA and UA obtained from the current HSC–CO$_2$ extraction procedure was higher than that obtained from a conventional solid-liquid extraction. Therefore, food grades OA and UA can be obtained in high yields at a low cost. Therefore, HSC–CO$_2$ extraction with aqueous ethanol as a cosolvent might be a viable new approach for obtaining valuable components, such as OA and UA, from *H. diffusa*;

this process is also considered the most environmentally friendly extraction method.

References

[1] J. Zhao, J. W. Deng, Y. W. Chen, and S. P. Li, "Advanced phytochemical analysis of herbal tea in China," *Journal of Chromatography A*, vol. 1313, pp. 2–23, 2013.

[2] M. Li, Y.-L. Wonga, L.-L. Jiang et al., "Application of novel loop-mediated isothermal amplification (LAMP) for rapid authentication of the herbal tea ingredient *Hedyotis diffusa* Willd," *Food Chemistry*, vol. 141, no. 3, pp. 2522–2525, 2013.

[3] C. Li, X. Xue, D. Zhou et al., "Analysis of iridoid glucosides in *Hedyotis diffusa* by high-performance liquid chromatography/electrospray ionization tandem mass spectrometry," *Journal of Pharmaceutical and Biomedical Analysis*, vol. 48, no. 1, pp. 205–211, 2008.

[4] Z. Liu, M. Liu, and J. Li, "Methylanthraquinone from *Hedyotis diffusa* WILLD induces Ca^{2+}-mediated apoptosis in human breast cancer cells," *Toxicology in Vitro*, vol. 24, no. 1, pp. 142–147, 2010.

[5] G.-H. Xu, Y.-H. Kim, S.-W. Chi et al., "Evaluation of human neutrophil elastase inhibitory effect of iridoid glycosides from *Hedyotis diffusa*," *Bioorganic and Medicinal Chemistry Letters*, vol. 20, no. 2, pp. 513–515, 2010.

[6] Y. Zhang, Y. Chen, C. Fan, W. Ye, and J. Luo, "Two new iridoid glucosides from *Hedyotis diffusa*," *Fitoterapia*, vol. 81, no. 6, pp. 515–517, 2010.

[7] H. Y. Cheung, S. H. Cheung, M. L. Law, and W. P. Lai, "Simultaneous determination of key bioactive components in *Hedyotis diffusa* by capillary electrophoresis," *Journal of Chromatography B: Analytical Technologies in the Biomedical and Life Sciences*, vol. 834, no. 1-2, pp. 195–198, 2006.

[8] Y. Fang, Y. Zhang, M. Chen, H. Zheng, and K. Zhang, "The active component of *Hedyotis diffusa* Willd," *Chinese Tradition Plant Medicine*, vol. 26, pp. 577–579, 2004.

[9] S. Gupta, D. Zhang, J. Yi, and J. Shao, "Anticancer activities of *Oldenlandia diffusa*," *Journal of Herbal Pharmacotherapy*, vol. 4, no. 1, pp. 21–33, 2004.

[10] Y.-C. Yang, M.-C. Wei, S.-J. Hong, T.-C. Huang, and S.-Z. Lee, "Development/optimization of a green procedure with

ultrasound-assisted improved supercritical carbon dioxide to produce extracts enriched in oleanolic acid and ursolic acid from *Scutellaria barbata* D. Don," *Industrial Crops and Products*, vol. 49, pp. 542–553, 2013.

[11] B. Claude, P. Morin, M. Lafosse, and P. Andre, "Evaluation of apparent formation constants of pentacyclic triterpene acids complexes with derivatized β- and γ-cyclodextrins by reversed phase liquid chromatography," *Journal of Chromatography A*, vol. 1049, no. 1-2, pp. 37–42, 2004.

[12] M.-C. Wei and Y.-C. Yang, "Extraction characteristics and kinetic studies of oleanolic and ursolic acids from *Hedyotis diffusa* under ultrasound-assisted extraction conditions," *Separation and Purification Technology*, vol. 130, pp. 182–192, 2014.

[13] Y.-C. Yang, M.-C. Wei, T.-C. Huang, and S.-Z. Lee, "Extraction of protocatechuic acid from *Scutellaria barbata* D. Don using supercritical carbon dioxide," *Journal of Supercritical Fluids*, vol. 81, pp. 55–66, 2013.

[14] Y.-C. Yang, M.-C. Wei, and S.-J. Hong, "Ultrasound-assisted extraction and quantitation of oils from *Syzygium aromaticum* flower bud (clove) with supercritical carbon dioxide," *Journal of Chromatography A*, vol. 1323, pp. 18–27, 2014.

[15] R. M. A. Domingues, M. M. R. de Melo, E. L. G. Oliveira, C. P. Neto, A. J. D. Silvestre, and C. M. Silva, "Optimization of the supercritical fluid extraction of triterpenic acids from *Eucalyptus globulus* bark using experimental design," *Journal of Supercritical Fluids*, vol. 74, pp. 105–114, 2013.

[16] D. J. S. Patinha, R. M. A. Domingues, J. J. Villaverde et al., "Lipophilic extractives from the bark of *Eucalyptus grandis x* globulus, a rich source of methyl morolate: selective extraction with supercritical CO_2," *Industrial Crops and Products*, vol. 43, no. 1, pp. 340–348, 2013.

[17] K. W. Chan and M. Ismail, "Supercritical carbon dioxide fluid extraction of *Hibiscus cannabinus* L. seed oil: a potential solvent-free and high antioxidative edible oil," *Food Chemistry*, vol. 114, no. 3, pp. 970–975, 2009.

[18] Y.-C. Yang, M.-C. Wei, T.-C. Huang, S.-Z. Lee, and S.-S. Lin, "Comparison of modified ultrasound-assisted and traditional extraction methods for the extraction of baicalin and baicalein from *Radix Scutellariae*," *Industrial Crops and Products*, vol. 45, pp. 182–190, 2013.

[19] Y.-C. Yang, M.-C. Wei, and T.-C. Huang, "Optimisation of an ultrasound-assisted extraction followed by RP-HPLC separation for the simultaneous determination of oleanolic acid, ursolic acid and oridonin content in *Rabdosia rubescens*," *Phytochemical Analysis*, vol. 23, no. 6, pp. 627–636, 2012.

[20] Y.-C. Yang, M.-C. Wei, F.-Y. Lian, and T.-C. Huang, "Simultaneous extraction and quantitation of oleanolic acid and ursolic acid from *Scutellaria barbata* D. Don by ultrasound-assisted extraction and high-performance liquid chromatography," *Chemical Engineering Communications*, vol. 201, no. 4, pp. 482–500, 2014.

[21] M.-C. Wei, Y.-C. Yang, H.-F. Chiu, and S.-J. Hong, "Development of a hyphenated procedure of heat-reflux and ultrasound-assisted extraction followed by RP-HPLC separation for the determination of three flavonoids content in *Scutellaria barbata* D. Don," *Journal of Chromatography B: Analytical Technologies in the Biomedical and Life Sciences*, vol. 940, pp. 126–134, 2013.

[22] Y. B. Zhang, L. H. Wang, D. Y. Zhang, L. L. Zhou, and Y. X. Guo, "Ultrasound-assisted extraction and purification of schisandrin B from *Schisandra chinensis* (Turcz.) Baill seeds: optimization by response surface methodology," *Ultrasonics Sonochemistry*, vol. 21, no. 2, pp. 461–466, 2014.

[23] C. Desgrouas, B. Baghdikian, F. Mabrouki et al., "Rapid and green extraction, assisted by microwave and ultrasound of cepharanthine from *Stephania rotunda* Lour," *Separation and Purification Technology*, vol. 123, pp. 9–14, 2014.

[24] G.-Q. He, H.-P. Xiong, Q.-H. Chen, H. Ruan, Z.-Y. Wang, and L. Traoré, "Optimization of conditions for supercritical fluid extraction of flavonoids from hops (*Humulus lupulus* L.)," *Journal of Zhejiang University Science B*, vol. 6, no. 10, pp. 999–1004, 2005.

[25] H. Içen and M. Gürü, "Effect of ethanol content on supercritical carbon dioxide extraction of caffeine from tea stalk and fiber wastes," *Journal of Supercritical Fluids*, vol. 55, no. 1, pp. 156–160, 2010.

[26] W. Qu, Z. Pan, and H. Ma, "Extraction modeling and activities of antioxidants from pomegranate marc," *Journal of Food Engineering*, vol. 99, no. 1, pp. 16–23, 2010.

[27] Y.-H. Lee, A. L. Charles, H.-F. Kung, C.-T. Ho, and T.-C. Huang, "Extraction of nobiletin and tangeretin from *Citrus depressa* Hayata by supercritical carbon dioxide with ethanol as modifier," *Industrial Crops and Products*, vol. 31, no. 1, pp. 59–64, 2010.

[28] D. Westerman, R. C. D. Santos, J. A. Bosley, J. S. Rogers, and B. Al-Duri, "Extraction of Amaranth seed oil by supercritical carbon dioxide," *Journal of Supercritical Fluids*, vol. 37, no. 1, pp. 38–52, 2006.

[29] A. C. Kumoro and M. Hasan, "Supercritical carbon dioxide extraction of andrographolide from *Andrographis paniculata*: effect of the solvent flow rate, pressure, and temperature," *Chinese Journal of Chemical Engineering*, vol. 15, no. 6, pp. 877–883, 2007.

[30] M. D. A. Saldaña, F. Temelli, S. E. Guigard, B. Tomberli, and C. G. Gray, "Apparent solubility of lycopene and β-carotene in supercritical CO_2, CO_2 + ethanol and CO_2 + canola oil using dynamic extraction of tomatoes," *Journal of Food Engineering*, vol. 99, no. 1, pp. 1–8, 2010.

[31] U. Topal, M. Sasaki, M. Goto, and K. Hayakawa, "Extraction of lycopene from tomato skin with supercritical carbon dioxide: effect of operating conditions and solubility analysis," *Journal of Agricultural and Food Chemistry*, vol. 54, no. 15, pp. 5604–5610, 2006.

[32] B. P. Nobre, A. F. Palavra, F. L. P. Pessoa, and R. L. Mendes, "Supercritical CO_2 extraction of *trans*-lycopene from Portuguese tomato industrial waste," *Food Chemistry*, vol. 116, no. 3, pp. 680–685, 2009.

[33] P. Tonthubthimthong, S. Chuaprasert, P. Douglas, and W. Luewisutthichat, "Supercritical CO_2 extraction of nimbin from neem seeds—an experimental study," *Journal of Food Engineering*, vol. 47, no. 4, pp. 289–293, 2001.

[34] S. G. Özkal, U. Salgin, and M. E. Yener, "Supercritical carbon dioxide extraction of hazelnut oil," *Journal of Food Engineering*, vol. 69, no. 2, pp. 217–223, 2005.

Research Article

Measuring Agarwood Formation Ratio Quantitatively by Fluorescence Spectral Imaging Technique

Botao Huang,[1] Duykien Nguyen,[2,3] Tianyi Liu,[2,3] Kaibin Jiang,[2,3] Jinfen Tan,[2,3] Chunxin Liu,[2,3] Jing Zhao,[1] and Shaowei Huang[2,3]

[1]*College of Science, South China Agricultural University, Guangzhou, Guangdong 510640, China*
[2]*Guangdong Key Laboratory for Innovative Development and Utilization of Forest Plant Germplasm, South China Agricultural University, Guangzhou, Guangdong 510640, China*
[3]*College of Forestry, South China Agricultural University, Guangzhou, Guangdong 510640, China*

Correspondence should be addressed to Jing Zhao; edithzj@gmail.com and Shaowei Huang; shwhuang@scau.edu.cn

Agarwood is a kind of important and precious traditional Chinese medicine. With the decreasing of natural agarwood, artificial cultivation has become more and more important in recent years. Quantifying the formation of agarwood is an essential work which could provide information for guiding cultivation and controlling quality. But people only can judge the amount of agarwood qualitatively by experience before. Fluorescence multispectral imaging method is presented to measure the agarwood quantitatively in this paper. A spectral cube from 450 nm to 800 nm was captured under the 365 nm excitation sources. The nonagarwood, agarwood, and rotten wood in the same sample were distinguished based on analyzing the spectral cube. Then the area ratio of agarwood to the whole sample was worked out, which is the quantitative information of agarwood area percentage. To our knowledge, this is the first time that the formation of agarwood was quantified accurately and nondestructively.

1. Introduction

Agarwood (*Aquilaria sinensis* Lour. Gilg) is a dark resinous heartwood that forms in *Aquilaria* trees, which was distributed in South China such as Hainan province, Guangxi province, and Guangdong province [1–3]. It forms when *Aquilaria* trees are infected with a type of mould. Prior to infection, the heartwood is relatively light and pale coloured; however, as the infection progresses, the tree produces a dark aromatic resin in response to the attack, which results in a very dense, dark, resin embedded heartwood [4].

Agarwood is valued in many cultures for its distinctive fragrance and thus is used for incense and perfumes. It is also known as a kind of famous traditional Chinese medicine. It can be used as sedative, analgesic, and digestive medicine in the orient [5–7]. Moreover, it had been reported that agarwood can help healing rheumatism, cardiovascular and cerebrovascular diseases, and many other diseases related to the artery and the heart [8, 9].

One of the main reasons for the relative rarity and high cost of agarwood is the depletion of the wild resource. Since 1995, *Aquilaria malaccensis*, the primary source, has been listed in potentially threatened species by the Convention on International Trade in Endangered Species of Wild Fauna and Flora. In 2004 all *Aquilaria* species were listed in potentially threatened species. For China, it had been claimed in China Plant Red Data Book in 1992 that, because of the deforestation of the nonagarwood which can generate the agarwood and lead to the rare situation of agarwood now, the way of cultivating should be the main method to get agarwood [10]. Nowadays the most common way of cultivating the agarwood is the Hong inoculated knot [2, 11]. For better quality control of agarwood cultivation, it is essential to choose the suitable *Aquilaria* trees. There are several factors to show which trees are suitable, of which agarwood formation ratio is one of the most significant factors. Agarwood formation is the ratio of agarwood cross-sectional area to tree cross-sectional area. The larger the area of the agarwood is, the better the tree is for

formation agarwood. So it is necessary to test the area of the agarwood in different trees and then use the statistical data to determine which is the more suitable tree. It is essential and important for selective breeding and evaluating quality of agarwood. However, there is no effective method to measure the area except rough estimation by human eyes. In this paper, the technology of fluorescence spectral imaging was presented to measure the area of the agarwood. As far as we know, this is the first time that the agarwood formation ratio was measured quantitatively.

Spectral imaging is a new technology by which the signal light of detected sample is divided into several narrow bands, and then the images at each band are captured by the detector in sequence. Both the spatial data and the spectra data can be obtained simultaneously. Spectral imaging technology has been applied in many fields such as food safety [12], fruit quality [13, 14], and medicine testing [15, 16]. In this paper, fluorescence spectral imaging method was used to work on the formation ratio of agarwood.

2. Materials and Methods

2.1. Sample Preparation. The tested samples were cut from seven-year-old *Aquilaria sinensis* at height of 1.3 meters above the ground. *Aquilaria sinensis* grew in an artificial forest in Huazhou, Guangdong province, China, and were treated by liquid transfusion technology of agarwood formation in the whole body and then were cut two years later. The samples were dried, polished to flat surface, and then stored at $25°C \pm 3$ before measuring.

2.2. Testing System. The testing system was designed in Guangdong Key Laboratory for Innovative Development and Utilization of Forest Plant Germplasm, South Agricultural University. The main components of the system are two 365 nm UV lamps (EA-160/FA, Spectronics Corp., NY, USA), optical filters (300 nm–800 nm, Thorlabs Inc., NJ, USA), a CCD (1/2″, 1280 × 1024) and camera lens (M0814-MP, Computer Company, Japan), and a host computer.

The two UV lamps are used as excitation light source which could excite sample plan uniformly. The optical filters are used to select the wavelengths of emission signals of samples. The working wavelength range is from 450 nm to 800 nm with the interval 10 nm. The spatial resolution is 5 lp/mm. The ray path of the system was shown in Figure 1. The UV light coming from the light source reached the samples on the underlay, and then the samples were stimulated to emit fluorescence light. The emission light was filtered by the filters and captured by the CCD. At last, a spectral cube of samples was got and analyzed. Each sample has one spectral cube.

2.3. Data Analysis. A spectral cube is shown in Figure 2, which consisted of 16 spectral images. The pictures in the same cube are spatially matched, but spectrally different.

There are four parts in each picture, nonagarwood, agarwood, rotten wood, and the background. Since the spatial distribution of nonagarwood, agarwood, and rotten wood is
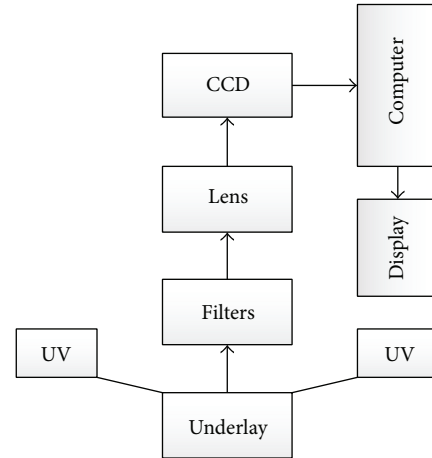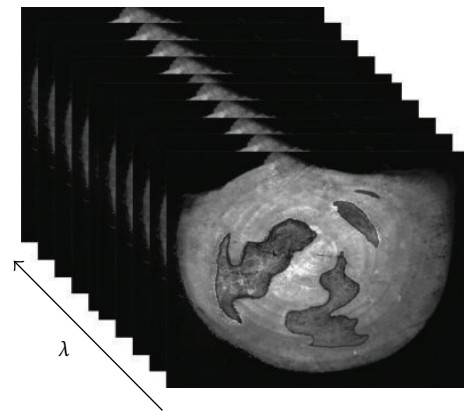

Figure 1: The fluorescence spectral imaging system.

Figure 2: Spectral cube of a sample.

irregular, the spectra differences of these parts were invited to determine the spatial position pixel by pixel. Here the pictures whose wavelength was between 500 nm and 650 nm were used because the spectral differences were the biggest in this wavelength range. There are four steps to analyze data here.

2.3.1. Obtaining the Spectral Curve of Each Part. For positioning the spatial distribution of nonagarwood, agarwood, and rotten wood in one sample, the spectral cube of the sample should be analyzed to get the spectral curve of each part. As an example, to get the spectral curve of agarwood, first, the mask was designed based on prior knowledge for choosing a 3×3 area of nonagarwood on one picture of the spectral cube; second, the average intensity of chosen area was calculated, which could represent the intensity of nonagarwood at the wavelength of this picture; third, the same areas of other pictures were analyzed like the first and second steps to get a group of intensities at different wavelength, which is the spectral curve data of the agarwood. The spectral curve of the nonagarwood and the rotten wood was also obtained by the same way.

2.3.2. Obtaining the Outline of the Sample. The outline of the whole sample is needed for getting the relative area of the whole sample. To obtain the outline of the sample, a high-pass filter [17, 18] in the spatial domain had been used, which was shown in the following expresion:

$$I = \begin{cases} I & (I \geq A) \\ 0 & (I < A), \end{cases} \tag{1}$$

in which I is the intensity of a pixel and A is the cutoff intensity. The signal which is higher than or equal to A could pass the filter, but the signal which is lower than A would be attenuated.

The filter shown in expression (1) was used to scan the spectral image line by line from left side. The scanning would not stop until the first pixel which could pass the filter appears. The pixel is the left edge of the sample in corresponding line. Then the filter begins second scanning from right side to look for the right edge.

2.3.3. Distinguishing Nonagarwood and Rotten Wood. Distinguishing agarwood directly from sample is difficult here, so the nonagarwood and rotten wood were distinguished, respectively, at first. Which wavelengths were selected was based on the differences of spectral curve of these three parts. Edge detection filter [19–22] was designed to detect the edge of nonagarwood. The edge detection filter worked with four steps. First, smooth the picture to reduce the noise by Gaussian filter. Second, calculate the local gradient and the edge direction of each spot to get the ridges with the following expression:

$$g(x, y) = \left[G_x^2 + G_y^2\right]^{1/2},$$
$$\alpha(x, y) = \arctan\left(\frac{G_y}{G_x}\right). \tag{2}$$

Here, $g(x, y)$ is the local gradient of each point, G_x is the partial derivative of pixel (i, j) in direction x, and G_y is the partial derivative of pixel (i, j) in direction y. $a(x, y)$ is the direction of the edge. The edge point is defined as the largest gray value point of the local area on the gradient direction. All these edge points could form the ridges of the gradient magnitude. Third, track the top of all the ridges and let all the pixels that are not on the top of the ridges be zero, which was known as nonmaximum suppression processing. Fourth, define the effective range of gray value of the ridges based on the tested sample. Here, range $[0.2, 0.25]$ was used. Every 8 connection ridge pixels in the range were integrated and linked into the strong ridge pixels, which were the edge between nonagarwood and agarwood.

The band ratio algorithms were used for rotten wood distinguishing. Band ratio is created by dividing spectral values of one band by spectral values of another band from a spectral cube. It is used to enhance the spectral differences between bands and to reduce the effects of topography [23, 24]. Here, band ratio algorithms were used to enhance the differences between the rotten wood and the other part of the sample. The band ratio method is expressed in

$$BV_{i,j,r} = \frac{BV_{i,j,k}}{BV_{i,j,l}}, \tag{3}$$

in which $V_{i,j,k}$ and $V_{i,j,l}$ are the gray value of the pixel (i, j) on k band and l band pictures and $BV_{i,j,r}$ is the ratio value of the pixel (i, j). If the denominator of the expression is zero, $BV_{i,j,r}$ will be assigned to zero.

To express the range of function (3) by linear fashion and use the standard 8-bit encodings (range from 0 to 255), normalized function should be used to maintain further processing, and the following are the formulas:

$$BV_{i,j,n} = \begin{cases} 0 & BV_{i,j,r} = 0 \\ \text{Int}\left[\left(BV_{i,j,r} * 127\right) + 1\right] & BV_{i,j,r} \in \left[\frac{1}{255}, 1\right] \\ \text{Int}\left(\frac{BV_{i,j,r}}{2} + 128\right) & BV_{i,j,r} \in (1, 255), \end{cases} \tag{4}$$

in which $BV_{i,j,n}$ refers to the output gray value of the pixel (i, j) and the "Int" refers to integer conversion.

After the enhanced image by band ratio algorithms was proceeded by the edge detection filter mentioned, the edge between agarwood and rotten wood was obtained.

2.3.4. Obtaining the Agarwood Formation Ratio. Since the area of no rotten wood and the area of no nonagarwood are obtained, for obtaining the agarwood formation ratio, two steps are needed, obtaining the edge of the agarwood and connecting the region. Function (5) was used to obtain the edge:

$$C = A \cap B, \tag{5}$$

in which A and B refer to the two images which were got in Section 2.3.3. C refers to the edge of agarwood. The edge of agarwood could be got by intersecting the complementary sets of nonagarwood and rotten wood area. For getting the area of agarwood, the region surrounded by the edge should be connected. The edge just like a ring which has two sides. Track the outside of the edge and the corresponding inside of the edge, and then connect both sides to get the agarwood area.

3. Results

3.1. Spectral Curve. The picture at 550 nm was used to select the area of agarwood, nonagarwood, and rotten wood. The selected areas were shown in Figure 3. The three spectral curves were shown in Figure 4. The differences of three spectral curves were obvious by analyzing Figure 4. The fluorescence intensity at each wavelength of nonagarwood is much higher than that of agarwood and rotten wood. Here, the picture at 550 nm was used. Comparing the spectra of agarwood and rotten wood, both of them had peaks at 510 nm and 570 nm. The peak of agarwood at 510 nm is higher

FIGURE 3: The spatial distribution of nonagarwood, agarwood, and rotten wood.
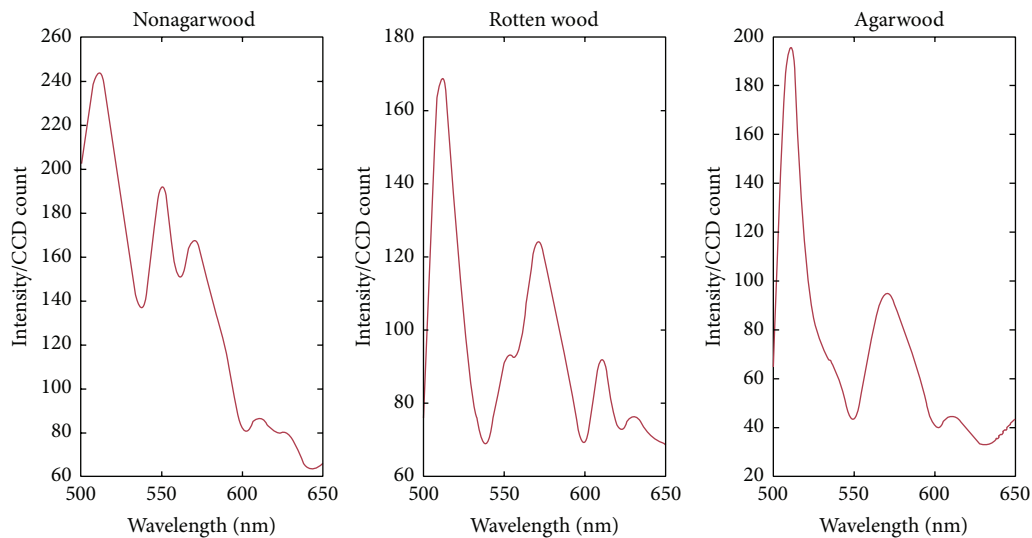

FIGURE 4: The spectral graphs of nonagarwood, rotten wood, and agarwood.

than that of rotten wood. However, the peak of agarwood at 570 nm is lower than that of rotten wood. So the band ratio of 510 nm and 570 nm was used to enhance the differences of rotten wood and agarwood.

3.2. The Outline of the Sample. The outline of the sample was shown in Figure 5, which was got by high-pass filter. Comparing Figure 5 with Figure 3, the outline of the sample had been got accurately.

3.3. The Area Ratio of Agarwood. The results of distinguished nonagarwood and rotten wood were shown in Figure 6. In Figure 6(a), the area of nonagarwood was all in the dark, but the area of the agarwood and rotten wood was filled by bright pixels. In Figure 6(b), the area of rotten wood was all in the dark, but the area of the agarwood and nonagarwood was full of bright pixels. The common area of bright pixels in two pictures is the area of agarwood.

The result got by intersecting Figures 6(a) and 6(b) was shown in Figure 7(a). The edges of the agarwood were tracked accurately. Filling the area between the inside and outside edges, the agarwood could be got, which was shown in Figure 7(b). The results are consistent with the judgment

FIGURE 5: The outline of the sample.

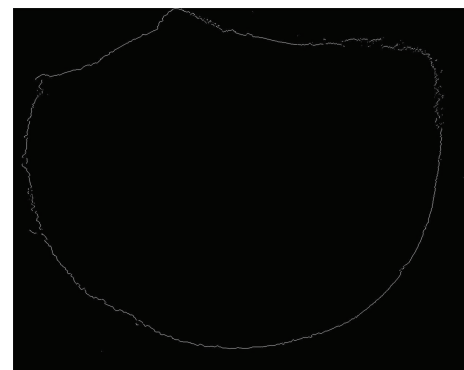made by the expert in traditional Chinese medicines [25, 26]. The relative area of agarwood could be got by counting the number of bright pixels in Figure 7(b).

Counting the number of pixels surrounded by the outline, the relative area of the whole sample could be got. The area percentage of agarwood is the ratio of relative area of agarwood to relative area of the whole sample. For the sample
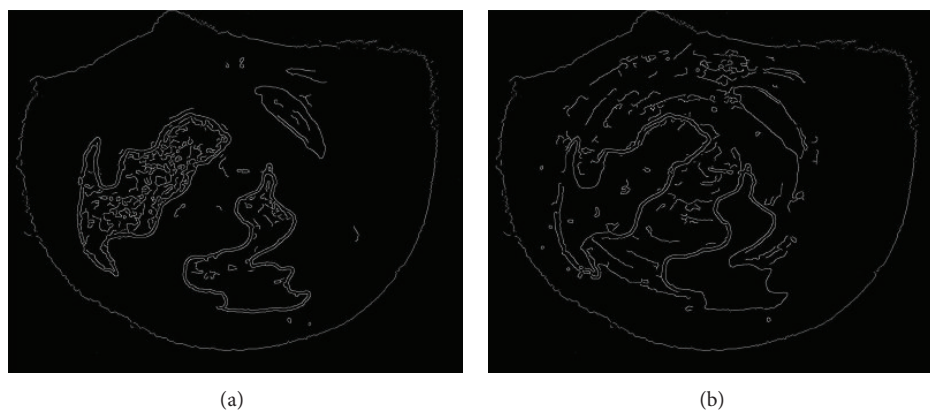
(a)

(b)

FIGURE 6: (a) Exclude the nonagarwood; (b) exclude the rotten wood.
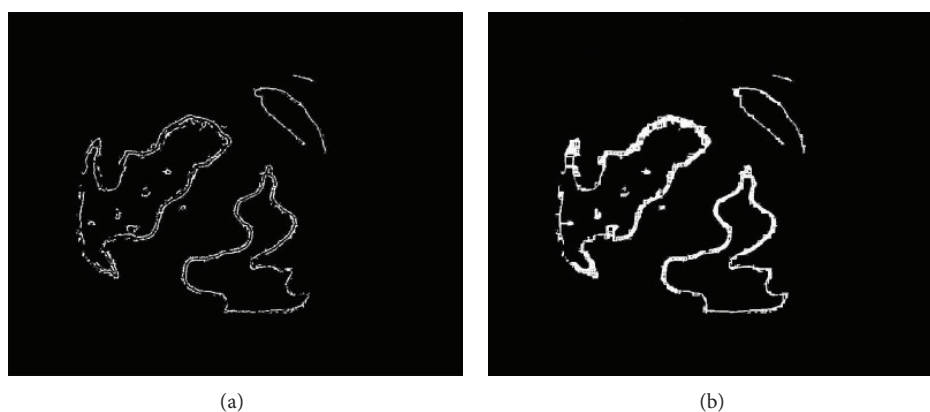

(a)

(b)

FIGURE 7: (a) The intersection of nonagarwood and rotten wood; (b) the area of the Chinese agarwood.

TABLE 1: Agarwood formation ratio of six samples.

No. 1	No. 2	No. 3	No. 4	No. 5	No. 6
0.48%	1.24%	0.68%	2.45%	0.44%	0.90%

showed in the paper, the area percentage of agarwood is 2.06%.

4. Discussion

35 samples were analyzed by fluorescence spectral imaging technique to evaluate the validity of the method. Six of them were shown in Figure 8. Line (a) is spectral images at 550 nm, Line (b) is the outlines of samples, and Line (c) is the spatial distribution of agarwood in samples. The area percentage of agarwood of these six samples was shown in Table 1. The results show that the technique works well on detecting the agarwood formation ratio.

The fluorescence spectral imaging technique tested samples pixel by pixel by the spectral information, which had been applied successfully to test spatial distribution of the constituents in traditional Chinese medicines by our group [16, 27]. Spatial distribution of agarwood was detected by fluorescence spectra of agarwood in this paper. Before the fluorescence spectral imaging technique was presented, the agarwood only can be judged manually. The experts could point out the distribution of agarwood but could not provide quantitative data. The new technique can test formation ratio quantitatively. The validity of the results was proved by the expert in field of identification of Chinese medicine.

5. Conclusions

The agarwood which formed in *Aquilaria sinensis* was measured by fluorescence spectral imaging technique in this paper. The agarwood formation ratio is an important factor to indicate the better trees, better liquid transfusion, and better planting technique for agarwood formation. To our knowledge, this is the first time that the agarwood formation ratio was measured quantitatively. Comparing to qualitative estimation by manual watching, the technique is much more accurate. It is concluded that fluorescence spectral imaging is a precise, noninvasive, and fast technique for measuring agarwood formation ratio and quality control of agarwood cultivation.
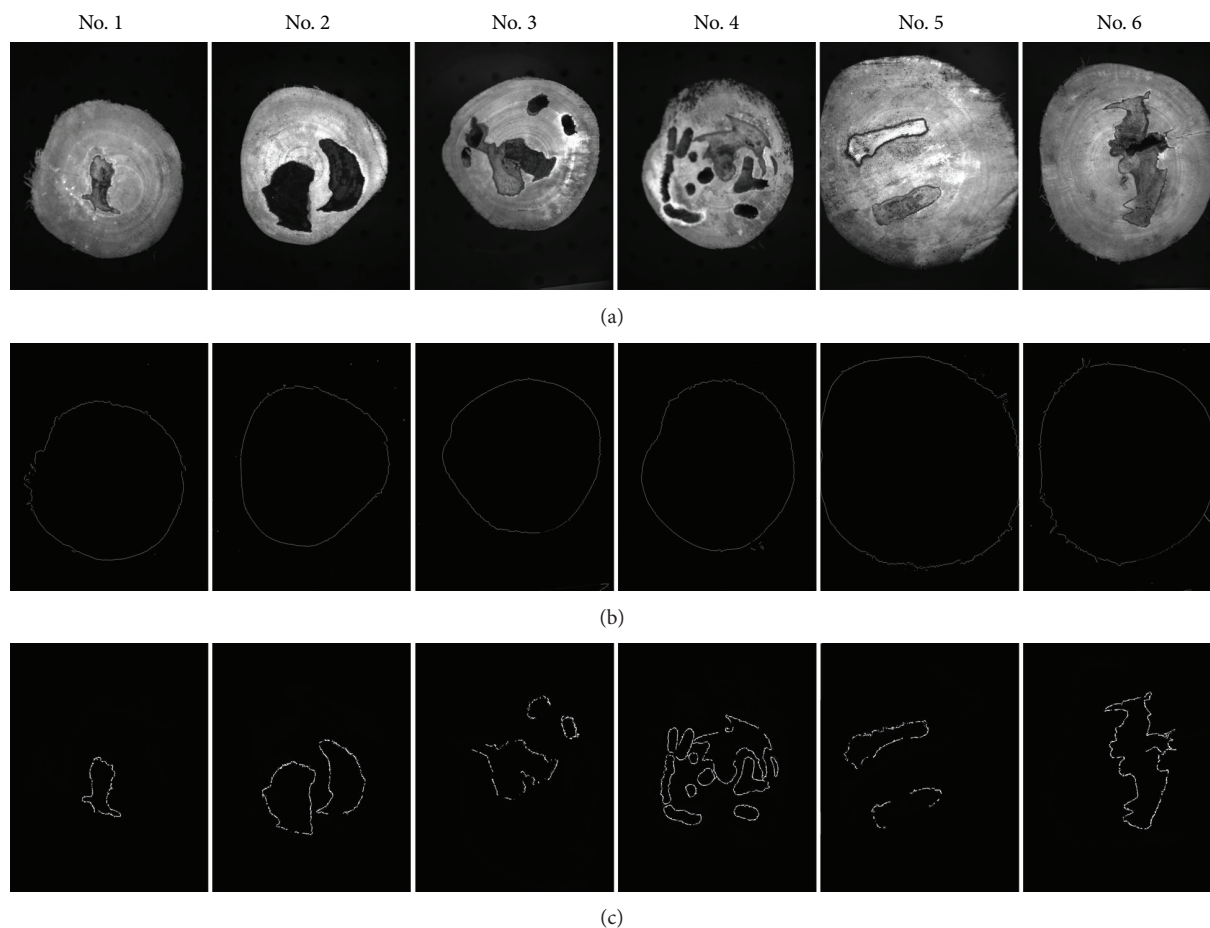
No. 1   No. 2   No. 3   No. 4   No. 5   No. 6

(a)

(b)

(c)

FIGURE 8: Agarwood formation ratio of six samples.

Conflict of Interests

The authors declare that there is no conflict of interests regarding the publication of this paper.

Authors' Contribution

Botao Huang and Duykien Nguyen contributed equally to this work.

Acknowledgments

References

[1] E. O. Espinoza, C. A. Lancaster, N. M. Kreitals, M. Hata, R. B. Cody, and R. A. Blanchette, "Distinguishing wild from cultivated agarwood (*Aquilaria* spp.) using direct analysis in real time and time of-flight mass spectrometry," *Rapid Communications in Mass Spectrometry*, vol. 28, no. 3, pp. 281–289, 2014.

[2] Y. Liu, H. Chen, Y. Yang et al., "Whole-tree agarwood-inducing technique: an efficient novel technique for producing high-quality agarwood in cultivated *Aquilaria sinensis* trees," *Molecules*, vol. 18, no. 3, pp. 3086–3106, 2013.

[3] T. Ito, M. Kakino, S. Tazawa et al., "Quantification of polyphenols and pharmacological analysis of water and ethanol-based extracts of cultivated agarwood leaves," *Journal of Nutritional Science and Vitaminology*, vol. 58, no. 2, pp. 136–142, 2012.

[4] R. Naef, "The volatile and semi-volatile constituents of agarwood, the infected heartwood of *Aquilaria* species: a review," *Flavour and Fragrance Journal*, vol. 26, no. 2, pp. 73–89, 2011.

[5] H. Takemoto, M. Ito, T. Shiraki, T. Yagura, and G. Honda, "Sedative effects of vapor inhalation of agarwood oil and spikenard extract and identification of their active components," *Journal of Natural Medicines*, vol. 62, no. 1, pp. 41–46, 2008.

[6] M. Kakino, S. Tazawa, H. Maruyama et al., "Laxative effects of agarwood on low-fiber diet-induced constipation in rats," *BMC Complementary and Alternative Medicine*, vol. 10, article 68, 2010.

[7] M. Kakino, H. Izuta, T. Ito et al., "Agarwood induced laxative effects via acetylcholine receptors on loperamide-induced constipation in mice," *Bioscience, Biotechnology and Biochemistry*, vol. 74, no. 8, pp. 1550–1555, 2010.

[8] J.-Y. Ueda, L. Imamura, Y. Tezuka, Q. L. Tran, M. Tsuda, and S. Kadota, "New sesquiterpene from Vietnamese agarwood and its induction effect on brain-derived neurotrophic factor mRNA expression in vitro," *Bioorganic & Medicinal Chemistry*, vol. 14, no. 10, pp. 3571–3574, 2006.

[9] J.-L. Cui, S.-X. Guo, and P.-G. Xiao, "Antitumor and antimicrobial activities of endophytic fungi from medicinal parts of *Aquilaria sinensis*," *Journal of Zhejiang University Science B*, vol. 12, no. 5, pp. 385–392, 2011.

[10] M. Ito and G. Honda, "Taxonomical identification of agarwood-producing species," *Natural Medicines*, vol. 59, no. 3, pp. 104–112, 2005.

[11] A. Barden, *Heart of the Matter: Agarwood Use and Trade and CITES Implementation for Aquilaria malaccensis*, TRAFFIC International, Cambridge, UK, 2000.

[12] A. A. Gowen, C. P. O'Donnell, P. J. Cullen, G. Downey, and J. M. Frias, "Hyperspectral imaging—an emerging process analytical tool for food quality and safety control," *Trends in Food Science & Technology*, vol. 18, no. 12, pp. 590–598, 2007.

[13] F. Mendoza, R. F. Lu, and H. Y. Cen, "Grading of apples based on firmness and soluble solids content using Vis/SWNIR spectroscopy and spectral scattering techniques," *Journal of Food Engineering*, vol. 125, no. 1, pp. 59–68, 2014.

[14] P. P. Subedi and K. B. Walsh, "Non-invasive techniques for measurement of fresh fruit firmness," *Postharvest Biology and Technology*, vol. 51, no. 3, pp. 297–304, 2009.

[15] J. Zhao, Q. C. Pang, J. Ma, C. M. Liu, L. Wang, and D. J. Cui, "In vivo identification of Radix Panacis Quinquefolii by spectral imaging technology," *Spectroscopy and Spectral Analysis*, vol. 31, no. 1, pp. 210–213, 2011.

[16] J. Zhao, Q.-C. Pang, J. Ma et al., "The research on active constituent distribution of rhizoma coptidis pieces," *Spectroscopy and Spectral Analysis*, vol. 31, no. 6, pp. 1692–1696, 2011.

[17] H.-L. Zhang and S.-Y. Wang, "A new steganalysis method using high-pass filter for JPEG image," in *Proceedings of the International Symposium on Electronic Commerce and Security (ISECS '08)*, pp. 165–168, August 2008.

[18] X. Chen, J. Yang, Q. Wu, J. Zhao, and X. He, "Directional high-pass filter for blurry image analysis," *Signal Processing: Image Communication*, vol. 27, no. 7, pp. 760–771, 2012.

[19] F. Hao, J. F. Shi, Z. S. Zhang, R. W. Chen, and S. Q. Zhu, "Canny edge detection enhancement by general auto-regression model and bi-dimensional maximum conditional entropy," *Optik*, vol. 125, no. 15, pp. 3946–3953, 2014.

[20] D. Song, Z. S. Dong, and Y. H. Ha, "Canny edge detection and its MATLAB realization," in *Proceedings of the 6th International Symposium on Test and Measurement, Vols 1–9, Conference Proceedings (ISTM '05)*, pp. 5152–5154, 2005.

[21] K. P. Lam and A. Furness, "K-AVE+GNN+Sobel equals an effective, highly parallel edge detector approach," *Parallel and Distributed Methods for Image Processing*, vol. 3166, pp. 190–198, 1997.

[22] J. Schou, H. Skriver, A. Nielsen, and K. Conradsen, "CFAR edge detector for polarimetric SAR images," *IEEE Transactions on Geoscience and Remote Sensing*, vol. 41, no. 1, pp. 20–32, 2003.

[23] J. Li, X. Rao, J. Guo, and Y. Ying, "Hyperspectral reflectance imaging for detecting citrus canker based on dual-band ratio image classification method," in *Proceedings of the 5th International Symposium on Advanced Optical Manufacturing and Testing Technologies: Optical Test and Measurement Technology and Equipment*, April 2010.

[24] A. Morel and B. Gentili, "A simple band ratio technique to quantify the colored dissolved and detrital organic material from ocean color remotely sensed data," *Remote Sensing of Environment*, vol. 113, no. 5, pp. 998–1011, 2009.

[25] P. Pripdeevech, W. Khummueng, and S.-K. Park, "Identification of odor-active components of agarwood essential Oils from Thailand by solid phase microextraction-GC/MS and GC-O," *Journal of Essential Oil Research*, vol. 23, no. 4, pp. 46–53, 2011.

[26] China TSPCoPsRo, *Pharmacopoeia of the People's Republic of China*, Chemical Industry Press, Beijing, China, 2005.

[27] J. Zhao, Q. Pang, J. Ma et al., "Spectral imaging technology applied to adulteration of traditional Chinese medicine powder," *Acta Optica Sinica*, vol. 30, no. 11, p. 4, 2010.

Research Article

Traceability and Quality Control in Traditional Chinese Medicine: From Chemical Fingerprint to Two-Dimensional Barcode

Yong Cai,[1,2] Xiwen Li,[1,3] Mei Li,[2] Xiaojia Chen,[1] Hao Hu,[1] Jingyun Ni,[1] and Yitao Wang[1]

[1]*State Key Laboratory of Quality Research in Chinese Medicine, Institute of Chinese Medical Sciences, University of Macau, Macau*
[2]*Information Technology College of Beijing Normal University, Zhuhai Campus, Zhuhai 519087, China*
[3]*Research Center for Pharmacognosy, Institute of Chinese Materia Medica, China Academy of Chinese Medical Sciences, Beijing 100700, China*

Correspondence should be addressed to Xiwen Li; xiweijia2004@aliyun.com and Hao Hu; haohu@umac.mo

Chemical fingerprinting is currently a widely used tool that enables rapid and accurate quality evaluation of Traditional Chinese Medicine (TCM). However, chemical fingerprints are not amenable to information storage, recognition, and retrieval, which limit their use in Chinese medicine traceability. In this study, samples of three kinds of Chinese medicines were randomly selected and chemical fingerprints were then constructed by using high performance liquid chromatography. Based on chemical data, the process of converting the TCM chemical fingerprint into two-dimensional code is presented; preprocess and filtering algorithm are also proposed aiming at standardizing the large amount of original raw data. In order to know which type of two-dimensional code (2D) is suitable for storing data of chemical fingerprints, current popular types of 2D codes are analyzed and compared. Results show that QR Code is suitable for recording the TCM chemical fingerprint. The fingerprint information of TCM can be converted into data format that can be stored as 2D code for traceability and quality control.

1. Introduction

The industrial chain of traditional Chinese medicine (TCM), from the production of raw materials to the sale of their finished products, is a complicated multilink process. It is an absolutely important task to ensure the quality of TCM to be safe, effective, stable, and controllable in the whole process. Although the advent of modern analytical technologies made a positive impact on component determination [1–3] and undoubtedly will continue to make a substantial contribution to quality control, current quality test in each part of the process is relatively independent and testing results can hardly be shared, which bring regulatory blind spots and difficulty of quality traceability. None of the available tools can combine all links and work for TCM traceability in the whole production process. Current traceability technologies included radio frequency identification [4–6], barcode [7],

and other combined techniques based on web [8]. However, these technologies were mainly used in circulation links and they could not provide quality information of products. A new method is required to run through each link of TCM and can carry quality traceability information.

Chemical fingerprinting was a comprehensive and quantified testing method. It can be constructed based on the systematic research on the chemical constituents for the evaluation of authentication [9, 10], reliability [11, 12], and stability [13–15] of TCM and their semifinished products, and it has now become a main method for quality determination and was accepted in Chinese Pharmacopoeia. However chemical fingerprints cannot be directly applied to Chinese medicine traceability due to several limitations. First, chemical fingerprints are stored in image format which has a large data capacity. It is difficult to be compressed and exported for a batch of information management. Second, quality
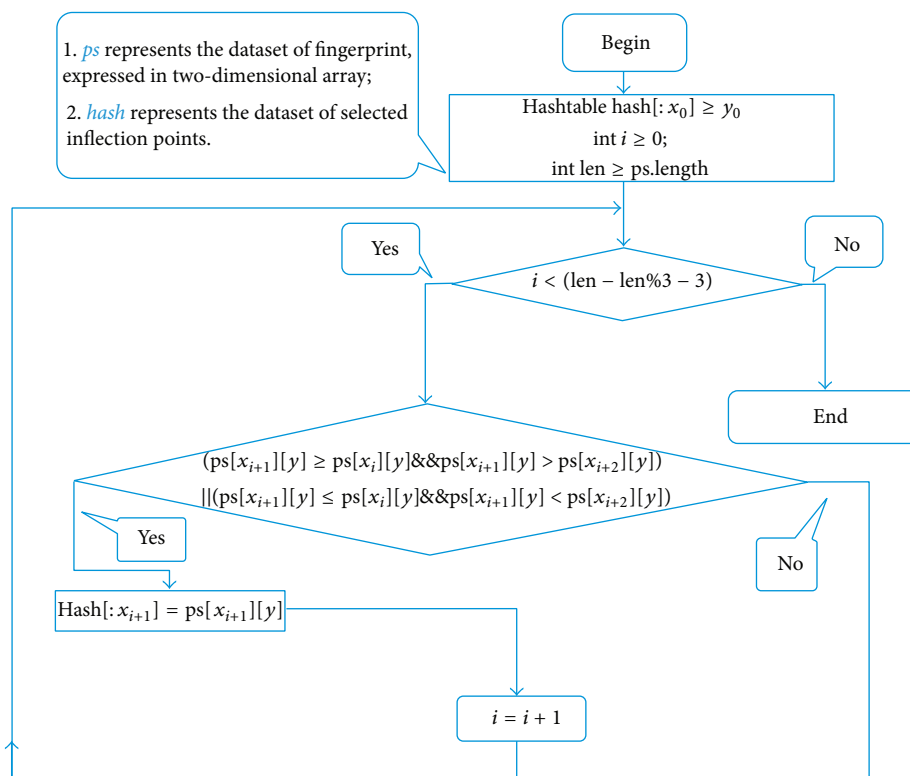
FIGURE 1: Program for selecting inflexion points.

information cannot be obtained through direct scanning of chemical fingerprints. It is not easy to transport quality information and the information cannot easily be shared between different links in the process of the production and the circulation of TCM.

Barcode technology is an important tool for modern logistics management due to its ability in quick and accurate information extraction and batch management. It has been widely used in the manufacturing [7, 8, 16], medication administration [17–19], and retailing industries [20, 21]. It was recently reported that DNA barcoding could be used for traceability [22]. The DNA molecular sequence cannot be automatically recognized by direct scanning, and the large size of printout is inconvenient to the application of distribution management; researchers conducted studies on converting DNA sequences into 2D barcode [23–25]. Chemical fingerprints share the similar vector features with the molecule sequence and the fingerprint, but so far no literature can be found on converting TCM fingerprint into 2D barcode. In this paper, with the high performance liquid chromatography (HPLC) technology, the chemical fingerprints were constructed based on the quality testing results and chemical quality data were extracted. After data normalization, the fingerprint information can be converted into the data format that can be stored by barcode and then further converted into the 2D barcode of TCM fingerprint. By comparing different encoding types, QR Code is finally recommended as the best barcode for quality traceability.

2. Materials and Methods

2.1. Construction of Chemical Fingerprints. Three Chinese medicines were randomly selected and their chemical fingerprints were constructed using HLPC technology (Yin-YangHuo and RouCongRong refer to [26, 27], resp.). The detailed method of MuDanPi detection was as follows: a Zorbax SB-C18 column (250 × 4.6 mm I.D., 5 μm) with a Zorbax SB-C18 guard column (12.5 × 4.6 mm I.D., 5 μm) was used. The samples were separated using a gradient mobile phase consisting of 0.5% acetic acid (A) and acetonitrile (B). The gradient condition is 0–40 min, 10%–50% B; 40–60 min, 50%–100% B; 60–65 min, 100% B. The separation was performed on an Agilent series 1200 liquid chromatography (Agilent Technologies, Santa Clara, CA, USA), equipped with a vacuum degasser, a quaternary pump, an autosampler, and a diode array detector (DAD).

2.2. Data Analysis. DIF (or TXT, CSV) data (see File S1 of the Supplementary Material available online at http://dx.doi.org/10.1155/2014/251304) were downloaded from HPLC instrument and were saved as excel files. These files were processed for data standardization: remove negative time and absorbance data; find inflexion points in chemical fingerprints; keep one decimal fraction of time data and remove duplicate ones; cut some redundant no-absorbance data. A software program under the environment of Ruby (Netbeans IDE 6.5, Ruby 1.8.7, Gem spreadsheet 0.9.5) was created

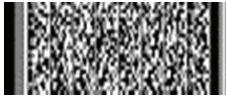TABLE 1: Comparison between different two-dimensional barcodes.

Code system	QR Code	Data matrix	PDF 417
Developer	DENSO (Japan)	RVSI Acuity CiMatrix (USA)	Symbol Technologies Inc. (USA)
Type	Matrix	Matrix	Stacked barcode
Data capacity			
Numeric	7,089	3,116	2,710
Alphanumeric	4,296	2,355	1,850
Binary	2,953	1,556	1,018
Kanji	1,817	778	554
Error correction level	Max 30%	Max 25%	Max 50%
Identification speed	30/s	2~3/s	3/s
Readable direction	360°	360°	+/−10°
Main features	Large capacity Small printout size	Small printout size	Large capacity
Main usages	All categories	FA	OA
Standardization	AIM International JIS, ISO	AIM International ISO	AIM International ISO
Sample picture			

TABLE 2: Changes of length of string and data points during data filtering process.

Sample	Step 1 bytes/points	Step 2 bytes/points	Step 3 bytes/points	Compression ratio
YinYangHuo	277508/9001	57311/8320	1228/185	0.44%/2.05%
Roucongrong	306359/9751	16581/2481	713/110	0.23%/1.12%
MUDANPI	359105/11250	53758/7328	2108/291	0.58%/2.58%

Step 1: download raw data from liquid chromatograph; step 2: remove negative data; step 3: find inflexion points and keep one decimal fraction of time data, remove duplicate time data, and redundant no-absorbance data.

to carry out data filtering, and the detailed process can be referred to Figure 1. The processed data would then be saved as the format of text and excel (see Files S2 and S3). The text format will be strung for converting into 2D code, while the excel format will be used to convert into chemical fingerprints.
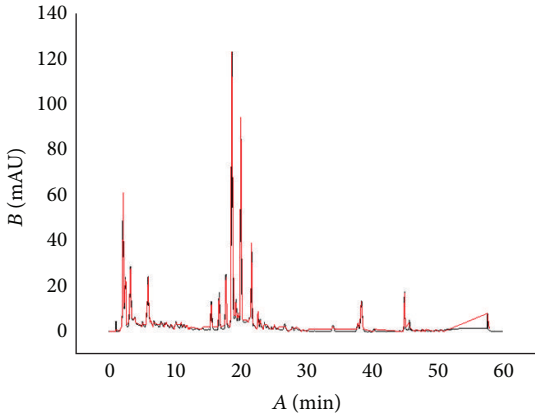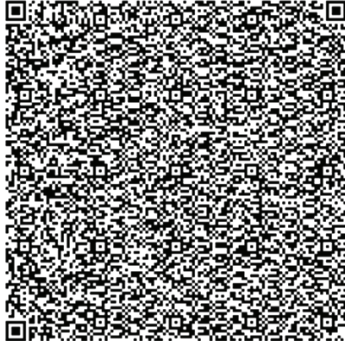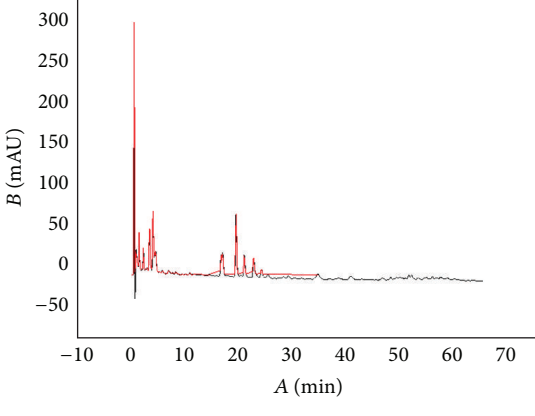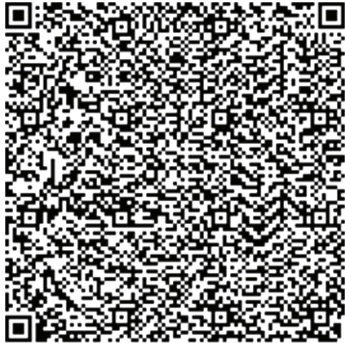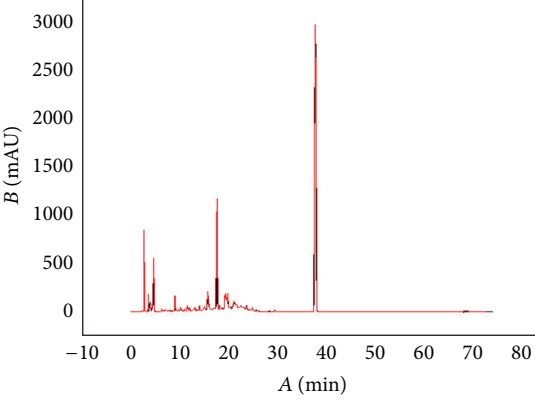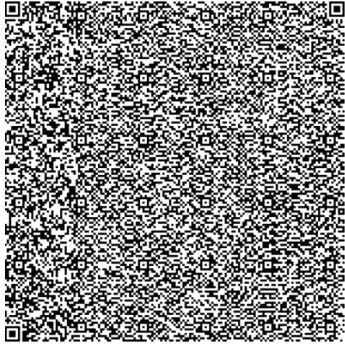
2.3. Selection of Barcode Type and Evaluation of Processed Data. In order to select suitable barcode types for storing data from chemical fingerprints, different 2D barcode types were compared in the aspect of encoding features. Filtered data stored in the excel file were inputted to liquid chromatograph and reanalyzed peak areas to evaluate whether data treatment has a significant influence on corresponding chemical composition content. OriginPro software was used to regenerate the TCM fingerprints. QR Code Generators were used to output 2D barcodes online (http://qrgenerator.qrcreator.net) and the parameters involved are listed as follows: ECC (Error Correcting Code): L-smallest; Size: 2.

3. Results and Discussion

With the development of modern industry of Chinese medicine, demand for Chinese medicinal herbs has grown rapidly over past decades. Although the HPLC technology can make a positive impact on quality control, quality traceability is still hard to implement because chemical fingerprints cannot be easily transported. This study successfully created a way to convert chemical information to barcodes for TCM quality traceability.

Based on the analysis of the test data of three different TCM chemical fingerprints (Figure 1), it was found that the sampling frequency was 0.4 seconds, and the sizes range of dataset was from 200 kilobytes to 370 kilobytes. However, all kinds of barcodes available cannot store such huge data of chemical fingerprints and therefore data filtering is required. After data filtering using Ruby program, the data sizes were from 0.7 kilobyte to 2.8 kilobyte and their main content was numeric characters. Compared to the original data, the compression ratio in terms of length of string is between

TABLE 3: Comparison of chemical fingerprints between raw data and processed data and generated QR Codes.

Sample	Chemical fingerprints from raw data and processed data	QR Code
YinYanghuo		
Roucongrong		
Mudanpi		

0.23% and 0.64%, ranging from 713 to 2323, while the compression ratio in terms of data point is between 1.12% and 2.99%, ranging from 110 to 337 (Table 2). With the algorithm (Figure 1), the dataset of the key inflexion point of the original fingerprint was retained and the data amount is hugely reduced, which created conditions for the generation of 2D barcode. The result from the above experiment shows that the curve after processing was fitted highly with the curve before processing; the main peak time and the peak delay are basically the same (Table 3). In order to test whether data processing has an influence on peak area of chemical fingerprint, we made a comparison between the two peak areas of raw data and processed data. Results showed that there was no significant difference ($P < 0.05$) between them (Table 3), which demonstrated that data standardization in this study can be used for converting chemical information to barcodes for quality traceability.

Barcode has two encoding types, one-dimensional code and two-dimensional code (Tables S1 and S2). The former one can be read with a fast speed and is more commonly used in retailing industries or manufacturing such as commodity packaging and electronic tickets. However one-dimensional code has a smaller data storage capacity (20 bytes) and cannot be used to hold bigger data. The latter one can store more information (2000 bytes) including text, images, fingerprint, and signature in limited space and can be used without the computer. Two-dimensional code becomes more and more popular in recent years. It was found that the size of chemical fingerprint data after filtering was still beyond 2 kilobytes. Such big data are difficult to be converted into barcode directly and they are difficult to be read. In addition, most 2D barcodes can store less than 2 kilobytes. Therefore, the capacity and the compression ratio become the most important filtering criteria in the choice of barcode type. Among all 2D barcodes, Data Matrix, Aztec Code, QR Code, Vericode, PDF 417, PDF 417 Truncated, Codablock F, and Code One meet the criteria. With further analysis to the above eight types of 2D barcodes, QR Code, Data Matrix, and PDF 417 are the most appropriate ones for storing numeric character. Comparative results (Table 1) show that QR Code is far more appropriate than the other two types in terms of storage capacity, identification speed, and readable direction. In addition, reconstructed chemical fingerprints from processed data recommended QR Code as the best 2D barcode for TCM quality traceability (Table 3).

4. Conclusion

The production chain of traditional Chinese medicine includes multiple links. Traceability is very important for guaranteeing TCM quality. This study takes the first step in the combination between quality detection and traceability. It was demonstrated that the data from TCM chemical fingerprints can be converted into 2D barcodes which can be used in the whole TCM industrial process. Similarly, the conversion from data of UV, IR, MS, NMR, and TLC to 2D barcode is also a potential topic for further traceability study. There is further space for improvement of data filtering. TCM

fingerprints from different kinds of detecting devices require data preprocessing. The optimal data algorithm depends on whether the processed data is consistent with the original data and how much space will be required.

Conflict of Interests

The authors declare that there is no conflict of interests regarding the publication of this paper.

Authors' Contribution

Yong Cai and Xiwen Li contributed equally to this work.

References

[1] Y. Jiang, B. David, P. Tu, and Y. Barbin, "Recent analytical approaches in quality control of traditional Chinese medicines—a review," *Analytica Chimica Acta*, vol. 657, no. 1, pp. 9–18, 2010.

[2] F. Gong, Y.-Z. Liang, P.-S. Xie, and F.-T. Chau, "Information theory applied to chromatographic fingerprint of herbal medicine for quality control," *Journal of Chromatography A*, vol. 1002, no. 1-2, pp. 25–40, 2003.

[3] M. Gu, F. Ouyang, and Z. Su, "Comparison of high-speed counter-current chromatography and high-performance liquid chromatography on fingerprinting of Chinese traditional medicine," *Journal of Chromatography A*, vol. 1022, no. 1-2, pp. 139–144, 2004.

[4] T. Kelepouris, K. Pramatari, and G. Doukidis, "RFID-enabled traceability in the food supply chain," *Industrial Management and Data Systems*, vol. 107, no. 2, pp. 183–200, 2007.

[5] U. Barchetti, A. Bucciero, M. de Blasi, L. Mainetti, and L. Patrono, "RFID, EPC and B2B convergence towards an item-level traceability in the pharmaceutical supply chain," in *Proceedings of the IEEE International Conference on RFID-Technology and Applications (RFID-TA '10)*, pp. 194–199, Guangzhou, China, June 2010.

[6] C. Shanahan, B. Kernan, G. Ayalew, K. McDonnell, F. Butler, and S. Ward, "A framework for beef traceability from farm to slaughter using global standards: an Irish perspective," *Computers and Electronics in Agriculture*, vol. 66, no. 1, pp. 62–69, 2009.

[7] S. P. Liu, Y. P. Zhu, and S. J. Li, "Research on agent-based bee product traceability platform and barcode system," in *Computer and Computing Technologies in Agriculture V*, vol. 368 of *IFIP Advances in Information and Communication Technology*, pp. 445–454, Springer, Berlin, Germany, 2012.

[8] J. P. Qian, X. T. Yang, X. M. Wu, L. Zhao, B. L. Fan, and B. Xing, "A traceability system incorporating 2D barcode and RFID technology for wheat flour mills," *Computers and Electronics in Agriculture*, vol. 89, pp. 76–85, 2012.

[9] P. Drašar and J. Moravcova, "Recent advances in analysis of Chinese medical plants and traditional medicines," *Journal of Chromatography B*, vol. 812, no. 1-2, pp. 3–21, 2004.

[10] G. H. Lu, K. Chan, Y. Z. Liang et al., "Development of high-performance liquid chromatographic fingerprints for distinguishing Chinese Angelica from related umbelliferae herbs," *Journal of Chromatography A*, vol. 1073, no. 1-2, pp. 383–392, 2005.

[11] S.-K. Yan, W.-F. Xin, G.-A. Luo, Y.-M. Wang, and Y.-Y. Cheng, "An approach to develop two-dimensional fingerprint for the quality control of Qingkailing injection by high-performance liquid chromatography with diode array detection," *Journal of Chromatography A*, vol. 1090, no. 1-2, pp. 90–97, 2005.

[12] I.-H. Lin, M.-C. Lee, and W.-C. Chuang, "Application of LC/MS and ICP/MS for establishing the fingerprint spectrum of the traditional Chinese medicinal preparation Gan-Lu-Yin," *Journal of Separation Science*, vol. 29, no. 1, pp. 172–179, 2006.

[13] X.-M. Liang, Y. Jin, Y.-P. Wang, G.-W. Jin, Q. Fu, and Y.-S. Xiao, "Qualitative and quantitative analysis in quality control of traditional Chinese medicines," *Journal of Chromatography A*, vol. 1216, no. 11, pp. 2033–2044, 2009.

[14] P.-S. Xie and A. Y. Leung, "Understanding the traditional aspect of Chinese medicine in order to achieve meaningful quality control of Chinese materia medica," *Journal of Chromatography A*, vol. 1216, no. 11, pp. 1933–1940, 2009.

[15] Y. Liang, P. Xie, and F. Chau, "Chromatographic fingerprinting and related chemometric techniques for quality control of traditional Chinese medicines," *Journal of Separation Science*, vol. 33, no. 3, pp. 410–421, 2010.

[16] V. A. Z. Monica Cristine Scherer and V. A. Z. Maria Salete Marcon Gomes, "Information technology applied to the process of traceability in the wheat supply chain," *Afriacan Journal of Agricultural Research*, vol. 9, no. 17, pp. 1318–1325, 2014.

[17] E. G. Poon, C. A. Keohane, C. S. Yoon et al., "Effect of barcode technology on the safety of medication administration," *The New England Journal of Medicine*, vol. 362, no. 18, pp. 1698–1707, 2010.

[18] A. A. Leung, C. R. Denham, T. K. Gandhi et al., "A safe practice standard for barcode technology," *Journal of Patient Safety*, 2014.

[19] A. Wang, "Use of bar-code technology to reduce drug administration errors," *American Medical Association Journal of Ethics*, vol. 3, pp. 167–169, 2011.

[20] B. C. Watson, "Barcode empires: politics, digital technology, and comparative retail firm strategies," *Journal of Industry, Competition and Trade*, vol. 11, no. 3, pp. 309–324, 2011.

[21] L. S. Cai, L. Y. Beng, C. A. Lasuin, T. S. Fun, and C. P. Yee, "Multifunctional barcode inventory system for retailing. Are you ready for it?" *World Academy of Science, Engineering and Technology*, vol. 59, pp. 267–271, 2009.

[22] A. Galimberti, F. de Mattia, A. Losa et al., "DNA barcoding as a new tool for food traceability," *Food Research International*, vol. 50, no. 1, pp. 55–63, 2013.

[23] N. P. Kumar, A. R. Rajavel, and P. Jambulingam, "Application of PDF417 symbology for "DNA Barcoding"," *Computer Methods and Programs in Biomedicine*, vol. 90, no. 2, pp. 187–189, 2008.

[24] C. Liu, L. Shi, X. Xu et al., "DNA barcode goes two-dimensions: DNA QR code web server," *PLoS ONE*, vol. 7, no. 5, Article ID e35146, 2012.

[25] L. Liu, Y. Wang, Q. Song, and Y. P. Bao, "Fingerprint identification system based on two-dimensional barcode and DSP," *Advanced Materials Research*, vol. 479, pp. 2082–2085, 2012.

[26] X. J. Chen, B. L. Guo, S. P. Li, Q. W. Zhang, P. F. Tu, and Y. T. Wang, "Simultaneous determination of 15 flavonoids in *Epimedium* using pressurized liquid extraction and high-performance liquid chromatography," *Journal of Chromatography A*, vol. 1163, no. 1-2, pp. 96–104, 2007.

[27] Y. Jiang, S. P. Li, Y. T. Wang, X. J. Chen, and P. F. Tu, "Differentiation of Herba Cistanches by fingerprint with high-performance liquid chromatography-diode array detection-mass spectrometry," *Journal of Chromatography A*, vol. 1216, no. 11, pp. 2156–2162, 2009.

Research Article

Rapid Identification and Verification of Indirubin-Containing Medicinal Plants

Zhigang Hu,[1,2] Yuan Tu,[1,2] Ye Xia,[1,2] Peipei Cheng,[1] Wei Sun,[2] Yuhua Shi,[2] Licheng Guo,[1,2] Haibo He,[2] Chao Xiong,[1,2] Shilin Chen,[2] and Xiuqiao Zhang[1]

[1]*College of Pharmacy, Hubei University of Chinese Medicine, No. 1 Huangjiahu West Road, Hongshan District, Wuhan 430065, China*
[2]*Institute of Chinese Materia Medica, China Academy of Chinese Medical Sciences, Beijing 100700, China*

Correspondence should be addressed to Shilin Chen; slchen@implad.ac.cn and Xiuqiao Zhang; qiaoxzh2000@163.com

Indirubin, one of the key components of medicinal plants including *Isatis tinctoria, Polygonum tinctorium*, and *Strobilanthes cusia*, possesses great medicinal efficacy in the treatment of chronic myelocytic leukemia (CML). Due to misidentification and similar name, materials containing indirubin and their close relatives frequently fall prey to adulteration. In this study, we selected an internal transcribed spacer 2 (ITS2) for distinguishing these indirubin-containing species from five of their usual adulterants, after assessing identification efficiency of *matK, rbcL, psbA-trnH*, and ITS2 among these species. The results of genetic distances and neighbor-joining (NJ) phylogenetic tree indicated that ITS2 region is a powerful DNA barcode to accurately identify these indirubin-containing species and discriminate them from their adulterants. Additionally, high performance liquid chromatography (HPLC) was used to verify indirubin in different organs of the above species. The results showed that indirubin had been detected in the leaves of *Is. tinctoria, P. tinctorium, S. cusia*, and Indigo Naturalis (made from their mixture), but not in their roots, or in the leaves of their adulterants. Therefore, this study provides a novel and rapid method to identify and verify indirubin-containing medicinal plants for effective natural treatment of CML.

1. Introduction

Chronic myelocytic leukemia (CML) is a malignant cancer that destroys the blood and marrow [1]. In 1967, a group of scientists discovered that the traditional Chinese medicine prescription, Danggui Luhui Wan, which contains 11 Chinese herbal medicines, had a significant curative effect on CML [2, 3]. More recently, indirubin from the Chinese herbal medicine Indigo Naturalis (Qingdai), prepared from the leaves of *Isatis tinctoria*, *Polygonum tinctorium,* and *Strobilanthes cusia*, was found to be the active ingredient [4–11]. Indirubin has since been found in additional Chinese herbal medicines derived from each of these species, respectively, including Isatidis Folium (the leaf of *Is. tinctoria*), Polygoni Tinctorii Folium (the leaf of *P. tinctorium*), and Baphicacanthis Cusiae Rhizoma et Radix (the root and rhizome

of *S. cusia*) [12–14]. However, few studies have determined the presence and containing of indirubin in the above medicinal plants and their adulterants. These adulterants include *P. hydropiper, P. chinense, Clerodendrum cyrtophyllum, Indigofera tinctoria,* and *S. dimorphotricha* (Figure 1) and are extremely difficult to discriminate from their true medicinal counterparts morphologically [15–18]. The confusion between true medicinal plants and their adulterants has adverse effects on the clinical efficacy and safety of traditional medicines. It is thus paramount that traditional medicinal herbs and their active components can be reliably and cost-effectively discriminated from their false counterparts.

In order to achieve the rapid identification and verification of the indirubin-containing medicinal plants, two important problems must be resolved. First, the original plant species known to contain indirubin must be effectively
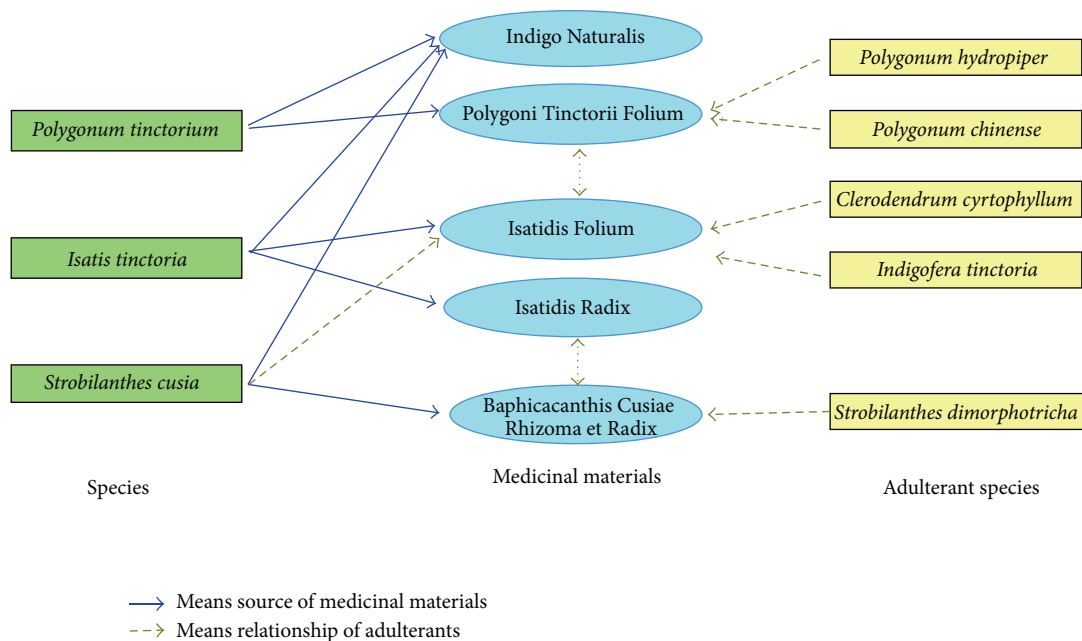
FIGURE 1: The relationship among indirubin-containing medicinal materials (plant organs/formulations), their plants of origin, and adulterants.

discriminated from their adulterants. DNA barcoding technology offers the best technique for this to date, involving specific amplification of a short, standardized DNA fragment with universal primers across multiple samples [19, 20]. In recent years, several candidate DNA regions, such as *matK*, *rbcL*, *psbA-trnH*, and ITS/ITS2, have been assessed for their potential as DNA barcodes in plants [21–25]. Analysis of 50,790 plant ITS2 sequences revealed this region to be highly effective in discriminating medicinal plants and their closely related species [23, 26], more so than *matK*, *rbcL*, and *psbA-trnH*. As such, ITS sequences have been recommended as the core barcode region for seed plants [27]. Here, we reveal the first rapid and effective method to reliably discriminate indirubin-containing species in traditional medicinal formulations from their adulterants, using ITS2 barcoding. Secondly, it is necessary that the different plant organs comprising traditional medicinal materials (Figure 1) can be analysed for indirubin levels effectively. High performance liquid chromatography (HPLC) offers an effective screening technique in this regard.

2. Materials and Methods

2.1. Plant Materials. A total of 57 samples from 8 species were gathered from various geographical areas in China, as detailed in Table 1. All the specimens were carefully visually identified using standard expert identification parameters at the Institute of Medicinal Plant Development (IMPLAD), Chinese Academy of Medical Sciences. The specimens were deposited in the herbarium of the Hubei University of Chinese Medicine.

2.2. DNA Extraction, PCR Amplification, and Sequencing. Samples comprising 30~40 mg of dried leaves or 60~70 mg of roots were crushed into powder in 2 mL microfuge tubes at 30 Hz using stainless steel ball milling for 1 min. Total genomic DNA was extracted using a Plant Genomic DNA Kit (Tiangen Biotech Co., China) with modifications as follows. Initial incubation was at 65°C in 750 μL GP1 (Tiangen) buffer for 1 h for dried leaves or 5 h for roots and rhizomes. The remaining steps followed the manufacturer's protocol.

For *matK*, *rbcL*, *psbA-trnH*, and ITS2 DNA barcodes, universal primers and general PCR reaction conditions were used as presented in Table S1 (see Table S1 in Supplementary Material available online at http://dx.doi.org/10.1155/2015/484670) [23, 28]. PCRs were in a 25 μL reaction mixture, containing 30–100 ng of genomic DNA template, 12.5 μL 2 × Taq PCR Master Mix (Aidlab Biotechnologies Co., China), and 1 μL of forward and reverse primers (2.5 μmol/L). After PCR, a 4 μL aliquot was examined by 0.5% TBE agarose gel electrophoresis, and purified PCR products were sequenced in both directions using the primers used for PCR on an ABI3730XL sequencer (Applied Biosystems Co., USA).

2.3. Cloning and Sequencing of the ITS2 Region. The ITS2 PCR products of *S. cusia* and *S. dimorphotricha* were unsuccessfully directly sequenced. Therefore, purified products (TIANquick Midi Purification Kit; Tiangen Biotech Co., China) were ligated into the pMD18-T vector (Takara Biotech Co., China) and transformed into *E. coli* DH5 cells using standard recombinant DNA techniques. Positive transformants were selected on LB containing 0.1 mg/mL ampicillin and confirmed with colony PCR using the above PCR conditions.

TABLE 1: Detailed description of all the samples in this study.

Species	Medicinal part	Locality	Voucher number	GenBank number of ITS2
Isatis tinctoria	Leaves	Hebei, China	YC0021MT02	KJ939152
Is. tinctoria	Leaves	Anhui, China	YC0021MT09	KJ939157
Is. tinctoria	Leaves	Chongqing, China	YC0021MT10	KJ939158
Is. tinctoria	Leaves	Chongqing, China	YC0021MT12	KJ939159
Is. tinctoria	Leaves	Chongqing, China	YC0021MT13	KJ939160
Is. tinctoria	Leaves	Yunnan, China	YC0021MT14	KJ939161
Is. tinctoria	Leaves	Beijing, China	YC0021MT15	KJ939162
Is. tinctoria	Leaves	Beijing, China	YC0021MT04	KJ939154
Is. tinctoria	Leaves	Beijing, China	YC0021MT05	KJ939155
Is. tinctoria	Leaves	Beijing, China	YC0021MT06	KJ939156
Is. tinctoria	Roots	Sichuan, China	YC0021MT01	KJ939151
Is. tinctoria	Roots	Hebei, China	YC0021MT03	KJ939153
Is. tinctoria	Roots	Beijing, China	YC0021MT20	KJ939163
Is. tinctoria	Roots	Beijing, China	YC0021MT21	KJ939164
Is. tinctoria	Roots	Beijing, China	YC0021MT22	KJ939165
Is. tinctoria	Roots	Beijing, China	YC0021MT23	KJ939166
Is. tinctoria	Roots	Sichuan, China	YC0021MT29	KJ939167
Is. tinctoria	Roots	Hubei, China	YC0021MT30	KJ939168
Polygonum tinctorium	Leaves	Beijing, China	YC0390MT04	KJ939177
P. tinctorium	Leaves	Beijing, China	YC0390MT05	KJ939178
P. tinctorium	Leaves	Beijing, China	YC0390MT01	KJ939174
P. tinctorium	Leaves	Beijing, China	YC0390MT07	KJ939179
P. tinctorium	Leaves	Beijing, China	YC0390MT09	KJ939181
P. tinctorium	Leaves	Fujian, China	PS2901MT01	FJ503014
Strobilanthes cusia	Leaves	Guangdong, China	YC0389MT01	KJ939116-KJ939119
S. cusia	Leaves	Chongqing, China	YC0389MT02	KJ939109-KJ939112
S. cusia	Leaves	Chongqing, China	YC0389MT03	KJ939113-KJ939115
S. cusia	Leaves	Hainan, China	YC0389MT04	KJ939125-KJ939127, KJ939104
S. cusia	Leaves	Yunnan, China	YC0389MT07	KJ939139, KJ939140
S. cusia	Leaves	Yunnan, China	YC0389MT08	KJ939141-KJ939143
S. cusia	Leaves	Guangxi, China	YC0389MT10	KJ939105, KJ939137, KJ939138
S. cusia	Leaves	Fujian, China	YC0389MT11	KJ939133-KJ939136
S. cusia	Leaves	Guangxi, China	YC0389MT12	KJ939120-KJ939122
S. cusia	Leaves	Guangxi, China	YC0389MT13	KJ939123, KJ939124
S. cusia	Roots and rhizomes	Hainan, China	YC0389MT05	KJ939128-KJ939130
S. cusia	Roots and rhizomes	Hainan, China	YC0389MT06	KJ939131, KJ939132
S. cusia	Roots and rhizomes	Guangdong, China	YC0389MT14	KJ939106-KJ939108
Polygonum hydropiper	Leaves	Guangdong, China	YC0509MT01	KJ939169
P. hydropiper	Leaves	Guangdong, China	YC0509MT02	KJ939170
P. hydropiper	Leaves	Guangdong, China	YC0509MT03	KJ939171
P. hydropiper	Leaves	Guangdong, China	YC0509MT04	KJ939172
P. hydropiper	Leaves	Guangdong, China	YC0509MT05	KJ939173
Polygonum chinense	Leaves	Guangxi, China	YC0510MT01	KJ939182
P. chinense	Leaves	Guangxi, China	YC0510MT02	KJ939183
P. chinense	Leaves	Guangdong, China	YC0510MT03	KJ939184
P. chinense	Leaves	Guangdong, China	YC0510MT04	KJ939185
Clerodendrum cyrtophyllum	Leaves	Guangxi, China	YC0508MT01	KJ939144

TABLE 1: Continued.

Species	Medicinal part	Locality	Voucher number	GenBank number of ITS2
C. cyrtophyllum	Leaves	Guangxi, China	YC0508MT02	KJ939145
C. cyrtophyllum	Leaves	Guangxi, China	YC0508MT03	KJ939146
C. cyrtophyllum	Leaves	Guangxi, China	YC0508MT04	KJ939147
Strobilanthes dimorphotricha	Leaves	Guangdong, China	YC0511MT01	KJ939187, KJ939188, KJ939191
S. dimorphotricha	Leaves	Guangdong, China	YC0511MT02	KJ939189, KJ939190
S. dimorphotricha	Leaves	Guizhou, China	YC0511MT03	KJ939192, KJ939193
Indigofera tinctoria	Leaves	Guangxi, China	YC0707MT01	KJ939148
In. tinctoria	Leaves	Guangxi, China	YC0707MT02	KJ939149
In. tinctoria	Leaves	Guangxi, China	YC0707MT03	KJ939150
In. tinctoria	Leaves	Guangxi, China	PS0251MT02	GU217625

Four positive clones from each sample were sequenced on an ABI3730XL sequencer. In total, 40 clones from 13 samples of *S. cusia* and 7 clones from 3 samples of *S. dimorphotricha* (excluding fungal sequences) were obtained.

2.4. Sequence Analyses. Sequence editing and contig assembly were performed using CodonCode Aligner v4.25 (CodonCode Co., USA). The ITS2 region was obtained based on the HMMER annotation method to remove the 5.8S and 28S sections at both ends of the sequences [29]. Obtained DNA sequences were aligned and the intraspecific variation and interspecific divergence calculated by Kimura two-parameter method. Phylogenetic trees were constructed using the Neighbor-Joining method with molecular evolutionary genetics analysis (MEGA) software version 5.0 [30].

2.5. HPLC Analyses. The reference standard of indirubin was purchased from Shanghai Yuanye Bio-Technology Company (HPLC-tested purity >98%). 1.25 mg of indirubin was dissolved in N,N-dimethyl formamide in a 25 mL volumetric flask. Five milliliters of solution was transferred to another 50 mL volumetric flask containing N,N-dimethyl formamide to make a standard stock solution of 5μg/mL indirubin. Two-three replicate samples from each tested plant organ and species were randomly sampled for indirubin content. Specifically, 75 mg of powdered crude materials was sonicated in 10 mL of N,N-dimethyl formamide for 30 min at room temperature and filtered. A 20μL aliquot of the filtrate was applied to a HPLC column (Angilent TC-C$_{18}$, 5.0 μm, 4.6 mm × 250 mm). The optimum separation of HPLC was carried out with a mobile phase composed of methanol-water (75 : 25, v/v) at a flow-rate of 1 mL/min. Peaks were detected at a wavelength and column temperature of 290 nm and 25°C, respectively.

3. Results

3.1. Efficiency of Amplification and Identification for Four Candidate Barcodes. For all eight species tested, 24 samples were selected randomly for amplification efficiency. The efficiency of amplification of *matK, rbcL, psbA-trnH,* and ITS2 was 62.5%, 79.2%, 100%, and 100%, respectively. High-quality bidirectional sequences were obtained for all PCR products. All the GenBank No. were listed in Table S2 and Table 1. Alignment revealed no interspecific divergence between *S. cusia* and *S. dimorphotricha* using both *psbA-trnH* and *rbcL*. In addition, *matK* had low amplification efficiency (62.5%), making this less applicable for barcoding of these species. In comparison with the other barcodes, all 24 samples were successfully classified into eight species using the ITS2 sequence. Therefore, only the ITS2 barcode was used for further analysis.

3.2. Measurement of DNA Divergence for ITS2. Song et al. (2012) used sequence-tagged pyrosequencing and genome-wide analyses to describe intragenomic variations of ITS2 regions from 178 plant species. This study defined "major variants" as any variant whose relative variant abundance (RVA) was greater than 5% [31]. In this study we obtained 40 clones of *S. cusia* and only 2 of them (KJ939104, KJ939105) showed significant differences when compared with the other sequences. The remaining 38 sequences were considered major variants of ITS2 in this paper.

In this study, 86 sequences of ITS2 were obtained from all samples. Two ITS2 sequences (EU196919, JN235085) of *P. tinctorium* were downloaded from GenBank. The sequence length, GC average content, haplotype number and number of variable sites in each species (MEGA 5.0 software) are presented in Table 2. ITS2 sequence length ranged from 191 bp to 263 bp and GC average content ranged from 45.9% to 73.6%. The GC average contents of clones of *S. cusia* (73.6%) and *S. dimorphotricha* (73.0%) were at least 4% greater than those of the other species. Based on the variable sites, *Is. tinctoria, P. tinctorium,* and *S. cusia* were divided into 5, 1, and 15 haplotypes, respectively.

Interspecific and intraspecific distances using Kimura two-parameter method are shown in Table 3. The maximum intraspecific distances of *Is. tinctoria, P. tinctorium,* and *S. cusia* were 0.027, 0.000, and 0.036, respectively, while the minimum interspecific distance was 0.401. Furthermore, the minimum interspecific distances between any one of these

TABLE 2: Sequence characteristics of the related species.

Species/(number of sequences)	Length of ITS2 (bp)	GC average content (%)	Number of haplotypes	Number of variable sites
Is. tinctoria (18)	191	56.7	5	5
P. tinctorium (8)	245	68.2	1	1
S. cusia (38)	230~235	73.6	15	20
P. hydropiper (5)	244	68.9	1	1
P. chinense (4)	263	65.8	1	1
C. cyrtophyllum (4)	224	56.7	1	1
S. dimorphotricha (7)	224~233	73.0	6	13
In. tinctoria (4)	219	45.9	1	1

TABLE 3: Data of interspecific and intraspecific distances of the related species.

Parameter	Range
Intraspecific distances of *Is. tinctoria*	0.000~0.027
Intraspecific distances of *P. tinctorium*	0.000
Intraspecific distances of *S. cusia*	0.000~0.036
Interspecific distance among the above three species	0.401~0.684
Interspecific distance between *Is. tinctoria* and its adulterants	0.514~0.684
Interspecific distance between *P. tinctorium* and its adulterants	0.025~0.755
Interspecific distance between *S. cusia* and its adulterants	0.065~0.931

three species and its adulterants were 0.514, 0.025, and 0.065, respectively.

3.3. Identification of ITS2 Using NJ Tree. Phylogenetic analysis demonstrated that every species clustered into their own clade, supported with at least 81% bootstrapping (Figure 2). In addition, three closely related species of the genus *Polygonum* were strongly supported (99%, 81% and 100% bootstrap, resp.), and clustered into a larger branch with 97% bootstrap. All cloned sequences of *S. cusia* (96% bootstrap) and *S. dimorphotricha* (92% bootstrap) in Acanthaceae family formed a larger group (93% bootstrap).

3.4. Detection of Indirubin in Crude Drugs and Their Adulterants. HPLC detected indirubin in the leaves of *Is. tinctoria, P. tinctorium, S. cusia,* and Indigo Naturalis (Figure 3). Indirubin was not detected in the roots and rhizomes of these three taxa or in the leaves of their adulterants (*P. hydropiper, P. chinense, C. cyrtophyllum, In. tinctoria,* and *S. dimorphotricha*).

4. Discussion

In previous studies, the identification methods of medicinal plants including *Is. tinctoria*, *P. tinctorium,* and *S. cusia* have primarily focused on characterization of morphology, chromatographic fingerprints, and microstructures [32–34]. However, these methods all have their disadvantages. The

recent, rapid development of DNA molecular marker techniques provides a powerful tool for the accurate identification of medicinal materials. In recent years, DNA barcoding has been successfully employed in species identification of medicinal herbs, with the ITS2 barcode exhibiting remarkable stability and accuracy in this field. ITS/ITS2 regions were demonstrated to successfully distinguish Corni Fructus (the flesh of *Cornus officinalis*) from its adulterants [35]. Xin et al. (2013) presented the ITS2 barcode as a powerful tool for tracing Goji (the fruit of *Lycium barbarum*) [36], while it was also used to accurately identify Ephedrae Herba (the stem taken from three species of *Ephedra*) and their closely related species [37]. Consequently, the rapidly developing DNA barcoding can effectively supplement the traditional identification methods. In this study, the ITS2 region was selected from four candidate barcodes to identify three species and their adulterants because of 100% amplification efficiency herein, high interspecific divergence, and low intraspecific variation. Based on the ITS2 barcode, the maximum intraspecific distance of the three species (*Is. tinctoria, P. tinctorium* and *S. cusia*) was less than the minimum interspecific distance, not only among the three species, but also among each species and its adulterants. Furthermore, the NJ tree indicated that *Is. tinctoria, P. tinctorium,* and *S. cusia* were clustered into their own monophyletic group, separated from the other species. Moreover, NJ tree analysis using ITS2 reliably distinguished individuals of the genus *Polygonum* and the family of Acanthaceae, supporting the powerful identification ability of ITS2 barcode in plants.
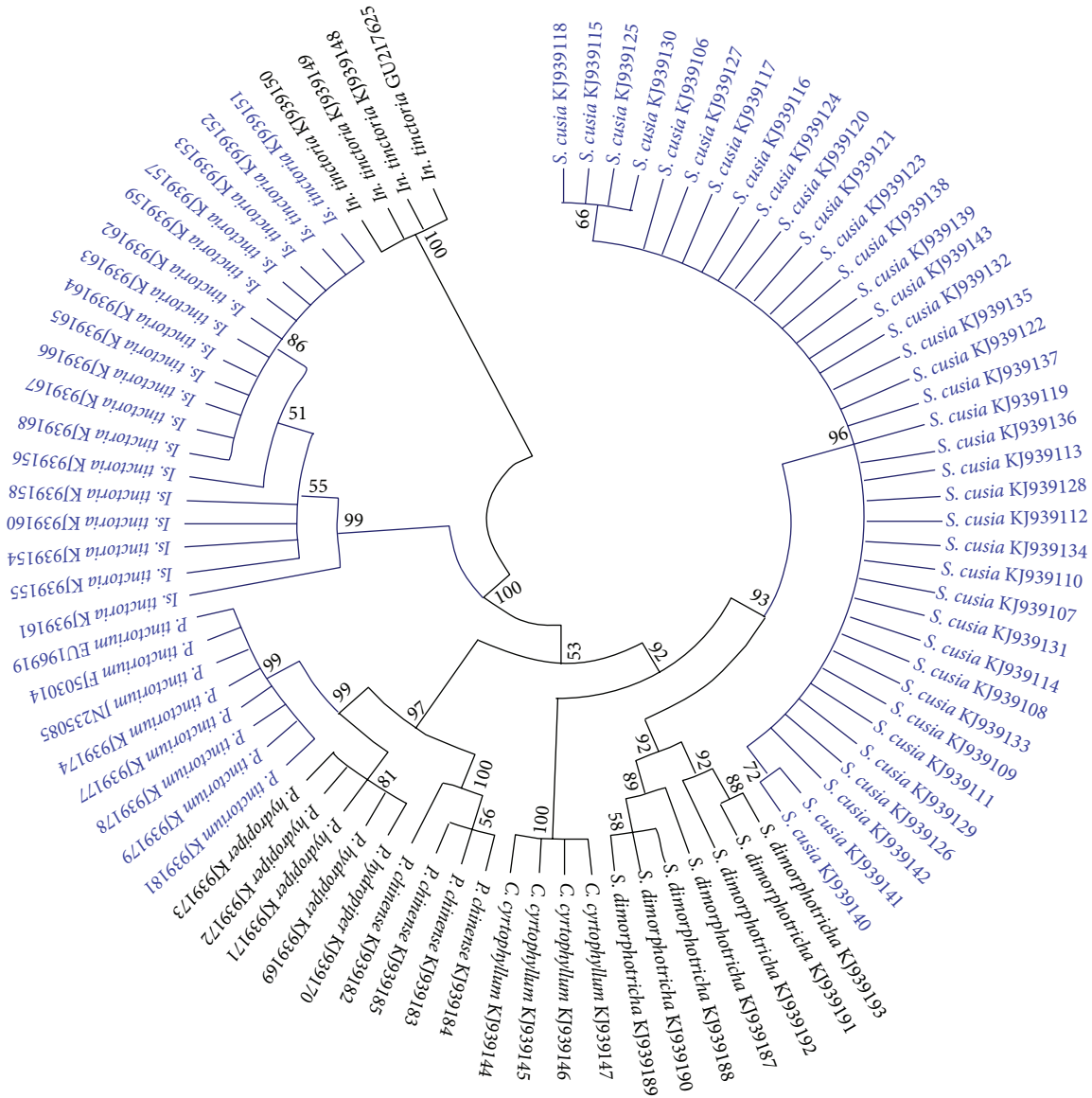
FIGURE 2: Phylogenetic tree of all the medicinal plants containing indirubin and their adulterants constructed with the ITS2 sequences using NJ method (Bootstrap scores ≥50%). The samples marked with blue represent the medicinal plants containing indirubin, and the others represent their adulterants.

Therefore, both the results of nearest distance method and NJ tree strongly support that ITS2 as DNA barcode can successfully distinguish *Is. tinctoria, P. tinctorium,* and *S. cusia* from each other and from their respective adulterants.

The demonstrated anticancer function of indirubin in the treatment of Chronic myelocytic leukemia (CML), warrants its further investigation and ability to be identified accurately in natural medicines. In this study, HPLC detection found that indirubin could only be detected in the leaves of *Is. tinctoria, P. tinctorium, S. cusia* and Indigo Naturalis. Meanwhile it could not be found in the root tissues of these species, or in the adulterant species tested herein. These results confirm that *Is. tinctoria, P. tinctorium,* and *S. cusia* cannot be replaced by their adulterants as indirubin-containing tinctures. And

not only that, the species used for traditional medicinal herbs can be extremely disordered because of a general divergence in regional customs and species identification abilities [38]. All of these strongly supported the need for accurate discrimination of these ineffective false "pseudo"-medicines.

5. Conclusion

Together with HPLC detection of indirubin in various organs, ITS2 DNA barcoding enables the rapid, efficient, and cost-effective discrimination of the truly effective preparations of medicinal plants from their noneffective organs and adulterants that do not contain indirubin. This provides an efficient
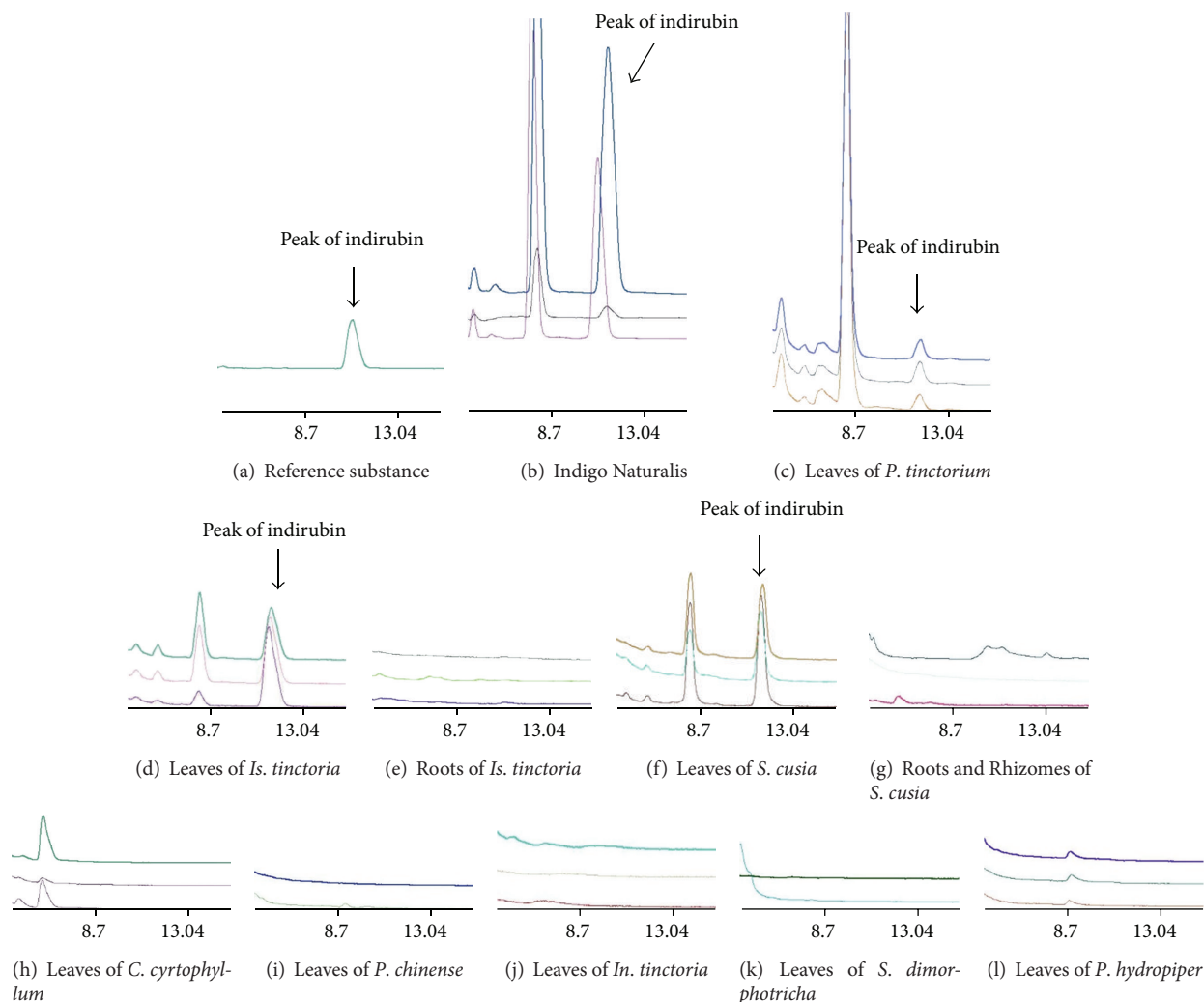
FIGURE 3: HPLC profiles of N,N-dimethyl formamide extract prepared from different organs of medicinal plants and five of their usual adulterants. Each profile was made up of two-three replicate samples from each tested plant organ and species.

and new method to verify indirubin-containing medicines for the natural treatment of CML.

Conflict of Interests

All the authors declare that there is no conflict of interests regarding the publication of this paper.

Authors' Contribution

Zhigang Hu and Yuan Tu were equal contributors to this paper.

Acknowledgments

References

[1] H. M. Kantarjian, A. Deisseroth, R. Kurzrock, Z. Estrov, and M. Talpaz, "Chronic myelogenous leukemia: a concise update," *Blood*, vol. 82, no. 3, pp. 691–703, 1993.

[2] The Sixth Groups of Chinese Academy of Medical Sciences, "The study on anti-leukemia of Dang Gui Lu Hui Wan," *Bulletin of Medical Research*, no. 7, pp. 28–30, 1975.

[3] R. Hoessel, S. Leclerc, J. A. Endicott et al., "Indirubin, the active constituent of a Chinese antileukaemia medicine, inhibits cyclin-dependent kinases," *Nature Cell Biology*, vol. 1, no. 1, pp. 60–67, 1999.

[4] S. Nam, R. Buettner, J. Turkson et al., "Indirubin derivatives inhibit Stat3 signaling and induce apoptosis in human cancer cells," *Proceedings of the National Academy of Sciences of the United States of America*, vol. 102, no. 17, pp. 5998–6003, 2005.

[5] M. Z. Ma, "The observation on curative effect of treating chronic myelogenous leukemia of Indigo Naturalis," *Chinese Journal of Medicine*, vol. 4, pp. 22–25, 1979.

[6] G. Y. Wu, F. D. Fang, J. Z. Liu et al., "Research on the principle using indigo for the curative effect of chronic myelogenous leukemia (1): the influence on the DNA, RNA and protein synthesis of peripheral leukemia cells to the person," *National Medical Journal of China*, vol. 60, no. 8, pp. 451–454, 1980.

[7] G. Y. Wu, J. Z. Liu, D. F. Fang, and J. Zuo, "Research on the principle using indigo for the curative effect of chronic myelogenous leukemia: identification on the function and bond types of the combination of indigo and DNA," *Science in China B*, no. 5, pp. 436–443, 1982.

[8] Z. Xiao, Y. Hao, B. Liu, and L. Qian, "Indirubin and Meisoindigo in the treatment of chronic myelogenous leukemia in China," *Leukemia & Lymphoma*, vol. 43, no. 9, pp. 1763–1768, 2002.

[9] D. Marko, S. Schätzle, A. Friedel et al., "Inhibition of cyclin-dependent kinase 1 (CDK1) by indirubin derivatives in human tumour cells," *British Journal of Cancer*, vol. 84, no. 2, pp. 283–289, 2001.

[10] Q. W. Wu, Z. L. Ge, Y. Gao, and L. Zhang, "Inhibitory effect of indirubin on growth of some cancer cells and its mechanism," *Tianjin Journal of Traditional Chinese Medicine*, vol. 25, no. 1, pp. 55–58, 2008.

[11] J. Liu, C. Zeng, L. P. Hu, and H. C. Chen, "Mechanism of proliferative inhibition of indirubin on K562 cells," *Guiding Journal of Traditional Chinese Medicine and Pharmacy*, vol. 15, no. 2, pp. 10–12, 2009.

[12] H.-C. Hou and S.-Z. Liang, "Determination of indirubin and indigo in *Baphicacanthus cusia* (Nees) Bremek by HPLC," *Journal of Chinese Medicinal Materials*, vol. 29, no. 7, pp. 681–682, 2006.

[13] Y. X. Zhan, Q. Fu, R. Duan et al., "Study on determination of indigo and indirubin contents and HPLC fingerprints of Isatidis Folium from various sources," *Modern Chinese Medicine*, vol. 13, no. 6, pp. 20–23, 2011.

[14] Chinese Pharmacopoeia Commission, *Pharmacopoeia of the People's Republic of China*, vol. 1, Chinese Medical Science and Technology Press, Beijing, China, 2010.

[15] Z. Y. Sun, H. M. Luo, and S. L. Chen, "Molecular identification of Isatidis Folium and its adulterants by ITS2 sequences," *World Science and Technology /Modernization of Traditional Chinese Medicine and Materia Medica*, vol. 13, no. 2, pp. 395–399, 2011.

[16] B.-Z. He, J.-J. Qin, Y.-L. Zhu, and Y.-K. Liao, "Identification characters of leaf morphological and venation pattern of *Baphicacanthus cusia* with its confused herb *Clerodendrum cyrtophyllum*," *Journal of Chinese medicinal materials*, vol. 35, no. 3, pp. 385–391, 2012.

[17] G. Q. Li, Z. T. Wang, X. B. Li, and G. J. Xu, "Determination of nrDNA ITS sequence of Liaodaqingye (Folium Polygoni Tinctorii) and its counterfeit," *Chinese Wild Plant Resources*, vol. 20, no. 3, pp. 43–46, 2001.

[18] H. Xu, R. Z. Du, P. M. Yang, Y. Zeng, P. J. Chu, and Z. L. Shi, "Identification of Baphicacanthis Cusiae Rhizoma et Radix and its adulterants," *Research and Practice of Chinese Medicines*, vol. 17, no. 6, pp. 54–55, 2003.

[19] P. D. N. Hebert, A. Cywinska, S. L. Ball, and J. R. Waard, "Biological identifications through DNA barcodes," *Proceedings of the Royal Society B: Biological Sciences*, vol. 270, no. 1512, pp. 313–321, 2003.

[20] R. Lahaye, M. Van Der Bank, D. Bogarin et al., "DNA barcoding the floras of biodiversity hotspots," *Proceedings of the National Academy of Sciences of the United States of America*, vol. 105, no. 8, pp. 2923–2928, 2008.

[21] M. W. Chase, N. Salamin, M. Wilkinson et al., "Land plants and DNA barcodes: short-term and long-term goals," *Philosophical Transactions of the Royal Society B: Biological Sciences*, vol. 360, no. 1462, pp. 1889–1895, 2005.

[22] CBOL Plant Working Group, "A DNA barcode for land plants," *Proceedings of the National Academy of Sciences of the United States of America*, vol. 106, no. 31, pp. 12794–12797, 2009.

[23] S. Chen, H. Yao, J. Han et al., "Validation of the ITS2 region as a novel DNA barcode for identifying medicinal plant species," *PLoS ONE*, vol. 5, no. 1, Article ID e8613, 2010.

[24] D. Hou, J. Song, L. Shi et al., "Stability and accuracy assessment of identification of traditional chinese materia medica using DNA barcoding: a case study on Flos Lonicerae Japonicae," *BioMed Research International*, vol. 2013, Article ID 549037, 8 pages, 2013.

[25] X. W. Li, Y. Yang, R. J. Henry, M. Rossetto, Y. T. Wang, and S. L. Chen, "Plant DNA barcoding: from gene to genome," *Biological Reviews*, 2014.

[26] H. Yao, J. Song, C. Liu et al., "Use of ITS2 region as the universal DNA barcode for plants and animals," *PLoS ONE*, vol. 5, no. 10, Article ID e13102, 2010.

[27] D.-Z. Li, L.-M. Gao, H.-T. Li et al., "Comparative analysis of a large dataset indicates that internal transcribed spacer (ITS) should be incorporated into the core barcode for seed plants," *Proceedings of the National Academy of Sciences of the United States of America*, vol. 108, no. 49, pp. 19641–19646, 2011.

[28] S. L. Chen, *Molecular Identification of Chinese Materia Medica Using DNA Barcodes*, People's Publishing House, Beijing, China, 2010.

[29] A. Keller, T. Schleicher, J. Schultz, T. Müller, T. Dandekar, and M. Wolf, "5.8S–28S rRNA interaction and HMM-based ITS2 annotation," *Gene*, vol. 430, no. 1-2, pp. 50–57, 2009.

[30] K. Tamura, D. Peterson, N. Peterson, G. Stecher, M. Nei, and S. Kumar, "MEGA5: molecular evolutionary genetics analysis using maximum likelihood, evolutionary distance, and maximum parsimony methods," *Molecular Biology and Evolution*, vol. 28, no. 10, pp. 2731–2739, 2011.

[31] J. Song, L. Shi, D. Li et al., "Extensive pyrosequencing reveals frequent intra-genomic variations of internal transcribed spacer regions of nuclear ribosomal DNA," *PLoS ONE*, vol. 7, no. 8, Article ID e43971, 2012.

[32] P. Zou, Y. Hong, and H. L. Koh, "Chemical fingerprinting of *Isatis indigotica* root by RP-HPLC and hierarchical clustering analysis," *Journal of Pharmaceutical and Biomedical Analysis*, vol. 38, no. 3, pp. 514–520, 2005.

[33] Y. Shi, Z. Xie, R. Wang, S. Huang, Y. Li, and Z. Wang, "Chromatographic fingerprint study on water-soluble extracts of radix isatidis, folium isatidis, and their preparations by HPLC-DAD technique," *Journal of Liquid Chromatography and Related Technologies*, vol. 36, no. 1, pp. 80–93, 2012.

[34] S. Nie, Y. Zu, L. Zhang, and Y. Pei, "A comparative study on microstructure between *Isatis indigotica* Fort. and *Baphicacanthus cusia* (Nees) Bremek," *Agricultural Science & Technology—Hunan*, vol. 13, no. 4, pp. 763–826, 2012.

[35] D.-Y. Hou, J.-Y. Song, H. Yao et al., "Molecular identification of *Corni fructus* and its adulterants by ITS/ITS2 sequences," *Chinese Journal of Natural Medicines*, vol. 11, no. 2, pp. 121–127, 2013.

[36] T. Y. Xin, H. Yao, H. H. Gao et al., "Super food *Lycium barbarum* (Solanaceae) traceability via an internal transcribed spacer 2 barcode," *Food Research International*, vol. 54, no. 2, pp. 1699–1704, 2013.

[37] X. H. Pang, J. Y. Song, H. B. Xu, and H. Yao, "Using ITS2 barcode to identify *Ephedrae herba*," *China Journal of Chinese Materia Medica*, vol. 37, no. 8, pp. 1118–1121, 2012.

[38] Z. Zhao, J. P. S. Yuen, J. Wu, T. Yu, and W. Huang, "A systematic study on confused species of Chinese materia medica in the Hong Kong market," *Annals of the Academy of Medicine Singapore*, vol. 35, no. 11, pp. 764–769, 2006.

Review Article

Sustainable Utilization of Traditional Chinese Medicine Resources: Systematic Evaluation on Different Production Modes

Xiwen Li,[1,2] Yuning Chen,[3] Yunfeng Lai,[3] Qing Yang,[4] Hao Hu,[3] and Yitao Wang[3]

[1] Research Center for Pharmacognosy, Institute of Chinese Materia Medica, China Academy of Chinese Medical Sciences, Beijing 100700, China
[2] Institute of Medicinal Plant Development, Chinese Academy of Medical Sciences, Peking Union Medical College, Beijing 100193, China
[3] State Key Laboratory of Quality Research in Chinese Medicine, Institute of Chinese Medical Sciences, University of Macau, Macau
[4] State Key Laboratory of Hydraulics and Mountain River Engineering, Sichuan University, Chengdu 610065, China

Correspondence should be addressed to Qing Yang; youngking411@126.com and Hao Hu; haohu@umac.mo

The usage amount of medicinal plant rapidly increased along with the development of traditional Chinese medicine industry. The higher market demand and the shortage of wild herbal resources enforce us to carry out large-scale introduction and cultivation. Herbal cultivation can ease current contradiction between medicinal resources supply and demand while they bring new problems such as pesticide residues and plant disease and pests. Researchers have recently placed high hopes on the application of natural fostering, a new method incorporated herbal production and diversity protecting practically, which can solve the problems brought by artificial cultivation. However no modes can solve all problems existing in current herbal production. This study evaluated different production modes including cultivation, natural fostering, and wild collection to guide the traditional Chinese medicine production for sustainable utilization of herbal resources.

1. Introduction

Traditional Chinese medicine (TCM) recently is widely accepted by patients and attracting more and more attention of researchers with the change of disease modes and the rise of "return to nature" in the world. Currently 45% of all countries (regions) in the world are using TCM, and the global trade of TCM has reached 40 billion USD a year, with an increasing rate of 10% per year [1]. China exported 25% of the global demand of TCM while 75% of which was raw materials [2]. Currently, a total of 80% of TCM are from continuous wild collection without scientific plans [3]. The natural reserves can hardly meet the rapidly increasing demand. At the same time, the wild herbal resources are quickly decreasing by 30% every year. Consequently 80% of the most usually used species cannot meet medical demand [4]. Data analysis showed that 1,800–2,100 medicinal species were facing the challenge of extinction in China [5]. Even

though some of the wild herbs can recover naturally within 3–5 years, the recovery speed falls much behind the one of the rising demand. As a result, TCM resources are facing more and more challenges of sustainable utilization.

Long-term sustainable utilization of TCM resources should combine market demand of raw materials, ecological stability, and social benefits [6]. Currently cultivation and natural fostering were the main production modes to ease contradictions between the decrease of natural reserves and the increase of market demand of wild medicinal resources [7]. Cultivation can be implemented in a large scale and is an efficient method to rapidly provide sufficient urgent raw medicinal materials compared with other methods. However cultivation requires massive cultivated land and plant disease and pests, heavy metal and pesticide residue are the major obstacles to limit its application to all medicinal plants. Moreover the quality of its output (raw materials) sometimes cannot satisfy the clinical criteria. Natural fostering, also

TABLE 1: The yield of mostly used Chinese materia medica through wild collection.

Materia medica	Output (10^7 kg)	Main producing areas	Reference
Huzhang	1	Huaihua, Jingmen	[43]
Jixueteng	0.5–1	Lincang, Simao, Dehong, Yulin	[43]
Yimucao	0.5–1	Tanghe, Zaoyang, Huxian	[43]
Lianqiao	0.6	Lushi, Yuncheng, Xinjiang	[44]
Caihu	0.6	Li and Dangchang in Gansu Province; Chengcheng and Wenxi in Shanxi Province	[45]
Chonglou	0.3	Qujing, Dali, Lijiang, Yuxi, Zhaotong, Chuxiong	[46]
Changzhou	0.28–0.3	Acheng, Wuchang, Bingxian, Huadian, Tonghua, Yongji	[47]
Duyiwei	0.25	Gannan, Yushu; Yunnan, Sichuan; and Tibet Province	[36]
Guanfangfeng	0.15	Heilongjiang, Jilin, Liaoning Province, Inner Mongolia, Hebei, and Shandong Province	[48]
Baiji	0.85	Anlong, Xingyi, Duyun, Neijiang, Wenjiang	[49]

named as wild nursery or semi-imitational cultivation, is a new kind of herb production method. It can combine economic benefit and diversity protecting practically and can solve the problem between subsistence and biodiversity conservation effectively. In China emphasis is given to natural fostering which aims to maintain and recover viable populations of wild species in nature. But it has still limitations such as the long-time process and low output, which cannot meet the rapid increase of market demand in short term. Though wild collection, natural fostering, and cultivation own advantages in yielding raw medicinal materials, they cannot completely solve the current problem of herbal resource sustainable utilization alone. How to choose production mode depends on natural reserves, usage amount, and biological characteristics of medicinal plant species. This study performs a systematic evaluation on these three production modes in different dimensions including current application status, technological challenges, input-output ratio, and ecological impact. In addition, we present illustrations to indicate the characteristics of each method, which can practically guide the selection of TCM production modes for resource sustainable utilization.

2. Current Status of Different Production Modes

2.1. Wild Collection. TCM resources mean the healing herbal materials. According to the statistics, there are 11,146 medicinal plants species, belonging to 383 families, and 2,313 genera [8]. The herbal geographical distribution covers different longitude, latitude, and altitude in China. Different ecological habitat causes different genuine medicinal materials. Nowadays there were 100,000 traditional Chinese medicine prescriptions and these prescriptions used 700 Chinese herbal species, 80% of which comes from wild collection [9] such as *Polygonum cuspidatum*, *Leonurus japonicus*, *Forsythia suspensa,* and *Bupleurum chinense*. Table 1 summarizes the mostly used Chinese herbs that need wild collection. Due to the finite herbal storage, the increasing demand, and the harsh living conditions, the output of wild herb collection is reducing every year.

Even though the Chinese government has started to improve ecological environment to protect the Chinese herbal habitat, the increasing demand of the whole world market still makes a great deal of medicinal plants face the possible extinction. The problems including the lack of wild herbal collecting plan, biomes' destruction, and degraded ecologic environment are becoming more and more serious. Some famous wild herbs, such as *Cordyceps sinensis*, *Dendrobium officinale*, *Fritillaria cirrhosa,* and *Saussurea involucrata*, are becoming more and more difficult to be found in wild habitat. Although some medicinal plants have been successfully cultivated, their wild species can still no longer be found within the latest decades of years, just like *ginseng*, *notoginseng*, and *Gastrodiae*. It would lead to great obstacles in future when these genuine medicinal plants need to be selected from wild resources for breeding.

The main reasons that endanger the wild Chinese herbal resources are the following. Firstly, the national and international market demand is boosting. There are 1.35 billion people in China in 2014. This is a huge consumption group. Besides, Chinese herbal trade has extended to 120 countries in the world market. The herbal varieties have reached 500 species and mainly were transported abroad as raw materials [10]. Secondly, the worsening global climate and Chinese ecological environment are threatening medicinal plant habitat. In the past 30 years the rapid industrialization of China caused a huge pressure to wild environment. The changing environment lowered the recovery speed of wild herbal plants. Some herbal plants even cannot be recovered at all because of the damage of their natural environment. Thirdly, wild collection was not scientifically carried out. In China the people who work on wild herb collection are almost the peoples with a low education level. Most of them have little knowledge on herbal sustainable utilization. They tended to follow their own habit and economic motivation to collect wild herbs, which caused that some herbs and their habitats were destroyed destructively. For example, digging a wild licorice has to destroy accompanying plants of 10 m^2. And digging up wild plants of *Ephedra* species destroyed $3,200 \text{ hm}^2$ meadow every year [11]. Therefore current wild collection cannot guarantee the sustainable development of Chinese herbal resources.

2.2. Natural Fostering. Natural fostering mainly focuses on increasing the number of herbal population to provide raw

TABLE 2: Main Chinese materia medica under natural fostering in China.

Chinese herb	Location	Area (km^2)	Reference
Chuanbeimu	Kangding	20	[50]
Gancao	Yanchi, Lingwu, Tongxin, Taole	49	[51]
Huanglian	Fugong district in Nujiang	1	[14]
Mahuang	Inner Mongolia Alukerqin	1000	[52]
Wuweizi	Qingyuan, Xinbin, Fengcheng	32	[53]
Luobuma	Bazhou in Xinjiang Province	—	[54]
Ciwujia	Cuiluan district in Yichun city	—	[55]
Huangqi	Along the Golmud section of the Qinghai-Tibet Railway to Amdo	—	[56]
Shizhushen	Kuandian district in Dandong	0.2	[57]
Zhuling	Neiqiu County	—	[58]
Yinyanghuo	Leishan, Xiuwen and Longli County	27	[59]
Jinlianhua	Weichang County in Hebei Province	20	[60]
Bajiaolian	Nanchuan, Chongqing	—	[61]
Tangbanxia	Tanghe County	1.25	[62]
Lianqiao	Zhongtiao Mountain	6.7	[44]
Xuelian	Yili city	0.02	[63]
Roucongrong	Hetian in Xinjiang Province	129	[64]
Zhongjiefeng	Guangzhou	—	[65]

medicinal materials. This method should be implemented in original habitats, which is different from artificial cultivation. Natural fostering can effectively combine medicinal plant production and economic benefit. It can increase the recovery ratio of original population. Finally, it does not change the basic community trait of original habitat. Therefore, natural fostering unites industrialized production of TCM and ecological protection. Natural fostering has been carried out in many Chinese herbs, such as *Fritillaria cirrhosa*, *F. unibracteata*, *Glycyrrhiza uralensis*, *G. inflate*, *G. glabra*, *Panax ginseng*, *Ephedra sinica*, *E. intermedia*, *Coptis chinensis*, *C. deltoidea*, *C. teeta*, *Gastrodia elata*, *Saussurea involucrata*, and *Cordyceps sinensis*. Practice proved it to be a pragmatic way to produce TCM materials and conserve biological diversity.

Natural fostering is mostly suitable for such herbs. Firstly, their original habitats are special and cultivation cost is very high. Secondly, their commercial characters and quality have great variations after being cultivated. Thirdly, their wild distribution areas are concentrated and great achievement of production will be made by natural fostering.

Natural fostering is an innovative method for Chinese herbal production. More than 19 Chinese herbs have been used to produce raw materials through natural fostering (Table 2) and among which 12 herbs have realized large-scale production. The key advantage of natural fostering is that the herbal quality from its output is very close to that from wild collection. For example, the polysaccharide content of wild *Ranunculus ternatus* was 14.1% and 10% from natural fostering. However the content of total amino acids of *Ranunculus ternatus* was 2-3% higher from natural fostering than from wild collection [12]. But they almost had the same kinds of amino acids. Similarly, wild *Cordyceps sinensis* had the same varieties of amino acids as that from natural fostering and both of their adenosine contents are

more than 0.1 mg/g, which meet the quality requirement of Chinese Pharmacopoeia [13]. The profit motivation was the main drive to prompt peasants to implement natural fostering of medicinal plants. For example, the income from fostering *Coptis* was 15 times higher than the one from planting crops [14].

Natural fostering is a promising herbal producing method which is a combination of wild collection and cultivation [6]. But its technology is still not mature and the germ plasm for natural fostering has not been identified completely. The production scale is not as large as artificial cultivation and stays at the primary phrase. Although there were numbers of experimental project of natural fostering in China, they were limited by the weakness of basic studies and long-term process. The success of natural fostering also depends on the further study of specie characteristics.

2.3. Cultivation. Herbal cultivation is one of the most effective methods which can not only satisfy market demand but also release the ecological pressure caused by wild collection. In China, the area of herbal cultivation has increased from 400,000 hm^2 in 1950s to current 9,330,000 hm^2. There were altogether 200 herbs that can be artificially cultivated, 100 of which have achieved large-scale cultivation including *Eucommia ulmoides*, *Magnolia officinalis*, *Bupleurum chinense*, and *Platycodon grandiflorum* [15]. The output of herbal production by cultivation has reached 400,000 tons per year. The yield of 200 usually used Chinese herbal medicine from cultivation accounted for more than 60% of the whole market demand per year in China. In particular some herbs such as *ginseng* and *notoginseng* were provided absolutely by cultivation. More and more companies are beginning to recognize the supply crisis of raw medicinal materials, and the Good Agriculture Practice (GAP) was implemented widely.

Table 3: Main Chinese materia medica under cultivation.

Chinese materia medica	Main producing area	Area (km^2)
Dangshen	Linchuan	3.3
Danshen	Shangluo, Fangcheng, Zhongjiang, Linqi	51
Panax pseudoginseng	Wenshan	67
Banlangen	Fuyang, Daqing	40
American ginseng	Jingyu	10
Panax ginseng	Jingyu, Fusong, Ji'an	10
Coptis	Shizhu, Zhenping, Enshi city	45
Huajuhong	Huazhou	10
Xuanshen	Zhenping	7
Changzhou	Luotian	2
Touhualiao	Shibing	20
Ginkgo	Chongming, Pizhou	24
Jinyinhua	Pingyi, Fengqiu	12
Tiepishihu	Wuyi, Tiantai, Xinshuangbannan	6
Chuanxiong	Pengzhou	67
Dihuang	Wushe	200
Fuzi	Jiangyou	2
Shanmaidong	Quanzhou	5
Chuanxinlian	Qingyuan	3
Dengzhanhua	Luxi	7
Chuanbei	Songpan and Mao County	2
Shanzhuyu	Xixia County	147
Yanhusuo	Fuzhou in Jiangxi province	24
Kushen	Changzhi	67
Longdan	Qingyuan	13

Table 3 summarized the main artificially cultivated herbal species.

TCM cultivation not only provides raw medicinal materials but also brings additional essential problems such as excessive heavy metal and pesticide residues. Although the number of herbs which can be cultivated is increasing, artificial breeding has been carried out on only 20 kinds of herbs [16]. The degeneration of germ plasm leads to plant diseases and insect pests and significant output reduction. It was estimated that the planting area in 2008 decreased by 40% compared with the area in 2002. Plant diseases and insect pests were one of the main reasons [17, 18]. Another problem of herbal planting was the lack of scientific design due to profit issues. When planting fruits, crops, and economic forest can bring more income than planting herbs, farmers will give up herbal cultivation. For example, the scale of *Polygonum multiflorum* in 1977 had reached 453.3 hm^2 in Deqing County in Guangdong Province while the planting area decreased by 90% in 2012 because planting citrus and other fruits can bring more income.

Although herbal cultivation can increase production and economic profit rapidly in single population, it is not a sustainable way for the development of herbal resources. Compared with crop cultivation which aims to get the first metabolite (protein, fat, sugar, etc.) of the plants, the main purpose of herbal production is to produce the secondary metabolites (such as alkaloids, saponins, terpenes). Herbal cultivation goes against plant natural growing regularity by escaping from community environment. It is suggested that improving cropping ratio and intercropping ratio may be able to solve the current problems in herbal cultivation.

3. Technological Challenges

3.1. Wild Collection. The key technological points of wild collection include collection methods, transportation, species identification, and collecting period. Among these factors, one of the most crucial technological difficulties is collection method. We should carefully design collection method to avoid possible damage on surrounding plants. At the same time, another difficulty of wild collection is transportation. The original distribution of wild medicinal plants is usually located in remote mountainous areas with poor establishments whose inconvenient traffic and poor information systems make it challenged to transport the wild collected herbs [7]. For example, wild liquorice, ephedra, and *Cistanche* mainly distribute in desert areas and are difficult to be transported. Moreover, long transportation process may also have influence on the quality of Chinese materia medica.

3.2. Cultivation. Germ plasm selection, breeding, fertilization, and prevention of diseases and insect pests should be paid more attention to in herbal cultivation.

3.2.1. Fertilization. Currently few basic studies on agrology of TCM were systematically carried out. We still do not know much about suitable soil conditions, balanced fertilization technology, and the relationship between soil environment and herbal intrinsic quality [19]. Fortunately, the varied soil conditions are being gradually recognized. Researchers found that, in the 29 cultivation areas of *Paris polyphylla* Smith var. *yunnanensis* in nine cities of Yunnan Province, the nutritional soil status was extremely uneven. Soil nitrogen in eight of these cultivated areas was below the normal level, which would affect herbal growth and output in the next year. The absorption of phosphorus and potassium was also influenced. The pH value of four cultivation areas was beyond the optimal growth range (4.5 to 6.3) [20]. People gradually realized that the rhizome of some herbs has the ability to enrich heavy metal elements. Even though the content of heavy metals was in a low level in soil, the actual amount of heavy metal in herbal materials still exceeded the standard. Han et al. found that the average content of copper, lead, arsenic, cadmium, and mercury exceeded the standard 21.0%, 12.0%, 9.7%, 28.5%, and 6.9%, respectively, after analyzing 312 kinds of Chinese herbs [21].

3.2.2. Pest Prevention. The basic researches on pest prevention of Chinese herbal species remained limited until recently.

The studies on the relationship among soil herbs and germ, as well as the physiological, biochemical, and molecular mechanic researches, were also in infancy. Because there are many differences between Chinese herbal species and crops including growth habit, stress resistance, and main target products, Chinese herbal cultivation cannot just apply the techniques used in ordinary crops completely. According to an investigation analyzing 300 kinds of Chinese herbal materia medica, the majority of the samples had residue of organic chlorine pesticides which can lead to hepatomegaly, degeneration of liver cell, damage of central nervous system, and bone marrow [22].

3.2.3. Seed Selecting and Breeding. Improper selection of original herbal species will lead to species confusion and reduction of diversity. For example, seeds from all kinds of *Cannabis* can be used as Huomaren materia medica, which causes the confusion of Huomaren germ plasm. Due to the divergence of stress resistance and growth habit, it is great difficult to introduce and cultivate *Cannabis sativa* according to the same protocol [23]. The most difficulty to select medicinal varieties was the intraspecies variation. Different classifications were divided according to the variation including subspecies, variety, and variant, which caused the quality divergence of herbal medicine and different clinical efficacy [24]. It is difficult to find good variety possessing not only the highest yield but also the best quality. Unfortunately there have been no new varieties with stable genetic property up to now.

3.3. Technological Challenges for Natural Fostering. The key technological points of natural fostering include selection of site, construction of seedlings base, density adjustment, and scientific harvesting. Among these technological points, the main challenges for natural fostering include the following.

3.3.1. Selection of Site. Natural fostering requires that the site should be in the original habitat or the ecological conditions similar to the original habitat areas. To determine whether an area is suitable for breeding, the most reliable and effective way is to carry out a longer period of experiment. However, it needs a lot of manpower, material, and observation for up to several years of growth cycle, and in practice the experiment is much difficult to carry out in a large scale [25]. A wild habitat may not be suitable for the growth of target medicinal species; at least most of the plants cannot be guaranteed to live in optimal living conditions and toward the development of population growth. So it is difficult to develop natural fostering to reach a large industrial scale in some situations [26]. Multicriteria assessment is essential to select suitable fostering site: (1) direct information on species distributions; (2) market analysis on potential medical plants; (3) community types or biotic units according to the evaluation of effective components; (4) transportation convenience; and (5) other goals.

3.3.2. Construction of Seedlings Base. The key part of base construction is how to produce vigorous seedlings or healthy seeds. Original funds and technologies are very important.

The aims of nursing seedlings are somewhat different from breeding in agriculture. Two methods are usually adopted: selection of germ plasm resources and crossbreeding. Selections of germ plasm resources are from wild species whose characters include ability of resisting adversity, high production, high content of effective chemical component, and so on. Sometimes, the selection needs to be adjusted in terms of relative medical aims such as medicinal organs (flower, radix, rhizome, and leaf), characters of effective component (volatile, poisonous), and values of medical goods ("daodi", shape). Crossbreed can be operated according to common approaches in agriculture [26]. One point needs to be announced that medical raw materials from crossbreed have not been verified through long-term experiments and not yet accepted by traditional Chinese herbalist doctors. From this view, crossbreed in natural fostering is used in yielding of medical materials for component of extraction, not for "yinpian" (semimanufactured goods for medicine through different physical methods). In addition, building and field construction is absolutely necessary [27].

3.3.3. Scientific Harvesting. Three parameters should be taken into account in natural fostering: quantity to harvest, time of harvest, and the condition of the plant community. The quantity of picking should not affect community structure and not pick in excess to ensure sustainable utilization in following years. It is absolutely necessary to pick medicinal materials in proper time because the content of effective chemistry component is different in different stages. As the extension of fostering time, herbal population density, medicinal ingredients, and biomass gradually increase. However, natural fostering may cause the degradation of competitiveness in licorice population after 5 years [28]. For some herbs, the shorter the growing years, the higher the content of the active ingredient such as calycosin glucoside and formononetin in *Astragalus membranaceus* [29]. Although early acquisition of these herbs could get better economic benefits, it may bring ecological loss. On the contrary, for some herbs the longer the growing years, the higher the content of medicinal ingredient such as ginseng. In order to achieve bigger production and high content of component, studies should be carried out on content dynamic curves of aimed medicinal materials in its life. The final objective is to find out key point of intersection between quantity and content to get the biggest effective biomass. All of the operations should preserve ecological stability, after all, which is our objective.

4. Economic Input and Output

4.1. Wild Collection. Wild collection depends on directly picking raw medicinal materials from natural resources. Therefore manpower is the main economic input. Local people do not need to invest any other economic resources to conduct wild collection, which generates great motivation for wild collection without considering systematic plan and the damage of ecological environment. Li et al. found that the annual income of farmers in Zhouzhi Country was 1,767.7 RMB/household in 2007 only by wild

Table 4: The cost of *Pinellia* production (RMB).

	Seed		Calcium fertilizer		Urea		Organic fertilizer		Pesticides	Employees		Equipment	Total
	Amount	Price	Amount	Price	Amount	Price	Amount	Price	Total	Amount	Price	Price	
Standard	2,250	36,000	1,500	1,050	225	450	45,000	4,500	150	480	14,400	2,100	58,650
Control	2,250	27,000	1,500	1,050	225	450	37,500	3,750	150	480	12,600	2,100	47,100
Difference		9,000		0		0	700	750	0	60	1,800	0	11,550

Table 5: The output-input ratio in *Pinellia* production.

	Output (kg per hm^2)	Value (RMB per hm^2)	Benefit (RMB per hm^2)	
			Net income	Input : output
Standard	3,093.43	134,564.21	75,914.21	1 : 2.294
Control	2,279.25	99,147.38	52,047.38	1 : 2.105
Difference	814.18	35,416.83	23,886.83	1 : 3.066

herbal collection [30]. Another study found that the annual income was 1,200 RMB/person in Ussuri area of Heilongjiang Province, which stimulated more than 3,000 persons to join in wild herbal collection [31].

4.2. Cultivation. The economic input of herbal cultivation includes land leasing, buying seeds, irrigation, fertilizers, pesticides, and manpower. Generally, the bigger the planting area, the higher the yield, the higher the economic income, and the higher the land cost. Most of leasing lands are located in the main producing areas, and the rents are different among different regions. According to the statistics of the National Agricultural Cost-benefit Data Assembly, the land rents of ginseng in Jilin, Liaoning, and Heilongjiang Province were 9.07 RMB/m^2, 0.54 RMB/m^2 and 0.46 RMB/m^2, respectively. Moreover, the land rents of cultivating different herbs in the same province were also different. For example, in Hubei Province the average land rent of *Coptis* was 0.14 RMB/m^2 but 0.07 RMB/m^2 for Kikyo. In addition, different planting methods also result in different output-to-input ratios. As shown in Tables 4 and 5, the input-outcome differences between the standard planting (demonstration group) and nonstandard planting (control group) for *Pinellia* are obviously apparent [32].

Comparing the two planting methods, there were significant differences between the cost of seeds, organic fertilizer, and employee. And the output-to-input ratio of standard planting methods was higher than the one of nonstandard planting. It indicated that more attention should be paid to seeds, soil management, and fertilization in herbal cultivation.

4.3. Natural Fostering. The economic input of natural fostering includes buying seeds, base construction, and harvest. Different fostering modes can bring different economic benefit. Table 6 showed that planting *Coptis* using three models (cultivation in greenhouse, fostering under *Cryptomeria japonica* and *Coriaria nepalensis* forest, resp.) caused different output-input ratios. Cultivation in greenhouse required the highest cost and fostering under *Cryptomeria japonica* forest brought the highest yielding. Natural fostering has a great advantage in planting Coptis. As shown in Table 7, it is proved

that natural fostering had higher benefit than cultivation in ginseng production (data from [33]). Compared with herbal cultivation, natural fostering was mainly implemented in mountainous areas, which caused higher cost of employees due to the poor traffic. As the examples of *Coptis* and *Rhizoma Paridis* fostering in Dujiangyan County of Sichuan Province, the human cost of transportation is 170 RMB from picking point to collection area [34]. Therefore, Chinese medicine enterprises have to build their factories close to the fostering area to reduce transportation cost.

5. Ecological Impact

5.1. Wild Collection. Wild collection generated great influence on ecological environment and biodiversity. Overexploitation had a damaging effect on plant vegetation, which made the surface exposed to air and led to land desertification and the subsequent severe soil loss. In addition, excessive wild collection destroyed community structure and the ecological balance. One of the main reasons for the ecological system imbalance of Inner Mongolia grassland was due to the excessive digging of wild licorice. The natural recovery of plant vegetation in the northwest arid areas was becoming more and more difficult. It has formed a vicious cycle of ecological problems among vegetation deterioration, soil erosion, resource exhaustion, and regional poverty.

Due to the deterioration of ecological environment by human impact, the amount of wildlife resources has been reducing while the amount of endangered species continued to increase. It is estimated that 15,000 of 72,000 species of medicinal plants in the world have been endangered by reason of overexcavation [35]. In China, there were 1,800–2,100 of 11,146 species of medicinal plants that have been endangered and 20% of all commonly used herbs were facing shortage [9]. The main endangered reason of medicinal plants was due to the lack of regulation and scientific planning in wild herbal collection. Typically, *Taxus chinensis* now was at the verge of extinction as the massive deforestation destruction when anticancer function of its main medicinal ingredient (taxol) was found in 1967.

Since the rapid development of the Chinese herbal medicine industry, wild herbal resources have suffered

TABLE 6: The cost under different *Coptis* production modes (RMB).

Model	Outcome	Input	Net income	Input : output
Cultivation in greenhouse	14,730	7,100	7,630	1 : 2.075
Natural fostering under *Japanese cedar* forest	14,250	4,800	9,450	1 : 2.968
Natural fostering under *Coriaria nepalensis* forest	13,605	4,800	9,005	1 : 2.834

TABLE 7: Comparison between different models of ginseng production (10,000 RMB/hectare).

	Input	Output	Cost-profit ratio	Net margin
Natural fostering	11.5	23.3	1.026	11.8
Cultivation	16.4	22.0	0.335	5.6

a predatory excavation. Furthermore, some herbal resources will still remain scarce, endangered, or extinct within a considerable period of time. For example, the natural reserve of wild *Lamiophlomis rotata* was 3,713–6,896 tons, the maximum allowable annual yield was about 1,700 tons, and the recovery period was 4-5 years. However, the actual amount of annual collection is about 2,520 tons. It would be unable to achieve sustainable utilization of wild *Lamiophlomis rotata* if picking keeps the current amount [36].

5.2. Cultivation. The shortage of wild medicinal resources and the development of modern Chinese medicine enterprises forced people to introduce and cultivate herbal medicine. But herbal cultivation has brought new ecological and environmental issues caused by deforestation, pesticide residues, and heavy metal pollution. Meanwhile original plant vegetation and secondary forests were inevitably destroyed more or less when cultivation of Chinese herbs was widely adopted. The ecosystem balance is facing the risk of severe damage by large-scale planting medicinal plants. In addition, soil structure was broken such as compaction due to excessive use of fertilizer. The phenomenon of soil heavy metal pollution is getting worse with the overuse or misuse of pesticides because of the lack of basic knowledge of diseases and pest control. It is common to see that both plant insect pests and their predators are killed because some current commonly used pesticides are too toxic. Sometimes several violent poisons were mixed to prevent or kill insect pests in order to achieve a quick and effective purpose. Although the yield of materia medica has been improved, they could not be used for clinical medicine. The final result was that environment became worse and the quality of Chinese herbal medicines could not meet standards [37]. Yi and Lu [38] found that pesticides and heavy metals not only existed in herbal medicines but also remained in soil.

5.3. Natural Fostering. The key point of natural fostering is not only to increase population density but also to involve human intervention as little as possible. Compared with cultivation, it can greatly reduce economic input and can provide Chinese herbal raw materials with high quality without influencing natural environment. In the process of fostering *Fritillaria* in Zheduo Mountain, there were 6 community types of wild *Fritillaria* and more than 40 kinds of main accompanying species which greatly exceeded the control areas. In addition, the biodiversity in fostering regions is also being increased [39]. Natural fostering in wild licorice made great achievements by using fence to limit excessive excavation in Hangjinqi area of Inner Mongolia. The coverage of licorice reached 63.3% and the continuous cover area reached 4,000 hm^2, which can be served as a barrier to prevent windstorms and fasten sand in the land [40].

Forest breeding is another kind of natural fostering. In the past 300 years, *Coptis* was planted under simple shacks that were built in the mountains without trees. In this way, all the trees and weeds were removed, and even the roots in soil must be cleared. Both the topsoil and network structure of the soil were destroyed, which can easily cause soil loss. Generally, a total of 3 m^2 forests need to be cut down for cultivating 1 m^2 *Coptis* [41]. On the contrary, *Coptis* production using natural fostering under forest not only improved the yield but also increase the forest coverage [42]. Natural fostering can increase the ability of community resilience. It integrates herbal medicine production with community conservation to address three crucial problems simultaneously, namely, funding, public participation, and rural living [40]. The logistic relationships among them can be explained in the following perspectives: (a) the raw materials of traditional medicine are largely derived from herbal medicine; (b) herbal medicines of high quality are closely correlated with the physical and chemical environments of communities; (c) only materials derived from intact communities are of high quality and may be sold at high prices; (d) Local communities will take the initiative to preserve community integrity so that they are able to harvest high quality natural products for improving income; (e) local people with surplus money can invest on community integrity conservation, which results in a good cycle.

6. Conclusion and Perspectives

As a result of the increasing demand for medicinal plants, most of which is still met by wild collection, a constant pressure is created on existing resources, leading to continuous depletion of some of the species in the forests, and at the same time forest land is losing its natural flora at an alarming rate. Although the shortage of medicinal materials is alleviated to some extent since more than 200 kinds of Chinese herbs could be artificially planted, the new problems of variety degeneration, pesticide residues, and the heavy metal pollution caused by cultivation under single species population have forced to seek more innovative methods. Researchers have placed high hopes on natural fostering to make up the deficiency of wild collection and artificial

cultivation. In particular, it has little impact on ecological environment and can produce raw herbal materials with a considerable high quality, also as an approach to conserve biological conservation. But it cannot completely replace the other two methods because of the long production cycle and the technological imperfections. More attention has been directed on the value of combined method from a holistic perspective, exploring the feasibility to solve the conflict between biodiversity and economy. Therefore, the sustainability of Chinese herbal resources should depend on systematic combination of wild collection, cultivation, and natural fostering, with comprehensive consideration of medical demand and herbal growth characteristics.

Conflict of Interests

The authors declare that there is no conflict of interests regarding the publication of this paper.

Authors' Contribution

All authors have contributed substantially to the design, analysis, discussion, and results and have approved the final version of this paper.

Acknowledgments

References

[1] W. Yang, "Development situation of China's traditional Chinese medicine export trade and its countermeasure study," *Guangdong Trace Elements Science*, vol. 15, no. 5, pp. 16–20, 2008.

[2] J. Jia and L. Jingping, "The position, problem and tactic of Chinese medicine industry," *Guangdong Agricultural Sciences*, vol. 1, pp. 207–109, 2011.

[3] C. Shilin and X. Peigen, *Introduction to the Sustainable Utilization of Chinese Herbal Medicine Resource*, China Medicinal Technology Publication, 2006.

[4] Y. Zhuyun, "Major tasks and challenges for resources science of Chinese Medicinal Materials," *Pharmacy and Clinics of Chinese Materia Medica*, vol. 3, no. 6, pp. 1–6, 2012.

[5] L. Huang, L. Guo, and G. Cui, "Basic theory research of traditional Chinese medicine resources," *Research and Information on Traditional Chinese Medicine*, vol. 7, no. 8, p. 29, 2005.

[6] S.-L. Chen, G.-Q. Su, J.-Q. Zou, L.-F. Huang, B.-L. Guo, and P.-G. Xiao, "The sustainable development framework of national Chinese medicine resources," *China Journal of Chinese Materia Medica*, vol. 30, no. 15, pp. 1141–1146, 2005.

[7] T. Gan, "Economic analysis of wild medicinal material depletion," *Rural Economic*, vol. 7, pp. 43–46, 2009.

[8] Y. Hai, H. Taikang, and W. Chunfu, "Processes and trends in the development of modern medicine," *Chinese Traditional and Herbal Drugs*, vol. 36, no. 1, pp. 147–149, 2005.

[9] L. Huang, H. Peng, and P. Xiao, "Development trend of traditional Chinese medicine resources," *China Journal of Chinese Materia Medica*, vol. 36, no. 1, pp. 1–4, 2011.

[10] M. Zhisheng, Z. Wensheng, and W. Yongyan, "The protection of wild herbs need to be improved in China," *Chinese Journal of Information on TCM*, vol. 15, no. 10, pp. 4–6, 2008.

[11] Y. Zhang, J. Si, and B. He, "Present situation of ephedra resources and their exploiting countermeasures," *World Science and Technology/Modernization of Traditional Chinese Medicine*, vol. 4, no. 4, pp. 63–68, 2002.

[12] C. Chi, H. Kaijia, and L. Buming, "The study on the comparison between wild and cultivated radix ranunculus ternatus," *Guangxi Sciences*, vol. 15, no. 1, pp. 70–74, 2008.

[13] S. Chen and D. Yun, "Comparison of semi-wild and wild Cordyceps chemical composition," *Journal of Chinese Medicinal Materials*, vol. 26, no. 3, pp. 163–165, 2003.

[14] J. Huang and L. Chunlin, "Traditional cultivation of Coptis teeta and its values in biodiversity conservation," *Biodiversity Science*, vol. 14, no. 1, pp. 79–86, 2006.

[15] R. Xu, J. Chen, and S. Chen, "Medicinal plant resources achieve rational development and sustainable using," *China Pharmaceuticals*, vol. 18, no. 6, pp. 1–2, 2009.

[16] H. Luqi, G. Lanping, C. Guanghong, X. Peigen, and W. Yongyan, "Basic theory of traditional Chinese medicine resources," *Research & Information of Traditional Chinese Medicine*, vol. 7, no. 8, pp. 4–6/29, 2005.

[17] Y. Yang, Y. Ma, and Z. Yang, "Current status and development of cultivation of wild medicinal herbs," *World Science and Technology (Modernization of Traditional Chinese Medicine and Materia Medica)*, vol. 22, no. 6, pp. 2217–2221, 2012.

[18] H. Wang and S. Chen, "On the implementation of good manufacturing practices and pest control of herbal medicines," *Lishizhen Medicine and Materia Medica Research*, vol. 20, no. 1, pp. 239–240, 2009.

[19] W.-W. Gao, Y.-J. Zhao, Y.-P. Wang, and S.-L. Chen, "A review of research on sustainable use of medicinal plants cropland in China," *China Journal of Chinese Materia Medica*, vol. 31, no. 20, pp. 1665–1669, 2006.

[20] Y.-H. Yang, L.-J. Dai, K.-H. He et al., "Relation between soil nutrient of artificially cultivated area and rhizome quality of Paris polyphylla var. yunnanensis," *Journal of Chinese Medicinal Materials*, vol. 35, no. 10, pp. 1557–1561, 2012.

[21] X.-L. Han, X.-B. Zhang, L.-P. Guo et al., "Statistical analysis of residues of heavy metals in Chinese crude drugs," *China Journal of Chinese Materia Medica*, vol. 33, no. 18, pp. 2041–2048, 2008.

[22] S. Chen and S. Jin, "A preliminary discussion on prevention and control of contamination of heavy metals and pesticides in Chinese medicinal plants," *World Science and Technology (Modernization of Traditional Chinese Medicine and Materia Medica)*, vol. 4, no. 4, pp. 72–74, 2002.

[23] F. Wu, M. Li, and B. Wang, "Experimental Study on the Resistance in *Fructus cannabis* Germplasm," *Journal of Anhui Agricultural Sciences*, vol. 38, no. 17, pp. 8982–8983, 2010.

[24] T.-J. Zhang, "Realization and evaluation of Chinese materia medica quality," *Chinese Traditional and Herbal Drugs*, vol. 42, no. 1, pp. 1–9, 2011.

[25] S. Chen, J. Wei, C. Sun et al., "Development of TCMGIS-I and its application in suitable producing area evaluation of Astragalus membranaceus," *World Science and Technology (Modernization of Traditional Chinese Medicine)*, vol. 8, no. 3, pp. 47–53, 2006.

[26] X.-W. Li and S.-L. Chen, "Conspectus of ecophysiological study on medicinal plant in wild nursery," *China Journal of Chinese Materia Medica*, vol. 32, no. 14, pp. 1388–1392, 2007.

[27] H. Guodong, G. Lanping, and H. Luqi, "Specialties and measures on variety breeding of chinese medicinal materials," *Resources Science*, vol. 30, no. 5, pp. 754–758, 2008.

[28] X. Li, C. Lin, and G. Li, "Influence of enclosure on *Glyeyrrhiza uralensis* community and distribution pattern in arid and semi-arid areas," *Acta Ecologica Sinica*, vol. 33, no. 13, pp. 3995–4001, 2013.

[29] Z.-Y. Shi, Z. Bao, Y. Jiang, and P.-F. Tu, "Quantitative analysis of calycosin glycoside and formononetin in Radix Astragali from different sources," *China Journal of Chinese Materia Medica*, vol. 32, no. 9, pp. 779–783, 2007.

[30] J. Li, Y. Li, and X. Tai, "On the rural households livelihood in the western poor areas after the slopping land conversion program within the sustainable livelihood analysis framework from the rural households survey in the Zhouzhi County, Shanxi Province," *China Rural Survey*, no. 5, pp. 29–38, 2009.

[31] Z. Wang, "Analysis of key issues which need to be resolved in the development of Chinese medicine industry," *China Journal of Chinese Materia Medica*, vol. 31, no. 1, pp. 81–84, 2006.

[32] R. M. B. Peijun, M. Yan, and W. Xiaohua, "Demonstration of standardized cultivation technology of Pinellia ternate," *Guizhou Agricultural Sciences*, vol. 38, no. 5, pp. 49–53, 2010.

[33] M. Li, Y. Quan, and L. Quan, "The progress and analysis of Panax ginseng cultivation in Yanbian State," *Journal of Agricultural Science Yanbian University*, vol. 29, no. 3, pp. 197–200, 2007.

[34] Ministry of Finance of the People Public of China, "Developments of Chinese herbal undergrowth financial which support by Sichuan Province make sense," *Country Finance and Financial Fair*, no. 6, pp. 20–21, 2013.

[35] U. W. E. Schippmann, D. Leaman, and A. B. A. Cunningham, "Comparison of cultivation and wild collection of medicinal and aromatic plants under sustainability aspects," *Frontis*, vol. 17, pp. 75–95, 2006.

[36] H. Sun, S.-Y. Jiang, C.-Q. Feng et al., "Status of wild resource of medicine plant Lamiophlomis rotata and its problems in sustainable use," *China Journal of Chinese Materia Medica*, vol. 37, no. 22, pp. 3500–3505, 2012.

[37] W. Rong, H. Guo, and H. Yang, "Current research status in China on pesticide contamination of plant material used in making Chinese herbal medicines," *Agrochemicals*, vol. 45, no. 5, pp. 302–305, 2006.

[38] X. Yi and Y. Lu, "Study on residues of pesticides and heavy metals in ligusticum wallichii Franch and other seven kinds of traditional Chinese medicine," *Research and Practice of Chinese Medicines*, vol. 18, no. 3, pp. 7–9, 2004.

[39] S.-L. Wei, W.-Q. Wang, and H. Wang, "Study on licorice resources and their sustainable utilization in center and western area of China," *China Journal of Chinese Materia Medica*, vol. 28, no. 3, pp. 202–206, 2003.

[40] X. Li and S. Chen, "Study on conditions of worldwide natural protected areas and construction of medicinal function and ecological industry protected areas in China," *Journal of Natural Resources*, vol. 24, no. 6, pp. 1124–1132, 2009.

[41] W. Liqun, X. Ye, and D. Fen, "Quality assessment for Coptis chinensis planted with ecological techniques," *Acta Academiae Medicinae Sinicae*, vol. 26, no. 6, pp. 608–610, 2004.

[42] C. Guifang and R. Cheng, "A preliminary study on the effect of growing Coptis Chinensis to ecological environment," *Yunnan Geographic Environment Research*, vol. 15, no. 4, pp. 61–65, 2003.

[43] P. Xiao, R. Zhao, X. Long, and B. Guo, "Macroscopic analysis on production and marketing of medicinal material resources for sustainable development," *China Journal of Chinese Materia Medica*, vol. 34, no. 17, pp. 2135–2139, 2009.

[44] J. Wang, R. Wang, and S. Fan, "Resources survey and analysis of wild *Forsythia suspensa* (Thunb.) Vahl," *Journal of Anhui Agricultural Sciences*, vol. 40, no. 15, pp. 8483–8484, 2012.

[45] X. Ying, "The marketing analysis of Bupleurum chinense DC," *Modern Chinese Medicine*, vol. 8, no. 12, pp. 43–44, 2006.

[46] B. Yang, S. Li, and X. Wang, "On Cultivation and Rational Utilization of Paris polyphylla var. yunnanensis," *Chinese Wild Plant Resources*, vol. 27, no. 6, pp. 70–73, 2008.

[47] D. Xiang, "The new investigation of Atractylodeschinensis (DC.) Koidz in Dong Bei," *Special Economic Animal and Plant*, vol. 13, no. 2, pp. 18–19, 2010.

[48] L. Ding, "The producing and selling analysis of *Saposhnikovia divaricata* (Turcz.) Schischk," *Modern Chinese Medicine*, vol. 14, no. 3, pp. 53–56, 2012.

[49] Z. Yongwei, J. Fusheng, W. Yin, and D. Zhishan, "Present status and sustainable development of Rhizoma Bletillae industry," *Chinese Archives of Traditional Chinese Medicine*, vol. 30, no. 10, pp. 2264–2267, 2012.

[50] S.-L. Chen, M.-R. Jia, Y. Wang, G. Xue, and P.-G. Xiao, "Study on the plant community of Fritillaria cirrhosa," *China Journal of Chinese Materia Medica*, vol. 28, no. 5, pp. 398–402, 2003.

[51] H. Yang, *Effect of the Grassland Enclosure on the Recovery of Gression Grassland and Field Liquorice Resource in Ningxia*, China Agricultural University, 2005.

[52] H. Hong, H. Chen, F. Xu et al., "Surveys on resources and varieties on Chinese markets of crude drug Mahuang," *China Journal of Chinese Materia Medica*, vol. 36, no. 9, pp. 1129–1132, 2011.

[53] L. Zefeng, L. Kun, and H. Yunliang, "The development status and tactics of Schisandra chinensis (Turcz.) Baill. industry in Liaoning Province," *Agricultural Economy*, no. 7, pp. 21–34, 2011.

[54] W. Han, L. Cao, Y. Hamid, and X. Xu, "Adaptation of Apocynum Venetum to saline water irrigation," *Journal of Desert Research*, vol. 32, no. 3, pp. 756–762, 2012.

[55] L. Cui, Q. Tong, C. Liang, C. Wang, and Q. Li, "Research progress of environmental factors on growth and medicinal components of Acanthopanax," *Northern Horticulture*, no. 4, pp. 182–184, 2011.

[56] X. Shengbo and Q. Jianju, "Analyses on the types, distributions andcharacteristics of vegetation and soil along Qinghai-Tibet Railway," *Journal of Anhui Agricultural Sciences*, vol. 41, no. 19, pp. 8268–8270, 2013.

[57] S.-L. Chen, J.-H. Wei, L.-F. Huang, B.-L. Guo, and P.-G. Xiao, "Probing into the theory and practice of wild medicinal materials tending," *China Journal of Chinese Materia Medica*, vol. 29, no. 12, pp. 1123–1126, 2004.

[58] D. Chunlian, Z. Xiaowu, L. Zhai, and S. Xiaopeng, "Hill County, Hebei Province, imitation of wild and cultivated Polyporus umbellatus (Pers.) Fries success in a sexual reproduction," *Edible and Medicinal Mushrooms*, vol. 4, 2012.

[59] R. Maoxiong, W. Desheng, Z. Jianling et al., "Wild resources of Epimedium brevicornum Maxim. with standardized planting and tending research," *The Chinese Academic Medical Magazine of Organisms*, no. 3, pp. 1–14, 2002.

[60] Y. Liqun, D. Wanlong, and Z. Dianlong, "Research advances on the wild medicinal materials tending and purposive cultivation of Trollius chinensis Bge," *Lishizhen Medicine and Materia Medica Research*, vol. 19, no. 2, pp. 286–288, 2008.

[61] Y. Liu, Z. Liu, and B. Xiao, "Wildlife tending of endangered herbal plant Dysosina versipellis," *Chinese Agricultural Science Bulletin*, vol. 26, no. 5, pp. 276–278, 2010.

[62] Y. Guoqing, "The history of 8 Chinese medicine in Henan," *Lishizhen Medicine and Materia Medica Research*, vol. 20, no. 1, article 143, 2009.

[63] H. Jihong and T. Guoyan, "Advances in studies of Snow Lotuses (Saussurea)," *Journal of Xinjiang Agricultural University*, vol. 25, no. 2, pp. 8–13, 2002.

[64] A. Bahargul, Y. Xu, Q. Guo, Gulibahaer, Rebiyaguli, and Gulibositan, "Cistanche tubulosa resources, investigation and analysis of trade and cultivation," *Chinese Wild Plant Resources*, vol. 32, no. 2, pp. 47–50, 2013.

[65] Y. Hongmei, C. Qingqian, and Qianlie, "Set of Sarcandra glabra (Thunb.) Nakai cultivation techniques," *Hunan Forestry Science & Technology*, vol. 37, no. 3, pp. 51–52, 2010.

Research Article

Effects of Total Ginsenosides on the Feeding Behavior and Two Enzymes Activities of *Mythimna separata* (Walker) Larvae

Ai-Hua Zhang,[1] Shi-Qiang Tan,[1,2] Yan Zhao,[1] Feng-Jie Lei,[1] and Lian-Xue Zhang[1]

[1]College of Chinese Medicinal Materials, Jilin Agricultural University, Changchun 130118, China
[2]Tianjin University of Traditional Chinese Medicine, Tianjin 300193, China

Correspondence should be addressed to Ai-Hua Zhang; fengjie_lei@163.com and Lian-Xue Zhang; zlx863@163.com

Ginsenosides, the main effective components of *Panax ginseng* C.A. Meyer and *Panax quinquefolius* L., are important allelochemicals of *ginseng*. Although many studies have targeted the pharmacological, chemical, and clinical properties of ginsenosides, little is known about their ecological role in *ginseng* population adaptation and evolution. Pests rarely feed on *ginseng*, and it is not known why. This study investigated the effects of total ginsenosides on feeding behavior and activities of acetylcholinesterase (AChE) and glutathione s-transferase (GST) in *Mythimna separata* (Walker) larvae. The results showed that the total ginsenosides had significant antifeeding activity against *M. separata* larvae, determined by nonselective and selective antifeeding bioassays. In addition, the total ginsenosides had inhibitory effects on the activities of GST and AChE. The antifeeding ratio was the highest at 8 h, then decreased, and was the lowest at 16 h. Both GST and AChE activities decreased from 0 h to 48 h in all total ginsenosides treatments but increased at 72 h. Total ginsenosides had antifeeding activity against *M. separata* larvae and inhibitory effects on the activities of GST and AChE.

1. Introduction

In the long process of adaptation to the environment, plants have developed a chemical response to stress called allelopathy, the release of allelochemicals [1, 2]. Terpenoids are a type of allelochemical and play an important role in regulating plant populations and ecological systems [3, 4].

Ligularia virgaurea secretes terpenoids that inhibit seed germination of other species [5, 6]. *Duranta repens* extracts have been shown to inhibit oviposition, feeding, and development of *Plutella xylostella* [7, 8]. Terpenoids from Meliaceae plants have shown insecticidal action against *Pieris occidentalis* and *Leucania separata* [9–12].

Ginseng (*Panax ginseng* C.A. Meyer) is a highly popular and valuable traditional Chinese medicine and tonic. The major *ginseng* producers of the world are China, Korea, Japan, and Russia [13, 14]. *Ginseng* can grow for more than one hundred years, but it requires strict ecological conditions that are limited. Wild *ginseng* populations maintain a specific distance internally between plants [15]. *Ginseng* has triterpene saponins, and few insects eat its stems or leaves. *Ginseng* triterpene saponins change the soil microbial population structure and inhibit *ginseng* seed and seed germination by other species [13–20].

Ginsenosides belong to the group triterpenes and are becoming a popular topic of research in pharmacology, medicine, and clinical drug development in both China and abroad. However, there is little information as to why *ginseng* synthetizes high levels of ginsenosides (contents of more than 3%) and the significance of ginsenosides for the plant's growth, development, and population dynamics. *Ginseng* contains a wide variety of triterpene saponins (found in more than 60 species), which suggests that there are a large number of metabolic pathways (including highly evolved metabolic pathways). Based on the scarcity of information, this study discusses the effects of total ginsenosides on the feeding behavior and two enzyme activities of *Mythimna separata* (Walker) larvae. The results of this study will enable further understanding of the effect of triterpenes on plant population adaptation and evolution. It is also useful to investigate

the mechanisms of Chinese herbal medicines and to add to the reference information for phytochemotaxonomy.

2. Materials and Methods

2.1. Insects. *Mythimna separata* (Walker) adults were collected at the test base of Jilin Agricultural University in the early summer of 2011. The offspring of these adults were reared on grain sorghum leaves under an LD 16 : 8 h photoperiod at $22 \pm 1°C$ with 70–80% relative humidity and never had contact with insecticides [21].

2.2. Chemicals. The total ginsenosides (purity $\geq$ 80%, UV method) were purchased from Jilin Hongjiu Biotech Co., Ltd. AChE and GST reagent kits were purchased from the Nanjing Jiancheng Bioengineering Institute. A Lowry Protein Assay Kit was purchased from Beijing Dingguo Changsheng Biotech Co., Ltd.

2.3. Bioassay for Feeding Behavior. A leaf disc bioassay was used to test *M. separata* larvae [22, 23]. The ginsenoside concentrations were 2.0%, 1.0%, and 0.5% (mass fraction (MF)). These concentrations are within the range of ginsenoside levels normally found in *P. ginseng*. One day prior to the assay, newly molted 4th-instar larvae were placed individually into Petri dishes (9 cm diameter). After starvation for 48 h, 6 excised grain sorghum leaf discs (Φ = 15 mm), soaked in solutions with different concentrations of ginsenosides for 30 min (control discs received distilled water only), were supplied to all larvae. The area of feeding on the leaves was measured every 8 h, and the corresponding antifeeding activity was calculated (nonselective and selective antifeeding ratios). Each test was repeated three times.

2.4. Enzymes Activity Tests. The effects of ginsenosides on larvae of *M. separata* larvae were tested at concentrations of 2.0%, 1.0%, and 0.5% (MF). The ginsenosides were dissolved with distilled water. Fresh clean grain sorghum leaves were punched into leaf discs with a puncher, and the leaf disc was soaked in different concentrations of ginsenoside solutions for 30 min and air-dried prior to use. The same volume of distilled water without ginsenosides was used for the control group. Fourth-instar larvae were maintained for 48 h without access to food. Larvae with the same weights were then selected and either were allowed to feed on the leaf discs containing ginsenosides or were placed in the control group. The leaves were replaced with the fresh ones every 2 days because of the possible degradation of the ginsenosides. Homogenates for the two enzyme activities (glutathione s-transferase (GST) and acetylcholinesterase (AChE) activity) of *M. separata* larvae were collected every 24 h. Each test was repeated three times.

Homogenates of the digestive tract of the larvae were prepared as follows. The digestive tract was dissected from individuals of each group and washed with phosphate-buffered saline (pH 7.0) to remove the gut contents. To this, 5 mL of cold PBS was added and the solution was centrifuged for 20 min (4°C, 10000 r/min). The supernatant is

the homogenate. The protein content of the supernatant fluid was measured using the Lowry Protein Assay Kit staining method [24, 25] with bovine serum albumin as the standard.

GST activity was assessed according to the method of Jaclyn and Min Lü [26, 27] by measuring GSH conjugation with 1-chloro-2,4-dinitrobenzene (CDNB). CDNB activity changes with the substrate concentration in a linear relationship. A visible-ultraviolet spectrophotometer measured absorption at 412 nm to detect product formation. All reactions took place in 0.1 M potassium phosphate-buffer containing 1 mM GSH and 0.01–3 mM CDNB. GST activity was determined according to the following equation:

$$Y = \frac{OD_\alpha - OD_\beta}{OD_\delta - OD_\varepsilon} \times C_\sigma \times N \div T * \left(A \times C_{prot} \right), \quad (1)$$

where Y represents GST activity (μmol/min/mg prot), OD_α represents the absorbance of the control group, OD_β represents the absorbance of the experiment group, OD_δ represents the absorbance of the reference group, OD_ε represents the absorbance of the blank group, C_σ represents the standard concentration (20 mM), N is the dilution factor of the reaction system (6), T is reaction time (10 min), A is the sample volume (mL), and C_{prot} represents the protein concentration of the sample.

AChE activity was determined using the method of Ellman et al. [28]. The enzyme activity was measured by assessing the increase of yellow color produced from thiocholine when it reacts with the dithiobisnitrobenzoate ion. It is based on the coupling of the following reactions:

$$acetylthiochline \xrightarrow{enzyme} thiocholine + acetate$$

$$thiocholine + dithiobisnitrobenzoate \longrightarrow yellow\ color \quad (2)$$
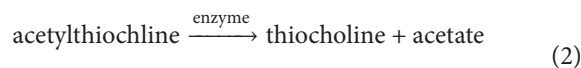
The AChE activity was spectrophotometrically measured at 412 nm (UV-754, Shandonggaomi, UV visible-ultraviolet spectrophotometer). The enzyme activities were expressed as μmol/min/mg protein. AChE activity was determined according to the following equation:

$$Y_0 = \frac{OD_1 - OD_2}{OD_3 - OD_4} \times C_0 \div C_{prot}. \quad (3)$$

In this equation, Y_0 represents AChE activity (μmol/min/mg prot), OD_1 represents the absorbance of the experiment group, OD_2 represents the absorbance of the control group, OD_3 represents the absorbance of the reference group, OD_4 represents the absorbance of the blank group, C_0 represents the standard concentration (1 mM), and C_{prot} represents the protein concentration of the sample.

2.5. Statistical Analyses. Nonselective and selective antifeeding ratios were calculated according to the following equations:

$$Y_1 = \frac{S_{ck} - S}{S_{ck}} \times 100\%,$$

$$Y_2 = \frac{S_{ck} - S}{S_{ck} + S} \times 100\%. \quad (4)$$

TABLE 1: Nonselective antifeeding ratio of different total ginsenoside concentrations on 4th-instar *M. separata* larvae.

Concentration of total ginsenosides (%)	8 h		16 h		24 h	
	Average feeding area (mm^2)	Nonselective antifeeding ratio (%)	Average feeding area (mm^2)	Nonselective antifeeding ratio (%)	Average feeding area (mm^2)	Nonselective antifeeding ratio (%)
Control	1664.67 ± 107.04 a	—	1770.00 ± 0.00 a	—	1770.00 ± 0.00 a	—
0.5	876.33 ± 333.10 b	47.36	1529.67 ± 28.02 a	13.58	1440.67 ± 89.80 a	18.61
1.0	592.67 ± 224.13 b	64.40	1524.00 ± 75.29 a	13.90	1408.00 ± 201.27 a	20.45
2.0	188.67 ± 81.59 c	88.67	757.67 ± 453.24 b	57.19	483.33 ± 358.60 b	72.69

Data are presented as the means ± SE. Means in the same column followed by different letters are significantly different at the level $P < 0.05$. Prior to analysis of variance (SPSS 18.0), the homogeneity of variance was tested in each statistic test.

TABLE 2: Selective antifeeding ratio of different total ginsenoside concentrations on 4th-instar *M. separata* larvae.

Concentration of total ginsenosides (%)	8 h		16 h		24 h	
	Average feeding area (mm^2)	Selective antifeeding ratio (%)	Average feeding area (mm^2)	Selective antifeeding ratio (%)	Average feeding area (mm^2)	Selective antifeeding ratio (%)
0.5	638.33 ± 34.53	34.19	450.33 ± 40.45	36.62	511.33 ± 9.61	23.28
Control	1301.67 ± 77.02	—	970.67 ± 52.78	—	821.67 ± 39.00	—
1.0	514.67 ± 80.75	44.29	470.67 ± 24.50	32.00	527.33 ± 25.74	29.23
Control	1332.33 ± 51.50	—	913.67 ± 33.47	—	963.00 ± 36.10	—
2.0	267.00 ± 95.79	62.49	285.33 ± 23.46	46.18	391.00 ± 22.37	42.46
Control	1156.67 ± 127.38	—	775.00 ± 50.48	—	968.00 ± 24.06	—

Data are presented as the means ± SE. Homogeneity of variance was tested in each statistic test.

In these equations, Y_1 represents the nonselective antifeeding ratio (%), Y_2 represents the selective antifeeding ratio (%), S_{ck} represents the average feeding area of the control group (mm), and S represents the average feeding area of the treated group (mm).

The nonselective and selective antifeeding ratios of larvae fed on diets containing different concentrations of ginsenosides were compared using SPSS Statistical 18.0. The effects of ginsenosides on the detoxification enzyme activity of *M. separata* larvae were also analyzed using SPSS Statistical 18.0. In all statistical tests, P values < 0.05 were considered statistically significant. All data are presented as the means ± SEM.

3. Results

3.1. Bioassay for Feeding Behavior. The nonselective antifeeding ratios of 4th-instar *M. separata* larvae at 8, 16, and 24 h are shown in Table 1. The total ginsenosides appeared to have significant antifeeding activity against *M. separata* larvae. The nonselective antifeeding ratios at different total ginsenoside concentrations were significantly different from those of the controls at 4, 8, and 12 h. As the total ginsenoside concentration increased, the nonselective antifeeding activity was enhanced. At 8 h, the antifeeding ratios of 2.0%, 1.0%, and 0.5% (MF) were 88.67%, 64.40%, and 47.36%, respectively.

The selective antifeeding ratios of the 4th-instar *M. separata* larvae are shown in Table 2. The 4th-instar *M. separata* larvae preferred to eat the leaves of the control; however, they

did consume a small amount of the treated leaves. The total ginsenosides had significant inhibitory effect on *M. separata* larvae, and this effect increased with an increase in total ginsenoside concentration.

3.2. Enzymes Activity Tests. As the total ginsenoside concentration increased, the activity of GST also increased. GST activities first decreased and then increased with the passage of time. The inhibition ratio was the highest at 48 h, with 75.15%, 468.98%, and 31.86% at 2.0%, 1.0%, and 0.5% concentrations, respectively (see Figure 2).

The AChE activity of 4th-instar *M. separata* larvae was 79.0546 μmol/min/mgprot before feeding on 2.0% (MF) total ginsenosides (see Figure 3); however, the AChE activities were depressed to 61.8998 (inhibition ratio, 21.70%), 31.5114 (inhibition ratio, 60.14%), and 35.0698 (inhibition ratio, 55.64%) μmol/min/mgprot at 24 h, 48 h, and 72 h, respectively (see Figure 4). The ginsenosides inhibited the AChE activity of 4th-instar *M. separata* larvae, and the inhibition effect increased with the increase in ginsenoside concentration but did not decrease over time.

4. Discussion

Plant secondary metabolic substances are formed via secondary metabolic pathways and play indispensable roles in the evolution of plants. They have repellency, antifeeding, and toxic effects on phytophagous insects. For example, Momordicin I and II have significant antifeedant activity

on second-instar larvae of *P. xylostella*, and the antifeeding rates were 80.39% and 74.09%, respectively [8]. Plant lectins also have repellency, antifeeding, and toxic effects on phytophagous insects such as caterpillars, tobacco hornworm, cotton leafworm, and beetles [29]. Azadirachtin causes mortality in *Nilaparvata lugens* (Stal) and destroys its ovarian follicle epithelial cells [30].

We compared the larval feeding behavior of *M. separata* on a diet containing different concentrations of total ginsenosides (MF: 2.0%, 1.0%, and 0.5%). The total ginsenosides imposed adverse effects on the feeding behavior of *M. separata* but to different extents (Tables 1 and 2). Comparison with control demonstrates that the consumption of leaves by *M. separata* was strongly affected by the total ginsenosides. If consumption is reduced, the energy required for physiological activities would also be reduced. Consequently, resistance is then reduced, and physiological metabolism would not be adequate. *M. separata* are sometimes found near cultivated *ginseng*; however, they rarely feed on the leaves of *ginseng*, which is the reason for choosing *M. separata* for this experiment.

Total ginsenosides inhibited GST and AChE activities of *M. separata* larvae. If the GST activity was inhibited, the detoxification was reduced. The *M. separata* changed feeding behaviors and fed on the grain sorghum leaves that were treated with total ginsenosides. In this way, they could reduce the damage from outsiders and protect themselves. It is the same for AChE; their neurotransmission slows down when AChE activity is inhibited and *M. separata* did feed on a small amount. The total ginsenosides had antifeeding activity against *M. separata* larvae and inhibitory effects on the activities of GST and AChE. Glutathione S-transferase (GST) and acetylcholinesterase (AChE) play important roles in insect metabolism and resistance to insecticides [31]. This study demonstrates that after treating *M. separata* with total ginsenosides GST activities decreased. This indicates that total ginsenosides have no toxic effects in vivo and activates the defense system of insects but could also inhibit GST activity. GSTs widely exist in insects and catalyze the nucleophilic reaction of glutathione (GSH) with a variety of electrophilic compounds. GSTs play an important role in exogenous substance biotransformation, drug metabolism, and protection of the organism against oxidative damage [32]. GST activity was inhibited by total ginsenosides, and detoxification was reduced in 4th-instar *M. separata* larvae (see Figure 1). Thus, they suffered damage from toxic substances and these substances are harmful to living larvae.

AChE is an important neurotransmitter enzyme mainly distributed in the brain and central nervous system [33]. AChE is localized at the surface of nerve cells and can decompose neurotransmitter acetylcholine, which is released from the nerve endings and guarantees normal nerve conduction [34]. If its activity is inhibited, the acetylcholine released in the synaptic gap cannot be degraded, and insects will have toxicity symptoms and possibly mortality [35]. Several essential oils from aromatic plants, monoterpenes, and natural products have all been shown to be inhibitors of AChE [36]. Pulegone-1,2-epoxide, isolated from a Verbenaceae medicinal
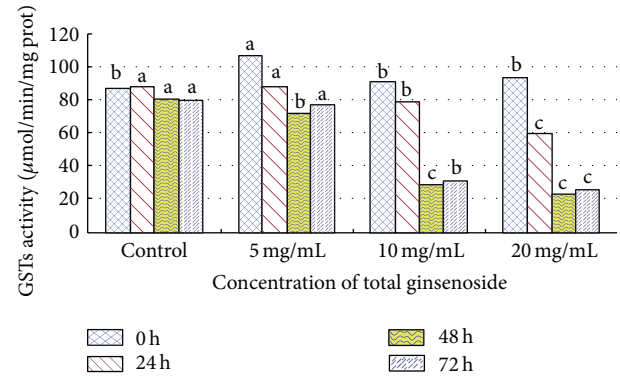

FIGURE 1: Effect of total ginsenosides on GST activity in 4th-instar *M. separata* larvae. Bars with different letters are significantly different from each other at $P < 0.05$ using the one-way ANOVA (SPSS 18.0). Data are means + SD.
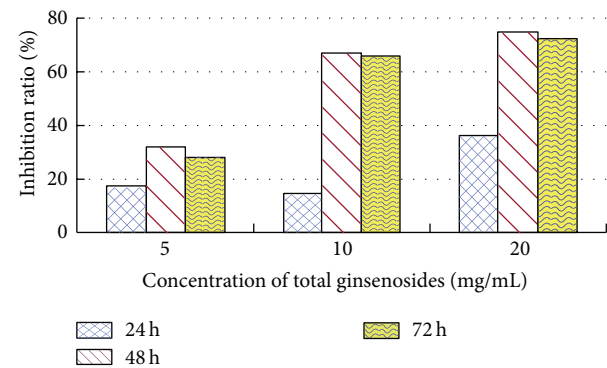

FIGURE 2: Inhibition ratio of total ginsenosides on GST activity in 4th-instar *M. separata* larvae.
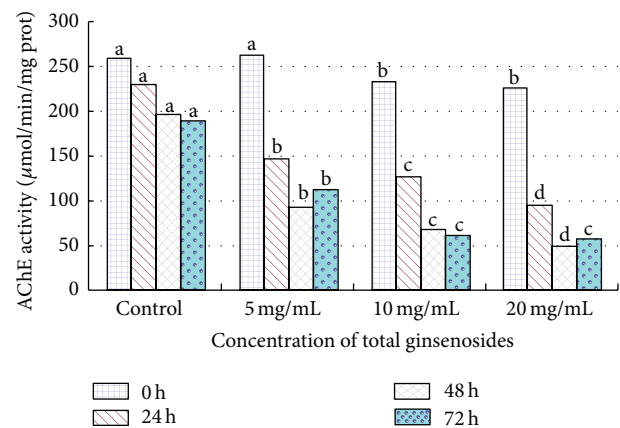
FIGURE 3: Effect of total ginsenosides on AChE activity in 4th-instar *M. separata* larvae. Bars with different letters are significantly different from each other at $P < 0.05$ using a one-way ANOVA (SPSS 18.0). Data are means + SD.

plant (*Lippia stoechadifolia* L. (Poleo)), showed an irreversible inhibition of the AChE in house fly and Madagascar roach [37]. This experiment indicates that the total ginsenosides inhibit AChE activity directly. On the basis of the research mentioned earlier and the comprehensive analysis of our findings, we conclude that the decline of AChE activity in

Figure 4: Inhibition ratio of total ginsenosides on AChE activity in 4th-instar *M. separata* larvae.

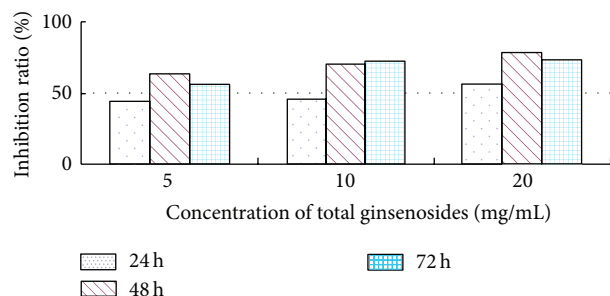*M. separata* larvae indirectly indicates damage to nerve cells, which induce AChE photoinactivation and death caused by the disruption of normal nerve conduction. Total ginsenosides have inhibitory allelopathic effects on *M. separata*, which were beneficial for researching the allelopathic potential of ginsenosides.

Conflict of Interests

The authors declare that there is no conflict of interests regarding the publication of this paper.

Authors' Contribution

Ai. Hua Zhang and Shi. Qiang Tan are cofirst authors; they contributed equally to the work.

Acknowledgments

References

[1] E. L. Rice, *Allelopathy*, Academic Press, New York, NY, USA, 1984.

[2] E. L. Rice, *Biological Control of Weeds and Plant Diseases: Advances in Applied Allelopathy*, University of Oklahoma Press, Norman, Okla, USA, 1995.

[3] S. L. Peng and P. Nan, "Terpenoids in higher plants and their roles in ecosystems," *Chinese Journal of Ecology*, vol. 21, pp. 33–38, 2002.

[4] W. X. Gu, S. S. Duan, and S. M. Luo, "Ecological characteristic of terpenoids and their allelopathic effects to plants," *Journal of South China Agricultural University*, vol. 19, pp. 108–112, 2005.

[5] R. Ma, M. Wang, X. Zhu, X. Lu, and K. Sun, "Allelopathy and chemical constituents of *Ligularia virgaurea* volatile," *Chinese Journal of Applied Ecology*, vol. 16, no. 10, pp. 1826–1829, 2005.

[6] R. Ma, M. Wang, K. Zhao, S. Guo, Q. Zhao, and K. Sun, "Allelopathy of aqueous extract from Ligularia virgaurea, a dominant weed in psychro-grassland, on pasture plants," *Chinese Journal of Applied Ecology*, vol. 17, no. 5, pp. 845–850, 2006.

[7] H. Wei, Y. Hou, G. Yang, and M. You, "Repellent and antifeedant effect of secondary metabolites of non-host plants on *Plutella xylostella*," *Chinese Journal of Applied Ecology*, vol. 15, no. 3, pp. 473–476, 2004.

[8] B. Ling, G.-C. Wang, J. Ya, M.-X. Zhang, and G.-W. Liang, "Antifeedant activity and active ingredients against plutella xylostella from *Momordica charantia* leaves," *Agricultural Sciences in China*, vol. 7, no. 12, pp. 1466–1473, 2008.

[9] X. D. Li and S. H. Zhao, "The toxic effects and mode of azadirachtin on insects," *Journal of South China Agricultural University*, vol. 17, pp. 118–122, 1995.

[10] X. Zhang, X. L. Wang, and J. T. Fen, "The development of botanical insecticides—toosendanin," *Journal of Northwest Sci-Tech University of Agriculture and Forestry*, vol. 21, pp. 1–5, 1993.

[11] W. L. Wang, S. H. Zhao, J. Han, and Y. S. Xu, "Effects of several Insecticidal principles from chinaberry, melia azedarach on the imported cabbage worm and Asiatic corn borer, *Ostrinia furnacalis*," *Acta Phytophylacica Sinica*, vol. 19, pp. 359–364, 1992.

[12] Y.-L. Shi and W.-P. Wang, "Biological effects of toosendanin, an active ingredient of herbal vermifuge in Chinese traditional medicine," *Acta Phytophylacica Sinica*, vol. 58, no. 5, pp. 397–406, 2006.

[13] L. Feng-Jie, Z. Ai-Hua, X. Yong-Hua, and Z. Lian-Xue, "Allelopathic effects of ginsenosides on in vitro growth and antioxidant enzymes activity of ginseng callus," *Allelopathy Journal*, vol. 26, no. 1, pp. 13–22, 2010.

[14] P. G. Xiao, "Preliminary investigation of wild ginseng in the Northeast," *Acta Pharmaceutica Sinica*, vol. 6, pp. 340–351, 1962.

[15] T. S. Wang, *Chinese Ginseng*, Liaoning Science and Technology Press, Shenyang, China, 2001.

[16] A.-H. Zhang, F.-J. Lei, Y.-H. Xu, G.-X. Zhou, and L.-X. Zhang, "Effects of ginsenosides on the germinating of ginseng seeds and on the activity of antioxidant enzymes of the radicles of ginseng seedlings *in vitro*," *Acta Ecologica Sinica*, vol. 29, no. 9, pp. 4934–4941, 2009.

[17] A. H. Zhang, F. J. Lei, S. W. Fang, M. H. Jia, and L. X. Zhang, "Effects of ginsenosides on the growth and activity of antioxidant enzymes in American ginseng seedlings," *Journal of Medicinal Plants Research*, vol. 5, pp. 3217–3223, 2011.

[18] A.-H. Zhang, F.-J. Lei, Z.-X. Guo, and L.-X. Zhang, "Allelopathic effects of ginseng root exudates on the seeds germination and growth of ginseng and American ginseng," *Allelopathy Journal*, vol. 28, no. 1, pp. 13–20, 2011.

[19] Y. Li, S.-L. Liu, X.-F. Huang, and W.-L. Ding, "Allelopathy of ginseng root exudates on pathogens of ginseng," *Acta Ecologica Sinica*, vol. 29, no. 1, pp. 161–168, 2009.

[20] Q. J. Zhang, W. R. Ben, and L. H. Xu, "Allelopathic effects of extract from old ginseng soil on seed germination and seedlings growth in rice," *Journal of North West A & F University (Natural Science Edition)*, vol. 40, pp. 49–54, 2012.

[21] H. C. Sharma, D. J. Sullivan, and V. S. Bhatnagar, "Population dynamics and natural mortality factors of the *Oriental armyworm, Mythimna separata* (Lepidoptera: Noctuidae), in South-Central India," *Crop Protection*, vol. 21, no. 9, pp. 721–732, 2002.

[22] F. M. Yan, *Chemical Ecology*, Science Press, Beijing, China, 2011.

[23] L. Z. Wen, *Introduction to Entomology Research Methods and Techniques*, Science Press, Beijing, China, 2010.

[24] O. H. Lowry, N. J. Rosebrough, A. L. Farr, and R. J. Randall, "Protein measurement with the Folin phenol reagent," *The Journal of Biological Chemistry*, vol. 193, no. 1, pp. 265–275, 1951.

[25] E. F. Hartree, "Determination of protein: a modification of the lowry method that gives a linear photometric response," *Analytical Biochemistry*, vol. 48, no. 2, pp. 422–427, 1972.

[26] L. Z. Wen, *Introduction to Entomology Research Methods and Techniques*, Science Press, Beijing, China, 2010.

[27] J. M. Goodrich and N. Basu, "Variants of glutathione s-transferase pi 1 exhibit differential enzymatic activity and inhibition by heavy metals," *Toxicology in Vitro*, vol. 26, no. 4, pp. 630–635, 2012.

[28] G. L. Ellman, K. D. Courtney, V. Andres Jr., and R. M. Featherstone, "A new and rapid colorimetric determination of acetylcholinesterase activity," *Biochemical Pharmacology*, vol. 7, no. 2, pp. 88–96, 1961.

[29] G. Vandenborre, G. Smagghe, and E. J. M. Van Damme, "Plant lectins as defense proteins against phytophagous insects," *Phytochemistry*, vol. 72, no. 13, pp. 1538–1550, 2011.

[30] S. Senthil Nathan, M. Young Choi, H. Yul Seo, C. Hoon Paik, K. Kalaivani, and J. Duk Kim, "Effect of azadirachtin on acetylcholinesterase (AChE) activity and histology of the brown planthopper *Nilaparvata lugens* (Stål)," *Ecotoxicology and Environmental Safety*, vol. 70, no. 2, pp. 244–250, 2008.

[31] R. M. E. Vos and P. J. van Bladeren, "Glutathione S-transferases in relation to their role in the biotransformation of xenobiotics," *Chemico-Biological Interactions*, vol. 75, no. 3, pp. 241–265, 1990.

[32] Z. S. Jiang, Z. G. Yan, Y. Z. Du, and Z. Z. Shang, "Effect of α-terthienyl on glutathione S-transferases in *Helicoverpa armigera* and *Ostrinia furnacalis* larvae," *Chinese Journal of Pesticide Science*, vol. 15, no. 3, pp. 76–79, 2003.

[33] J. I. Kim, C. S. Jung, Y. H. Koh, and S. H. Lee, "Molecular, biochemical and histochemical characterization of two acetyl-cholinesterase cDNAs from the German cockroach *Blattella germanica*," *Insect Molecular Biology*, vol. 15, no. 4, pp. 513–522, 2006.

[34] K. Yin, E.-B. Ma, C.-R. Xue, H.-H. Wu, Y.-P. Guo, and J.-Z. Zhang, "Study on insecticidal activities and effect on three kinds of enzymes by 5-aminolevulinic acid on oxya Chinensis," *Agricultural Sciences in China*, vol. 7, no. 7, pp. 841–846, 2008.

[35] Z. H. Tang, "Research status and perspectives of insect resistance to insecticides in China," *Entomological Knowledge*, vol. 37, pp. 97–103, 2000.

[36] E. Shaaya and A. Rafaeli, "Essential oils as biorational insecticides—potency and mode of action," in *Insecticides Design Using Advanced Technologies*, pp. 249–261, Springer, Berlin, Germany, 2007.

[37] D. L. Grundy and C. C. Still, "Inhibition of acetylcholinesterases by pulegone-1,2-epoxide," *Pesticide Biochemistry and Physiology*, vol. 23, no. 3, pp. 383–388, 1985.

Research Article

Effect of the Herbal Drug Guilu Erxian Jiao on Muscle Strength, Articular Pain, and Disability in Elderly Men with Knee Osteoarthritis

Chen-Chen Tsai,[1,2,3] Yin-Yi Chou,[4] Yi-Ming Chen,[4,5] Yih-Jing Tang,[6,7] Hui-Ching Ho,[8] and Der-Yuan Chen[4,5,9]

[1] *Department of Traditional Chinese Medicine, Taichung Veterans General Hospital, 1650 Taiwan Boulevard, Section 4, Taichung, 40705, Taiwan*

[2] *College of Chinese Medicine, China Medical University, No. 91, Hsueh-Shih Road, Taichung, Taiwan 40402, Taiwan*

[3] *Hungkuang University, No. 1018, Section 6, Taiwan Boulevard, Shalu District, Taichung 43302, Taiwan*

[4] *Division of Allergy, Immunology and Rheumatology, Department of Internal Medicine, Taichung Veterans General Hospital, 1650 Taiwan Boulevard, Section 4, Taichung 40705, Taiwan*

[5] *Faculty of Medicine, National Yang Ming University, No. 155, Section 2, Linong Street, Taipei, 112, Taiwan*

[6] *Department of Family Medicine, Center for Geriatrics and Gerontology, Taichung Veterans General Hospital 1650 Taiwan Boulevard, Section 4, Taichung 40705, Taiwan*

[7] *School of Medicine, Chung Shan Medical University, No. 110, Section 1, Jianguo North Road, Taichung 40201, Taiwan*

[8] *Biostatistics Task Force of Taichung Veterans General Hospital, 1650 Taiwan Boulevard, Section 4, Taichung 40705, Taiwan*

[9] *Institute of Biomedical Science, National Chung Hsing University, 250 Kuo Kuang Road, Taichung 402, Taiwan*

Correspondence should be addressed to Der-Yuan Chen; dychen@vghtc.gov.tw

Background. Guilu Erxian Jiao (GEJ) is a widely used Chinese herbal remedy for knee osteoarthritis, but its clinical efficacy is unknown. *Methods*. We enrolled 42 elderly male patients with knee OA, including 21 patients who received the herbal drug GEJ as the case group and 21 patients who did not receive GEJ as the control group. The effects of 12 weeks of GEJ treatment on muscle strength of lower limbs were measured by a Biodex dynamometer, with disability evaluated on the Lequesne index and articular pain measured on the visual analog scale (VAS) between the two groups on the baseline and after treatment. *Results*. There were significant increases in the levels of muscle strength of TQ/BW-ext-dominant and TQ/BW-flex-dominant between the two groups after treatment ($P < 0.05$). There were also significant increases in muscle strength of knee extensor muscles in the GEJ-treated group ($n = 21$) self-controlled before and after 12 weeks of treatment (all $P < 0.01$). There were significant decreases in articular pain ($P < 0.01$) and Lequesne index scores ($P < 0.01$) in the GEJ-treated group when compared to the non-GEJ-treated group. *Conclusions*. Our results showed that GEJ is effective and is tolerated well in elderly men with knee OA.

1. Introduction

Knee osteoarthritis (OA) is a common articular disease, affecting not only the joints but also the surrounding muscles and causing falls, disabilities, and dependency in older people [1, 2]. Quadricep strength deficits have been reported in 20%–70% of patients with knee OA [3, 4]. Any improvement in muscle strength or peak power of the lower extremities with decreased levels of articular pain may be important and is a strong predictor of functional ability [5–7].

There is no gold standard treatment for knee OA. Pharmacological approaches include analgesics, anti-inflammatory agents, intra-articular corticosteroids or hyaluronic acid, glucosamine sulphate, chondroitin sulphate, and some experimental treatments already widely used. However, these drugs have some adverse effects such as constipation, nausea, and excessive sedation in older people, and their effect on cartilage with OA symptoms remains controversial [8–15].

The herbal drug Guilu Erxian Jiao (GEJ) is a multicomponent Chinese herbal supplement that has been used for treatment of degenerative joint diseases without adverse effects for two thousand years [16–20]. However, understanding of the mechanisms responsible for the beneficial effects of GEJ is limited. Specifically, information on the effects of GEJ on muscle strength, articular pain, and disability in elderly men with knee osteoarthritis is scant. Therefore, it is very important to investigate the clinical effectiveness and safety of GEJ therapy for elderly men with knee OA.

The primary purpose of the present study was to investigate the therapeutic effects of 12 weeks of GEJ treatment on muscle strength in elderly male patients with knee OA. The secondary purpose was to investigate the effects of the same regimen on articular pain, the Lequesne disability index, and blood markers (liver and renal function).

2. Materials and Methods

2.1. Patients. A total of forty-two elderly men with knee OA who were regularly followed up at outpatient clinics of the departments of rheumatology and traditional Chinese medicine (TCM) were enrolled. Patients were included if they met the following criteria: males aged 65 years or older who could walk independently, fulfilled the 1986 American College of Rheumatology (ACR) classification of knee OA [21], received the same Western medication for OA regularly for 24 weeks before the study entry, had persistent articular pain and disability while under regular Western medication, and regular 12 weeks followed up during the study enrolled by a physician of rheumatology. Patients who had a history of coronary artery disease, previous knee surgery, severe visual impairment, stroke, severe pulmonary disease requiring the use of oxygen, hip fracture or lower extremity joint replacement in the past 6 months, and other inflammatory and/or infectious diseases, or who used other Chinese medicine or health products as indicated in their medical records, were excluded. The case group consisted of twenty-one patients who regularly received GEJ treatment (6 g/daily) for 12 weeks simultaneously and were followed up at the outpatient clinic of the department of TCM. The control group consisted of 21 patients who do not receive GEJ treatment and only continued to receive the same Western medication at the outpatient clinic of the department of rheumatology that had been prescribed for them before the study entry. Patient characteristics and variables, which were recorded at baseline and after treatment, included the following: age, BMI, Lequesne index, visual analog pain scale score (VAS), muscle power, liver function, and renal function. The study was approved by the Institutional Review Board (IRB) of Taichung Veterans General Hospital, Taiwan. A departmental database was searched to identify elderly patients with OA who were treated with GEJ between March 2007 and March 2008. The Ethics Committee of Taichung Veterans General Hospital approved this study (C06287) and the written consent of each participant was obtained according to the Declaration of Helsinki.

2.2. Study Design and Protocol. We enrolled 42 elderly men with knee OA, including 21 patients who received the herbal drug GEJ as the case group and 21 patients who did not receive GEJ and received the same Western medication as the control group. This study evaluated the effects of 12 weeks of GEJ treatment on muscle strength of lower limbs, physical function, and articular pain. The dominant side of the OA knee was defined as the joint with articular pain (VAS) > 5.

Twenty-one patients received four capsules three times a day of Guilu Erxian Jiao extract, 6 g/daily for 12 weeks. The GEJ capsules (batch number: CB118-091610) were prepared according to the well-documented TCM formula described in a TCM book known as "The Golden Mirror of Medicine," and provided by the Sun Ten Pharmaceutical Company, Ltd., Taiwan (drug permit license number-042004, Department of Health, Taiwan). The Sun Ten Pharmaceutical Company, Ltd. has received the herbal Good Manufacturing Practice (GMP) certification in Taiwan. The components of the GEJ capsules are Carapax and Plastrum Chrysemys (species: *Pseuclemys scripta elegans*, *Chrysemys scripta elegans*; Animal part: Plastrum); Cornu Cervi (species: *Rangifer tarandus*; animal part: antler); Ginseng Radix Rubra (species: *Panax ginseng* C. A. Mey; plant part: root) and *Lycii fructus* (species: *Lycium barbarum L.*; plant part: fruit). GEJ was prepared as follows: Carapax, Plastrum Chrysemys, and Cornu Cervi were stewed for 7 days, and then Ginseng Radix Rubra and Lycii Fructus were added into the mixture of Carapax, Plastrum Chrysemys, and Cornu Cervi [20]. A 2.8 g extract was derived from the ratio between the 4 components consisting of about 5 g (Carapax and Plastrum Chrysemys); 10 g (Cornu Cervi); 1.1 g (Ginseng Radix Rubra); 0.9 g (Lycii Fructus). Each 6 g/daily capsule contained 2.8 g extract and 3.2 g cornstarch in conformance to the drug permit license.

2.3. Measurement of Muscle Strength. Muscle strength of the knee extensors and flexors was assessed by an isokinetic dynamometer (Biodex Medical Systems, Inc., Shirley, NY, USA) according to the peak torque/body mass variable (Nm/kg) at a velocity of 60°/s. Maximum strength tests (one repetition maximum or 1RM) were performed fortnightly. Then, a new 80% load was prescribed during the interval between the strength tests. Participants were given 3% increments in load per session as tolerated [22, 23]. The calculation of muscle performance and the respective normalizations for body mass were performed by using the dynamometer software.

2.4. Measurement of Articular Pain. The pain severity of knee OA was evaluated by the visual analogue scale (VAS) at baseline and after 12 weeks in the two groups on a weight-bearing posture (walking) for 5 minutes. The instrument consists of horizontal lines 10 cm long, with anchor points of 0 (indicates no pain) and 10 (indicates maximum degree of pain.). The average of three measurements was recorded, and a 10-minute interval was set between tests to allow for more consistent measurement conditions [24].

2.5. Measurement of OA Disability. Disability of patients with knee OA was evaluated using the Lequesne index (LI) [25]. The questionnaire is divided into three parts: (I) pain or discomfort (5 questions), (II) maximum distance walked (2 questions), and (III) activities of daily living (4 questions). A score of 26 (maximum) indicates the greatest degree of dysfunction, and a score of 1–3 (minimum) indicates mild dysfunction [25, 26].

2.6. Statistical Analysis. Descriptive statistics were run on all variables. Associations among variables, including baseline characteristics, muscle strength, the Lequesne index, and pain outcomes, were evaluated with the Mann-Whitney U test. Incremental and decremental changes in quantitative variables after 12 weeks of treatment were compared with baseline data in the non-GEJ-treated group and the GEJ-treated group. The level of statistical significance was set at 0.05 for all hypothesis testing. When significant changes in the levels of muscle strength and decremental changes of VAS scores and Lequesne index scores between the two groups pre- and posttreatment were found, the variables of self-controlled were evaluated using the Wilcoxon signed-rank test in the GEJ-treated group before and after 12 weeks of treatment. Statistical significance for all tests was accepted with P values less than 0.05. A sample size calculation indicated that statistical significance could be achieved with 84% power using sample power 2.0 software.

We used logistic regression to estimate the ORs and 95% CIs for the association between the GEJ-treated group and the non-GEJ-treated group. Effects of herbal drug treatment were also assessed and the results were analyzed to identify any trends. The level of significance was established at $P < 0.05$ (tested by Wald statistic). The logistic regression was adjusted additionally for incremental changes of torque/body weight extension of the dominant and nondominant side (TQ/BW-ext-dominant and nondominant side); torque/body weight extension of the dominant side after treatment (TQ/BW-ext-dominant-side after treatment); torque/body weight flexion of the dominant side after treatment (TQ/BW-flex-dominant side after treatment); and decremental changes of subcategories in the Lequesne index: (I) change of pain or discomfort, (II) change of maximum distance walked, and (III) change of activities of daily living.

3. Results

3.1. Clinical Characteristics of OA Patients. Table 1 shows the baseline clinical characteristics of OA patients. There were no significant differences in age, body mass index (BMI), activities of daily living (ADL) scores, Lequesne index scores, balance tests, and muscle strength between the GEJ-treated group and the non-GEJ-treated group.

3.2. Changes in Muscle Strength after 12 Weeks of GEJ Treatment. Table 2 shows there were no significant incremental changes in the muscle strength of extensor and flexor muscles between the GEJ-treated group and the non-GEJ-treated group from baseline to the end of the 12 week GEJ treatment

period ($P > 0.05$, Table 2). Nevertheless, there were slightly higher incremental changes in the strength of TQ/BW-ext-nondominant and TQ/BW-ext-dominant extensor muscles ($P < 0.1$, Table 2) in the GEJ-treated group compared to those in the non-GEJ-treated group. There were no significant differences in the levels of TQ/BW-ext-dominant and TQ/BW-flex-dominant extensor muscles between the two groups at baseline ($P > 0.05$, Table 2). But there were significant increases in the levels of strength of TQ/BW-ext-dominant and TQ/BW-flex-dominant muscles in the GEJ-treated group compared to those in the non-GEJ-treated group ($P < 0.05$, Table 2 and Figure 1). Moreover, we also found that there were significant increases in strength of knee extensor muscles on the dominant side and nondominant side in the GEJ-treated group ($n = 21$) self-controlled before and after 12 weeks of treatment (all $P < 0.01$, Table 3 and Figure 3). Logistic regression analysis demonstrated a trend toward increase of extensor muscle strength on the dominant side (OR = 1.04; 95% CI 1.00–1.09; $P = 0.062$; Table 4).

3.3. Changes in Visual Analog Pain Scale Scores (VAS) after 12 Weeks of GEJ Treatment. Table 2 shows that there was a significantly greater decrease in articular pain scores in GEJ-treated patients than in non-GEJ-treated patients ($P < 0.01$) (Figure 2). Table 3 also shows that there was a significant decrease in articular pain scores in the GEJ-treated group before and after 12 weeks of treatment ($P < 0.01$) (Figure 4). Logistic regression analysis also demonstrated a significant decrease in articular pain scores after 12 weeks of GEJ therapy (OR = 2.33; 95% CI 1.09–4.98; $P = 0.029$; Table 4).

3.4. Changes in Lequesne Index Scores after 12 Weeks of GEJ Treatment. Table 2 shows there was a significantly greater decrease in Lequesne index (LI) scores of disability in GEJ-treated patients than in non-GEJ-treated patients ($P < 0.01$) (Figure 2). GEJ-treated patients also had a significant reduction in scores in all three parts of the Lequesne index: (I) pain or discomfort ($P < 0.01$), (II) maximum distance walked ($P < 0.01$), and (III) activities of daily living ($P < 0.05$). Table 3 shows there was a significant decrease in LI scores of disability observed in the GEJ-treated group before and after 12 weeks of treatment ($P < 0.05$). GEJ-treated patients also had a significant reduction in scores in two parts of the LI: (I) pain or discomfort ($P < 0.01$) and (III) activities of daily living ($P < 0.05$) in the GEJ-treated group before and after 12 weeks of treatment (Figure 4). Logistic regression analysis demonstrated a significant decrease in one component of the LI, (III) activities of daily living, after 12-weeks of GEJ therapy (OR = 2.28; 95% CI 1.12–4.65; $P = 0.023$) (Table 4).

3.5. Changes in Liver and Renal Function after 12 Weeks of GEJ Treatment. The levels of glutamic oxaloacetic transaminase (GOT) and glutamic pyruvic transaminase (GPT) were within normal limits after 12 weeks of GEJ treatment. There were no significant changes in renal function and urinalysis or urinary albumin-to-creatinine ratio (ACR = urine microalbumin/urine creatinine) after 12 weeks of GEJ treatment ($P > 0.1$). No cardiopulmonary dysfunction or

TABLE 1: Baseline clinical characteristics of the non-GEJ-treated group and the GEJ-treated group.

Variables	Non-GEJ-treated group ($n = 21$)			GEJ-treated group ($n = 21$)			P value
	Median	P_{25}	P_{75}	Median	P_{25}	P_{75}	
Age, years	83.00	81.00	87.00	82.00	80.00	86.00	0.528
BMI, kg/m^2	24.39	23.11	25.16	23.44	21.23	25.79	0.462
ADL	100.00	100.00	100.00	100.00	100.00	100.00	0.075
Lequesne index	4.00	0.00	6.00	6.00	3.00	9.00	0.108
Test for balance	0.00	0.00	0.00	0.00	0.00	0.00	0.317
PeakTQ-ext-nondominant (Nm)	31.60	21.50	52.90	38.80	18.20	45.90	0.725
PeakTQ-ext-dominant (Nm)	25.70	12.00	52.50	29.10	19.50	49.60	0.624
PeakTQ-flex-nondominant (Nm)	17.40	11.60	26.70	19.50	14.40	32.60	0.801
PeakTQ-flex-dominant (Nm)	17.30	10.80	28.90	18.80	15.70	33.20	0.345
TQ/BW-ext-nondominant (ft·lb/lb)	43.10	29.60	93.10	66.60	35.30	83.10	0.538
TQ/BW-ext-dominant (ft·lb/lb)	34.80	18.20	77.10	57.80	27.40	82.40	0.365
TQ/BW-flex-nondominant (ft·lb/lb)	26.30	16.40	40.20	33.00	24.40	51.20	0.473
TQ/BW-flex-dominant (ft·lb/lb)	25.50	17.90	46.10	37.30	24.20	53.80	0.204

Mann-Whitney U test; $^*P < 0.05$.

TABLE 2: Changes in muscle strength, VAS, and Lequesne index scores from baseline to 12 weeks in the non-GEJ-treated group and the GEJ-treated group.

Variables	Non-GEJ-treated group ($n = 21$)			GEJ-treated group ($n = 21$)			P-value
	Median	P_{25}	P_{75}	Median	P_{25}	P_{75}	
Incremental changes in muscle strength							
PeakTQ-ext-nondominant (Nm)	2.10	−4.80	14.30	17.70	3.90	28.20	0.090
PeakTQ-ext-dominant (Nm)	4.60	−1.60	11.70	14.80	3.30	23.20	0.105
PeakTQ-flex-nondominant (Nm)	3.30	−3.40	8.20	2.90	−1.20	10.20	0.308
PeakTQ-flex-dominant (Nm)	3.70	−1.40	8.80	2.80	−2.40	10.60	0.870
TQ/BW-ext-nondominant (ft·lb/lb)	4.70	−2.60	26.60	29.70	6.90	51.30	0.080
TQ/BW-ext-dominant (ft·lb/lb)	6.10	−2.90	20.40	29.30	6.00	37.30	0.063
TQ/BW-flex-nondominant (ft·lb/lb)	5.20	−6.00	11.60	4.90	−1.80	17.90	0.308
TQ/BW-flex-dominant (ft·lb/lb)	6.20	−2.50	12.70	4.80	−3.70	16.40	0.811
Levels of muscle strength of the two groups pre- and posttreatment							
TQ/BW-ext-dominant-pretreatment (ft·lb/lb)	34.80	18.20	77.10	57.80	27.40	82.40	0.365
TQ/BW-ext-dominant-posttreatment (ft·lb/lb)	50.20	26.50	70.00	87.10	58.90	99.40	0.012*
TQ/BW-flex-dominant-pretreatment (ft·lb/lb)	25.50	17.90	46.10	37.30	24.20	53.80	0.204
TQ/BW-flex-dominant-posttreatment (ft·lb/lb)	27.50	18.30	52.30	47.50	38.20	58.60	0.045*
Decremental change of visual analog pain scale score	0.00	−1.00	0.00	0.00	0.00	2.00	0.001**
Decremental change of Lequesne index score	−1.00	−3.00	0.00	2.00	1.00	4.00	0.0003**
(I) change of pain or discomfort	0.00	−1.00	0.00	1.00	0.00	2.00	0.002**
(II) change of maximum distance walked	0.00	−1.00	0.00	0.00	0.00	1.00	0.003**
(III) change of activities of daily living	0.00	−1.00	0.00	1.00	0.00	2.00	0.025*

Mann-Whitney U test; $^*P < 0.05$, $^{**}P < 0.01$.

adverse gastrointestinal effects were observed during the treatment period.

4. Discussion

To the best of our knowledge, the present study is the first attempt to investigate the therapeutic effects of the herbal drug GEJ on muscle strength, articular pain, and disability (Lequesne index) in elderly men with knee OA. Our results showed that elderly men displayed significant improvements in the muscle strength of the knee and a decrease of articular pain and Lequesne index scores after 12 weeks of GEJ treatment. All patients tolerated the therapy well and reported no adverse effects or changes in liver or renal function.

TABLE 3: Measurements of muscle strength, VAS, and Lequesne index scores in the GEJ-treated group ($n = 21$) before and after 12 weeks of treatment.

Variables	Pretreatment			Posttreatment			
	Median	P_{25}	P_{75}	Median	P_{25}	P_{75}	P value
Measurements of muscle strength							
PeakTQ-ext-nondominant (Nm)	38.80	18.20	45.90	52.10	37.90	65.30	0.007**
PeakTQ-ext-dominant (Nm)	29.10	19.50	49.60	51.60	40.10	62.60	0.001**
PeakTQ-flex-nondominant(Nm)	19.50	14.40	32.60	20.70	19.10	36.20	0.085
PeakTQ-flex-dominant (Nm)	18.80	15.70	33.20	30.80	21.70	36.70	0.092
TQ/BW-ext-nondominant (ft·lb/lb)	66.60	35.30	83.10	76.50	71.70	103.90	0.006**
TQ/BW-ext-dominant (ft·lb/lb)	57.80	27.40	82.40	87.10	58.90	99.40	0.001**
TQ/BW-flex-nondominant (ft·lb/lb)	33.00	24.40	51.20	39.70	31.40	55.80	0.092
TQ/BW-flex-dominant (ft·lb/lb)	37.30	24.20	53.80	47.50	38.20	58.60	0.076
Measurements of visual analog pain scale score (VAS)							
visual analog pain scale score	2.00	0.00	3.00	0.00	0.00	2.00	0.005**
Measurements of Lequesne index score							
Lequesne index score	6.00	3.00	9.00	3.00	0.00	6.00	0.001**
(I) Pain or discomfort	2.00	1.00	3.00	0.00	0.00	1.00	0.003**
(II) Maximum distance walked	1.00	1.00	3.00	1.00	0.00	2.00	0.150
(III) Activities of daily living	2.00	1.00	5.00	1.00	0.00	3.00	0.032*

Wilcoxon signed-rank test; *$P < 0.05$; **$P < 0.01$.

TABLE 4: Logistic regression analysis of the changes in the non-GEJ-treated group ($n = 21$) and the GEJ-treated group ($n = 21$).

Variable	Regression coefficient	S.E.	Odds ratio	95% CI of odds ratio	P value
Incremental change of TQ/BW-ext-dominant	0.041	0.022	1.04	1.00–1.09	0.062
Decremental change of visual analog pain scale score	0.846	0.388	2.33	1.09–4.98	0.029*
Change of (III) activities of daily living score	0.824	0.364	2.28	1.12–4.65	0.023*
Constant	−1.262	0.616	0.28		0.040

*$P < 0.05$ (tested by Wald statistic).
Accuracy of model = 78.6%.
Model III: backward regression.

Scientific data regarding the improvement of muscle strength after GEJ treatment in elderly men with knee OA are scant. In traditional Chinese medicine, GEJ has been used to treat kidney deficiency (qi, ying, and yang) and nourish blood, which plays an important role in treating joint disease at the cellular level [18, 20, 27]. The present study demonstrated a significant increase in muscle strength of extensor and flexor muscles after 12 weeks of GEJ treatment in elderly men with knee OA, with the most significant increase in the TQ/BW-ext-dominant. Improvement of muscle strength and balance and relief of articular pain are very important for elderly men with knee osteoarthritis who are prone to falls and may become disabled [3, 4]. GEJ may improve muscle strength and walking ability, which may in turn help these patients maintain functional independence [6, 28, 29]. Further studies are needed to elucidate the action mechanism of GEJ for improvement of muscle strength in elderly men with knee osteoarthritis.

Our results also showed a significant decrease in articular pain scores in GEJ-treated patients compared to non-GEJ-treated patients. An in vitro study revealed that GEJ could inhibit the apoptosis of chondrocyte-like phenotype bone mesenchymal stem cells (BMSCs), which reduced synovitis

and blocked cartilage destruction [30]. In mice, some results may be related to mechanisms regarding the chondroprotective effect of GEJ achieved through upregulation of bcl-2 mRNA expression and downregulation of caspase-3mRNA expression [18, 30]. In healthy volunteers, the results of a recent randomized, placebo-controlled, double-blind clinical trial study showed that the reversibility of the CD4+ to CD8+ lymphocyte ratio in the GEJ-treated group may explain the effectiveness of GEJ for treatment of knee OA [20]. No clinical changes in biochemical indicators of liver function, renal function, or hemograms were observed after GEJ treatment [20]. These results may explain the mechanism of the therapeutic effects of the herbal drug GEJ on articular pain. A previous study evaluated the effect of over-the-counter osteophyte capsules, which contain extracts of Radix Rehmannia *Rehamanniae* (Dihuang) and Herba Cistanches (Roucongrong), a traditional Chinese herb used for treatment of inflammation and articular pain in osteoarthritis. However, that study was limited by lack of placebo control and there was no double-blinding [31]. Another study investigated the effects of blood-nourishing and hard-softening (BNHS) capsules, a traditional Chinese formula used in the symptomatic treatment of inflammation and pain. BNHS capsules
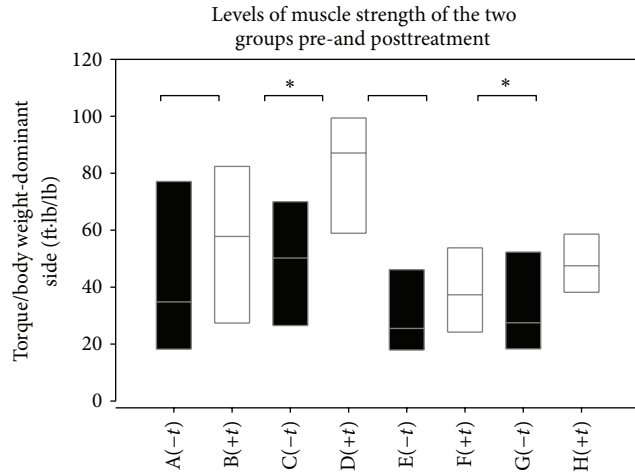
FIGURE 1: Box plots showing Torque/body weight of extension and flexion-dominant side for each subgroup. A ($-t$) group, TQ/BW-ext-pretreatment in Non-GEJ-treated group; B ($+t$) group, TQ/BW-ext-pretreatment in GEJ-treated group; C ($-t$) group, TQ/BW-ext-posttreatment in non-GEJ-treated group; D ($+t$) group, TQ/BW-ext-posttreatment in GEJ-treated group; E ($-t$) group, TQ/BW-flex-pretreatment in non-GEJ-treated group; F ($+t$) group, TQ/BW-flex-pretreatment in GEJ-treated group; G ($-t$) group, TQ/BW-flex-posttreatment in non-GEJ-treated group; H ($+t$) group, TQ/BW-flex-posttreatment in GEJ-treated group.

FIGURE 3: Box plots showing Torque/body weight of extension or flexion for each subgroup. A (pre) group, TQ/BW-ext-nondominant at pretreatment; B (post) group, TQ/BW-ext-nondominant at posttreatment; C (pre) group, TQ/BW-ext-dominant at pretreatment; D (post) group, TQ/BW-ext-dominant at posttreatment; E (pre) group, TQ/BW-flex-nondominant at pretreatment; F (post) group, TQ/BW-flex-nondominant at posttreatment; G (pre) group, TQ/BW-flex-dominant at pretreatment; H (post) group, TQ/BW-flex-dominant at posttreatment.
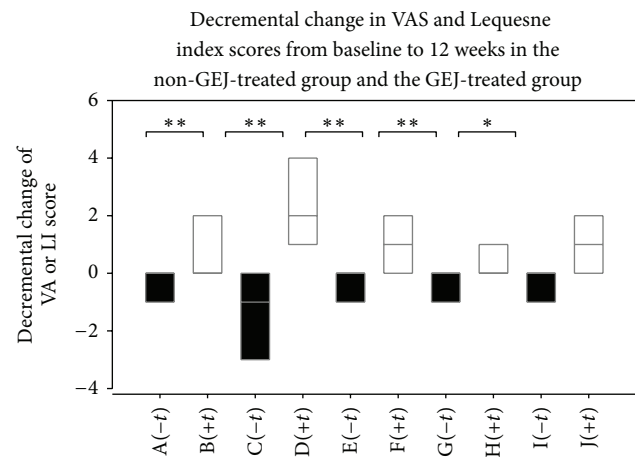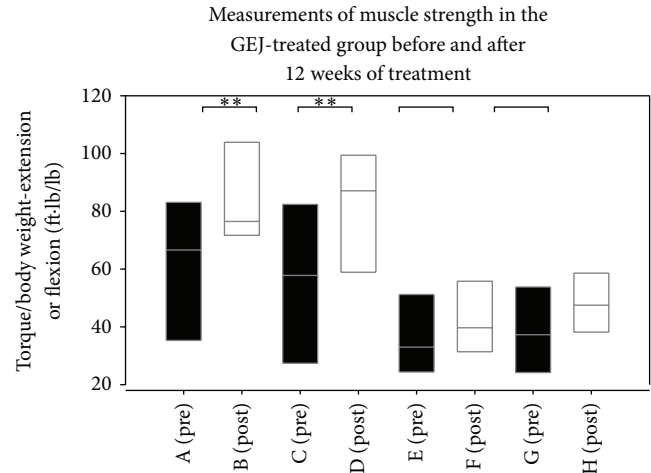

FIGURE 2: Box plots showing decremental change of VA or LI score for each subgroup. A ($-t$) group, decremental change of visual analog pain scale score in non-GEJ-treated group; B ($+t$) group, decremental change of visual analog pain scale score in GEJ-treated group; C ($-t$) group, decremental change of Lequesne index score in non-GEJ-treated group; D ($+t$) group, decremental change of Lequesne index score in GEJ-treated group; E ($-t$) group, (I) change of pain or discomfort in non-GEJ-treated group; F ($+t$) group, (I) change of pain or discomfort in GEJ-treated group; G ($-t$) group, (II) change of maximum distance walked in non-GEJ-treated group; H ($+t$) group, (II) change of maximum distance walked in GEJ-treated group; I ($-t$) group, (III) change of activities of daily living in non-GEJ-treated group; J ($+t$) group, (III) change of activities of daily living in GEJ-treated group.

consist of extracts from Bai Shao (*Radix Paeoniae Alba*), Qin Jiao (*Radix Gentianae Macrophyllae*), and Gan Cao (*Radix Glycyrrhizae*). This herbal drug can relieve disease-related symptoms within 4 weeks, such as pain and stiffness, as well as improving physical function in patients with painful knee OA [32]. In a clinical trial, Duhuo Jisheng Wan (DJW-herbal remedy) demonstrated clinical efficacy when compared to diclofenac after 4-weeks treatment. Only in the 4 weeks of treatment were the mean changes in VAS of the DJW-treated group significantly lower than those of the diclofenac-treated group. Afterwards, these mean changes became no different throughout the study [33]. The variables that may have influenced the results of the aforementioned studies are the age of patient populations, the severity of knee OA, the duration of medication taken, and the effectiveness of drugs used. The diverse results and lack of correlation in these studies may be due to several factors, including patient anxiety, motivation, habit of exercise, muscle atrophy, and aberrant joint mechanics [34]. In the present study, elderly men (mean age: 82-83 years) with knee OA who previously had poor compliance experienced a significant decrease in articular pain.

Moreover, there were decremental changes in all components of the Lequesne index in the GEJ-treated group compared to the non-GEJ-treated group after 12 weeks of treatment. In the GEJ-treated group, there was a significant reduction in two parts of the Lequesne index: (I) pain or discomfort and (III) activities of daily living. Our results were similar to the findings of some studies showing the efficacy of individualized Chinese herbal medication, which according to TCM diagnosis can reduce symptoms of OA. The results demonstrated statistically significant improvement in global

Measurements of VAS and Lequesne
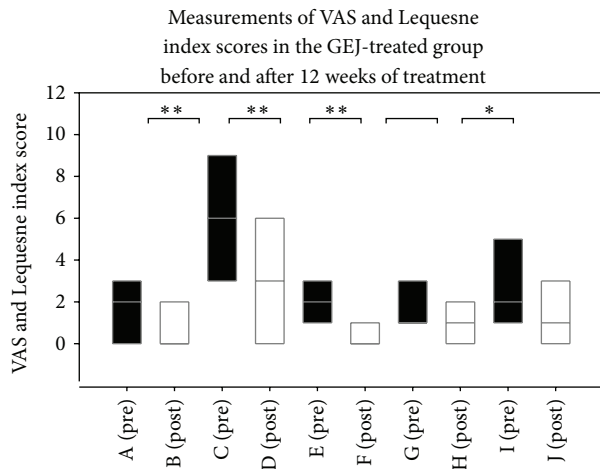index scores in the GEJ-treated group
before and after 12 weeks of treatment

FIGURE 4: Box plots showing VAS and Lequesne index score for each subgroup. A (pre) group, VAS at pretreatment; B (post) group, VAS at posttreatment; C (pre) group, Lequesne index score at pretreatment; D (post) group, Lequesne index score at posttreatment; E (pre) group, (I) pain or discomfort at pretreatment; F (post) group, (I) pain or discomfort at posttreatment; G (pre) group, (II) maximum distance walked at pretreatment; H (post) group, (II) maximum distance walked at posttreatment; I (pre) group, (III) activities of daily living at pretreatment; J (post) group, (III) activities of daily living at posttreatment.

WOMAC scores and WOMAC subscale scores (for pain, stiffness, and functional impairment) for knee OA [35]. It has previously been shown that patients with OA have impaired muscle activation compared with healthy controls and that pain in OA is assumed to be a major source of inhibition in the ability to voluntarily activate muscles surrounding arthritic joints [3, 36]. In the present study, the pain reduction after 12 weeks of GEJ treatment may have led to improved muscle activation in these patients. So, it may be related to increasing activities of daily living after having improvement on muscle strength and articular pain with GEJ treated. However, the exact mechanism of GEJ's effect on Lequesne index scores remains unclear.

Our results showed no significant influence of GEJ on liver or renal function, suggesting that it had no harmful impact on the biochemical profiles of patients. In a previous study, no adverse gastrointestinal effects, such as abdominal fullness, constipation, diarrhea, or nausea, were observed during 8 weeks of GEJ therapy [20]. If long-term ingestion of GEJ is feasible in the further treatment of elderly men with knee OA, we suggest regular follow-up of liver and kidney function via blood tests for a better understanding of the mechanisms of drug side effects and interactions.

The limitations of our study included the small sample size, the enrollment of men only, the short follow-up period, the advanced stage of knee OA, and the failure to measure life quality. It is possible that the statistical power of our study may not have been sufficient to detect potential differences between the two groups. Some patients might not have taken GEJ regularly during the study period. Some important confounding variables were also not fully addressed, such as diet or dietary supplements, which are known to affect articular pain. This may explain why there were only a few differences in muscle strength between the GEJ-treated group and the non-GEJ-treated group. It is possible that our selection criteria were too stringent. Patients who had a history of coronary artery disease, previous knee surgery, severe visual impairment, stroke, severe pulmonary disease requiring the use of oxygen, hip fracture or lower extremity joint replacement in the past 6 months, and other inflammatory and/or infectious diseases, or who used other Chinese medicine or health products as indicated in their medical records, were excluded. This makes it difficult to transfer the results to the general population with knee OA. However, the stringent selection criteria were necessary to ensure the homogeneity of the groups and, furthermore, to exclude people who were at high risk of having side effects. Furthermore, the elderly people with OA knee treated by GEJ are likely to be taking other drugs, such as analgesics or anti-inflammatory agents, so caution had to be exercised to avoid drug interactions that might lead to other medical problems.

5. Conclusions

Our results showed a significant improvement of the muscle strength of the lower limbs, above all the extensor muscle on the dominant side, in elderly men with OA knee who received 12 weeks of GEJ treatment. There were also significant decreases of articular pain scores and Lequesne index scores in these patients. GEJ treatment was well tolerated and caused no significant changes in liver or renal function. An improvement in physical function is clinically important in OA patients because it is a crucial predictor of the ability to perform daily activities and avoid falls. Future clinical trials will be required to extend and confirm these findings and a long-term follow-up is necessary to verify whether the benefits can be maintained.

List of Abbreviations

BMI:	Body mass index
ADL:	Activities of daily living
Peak TQ-ext-nondominant:	Peak torque extension of nondominant side
Peak TQ-ext-dominant:	Peak torque extension of dominant side
Peak TQ-flex-nondominant:	Peak torque flexion of nondominant side
Peak TQ-flex-dominant:	Peak torque flexion of dominant side
TQ/BW-ext-nondominant:	Torque/body weight extension of nondominant side
TQ/BW-ext-dominant:	Torque/body weight extension of dominant side
TQ/BW-flex-nondominant:	Torque/body weight flexion of nondominant side

TQ/BW-flex-dominant: Torque/body weight flexion
of dominant side
VAS: Visual analogue scale.

Conflict of Interests

The authors declare that there is no conflict of interests regarding the publication of this paper.

Authors' Contribution

Chen-Chen Tsai, Yin-Yi Chou, Yi-Ming Chen, Yih-Jing Tang, and Hui-Ching Ho contributed equally to this work.

Acknowledgment

References

[1] D. T. Felson, "Epidemiology of knee and hip osteoarthritis," *Epidemiologic Reviews*, vol. 10, pp. 1–28, 1988.

[2] S. R. Lord, C. Sherrington, and H. B. Menz, *Falls in Older People: Risk Factors and Strategies for Prevention*, Cambridge University Press, 2001.

[3] M. H. Arokoski, J. P. A. Arokoski, M. Haara et al., "Hip muscle strength and muscle cross sectional area in men with and without hip osteoarthritis," *Journal of Rheumatology*, vol. 29, no. 10, pp. 2185–2195, 2002.

[4] A. Chang, K. Hayes, D. Dunlop et al., "Thrust during ambulation and the progression of knee osteoarthritis," *Arthritis and Rheumatism*, vol. 50, no. 12, pp. 3897–3903, 2004.

[5] C. Jinks, K. Jordan, and P. Croft, "Osteoarthritis as a public health problem: the impact of developing knee pain on physical function in adults living in the community: (KNEST 3)," *Rheumatology*, vol. 46, no. 5, pp. 877–881, 2007.

[6] N. A. Sharkey, N. I. Williams, and J. B. Guerin, "The role of exercise in the prevention and treatment of osteoporosis and osteoarthritis.," *Nursing Clinics of North America*, vol. 35, no. 1, pp. 209–221, 2000.

[7] J. M. Chandler, P. W. Duncan, G. Kochersberger, and S. Studenski, "Is lower extremity strength gain associated with improvement in physical performance and disability in frail, community-dwelling elders?" *Archives of Physical Medicine and Rehabilitation*, vol. 79, no. 1, pp. 24–30, 1998.

[8] J. D. Bradley, K. D. Brandt, B. P. Katz, L. A. Kalasinski, and S. I. Ryan, "Comparison of an antiinflammatory dose of ibuprofen, an analgesic dose of ibuprofen, and acetaminophen in the treatment of patients with osteoarthritis of the knee," *The New England Journal of Medicine*, vol. 325, no. 2, pp. 87–91, 1991.

[9] T. J. Schnitzer, M. C. Hochberg, C. E. Marrero, B. Duquesroix, H. Frayssinet, and M. Beekman, "Efficacy and safety of naproxcinod in patients with osteoarthritis of the knee: a 53-week prospective randomized multicenter study," *Seminars in Arthritis and Rheumatism*, vol. 40, no. 4, pp. 285–297, 2011.

[10] F. M. Gloth III, "Pharmacological management of persistent pain in older persons: focus on opioids and nonopioids," *Journal of Pain*, vol. 12, no. 3, pp. S14–S20, 2011.

[11] F. Richy, O. Bruyere, O. Ethgen, M. Cucherat, Y. Henrotin, and J.-Y. Reginster, "Structural and symptomatic efficacy of glucosamine and chondroitin in knee osteoarthritis: a comprehensive meta-analysis," *Archives of Internal Medicine*, vol. 163, no. 13, pp. 1514–1522, 2003.

[12] T. E. Towheed, L. Maxwell, T. P. Anastassiades et al., "Glucosamine therapy for treating osteoarthritis," *Cochrane Database of Systematic Reviews*, no. 2, Article ID CD002946, 2005.

[13] A. Moore, S. Derry, and H. McQuay, "Differing results of trials of glucosamine for pain in arthritis," *Arthritis and Rheumatism*, vol. 58, no. 1, pp. 332–333, 2008.

[14] N. R. Dostrovsky, T. E. Towheed, R. W. Hudson, and T. P. Anastassiades, "The effect of glucosamine on glucose metabolism in humans: a systematic review of the literature," *Osteoarthritis and Cartilage*, vol. 19, no. 4, pp. 375–380, 2011.

[15] J. E. Pope, K. McCrea, A. Stevens, and J. Ouimet, "The relationship between NSAID use and osteoarthritis (OA) severity in patients with hip and knee OA: results of a case control study of NSAID use comparing those requiring hip and knee replacements to those in whom surgery was not recommended," *Medical Science Monitor*, vol. 14, no. 12, pp. CR604–CR610, 2008.

[16] L. Long, K. Soeken, and E. Ernst, "Herbal medicines for the treatment of osteoarthritis: a systematic review," *Rheumatology*, vol. 40, no. 7, pp. 779–793, 2001.

[17] Z. P. Zhang, Q. Liao, Y. Li, and W. G. Chen, "Experimental study of effects of PAP on metabolism of chondrocytes cultured in vitro," *Journal of Jiangxi University of Traditional Chinese Medicine*, vol. 17, no. 12, pp. 48–49, 2005 (Chinese).

[18] S.-Y. Lin, M.-H. Shen, and J. Chen, "Effect of guilu erxianjiao in suppressing splenic T-lymphocyte apoptosis in mice undergoing chemotherpy," *Chinese Journal of Integrated Traditional and Western Medicine*, vol. 28, no. 4, pp. 339–342, 2008 (Chinese).

[19] C. Mao, Y. Zhang, W. Yan, and X. Zheng, "Effects of serum containing oral liquid of Guilu-Erxian on the therapy of osteoporosis at the cellular level," *Shengwu Yixue Gongchengxue Zazhi*, vol. 25, no. 4, pp. 897–902, 2008 (Chinese).

[20] Y. H. Lin, H. Y. Chen, Y. C. Li, J. C. Chiu, and S. H. Yang, "Adverse events assessment of traditional Chinese herbal product, Guilu Erxian Jiao, in healthy volunteers," *Journal of Chinese Medicine*, vol. 22, no. 1-2, pp. 65–75, 2011.

[21] R. Altman, E. Asch, and D. Bloch, "Development of criteria for the classification and reporting of osteoarthritis. Classification of osteoarthritis of the knee," *Arthritis and Rheumatism*, vol. 29, no. 8, pp. 1039–1052, 1986.

[22] M. L. A. S. Santos, W. F. Gomes, D. S. Pereira et al., "Muscle strength, muscle balance, physical function and plasma interleukin-6 (IL-6) levels in elderly women with knee osteoarthritis (OA)," *Archives of Gerontology and Geriatrics*, vol. 52, no. 3, pp. 322–326, 2011.

[23] D. H. Perrin, *Isokinetic Exercise and Assessment*, Human Kinetics, Champaign, Ill, USA, 1993.

[24] M.-C. Weng, C.-L. Lee, C.-H. Chen et al., "Effects of different stretching techniques on the outcomes of isokinetic exercise in patients with knee osteoarthritis," *Kaohsiung Journal of Medical Sciences*, vol. 25, no. 6, pp. 306–315, 2009.

[25] S. C. O'Reilly, A. Jones, K. R. Muir, and M. Doherty, "Quadriceps weakness in knee osteoarthritis: the effect on pain and disability," *Annals of the Rheumatic Diseases*, vol. 57, no. 10, pp. 588–594, 1998.

[26] M. G. Lequesne, C. Mery, M. Samson, and P. Gerard, "Indexes of severity for osteoarthritis of the hip and knee," *Scandinavian Journal of Rheumatology*, vol. 16, no. 65 supplement, pp. 85–89, 1987.

[27] S. Tsuyoshi Ohnishi, K. Nishino, S. Uchiyama, T. Ohnishi, and M. Yamaguchi, "Ki-energy (life-energy) stimulates osteoblastic cells and inhibits the formation of osteoclast-like cells in bone cell culture models," *Evidence-Based Complementary and Alternative Medicine*, vol. 4, no. 2, pp. 225–232, 2007.

[28] M. Fransen, S. McConnell, and M. Bell, "Therapeutic exercise for people with osteoarthritis of the hip or knee: a systematic review," *Journal of Rheumatology*, vol. 29, no. 8, pp. 1737–1745, 2002.

[29] M. E. Van Baar, W. J. Assendelft, J. Dekker, R. A. Oostendorp, and J. W. Bijlsma, "Effectiveness of exercise therapy in patients with osteoarthritis of the hip or knee: a systematic review of randomized clinical trials," *Arthritis & Rheumatology*, vol. 42, pp. 1361–1369, 1999.

[30] W. S. Li, N. Li, H. M. Wang, X. H. Li, H. S. Zhan, and Y. Y. Shi, "Effects of guilu erxian decoction serum on apoptosis of chondrogenic phenotype bone marrow-derived mesenchymal stem cells in vitro," *Chinese Journal of Traumatology and Orthopaedics*, vol. 17, no. 1, pp. 5–7, 2009 (Chinese).

[31] L. BL, "Clinical report of counter-osteophytes capsule on the treatment of OA in 1,000 cases," *Liaoning Journal of Traditional Chinese Medicine*, vol. 3, pp. 40–41, 1982.

[32] Y. Cao, Y. Shi, Y. Zheng, M. Shi, and K. L. K. Sing, "Blood-nourishing and hard-softening capsule costs less in the management of osteoarthritic knee pain: a randomized controlled trial," *Evidence-Based Complementary and Alternative Medicine*, vol. 2, no. 3, pp. 363–368, 2005.

[33] S. Teekachunhatean, P. Kunanusorn, N. Rojanasthien et al., "Chinese herbal recipe versus diclofenac in symptomatic treatment of osteoarthritis of the knee: a randomized controlled trial [ISRCTN70292892]," *BMC Complementary and Alternative Medicine*, vol. 4, article 19, 2004.

[34] G. K. Fitzgerald, "Therapeutic exercise for knee osteoarthritis: considering factors that may influence outcome," *Europa Medicophysica*, vol. 41, no. 2, pp. 163–171, 2005.

[35] M. Lechner, I. Steirer, B. Brinkhaus et al., "Efficacy of individualized chinese herbal medication in osteoarthrosis of hip and knee: a double-blind, randomized-controlled clinical study," *Journal of Alternative and Complementary Medicine*, vol. 17, no. 6, pp. 539–547, 2011.

[36] J.-N. Lai, J.-S. Hwang, H.-J. Chen, and J.-D. Wang, "Finished herbal product as an alternative treatment for menopausal symptoms in climacteric women," *Journal of Alternative and Complementary Medicine*, vol. 11, no. 6, pp. 1075–1084, 2005.

Research Article

Pharmacokinetics of Two Alkaloids after Oral Administration of *Rhizoma Coptidis* Extract in Normal Rats and Irritable Bowel Syndrome Rats

Zipeng Gong,[1] Ying Chen,[1] Ruijie Zhang,[1] Yinghan Wang,[1,2] Qing Yang,[1] Yan Guo,[1] Xiaogang Weng,[1] Shuangrong Gao,[1] Hailin Wang,[1] Xiaoxin Zhu,[1] Yu Dong,[3] Yujie Li,[1] and Yajie Wang[1]

[1] *Institute of Chinese Materia Medica, China Academy of Chinese Medical Sciences, No. 16, Dongzhimen Nei Nanxiao Road, Dongcheng District, Beijing 100700, China*
[2] *Institute of Chinese Materia Medica, Chengde Medical University, Chengde 067000, China*
[3] *Guang'an Men Hospital, China Academy of Chinese Medical Sciences, No. 5, Beixiange Road, Xicheng District, Beijing 100053, China*

Correspondence should be addressed to Xiaoxin Zhu; zhuxiaoxin@icmm.ac.cn and Yu Dong; dongyu250541@sina.com

A comparative pharmacokinetic study of berberine and palmatine after oral administration of *Rhizoma Coptidis* extract (96 mg/kg, containing berberine 22 mg/kg and palmatine 5 mg/kg based on body weight) was performed in normal and postinflammation irritable bowel syndrome (PI-IBS) rats, induced by intracolonic instillation of acetic acid and restraint stress. Quantification of berberine and palmatine in rat plasma was achieved by using a sensitive and rapid UPLC-MS/MS method. Plasma samples were collected at 13 different time points and the pharmacokinetic parameters were analyzed by WinNonlin software. The significant differences in the pharmacokinetic behaviors, such as C_{max}, $\mathrm{AUC}_{(0-t)}$, V_d/F, and CL/F, of berberine and palmatine were found between normal and PI-IBS model rats. The results indicated that PI-IBS pathological conditions in rats could alter the pharmacokinetic behavior of drug. Preclinical pharmacokinetic studies are usually carried out on healthy animals. However, we should pay more attention to the fact that the change of pharmacokinetic behavior plays an important role on efficacy. It is essential to investigate the pharmacokinetics of the drug in disease status.

1. Introduction

Irritable bowel syndrome (IBS) is a chronic functional digestive tract disease, whose symptoms mainly involve not only abdominal pain or distention and abnormal defecation, but also psychological symptoms including anxiety and depression [1]. Postinflammation irritable bowel syndrome (PI-IBS) has been defined as an acute onset IBS symptoms (by Rome criteria) that develop after the individual, who has not previously met the Rome criteria, experiences a gastrointestinal infection with two or more of the following characteristics: fever, vomiting, diarrhea, or a stool culture positive for an infectious agent [2, 3]. However, the pathogenesis of PI-IBS is still unclear, which restrains the development of proper models and drugs for PI-IBS.

Rhizoma Coptidis (RC), known as Huang Lian, was officially recognized in the *Chinese Pharmacopoeia* [4] and has been reported to exert a number of pharmacological actions including antispasmodic [5], anti-Alzheimer's disease [6], hypolipidemic [7], anti-inflammatory [8], antitumor [9], and antibacterial [10]. In addition it was described to ameliorate radiation-induced skin injury [11]. Moreover, RC is also used to treat syndromes including abdominal pain and diarrhea [12], including PI-IBS. RC mainly consists of various alkaloids, including berberine, palmatine, coptisine, and epiberberine [13]. Berberine is an important and typical constituent in RC, which possesses a variety of activities including antitumor [14], anti-inflammation [15], and antiatherosclerosis and has also been used to treat infectious diarrhea [16]. The

other important constituent of RC is palmatine, which was reported to present some pharmacological effects such as liver-protective and cardiovascular protective effects [17, 18].

In the previous study, we found that the pharmacokinetic profiles of berberine after oral administration of hydrochloride berberine could be significantly altered in PI-IBS rats [19]. Compared with the control group, $AUC_{(0-t)}$ significantly increased in the PI-IBS group while CL/F considerably decreased. RC is a fundamental herb of traditional Chinese medicine prescriptions used to treat PI-IBS and its side effect is less than the pure berberine. Therefore, in the current study we compared the pharmacokinetics of berberine and palmatine in rat plasma after oral administration of RC extraction in normal and PI-IBS rats using WinNonlin software.

2. Materials and Methods

2.1. Materials. Rhizoma Coptidis is the dried rhizome of *Coptis chinensis* Franch, which was purchased from a local store (Sichuan, China) and identified by Professor Jinda Hao, a botanist and professor at the Institute of Chinese Materia Medica, China Academy of Chinese Medical Sciences. The voucher specimen (no. 110926) has been preserved in our laboratory. Berberine chloride with the purity of 86.7% and palmatine chloride with the purity of 86.1% were obtained from the National Institute for the Control of Pharmaceutical and Biological Products (Beijing, China). Methanol and acetonitrile of chromatographic grade were from Fisher Co., Ltd. (Waltham, USA). Formic acid was obtained from Merck KGaA Co. (Darmstadt, Germany). Deionized water purified by a Milli-Q water purification system (Milford, USA) was used throughout the study. All other reagents were of analytical grade from Beijing Chemical Reagent Co. (Beijing, China).

2.2. Preparation of Ethanol Extract of RC. The ethanol extract of RC was prepared by the Department of Pharmacy in China-Japan Friendship Hospital and its main constituents were reported to be alkaloids. The content of berberine and palmatine in the ethanol extract of RC was 23.03% and 5.52% [20].

2.3. Animals. Twenty male Sprague-Dawley rats (230–270 g) were obtained from Beijing Vital River Laboratory Animal Technology Co., Ltd. (Beijing, China), housed under standard conditions of temperature, humidity, and light, and had free access to standard rodent diet and water before the experiment. Animal welfare and experimental procedures were strictly in accordance with the Guide for the Care and Use of Laboratory Animals. The animal protocol was approved by the Animal Ethics Committee at the Institute of Chinese Materia Medica, China Academy of Chinese Medical Sciences. Animals were randomly divided into a control and a model group.

2.4. Induction of PI-IBS Rats and Administration. After an overnight fast, acute colonic inflammation of 10 rats was induced as PI-IBS model by intracolonic instillation of 4%

acetic acid (1 mL) by a silicone tube connected with injector at 8 cm proximal to the anus for 30 s. Then, phosphate buffered saline (1 mL) was instilled to dilute the acetic acid and rinse the colon. The control rats were handled identically except that saline was instilled instead of 4% acetic acid. One week later, the front upper limb, chest, and front porch of PI-IBS model rats were wrapped by adhesive tape for 1 h. The rats had free access to food and water, except when the procedure required deprivation. As previously described [19], distal colonic motility, motility index (MI), number of feces defecated in 2 h, and the time of glass bead output were performed to quantify the visceral hypersensitivity and altered colonic motility after subsidence of inflammation in rats before acetic acid enema and after being crimped.

RC was administered by gastric gavages at the 7 days and behavior tests periods. The control group rats were given distilled water (10 mL/kg).

2.5. Drug Analysis. Plasma concentrations of berberine and palmatine were determined by using the UPLC-MS/MS method previously developed and validated [20]. The qualitative chemical profile of these extracts was analyzed by UPLC-MS/MS as previously described [21]. And the content of berberine and palmatine in the ethanol extract of RC was 23.03% and 5.52%.

2.6. Pharmacokinetic Analysis. Before the experiment, the rats were fasted overnight and then subjected to the following surgical procedures under anesthesia induced by intraperitoneal injection of chloral hydrate at 150 mg/kg. A polyethylene catheter (0.50 mm i.d., 1.00 mm o.d.; Portex Limited, Hythe, China) was cannulated into the right jugular vein. The distal end of the catheter was led under the skin and exteriorized at the back of the neck. After surgery, the rat was then allowed to recover for 24 h and fasted overnight prior to drug administration. The RC extract freshly dissolves in pure water after dispersion with the aid of an ultrasonic instrument administered intragastrically (i.g.) into rats. After drug administration, the blood samples (200 μL) were collected from the catheter into heparinized centrifuge tubes at appropriate intervals (5 min, 15 min, 30 min, and 1, 1.5, 2, 3, 4, 6, 8, 10, and 12 h). After centrifugation at 3500 rpm for 15 min, 100 μL of plasma was collected and stored at −80°C until analysis. After each blood collection, 200 μL of physiological saline containing 20 units/mL of heparin was immediately injected back into the body to flush the catheter and prevent coagulation. The amounts of berberine and palmatine in plasma were estimated by UPLC-MS/MS analysis as described previously.

2.7. Pharmacokinetic Data Analysis. Noncompartmental methods using WinNonlin software (Pharsight Corporation, Mountain View, USA, Version 6.3) were used to analyze plasma concentration *versus* time profiles and estimate the following pharmacokinetic parameters: terminal elimination half-life ($t_{1/2}, \lambda_z$); area under the plasma concentration *versus* time curve from zero to the last sampling time (AUC_{0-t}); volume of distribution (V_d, λ_z); and total body clearance (CL). The peak plasma concentration (C_{max}) and the time to
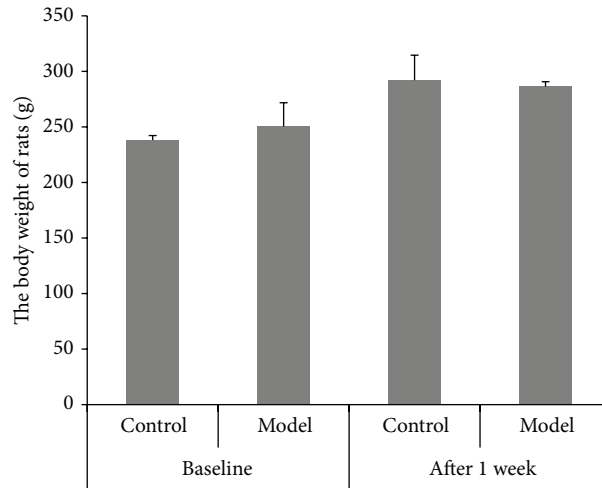
FIGURE 1: The change of body weight before enema and after stress in rats (mean ± SD, $n = 10$).

reach $C_{\max}$ ($T_{\max}$) for i.g. dose were read directly from the observed individual plasma concentration-time data.

2.8. Data Analysis. All reported values represent mean ± SD. The statistical difference was calculated using an unpaired t-test with a two-tailed distribution for comparison of two mean values. P value < 0.05 was considered statistically significant.

3. Results

3.1. The Change in Body Weight of Rats. Before enema and after stress, the body weights of rats were measured (Figure 1). The increase in body weight of rats in model group was slower than that of rats in control group (238 g *versus* 292 g for control group and 250 g *versus* 286 g for model group). However, the difference between the two groups before enema and after stress was not significant.

3.2. Recording of Distal Colonic Motility and Calculation of Motility Index (MI). Before enema and after stress, the distal colonic MI was observed (Figure 2) and calculated (Figure 3). At the time point before enema, there was no remarkable difference in MI between two groups. After given the stress, the distal colonic MI in the model group was significantly accelerated from 1126.83 mmHg·s to 2060.67 mmHg·s compared with the control group.

3.3. The Time of the Glass Bead Output and the Number of the Fecal Pellet Outputs in 2 Hours. Before enema and after stress, the time of the glass bead output (Figure 4) and the number of the fecal pellet outputs in 2 hours (Figure 5) were observed and calculated. At the time point before enema, there was no remarkable difference in the time of the glass bead output and the number of the fecal pellet outputs in 2 hours between the two groups. However, the time of the glass bead output in the model group was significantly shortened and the number of the fecal pellet outputs in model group was significantly

TABLE 1: The number of the mast cells in proximal colon (mean ± SD, $n = 5$).

Group	Mast cell count after stress (piece)
Control	3.27 ± 1.05
Model	6.77 ± 2.73[*]

[*] P < 0.05 compared with the control group.

increased compared with the control group after given the stress.

3.4. Histological Features of Colonic Tissue. Mucosal histological features in the lamina propria and the submucosa were observed by microscopy. Figure 6 shows a clear and integral structure of colonic mucosa, including a continuous and integral intestinal epithelium, regular glandular arrangement, and no abnormal cells. In addition, few inflammatory cell infiltrations are seen in the lamina propria. There is no remarkable inflammatory feature in the colon of the rats in the control as well as the model group.

3.5. Mast Cells Count and Degranulation Rate in the Proximal Colon. Figure 7 shows the distribution and quantity of the mast cells. Most of the mast cells were distributed in the submucosa and lamina propria, in line or around the digestive tract's vessels, lymphatic vessels, and peripheral nerves. Mast cells were round, oval, or irregular, featured as aubergine cytoplasm and blue karyon using a toluidine blue stain. Moreover, the smaller cells had less cytoplasm and clear periphery while the bigger ones had not only more cytoplasm and unclear peripheries but also aubergine granules around the karyon. The distribution of the mast cells in the model group was the same as the control group. However the number of mast cells in the model group was remarkably increased (Table 1). Also the cytomembrane of mast cells in the model group was ruptured and aubergine granules were dispersed in intercellular matrix. These results indicate that
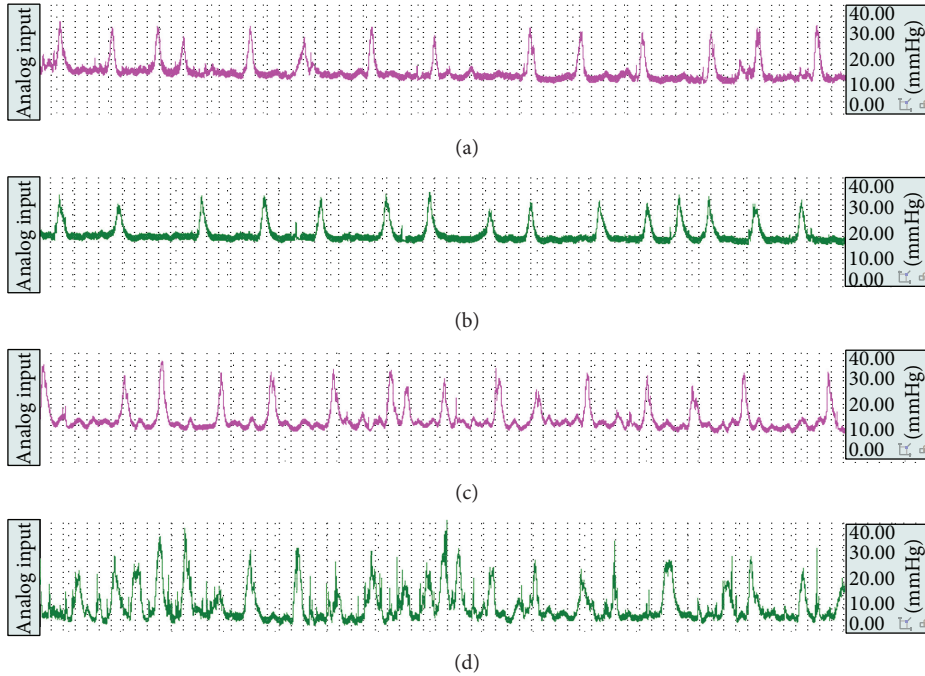
(a)

(b)

(c)

(d)

FIGURE 2: The representative curve of colonic movement in the control group (a) and the model group (b) before enema and in the control group (c) and the model group (d) after stress.
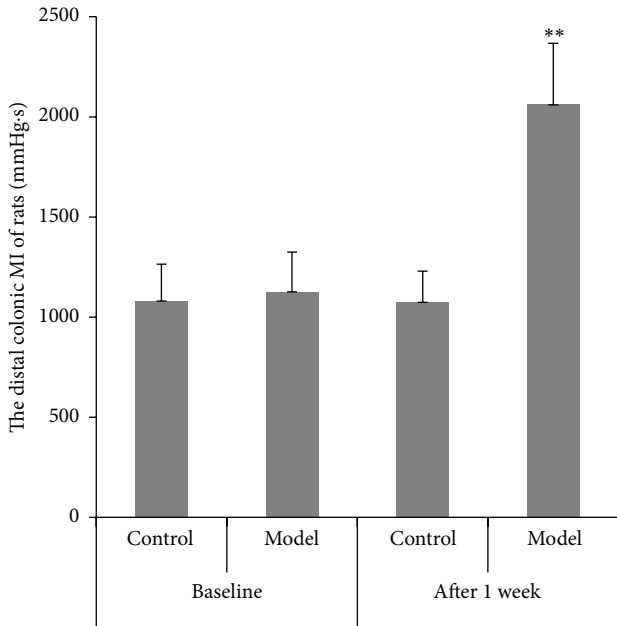

FIGURE 3: The distal colonic MI of rats in the control group and the model group (mean ± SD, $n = 10$). $^{**}P < 0.01$ compared with normal group.

FIGURE 4: Time of the glass bead output (s) (mean ± SD, $n = 10$). $^{**}P < 0.01$ compared with normal group.

intracolonic instillation of acetic acid with restraint stress can cause the anomaly of mast cells.

3.6. *Pharmacokinetic Analysis.* The mean plasma concentrationtime profiles of berberine and palmatine following intragastric (i.g.) administration of the RC extract are represented in Figure 8. Also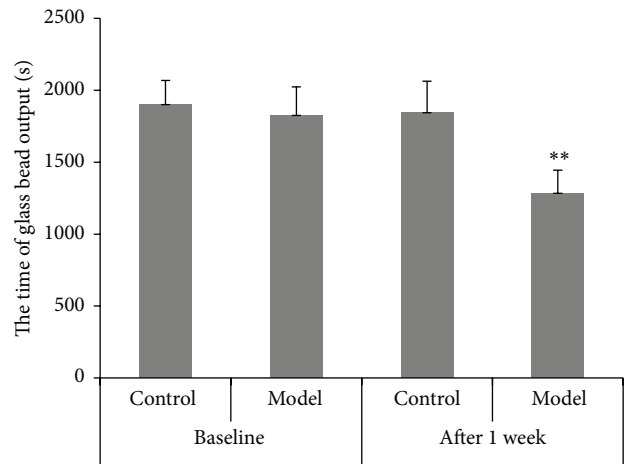, their pharmacokinetic parameters are summarized in Table 2. The results show that both berberine and palmatine were absorbed rapidly by the body 15 min after intragastric administration of RC extraction in both the control and model groups. Moreover, it is noteworthy that the C_{max} and the area under the plasma drug concentration *versus* time curves of berberine were significantly increased in the model group (39.18 ± 7.85 ng/mL; 9874.67 ± 2713.10 min·ng/mL) in comparison to the control group (20.04 ± 12.14 ng/mL; 4954.25 ± 784.34 min·ng/mL). On the other hand, compared with that in control group (5124.29 ± 1841.24 L/kg; 198.61 ± 75.35 L/h/kg), the marked decrease of V_d/F and CL/F of berberine in the model
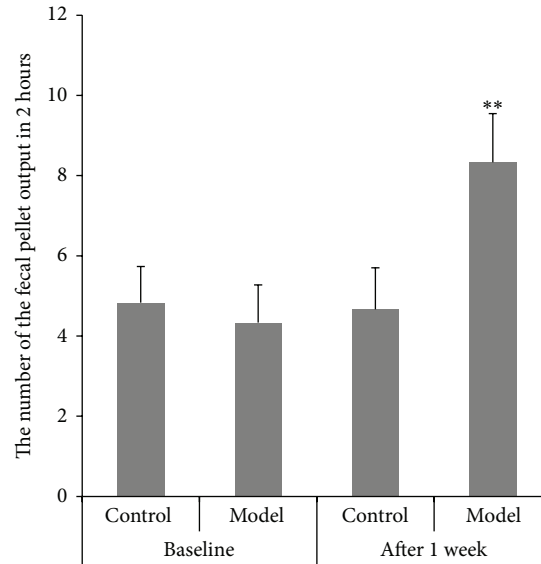
FIGURE 5: Number of the fecal pellet outputs in 2 hours (mean $\pm$ SD, $n = 10$). $^{**}P < 0.01$ compared with normal group.
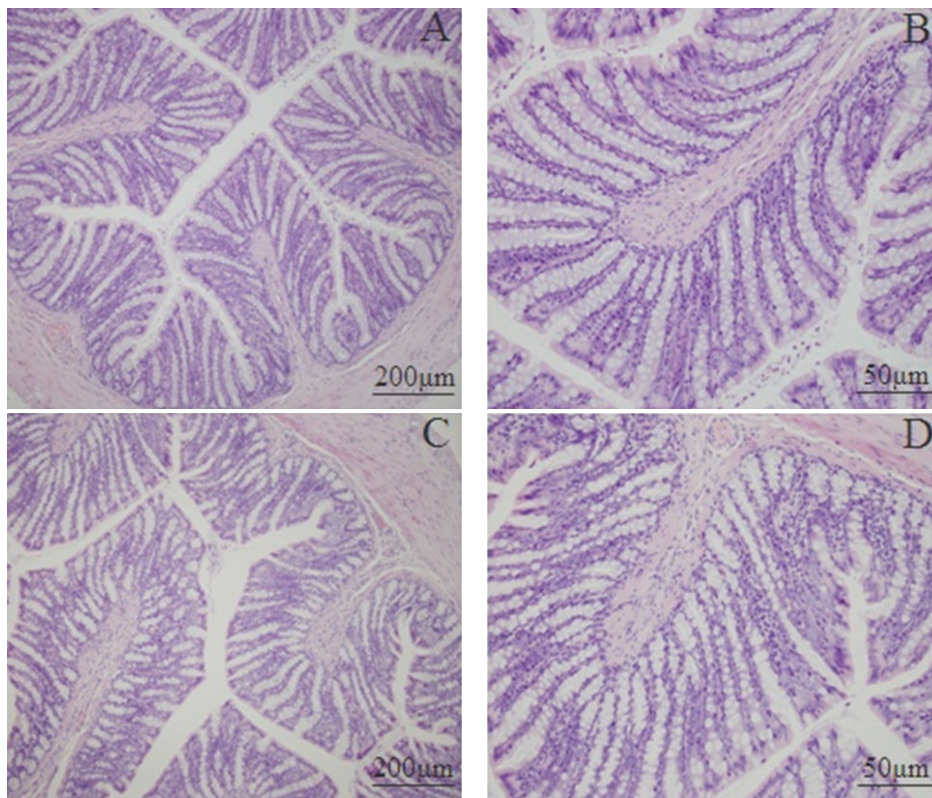

FIGURE 6: Photomicrographs of distal colons from the control group (A, ×100; B, ×400) and model group (C, ×100; D, ×400) by hematoxylin and eosin staining.

group (2503.89 $\pm$ 542.41 L/kg; 124.34 $\pm$ 27.42 L/h/kg) suggested that the elimination of berberine slowed down. For palmatine, the $\text{AUC}_{(0-t)}$ in the model group significantly increased (1470.61 $\pm$ 229.83 min·ng/mL *versus* 2186.61 $\pm$ 693.35 min·ng/mL). Additionally, a second peak at 3 hours for berberine and 4 hours for palmatine was observed in the model group.

4. Discussion

The curing PI-IBS effect of herbs has been paid more and more attention because of increasing incidence of PI-IBS and lack of effective drugs. Animal models of PI-IBS play an important role in the screening and evaluation of drugs for PI-IBS patients.
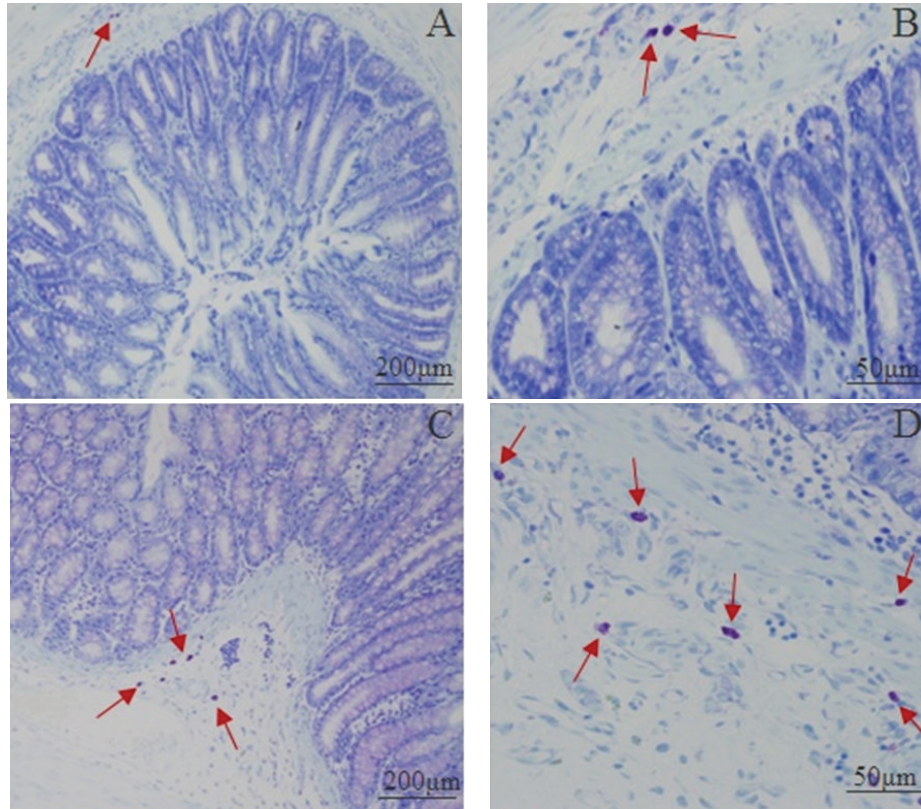
FIGURE 7: Photomicrographs of mast cell in proximal colons from the control group (A, ×100; B, ×400) and the model group (C, ×100; D, ×400) by toluidine blue staining. The red arrows indicated the mast cell.
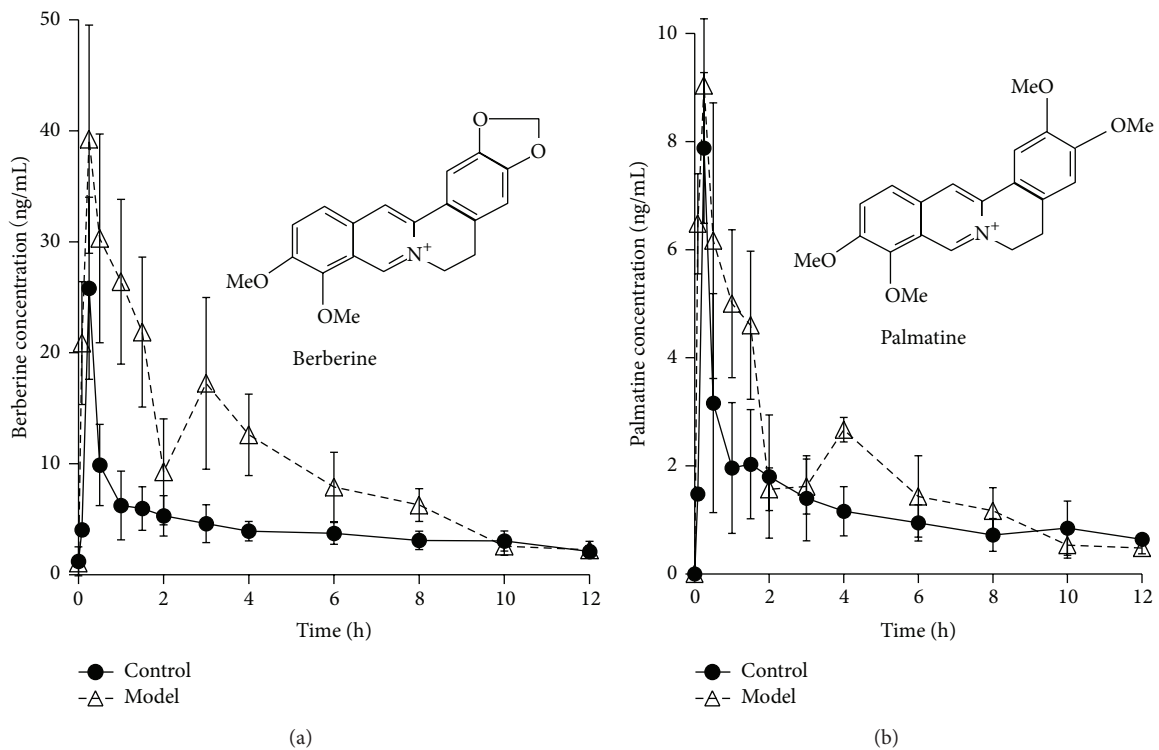

(a)

(b)

FIGURE 8: The mean plasma concentration (ng/mL) of berberine and palmatine *versus* time (h) profiles after oral administration of *Rhizoma Coptidis* extract in the control and PI-IBS model rats. Values were expressed as mean ± SD ($n = 5$).

TABLE 2: Pharmacokinetic parameters of berberine and palmatine in rat after oral administration of *Rhizoma Coptidis* extract at a dose of 96 mg/kg (mean ± SD, $n = 5$).

Parameters	Berberine		Palmatine	
	Control	Model	Control	Model
$T_{1/2,\lambda z}$ (min)	945.8 ± 349.5	836.2 ± 253.3	1611.7 ± 616.0	1521.7 ± 710.9
T_{max} (min)	15.0 ± 0.0	15.0 ± 0.0	15.0 ± 0.0	15.0 ± 0.0
C_{max} (ng/mL)	20.0 ± 12.1	39.2 ± 7.9[**]	8.1 ± 2.2	9.1 ± 1.2
AUC_{0-t} (min·ng/mL)	4954.3 ± 784.3	9874.7 ± 2713.1[**]	1470.6 ± 229.8	2186.6 ± 693.4[*]
$V_d/F_{\lambda z}$ (L/kg)	5124.3 ± 1841.2	2503.9 ± 542.4[**]	4869.6 ± 1237.6	4315.9 ± 1111.3
CL/F (L/h/kg)	198.6 ± 75.4	124.3 ± 27.4[*]	147.4 ± 45.3	119.3 ± 28.1

[**]$P < 0.01$ and [*]$P < 0.05$ compared with the control group.

In the present study, PI-IBS rat models were established by intracolonic instillation of acetic acid to induce acute inflammation of colon; after the inflammation resolved, wrap restraint stress was given to the rats. During the process of modeling, the rats in the model groups all have serious diarrhea in the three days after enema; this diarrhea gradually resolved in the following days. The body weight in the model group grew slowly while that in the control group grew faster. MI is significantly increased after given stress in the model group. Moreover, the number of mast cells in model group was dramatically increased. However, there was no remarkable inflammatory feature in the colon of the rats in control and model group. These results indicate that intracolonic instillation of acetic acid with wrap restraint stress can largely imitate the symptoms of human PI-IBS and be used as animal models of PI-IBS [22].

RC is a key component of many traditional Chinese medicine prescriptions used to treat syndromes including inflammation [23] and diarrhea, including PI-IBS. However, up to now, little attention has been paid to the pharmacokinetics of alkaloids in irritable bowel syndrome animals and human. Also, drugs are used to treat diseases and only patients are the ultimate consumers of drugs. It is necessary to study the pharmacokinetics of alkaloids in the pathological state. Therefore, in our study, we compared the pharmacokinetics of berberine and palmatine in rat plasma after oral RC at a dosage of 96 mg/kg between normal and PI-IBS rats. The findings showed that C_{max} and $AUC_{(0-t)}$ of berberine in the model group significantly increased while V_d/F and CL/F decreased. $AUC_{(0-t)}$ of palmatine in the model group significantly increased.

Interestingly, a second peak at 3 hours for berberine and 4 hours for palmatine was observed in model group. However, similar results had not happened in the control group. The difference is probably due to the abnormality of colonic motility in the model group. But the results are inconsistent with Deng and Yan's reports [24, 25]. Both of them observed three peaks in mean plasma concentration curves of berberine, palmatine, and jatrorrhizine after oral administration of the combination of *Coptis chinensis* and Fructus Evodiae or RC extraction in normal rats, which is probably concerned with the distribution, reabsorption, and enterohepatic circulation. And the discrepancy probably is because the pharmacokinetic experiments are so susceptible that the mean plasma concentration-time profiles would often differ when the experimental conditions were changed a little, such as investigator, herbs, animals, and sampling time.

In conclusion, the results indicate that the pharmacokinetics of berberine and palmatine after oral administration of RC extraction in rat plasma were significantly different between normal and PI-IBS rats, which indicates a dosage modification of *Rhizoma Coptidis* in PI-IBS pathological conditions.

5. Conclusions

The pharmacokinetic behavior of berberine and palmatine after oral administration of *Rhizoma Coptidis* extract was significantly altered in PI-IBS pathological conditions, which indicate the dosage modification of *Rhizoma Coptidis* in PI-IBS.

Conflict of Interests

The authors declare no conflict of interests.

Authors' Contribution

Zipeng Gong and Ying Chen contributed equally to this work. Zipeng Gong, Ying Chen, Xiaoxin Zhu, and Yu Dong designed the experimental protocol. Zipeng Gong, Ruijie Zhang, Yinghan Wang, Yan Guo, Qing Yang, Xiaogang Weng, Yujie Li, and Yajie Wang carried out the animal surgery and the blood collection. Shuangrong Gao and Hailin Wang contributed to the histological examination of inflammation and mast cells counting. Zipeng Gong and Ying Chen carried out data analysis and interpretation and wrote a draft of the paper. Xiaoxin Zhu and Yu Dong contributed to critical review of the paper.

Acknowledgments

References

[1] D. A. Drossman, "The Functional Gastrointestinal Disorders and the Rome III Process," *Gastroenterology*, vol. 130, no. 5, pp. 1377–1390, 2006.

[2] B. Zanini, C. Ricci, F. Bandera et al., "Incidence of post-infectious irritable bowel syndrome and functional intestinal disorders following a water-borne viral gastroenteritis outbreak," *The American Journal of Gastroenterology*, vol. 107, no. 6, pp. 891–899, 2012.

[3] R. Spiller and K. Garsed, "Post infectious irritable bowel syndrome," *Gastroenterology*, vol. 136, no. 6, pp. 1979–1988, 2009.

[4] The State Pharmacopoeia Commission of China, *Pharmacopoeia of the People's Republic of China*, pp. 285-286, Chemical Industry Press, Beijing, China, 2010, (Chinese Edition).

[5] M. Zhao, Y. Xian, S. Ip, H. H. S. Fong, and C. Che, "A new and weakly antispasmodic protoberberine alkaloid from rhizoma coptidis," *Phytotherapy Research*, vol. 24, no. 9, pp. 1414–1416, 2010.

[6] H. Hong, P.-Y. Chen, T. Shih et al., "Computational pharmaceutical analysis of anti-Alzheimer's Chinese medicine Coptidis Rhizoma alkaloids," *Molecular Medicine Reports*, vol. 5, no. 1, pp. 142–147, 2012.

[7] Y. Cao, W. Bei, Y. Hu et al., "Hypocholesterolemia of Rhizoma Coptidis alkaloids is related to the bile acid by up-regulated CYP7A1 in hyperlipidemic rats," *Phytomedicine*, vol. 19, no. 8-9, pp. 686–692, 2012.

[8] Y. Y. Choi, M. H. Kim, I. H. Cho et al., "Inhibitory effect of Coptis chinensis on inflammation in LPS-induced endotoxemia," *Journal of Ethnopharmacology*, vol. 149, no. 2, pp. 506–512, 2013.

[9] J. Tang, Y. B. Feng, S. Tsao, N. Wang, R. Curtain, and Y. Wang, "Berberine and Coptidis Rhizoma as novel antineoplastic agents: a review of traditional use and biomedical investigations," *Journal of Ethnopharmacology*, vol. 126, no. 1, pp. 5–17, 2009.

[10] W. Kong, J. Wang, X. Xiao, S. Chen, and M. Yang, "Evaluation of antibacterial effect and mode of Coptidis rhizoma by microcalorimetry coupled with chemometric techniques," *Analyst*, vol. 137, no. 1, pp. 216–222, 2012.

[11] X. Wang, S. Lin, H. Kang et al., "The effect of *RHIZOMA COPTIDIS* and *COPTIS CHINENSIS* aqueous extract on radiation-induced skin injury in a rat model," *BMC Complementary and Alternative Medicine*, vol. 13, article 105, 2013.

[12] Y. Tjong, S. Ip, L. Lao et al., "Analgesic effect of Coptis chinensis rhizomes (Coptidis Rhizoma) extract on rat model of irritable bowel syndrome," *Journal of Ethnopharmacology*, vol. 135, no. 3, pp. 754–761, 2011.

[13] S. Yu, X. Pang, Y. Deng et al., "A sensitive and specific liquid chromatography mass spectrometry method for simultaneous determination of berberine, palmatine, coptisine, epiberberine and jatrorrhizine from Coptidis Rhizoma in rat plasma," *International Journal of Mass Spectrometry*, vol. 268, no. 1, pp. 30–37, 2007.

[14] H. A. Jung, N. Y. Yoon, H. J. Bae, B. Min, and J. S. Choi, "Inhibitory activities of the alkaloids from Coptidis Rhizoma against aldose reductase," *Archives of Pharmacal Research*, vol. 31, no. 11, pp. 1405–1412, 2008.

[15] A. Remppis, F. Bea, H. J. Greten et al., "Rhizoma coptidis inhibits LPS-induced MCP-1/CCL2 production in murine macrophages via an AP-1 and NFκB-dependent pathway," *Mediators of Inflammation*, vol. 2010, Article ID 194896, 8 pages, 2010.

[16] C. Lin, L. T. Ng, F. Hsu, D. Shieh, and L. Chiang, "Cytotoxic effects of Coptis chinensis and Epimedium sagittatum extracts and their major constituents (berberine, coptisine and icariin) on hepatoma and leukaemia cell growth," *Clinical and Experimental Pharmacology and Physiology*, vol. 31, no. 1-2, pp. 65–69, 2004.

[17] W. C. Lee, J. K. Kim, J. W. Kang et al., "Palmatine attenuates D-galactosamine/lipopolysaccharide-induced fulminant hepatic failure in mice," *Food and Chemical Toxicology*, vol. 48, no. 1, pp. 222–228, 2010.

[18] Y. M. Kim, Y. M. Ha, Y. C. Jin et al., "Palmatine from Coptidis rhizoma reduces ischemia-reperfusion-mediated acute myocardial injury in the rat," *Food and Chemical Toxicology*, vol. 47, no. 8, pp. 2097–2102, 2009.

[19] Z. Gong, Y. Chen, R. Zhang et al., "Pharmacokinetic comparison of berberine in rat plasma after oral administration of berberine hydrochloride in normal and post inflammation irritable bowel syndrome rats," *International Journal of Molecular Sciences*, vol. 15, no. 1, pp. 456–467, 2014.

[20] X. Weng, Y. Li, Q. Yang et al., "Effects of Wuji Pill with different compatibility on the activity of cytochrome P450 1A2 in rat liver microsomes in vitro," *World Chinese Journal of Digestology*, vol. 18, no. 6, pp. 586–591, 2010.

[21] Y. Chen, Y. J. Li, Y. J. Wang et al., "Comparative pharmacokinetics of active alkaloids after oral administration of Rhizoma Coptidis extract and Wuji Wan formulas in rat using a UPLC-MS/MS method," *European Journal of Drug Metabolism and Pharmacokinetics*, 2014.

[22] J. Schwille-Kiuntke, J.-S. Frick, P. Zanger, and P. Enck, "Post-infectious irritable bowel syndrome—a review of the literature," *Zeitschrift fur Gastroenterologie*, vol. 49, no. 8, pp. 997–1003, 2011.

[23] Q. Wang, Y. Cui, T. Dong, X. Zhang, and K. Lin, "Ethanol extract from a Chinese herbal formula, "zuojin Pill", inhibit the expression of inflammatory mediators in lipopolysaccharide-stimulated RAW 264.7 mouse macrophages," *Journal of Ethnopharmacology*, vol. 141, no. 1, pp. 377–385, 2012.

[24] Y. Deng, Q. Liao, S. Li, K. Bi, B. Pan, and Z. Xie, "Simultaneous determination of berberine, palmatine and jatrorrhizine by liquid chromatography-tandem mass spectrometry in rat plasma and its application in a pharmacokinetic study after oral administration of coptis-evodia herb couple," *Journal of Chromatography B*, vol. 863, no. 2, pp. 195–205, 2008.

[25] R. Yan, Y. Wang, Y. Liu, and X. Di, "Comparative pharmacokinetics of berberine, palmatine and jatrorrhizine in rat plasma after oral administration of Rhizomacoptidis and Zuojinwan using liquid chromatography-tandem mass spectrometry," *Iranian Journal of Pharmaceutical Research*, vol. 11, no. 3, pp. 949–957, 2012.

Research Article

Integrated Analysis for Identifying Radix Astragali and Its Adulterants Based on DNA Barcoding

Sihao Zheng,[1] Dewang Liu,[2] Weiguang Ren,[1] Juan Fu,[1] Linfang Huang,[1] and Shilin Chen[3]

[1] *Institute of Medicinal Plant Development, Chinese Academy of Medical Sciences, Peking Union Medical College, Beijing 100193, China*
[2] *School of Pharmacy, Inner Mongolia Medical University, Inner Mongolia 010080, China*
[3] *Institute of Chinese Materia Medica, China Academy of Chinese Medical Sciences, Beijing 100700, China*

Correspondence should be addressed to Linfang Huang; lfhuang@implad.ac.cn

Radix Astragali is a popular herb used in traditional Chinese medicine for its proimmune and antidiabetic properties. However, methods are needed to help distinguish Radix Astragali from its varied adulterants. DNA barcoding is a widely applicable molecular method used to identify medicinal plants. Yet, its use has been hampered by genetic distance, base variation, and limitations of the bio-NJ tree. Herein, we report the validation of an integrated analysis method for plant species identification using DNA barcoding that focuses on genetic distance, identification efficiency, inter- and intraspecific variation, and barcoding gap. We collected 478 sequences from six candidate DNA barcodes (ITS2, ITS, *psb*A-*trn*H, *rbc*L, *mat*K, and COI) from 29 species of Radix Astragali and adulterants. The internal transcribed spacer (ITS) sequence was demonstrated as the optimal barcode for identifying Radix Astragali and its adulterants. This new analysis method is helpful in identifying Radix Astragali and expedites the utilization and data mining of DNA barcoding.

1. Introduction

Radix Astragali (Huang Qi), a commonly used Chinese medicinal material, is mainly sourced from the plants of *Astragalus membranaceus* and *Astragalus mongholicus* according to Chinese Pharmacopoeia (2010 edition). Radix Astragali is widely used for its antiperspirant, antidiuretic, and antidiabetic properties and as a tonic drug [1–3]. It possesses various beneficial compounds, including astragalosides, isoflavonoids, isoflavones, isoflavan, and pterocarpan glycosides [4–6].

Due to the high market demand for Radix Astragali, a diverse group of adulterants with similar-morphological characteristics from genuses, such as *Astragalus*, *Hedysarum*, and *Malva* are often used in its stead [7]. The traditional methods used to identify Radix Astragali for use as a medicinal material, such as morphological and microscopic identification [8], thin-layer chromatography and Ultraviolet spectroscopy [9], Fourier Transform infrared spectroscopy (FTIR) [10], and high performance liquid chromatography (HPLC) [11], all, require specialized equipment and training.

Several PCR-based molecular methods have been developed, providing an alternative means of identification. Multiplex PCR methods of DNA fragment analysis, such as randomly amplified polymorphic DNA (RAPD) [12] or amplified fragment length polymorphism (AFLP) [13], are unstable for the results to identify. DNA barcoding is a widely used molecular marker technology, first proposed by Hebert et al. [14, 15]. It uses a standardized and conserved, but diverse, DNA sequence to identify species and uncover biological diversity [16, 17]. In previous studies, various coding sequences for identifying Radix Astragali and its adulterants have been used, such as the 5S-rRNA spacer domain [18], $3'$ untranslated region ($3'$ UTR) [19], ITS (internal transcribed spacer region) and 18S rRNA [3, 20, 21], ITS2 [22], ITS1 [6], *mat*K (maturase K) and *rbc*L (ribulose 1, 5-bisphosphate carboxylase) of chloroplast genome, and coxI (cytochrome c oxidase 1) of the mitochondrial genome [23]. However, sequence analysis was mainly focused on genetic distance, variable sites, amplified polymorphisms, and the use of a modified neighbor-joining (NJ) algorithm, Bio-NJ tree, which were basic analyses limited to particular species. A more effective

TABLE 1: Taxon sampling information of astragalus and its adulterants.

Experiment number	species	Sampling spot	
S1-S5	*Astragalus membranaceus*	Shaanxi	China
SD1-SD9	*Astragalus membranaceus*	Shaanxi	China
GS1-GS6	*Astragalus mongholicus*	Gansu	China
NM1-NM10	*Astragalus mongholicus*	Neimeng	China
SX1-SX10	*Astragalus mongholicus*	Shanxi	China
HHQ1-HHQ7	*Astragalus chinensis*	Beijing	China
CY1-CY6	*Astragalus scaberrimus*	Beijing	China
JK1-JK3	*Malva pusilla*	Shaanxi	China
MX	*Medicago sativa*	Shaanxi	China
HH1-HH7	*Melilotus officinalis*	Shaanxi	China
HQ1-HQ12	*Hedysarum polybotrys*	Gansu	China
XJ	*Astragalus adsurgens*	Beijing	China

method of molecular identification is necessary. The current study evaluates the identification reliability and efficiency of DNA barcoding for the identification of Radix Astragali using six indicators of genetic distance, identification efficiency, intra- and interspecific variation, gap rate, and barcoding gap. Six barcodes were selected for identification because they are commonly used in plant, especially in medicinal plant. We collected Radix Astragaliand several of its adulterants reported in previous research and downloaded the genetic sequences from the GenBank database. A total of 29 species (including 19 species of *Astragalus*) and 478 sequences from six barcodes were used to validate the new method for identifying Radix Astragali and adulterants and to accelerate the data utilization of DNA barcoding.

2. Materials and Methods

2.1. Materials Information. A total of 77 specimens were collected from two origins of Radix Astragali, along with seven adulterants. Radix Astragali specimens were collected from Inner Mongolia, Shaan xi, and Gan su provinces in the People's Republic of China, which are the main producing areas. The collection information is shown in Table 1. All corresponding voucher specimens were deposited in the Herbarium of the Institute of Medicinal Plant Development at the Chinese Academy of Medical Sciences in Beijing, China. The GenBank accession number of the ITS2 in this experiment was orderly KJ999296–KJ999344, the accession number of ITS sequences was orderly KJ999345–KJ999416, and the accession number of *psbA-trn*H was orderly KJ999256–KJ999295. The sequences added in the subsequent analysis, including ITS, ITS2, *psbA-trn*H, *mat*K, and *rbc*L, were downloaded from the GenBank database.

2.2. DNA Extraction, PCR Amplification, and Sequencing. The material specimens were naturally dried and 30 mg of dried plant material was used for the DNA extraction. Samples were rubbed for two minutes at a frequency of 30 r/s in a FastPrep bead mill (Retsch MM400, Germany), and total genomic DNA was isolated from the crushed material according to the manufacturer's instructions (Plant

Genomic DNA Kit, Tiangen Biotech Co., China). We made the following modifications to the protocol: chloroform was diluted with isoamyl alcohol (24 : 1 in the same volume) and buffer solution GP2 with isopropanol (same volume). The powder, 700 μL of 65°C GP1, and 1 μL β-mercaptoethanol were mixed for 10–20 s before being incubated for 60 minutes at 65°C. Then, 700 μL of the chloroform:isoamyl alcohol mixture was added and the solution was centrifuged for 5 minutes at 12000 rpm (~13400 ×g). Supernatant was removed and placed into a new tube before adding 700 μL isopropanol and blending for 15–20 minutes. The mixture was centrifuged in CB3 spin columns for 40 s at 12000 rpm. The filtrate was discarded and 500 μL GD (adding quantitative anhydrous ethanol before use) was added before centrifuging at 12000 rpm for 40 s. The filtrate was discarded and 700 μL PW (adding quantitative anhydrous ethanol before use) was used to wash the membrane before centrifuging for 40 s at 12000 rpm. This step was repeated with 500 μL PW, followed by a final centrifuge for 2 minutes at 12000 rpm to remove residual wash buffer. The spin column was dried at room temperature for 3–5 minutes and then centrifuged for 2 minutes at 12000 rpm to obtain the total DNA.

General PCR reaction conditions and universal DNA barcode primers were used for the ITS, ITS2, and *psbA-trn*H barcodes, as presented in Table 2 [24–26]. PCR amplification was performed on 25-μL reaction mixtures containing 2 μL DNA template (20–100 ng), 8.5 μL ddH2O, 12.5 μL 2× Taq PCR Master Mix (Beijing TransGen Biotech Co., China), and 1/1-μL forward/reverse (F/R) primers (2.5 μM). The reaction mixtures were amplified in a 9700 GeneAmp PCR system (Applied Biosystems, USA). Amplicons were visualized by electrophoresis on 1% agarose gels. Purified PCR products were sequenced in both directions using the ABI 3730XL sequencer (Applied Biosystems, USA).

2.3. Sequence Assembly, Alignment, and Analysis. Sequencing peak diagrams were obtained and proofread, and then contigs were assembled using a CodonCode Aligner 5.0.1 (CodonCode Co., USA). Complete ITS2 sequences were obtained using the HMMer annotation method, based on the Hidden Markov model (HMM) [27]. All of the sequences were

TABLE 2: Primers and PCR reaction conditions.

Primer name	Primer sequences (5′-3′)	PCR reaction condition
ITS2		
2F	ATGCGATACTTGGTGTGAAT	94˚C 5 min;
3R	GACGCTTCTCCAGACTACAAT	94˚C 30 s, 56˚C 30 s, 72˚C 45 s, 40 cycles; 72˚C 10 min;
ITS		
4R	TCCTCCGCTTATTGATATGC	94˚C 5 min;
5F	GGAAGTAAAAGTCGTAACAAGG	94˚C 1 min, 50˚C 1 min, 72˚C 1.5 min + 3 s/cycle, 30 cycles; 72˚C 7 min;
*psb*A		
fwdPA	GTTATGCATGAACGTAATGCTC	94˚C 4 min;
*trn*H		
rev TH	CGCGCATGGTGGATTCACAATCC	94˚C 30 s, 55˚C 1 min, 72˚C 1 min, 35 cycles; 72˚C 10 min;

aligned using ClustalW, in combination with 317 sequences from six commonly used barcodes (ITS2, ITS, *psb*A-*trn*H, *mat*K, *rbc*L, and COI), which were downloaded from the GenBank database (Table 3). Sequence genetic distance and GC content were calculated using the maximum composite likelihood model. Maximum likelihood (ML) trees were constructed based on the Tamura-Nei model, and bootstrap tests were conducted using 1000 repeats to assess the confidence of the phylogenetic relationships by MEGA 6.0 software [28]. The barcoding gap, defined as the spacer region between intra- and interspecific genetic variations, and identification efficiency, based on BLAST1 and K2P nearest distance, were performed by the Perl language algorithm (Putty) [25, 29, 30].

3. Results

3.1. Sequence Information and Identification Efficiency. A total of 478 sequences for six barcodes were analyzed, from which 161 sequences were obtained from Astragalus Radix and its adulterants. Sequence information and identification success rates are listed in Table 4. The average GC content of six barcodes was discrepant, and ITS and ITS2 regions from nuclear ribosomal DNA performed higher than other barcodes (52.97% versus 50.80%). Among the six barcodes, ITS2 provided the largest average genetic distance (1.0792), and rbcL was the smallest (0.0349). All of the six barcodes obtained a zero value for the minimum genetic distance. In terms of identification efficiency, the nearest distance method was superior to the BLAST1 method for all of the six barcodes. Moreover, ITS and the *psb*A-*trn*H and *mat*K regions provided a higher rate of success than the other three barcodes using the BLAST1 method. However, *mat*K, ITS, and *psb*A-*trn*H performed better than the other three barcodes, based on the nearest distance method. ITS and *psb*A-*trn*H obtained higher genetic distances, so the *mat*K, ITS, and *psb*A-*trn*H barcodes were the preferable methods for identifying Radix Astragali

and its adulterants based on superior sequencing efficiency and identification efficiency.

3.2. Intra- and Interspecific Variation Analysis Using Six Parameters. Six parameters to analyze intraspecific variation and interspecific divergence were employed to assess the utility of six DNA barcodes (Table 5). We expected the "minimum interspecific distance" would be higher than the "coalescent depth" (maximum intraspecific distance). Therefore, we first utilized the "gap rate" to indicate the distinctness, calculated by the formula: (minimum interspecific distance − maximum intraspecific distance)/minimum interspecific distance. Results show that the ITS2, COI, *mat*K, and *rbc*L regions outperformed the ITS and *psb*A-*trn*H regions for gap rates. However, when we compared all of the average inter- and intraspecific distances, the ITS2, *rbc*L, *mat*K, and *psb*A-*trn*H regions performed better than the ITS and COI regions. Therefore, in terms of intra- and interspecific variation, ITS2, *mat*K, and *rbc*L are the preferable options for identifying Radix Astragali and its adulterants.

3.3. Barcoding Gap Analysis. Analysis of the DNA barcoding gap presents the divergence of inter- and intraspecies and indicates separate, nonoverlapping distribution between specimens in an ideal situation [25]. In our study (Figure 1), the *rbc*L, COI, ITS, and *mat*K regions possessed less relative distribution of inter- and intraspecific variation than *psb*A-*trn*H and ITS2, although there were no nonoverlapping regions for the six barcodes. Hence, the *rbc*L, COI, ITS, and *mat*K regions are more successful at identifying Radix Astragali and its adulterants, from the standpoint of barcoding gap analysis.

3.4. ML Tree Analysis. Maximum likelihood (ML) is a general statistical criterion in widespread use for the inference of molecular phylogenies [31]. An ML tree visually revealed the relationship between species. As the results show (Figure 2),

TABLE 3: Sequences from GenBank for identifying *Astragalus* and its adulterants.

Region	Family	Species	Accession number
	Fabaceae	*Melilotus officinalis*	U50765, Z97687
	Fabaceae	*Astragalus adsurgens*	L10757, GU217639, GU217640, GU217641
	Fabaceae	*Astragalus chinensis*	GQ434365, GQ434366
	Fabaceae	*Hedysarum polybotrys*	GQ434367
	Fabaceae	*Astragalus mongholicus*	GQ434368, GU217643
	Fabaceae	*Astragalus mongholicus var. dahuricus*	GU217635
ITS2	Fabaceae	*Astragalus membranaceus*	GU217642, JF421475
	Fabaceae	*Caragana sinica*	GU217654
	Fabaceae	*Medicago sativa*	GU217662, Z99236, AF028417, JN617208
	Fabaceae	*Medicago sativa subsp. caerulea*	AF028418
	Fabaceae	*Medicago sativa subsp. glomerata*	AF028419
	Fabaceae	*Medicago falcata*	AF028420
	Malvaceae	*Alcea rosea*	AF303023
	Fabaceae	*Astragalus membranaceus*	AF359749, EF685968, EU852042, FJ572044, GU289659 GU289660, GU289661, GU289662, GU289663, GU289664 HM142272, HM142273, HM142274, HM142275, HM142276 HM142277, HM142278, HM142279, HM142280, HM142281 HQ891827, JX017320, JX017321, JX017322, JX017323 JX017324, JX017325, JX017326, JX017327, JX017328 JX017329, JX017330, JX017331, JX017332, AF121675
	Fabaceae	*Astragalus mongholicus*	AF359750, EF685969, HM142282, HM142283, HM142284 HM142285, HM142286, HM142287, HM142288, HM142289 HM142290, JF736665, JF736666, JF736667, JF736668 JF736669, AB787166
	Fabaceae	*Astragalus propinquus*	AF359751
	Fabaceae	*Astragalus lepsensis*	AF359752
	Fabaceae	*Astragalus aksuensis*	AF359753, AB231091
	Fabaceae	*Astragalus hoantchy*	AF359754, AF521952
	Fabaceae	*Astragalus hoantchy subsp. dshimensis*	AF359755
	Fabaceae	*Astragalus lehmannianus*	AF359756
	Fabaceae	*Astragalus sieversianus*	AF359757
	Fabaceae	*Astragalus austrosibiricus*	AF359758
	Fabaceae	*Astragalus uliginosus*	EF685970
ITS	Fabaceae	*Astragalus scaberrimus*	AB051988
	Fabaceae	*Astragalus chinensis*	FJ980292, HM142297, AF121681
	Fabaceae	*Astragalus borealimongolicus*	HM142291, HM142292, HM142293, HM142294, HM142295 HM142296
	Fabaceae	*Astragalus adsurgens*	HM142298, HM142299, HQ199326
	Fabaceae	*Astragalus mongholicus var. dahuricus*	HM142300, KC262199
	Fabaceae	*Astragalus zacharensis*	HM142301
	Fabaceae	*Astragalus melilotoides*	HM142302
	Fabaceae	*Astragalus scaberrimus*	HM142303
	Fabaceae	*Astragalus sieversianus*	AB741299
	Fabaceae	*Oxytropis anertii*	EF685971
	Fabaceae	*Caragana sinica*	DQ914785, FJ537284, GQ338283
	Fabaceae	*Glycyrrhiza pallidiflora*	EU591998, GQ246130
	Fabaceae	*Melilotus officinalis*	AB546796, JF461307, JF461308, JF461309, DQ311985
	Fabaceae	*Medicago sativa*	GQ488541, AF053142, AY256392, JX017335, JX017336 JX017337, KF938697
	Fabaceae	*Oxytropis caerulea*	GU217599, HQ199316
	Fabaceae	*Hedysarum vicioides*	HM142304, HM142305
	Fabaceae	*Hedysarum polybotrys*	JX017333, JX017334, KF032294
	Malvaceae	*Malva neglecta*	EF419478, EF419479
	Malvaceae	*Alcea rosea*	AH010172, EF419544, EF679714, JX017319

TABLE 3: Continued.

Region	Family	Species	Accession number
psbA-trnH	Fabaceae	*Astragalus membranaceus f. pallidipurpureus*	GQ139474
	Fabaceae	*Astragalus adsurgens*	GU396749, GU396750, GU396751, KF011553
	Fabaceae	*Astragalus mongholicus*	GU396754, AB787167
	Fabaceae	*Astragalus membranaceus*	GQ139475, GQ139476, GQ139477, GQ139478, GQ139479 GQ139480, GQ139481, GQ139482, GQ139483, GU396752 GU396753
	Fabaceae	*Caragana sinica*	GU396767, KJ025053
	Fabaceae	*Oxytropis caerulea*	GU396771
	Fabaceae	*Medicago sativa*	GU396781, HQ596768, HE966707
	Fabaceae	*Glycyrrhiza pallidiflora*	GU396807
	Fabaceae	*Melilotus officinalis*	HE966710
	Malvaceae	*Malva neglecta*	EF419597, EF419598, HQ596765, HQ596765
	Malvaceae	*Alcea rosea*	EF419662, EF679744
matK	Fabaceae	*Astragalus membranaceus*	EF685992, HM142232, HM142233, HM142234, HM142235 HM142236, HM142237, HM142238, HM142239, HM142240 HM142254
	Fabaceae	*Astragalus mongholicus*	EF685993, HM142241, HM142242, HM142243, HM142244 HM142245, HM142246, HM142247, HM142255, HM142256
	Fabaceae	*Astragalus uliginosus*	EF685994, HM142262
	Fabaceae	*Astragalus mongholicus var. dahuricus*	HM049531, HM142260
	Fabaceae	*Astragalus chinensis*	HM049533, HM142263
	Fabaceae	*Astragalus adsurgens*	HM049537, HM142258, HM142259, AY920437
	Fabaceae	*Astragalus borealimongolicus*	HM142248, HM142249, HM142250, HM142251, HM142252 HM142253
	Fabaceae	*Astragalus zacharensis*	HM142261
	Fabaceae	*Astragalus melilotoides*	HM142264
	Fabaceae	*Astragalus scaberrimus*	HM142265
	Fabaceae	*Astragalus sieversianus*	AB741343
	Fabaceae	*Medicago sativa*	AF522108, HQ593363, HM851138, AY386881, HE967439 AF169289
	Fabaceae	*Oxytropis anertii*	EF685995, HM142266
	Fabaceae	*Oxytropis caerulea*	HM049544
	Fabaceae	*Glycyrrhiza pallidiflora*	EF685997, HM142269, JQ619944
	Fabaceae	*Hedysarum vicioides*	EF685996, HM142257, HM142267
	Fabaceae	*Caragana sinica*	HM049541
	Fabaceae	*Melilotus officinalis*	HE970723
	Malvaceae	*Malva neglecta*	EU346788, HQ593360, JN894566, JN894571, JN895781 JQ412262,
	Malvaceae	*Alcea rosea*	EU346805
rbcL	Fabaceae	*Medicago sativa*	Z70173
	Fabaceae	*Astragalus membranaceus*	EF685978, HM142199, HM142200, HM142201, HM142202 HM142203, HM142204, HM142205, HM142206, HM142207 HM142221
	Fabaceae	*Astragalus mongholicus*	EF685979, HM142208, HM142209, HM142210, HM142211 HM142212, HM142213, HM142214, HM142222, HM142223
	Fabaceae	*Astragalus uliginosus*	EF685980, HM142225
	Fabaceae	*Hedysarum vicioides*	EF685982, U74246, HM142224, HM142227,
	Fabaceae	*Astragalus adsurgens*	EF685984
	Fabaceae	*Astragalus borealimongolicus*	HM142215, HM142216, HM142217, HM142218, HM142219 HM142220,
	Fabaceae	*Oxytropis anertii*	EF685981, HM142226
	Fabaceae	*Glycyrrhiza pallidiflora*	EF685983, AB012129, HM142228
	Fabaceae	*Caragana sinica*	FJ537233
	Fabaceae	*Melilotus officinalis*	JQ933405, JX848463

TABLE 4: The information of identification efficiency for six barcodes.

Markers	COI	ITS2	ITS	*mat*K	*rbc*L	*psb*A-*trn*H
Number of sequences	39	72	185	65	43	74
Average GC content/%	43.29	50.80	52.97	31.14	42.88	21.77
Genetic distance						
Min	0.0000	0.0000	0.0000	0.0000	0.0000	0.0000
Max	0.0086	7.9494	5.3130	0.2801	0.0349	2.2701
Average	0.0019	1.0792	0.3508	0.0711	0.0116	0.5080
Identification efficiency/%						
BLAST 1/%	10.26	12.50	30.81	29.23	23.26	29.73
Nearest distance/%	33.33	27.78	52.43	66.15	37.21	41.89

TABLE 5: Analysis of interspecific divergence and intraspecific variation for six barcodes.

Marker (Mean ± SD)	COI	ITS2	ITS	*mat*K	*rbc*L	*psb*A-*trn*H
Theta	2.2260 ± 6.2961	0.0030 ± 0.0046	0.0271 ± 0.0404	0.0021 ± 0.0035	0.0011 ± 0.0020	0.2415 ± 0.4777
Coalescent depth	0.0001 ± 0.0004	0.0040 ± 0.0046	0.1423 ± 0.3958	0.0032 ± 0.0050	0.0016 ± 0.0030	0.4109 ± 0.5683
All intraspecific distance	9.3280 ± 0.0003	0.0021 ± 0.0024	0.1153 ± 0.3051	0.0014 ± 0.0022	0.0002 ± 0.0011	0.3093 ± 0.4300
Theta prime	0.0012 ± 0.0008	0.0617 ± 0.0302	0.0603 ± 0.0371	0.0091 ± 0.0061	0.0024 ± 0.0035	0.3083 ± 0.2887
Minimum interspecific distance	0.0008 ± 0.0010	0.0440 ± 0.0386	0.0168 ± 0.0196	0.0066 ± 0.0066	0.0023 ± 0.0035	0.0423 ± 0.0380
All interspecific distance	0.0007 ± 0.0010	0.0343 ± 0.0389	0.1066 ± 0.2833	0.0071 ± 0.0064	0.0015 ± 0.0029	0.3166 ± 0.4070
Gap rate/%	87.50	90.91	/	51.52	30.43	/

*psb*A-*trn*H successfully differentiated Radix Astragali and its adulterants. Furthermore, it produced areas of obvious separation for Radix Astragali. The remaining five barcodes also differentiated Radix Astragali and its adulterants. Each species clustered together, separate from other species. Considering the difficult amplification and sequencing and fast and accurate identification purpose of DNA barcoding, we did not add all the sequence data of ITS2 and *psb*A-*trn*H to build ML tree and subsequent analysis.

4. Discussion and Conclusions

Radix Astragali is reported to possess 47 bioactive compounds and has many bioactive properties [32–37]. Various Radix Astragali preparations are commercially available, not only in China as a TCM component, but also in the United States, as dietary supplements [38]. However, due to increasing demand, substitutes and adulterants have flooded the market. Traditional identification methods, such as morphological and microscopic methods, are limited by the lack of explicit criteria for character selection or coding and, thus, mainly depend on subjective assessments. Although chemical methods are able to distinguish between different species, it is difficult to differentiate sibling species that possess similar chemical compositions. In addition, chemical methods are unable to provide accurate species authentication. Several types of molecular markers for characterizing genotypes are useful in identifying plant species. For example, RAPD has been used to estimate genetic diversity in plant populations based on amplification of random DNA fragments and comparisons of common polymorphisms. DNA barcoding

is advocated for species identification, due to its universal applicability, simplicity, and scientific accuracy. However, the analysis methods for DNA barcodes were limited. With the development of molecular biology and bioinformatics, a more improved analytic method for DNA barcoding can be established to identify Radix Astragali and closely related species.

In this study, we validated a new analytical method for identifying Radix Astragali using DNA barcoding. Seventy-seven specimens of Radix Astragali and its adulterants were collected, and the sequences of 29 species reported in the literature were downloaded from the GenBank database. Based on the 478 sequences for six barcodes (ITS2, ITS from nuclear genome; *psb*A-*trn*H, *rbc*L, and *mat*K from chloroplast genome; COI from mitochondrial genome), genetic distance and ML Tree were calculated by MEGA 6.0 software, and identification efficiency, intra- and interspecific variation, and barcoding gap were calculated using the Perl language algorithm. Results of the six indicators assessed are shown in Table 6. ITS and *psb*A-*trn*H outperformed other barcodes in terms of identification efficiency. ITS2 performed better in terms of genetic distance, gap rate, and inter- and intraspecific variation. *Rbc*L performed better in terms of barcoding gap and inter- and intraspecific variation. Although ITS2 was part of the ITS sequence, it performed poorly in identification efficiency. Therefore, we suggest that the ITS sequence is the optimal barcode, and that the *psb*A-*trn*H region is a complementary barcode for identifying Radix Astragali and its adulterants.

In conclusion, we describe a new analytical method for the use of DNA barcoding in the identification of Radix
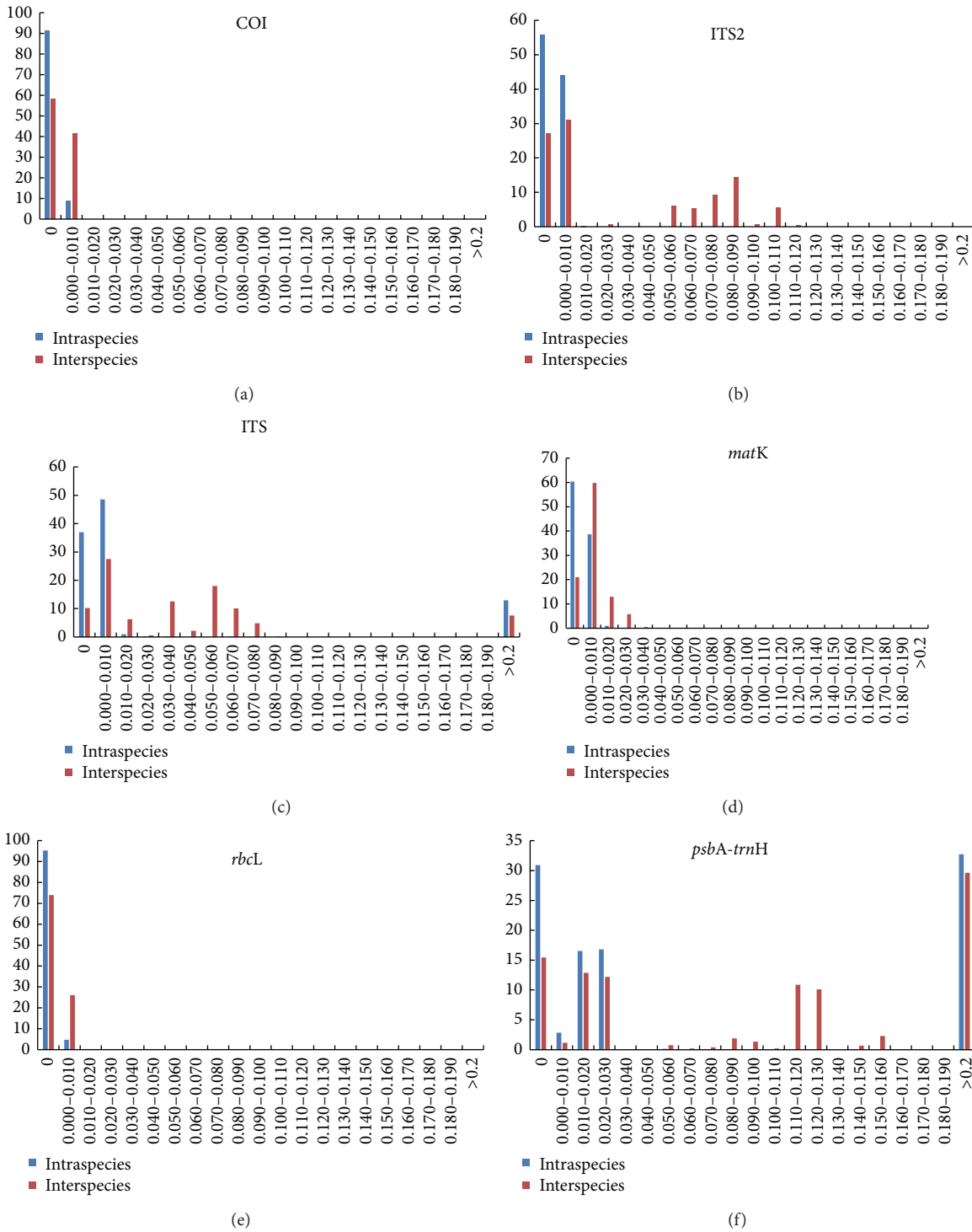
FIGURE 1: Barcoding gap for six barcodes.

Astragali. Six indicators, including average genetic distance, BLAST1 and the nearest distance method for identification efficiency, inter- and intraspecific variation, and gap rate were tested to evaluate six DNA barcodes using bioinformatics software and the Perl language algorithm. The ITS sequence was the optimal barcode for identifying Radix Astragali and its adulterants. This method provides a novel means for accurate identification of Radix Astragali and its adulterants and improves the utilization of DNA barcoding in identifying medicinal plant species.

(a)

(b)
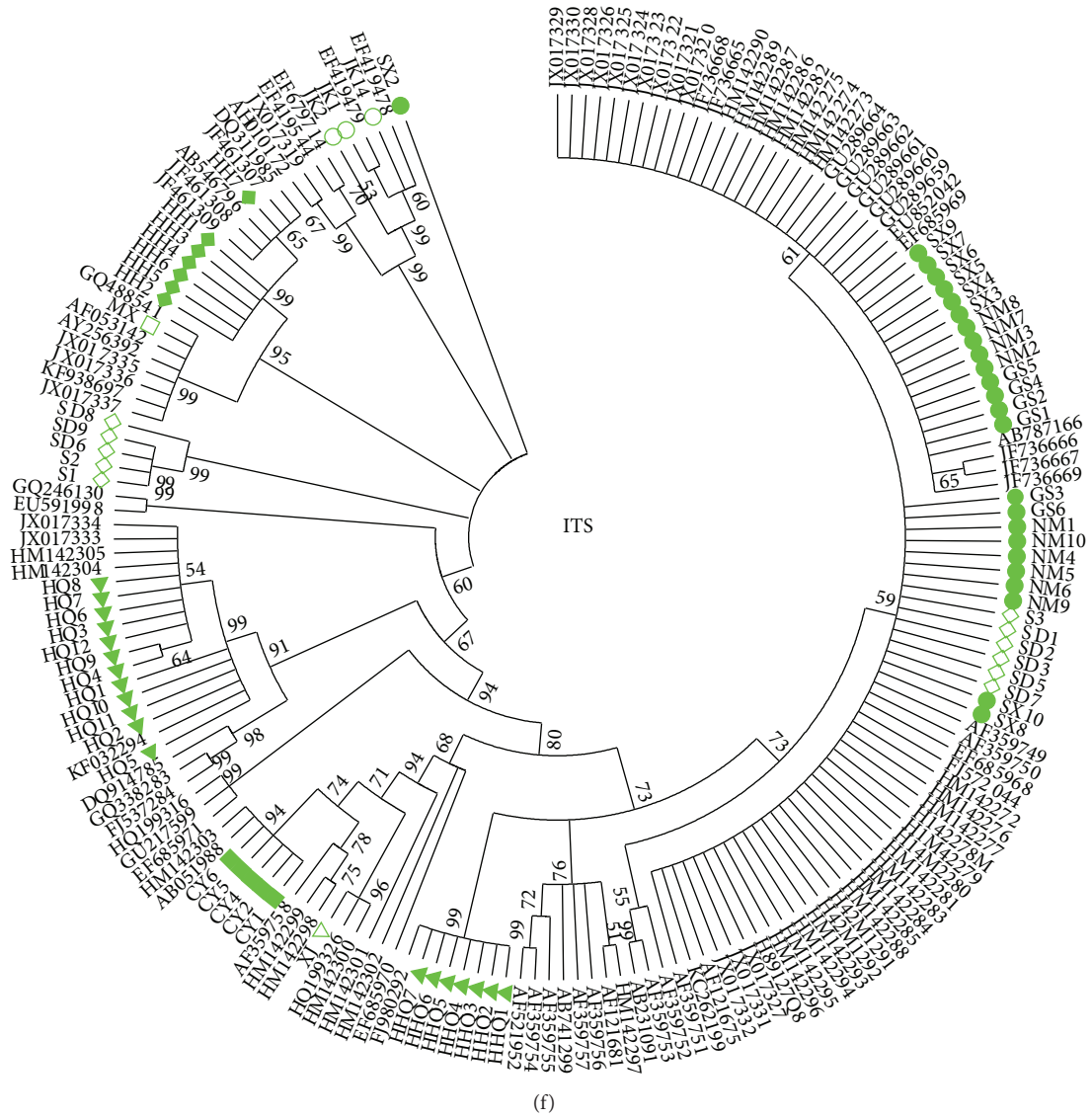
(c)

(d)

(e)
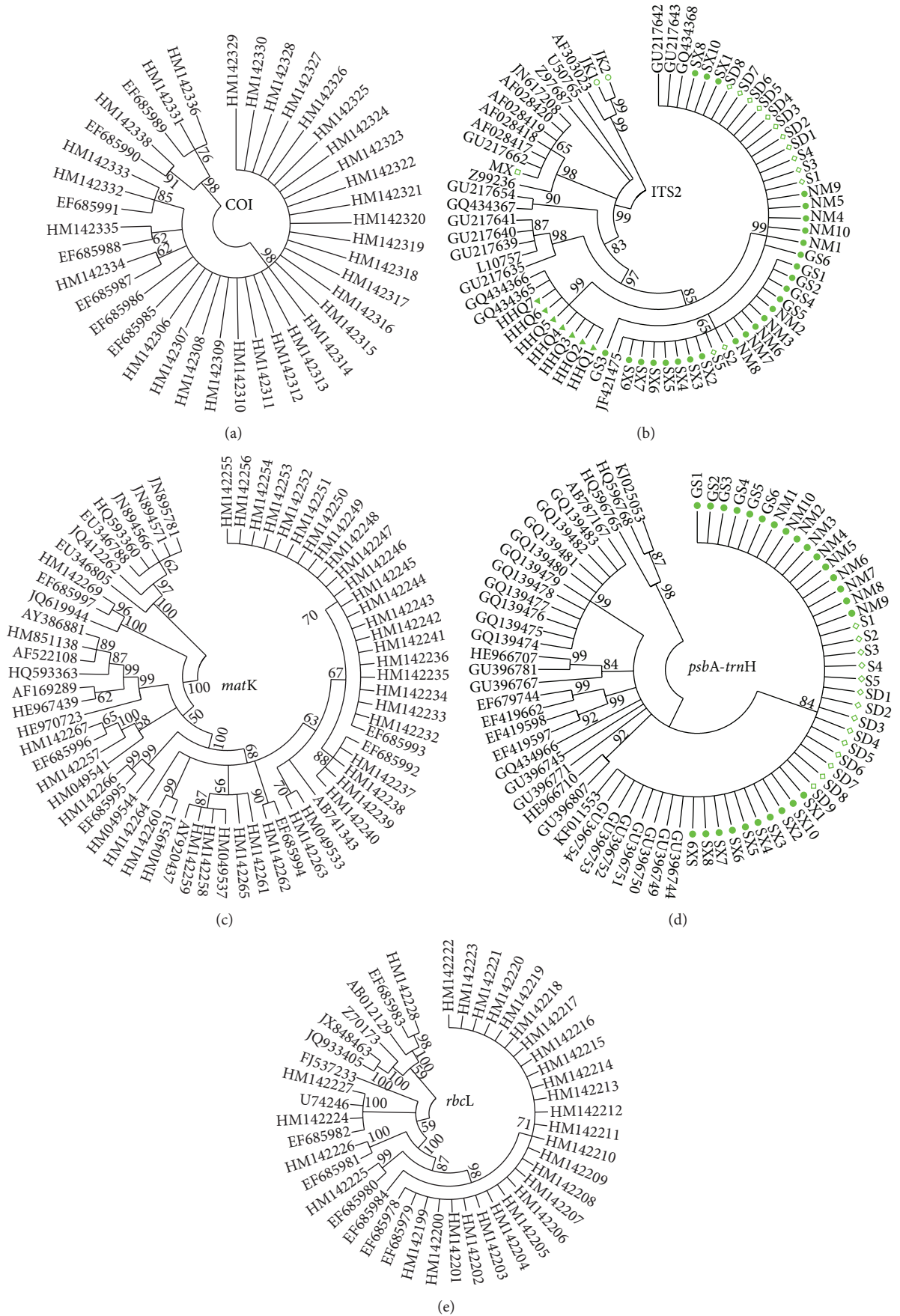
Figure 2: Continued.

(f)

Figure 2: ML tree for six barcodes. *The different color and shape for different species in clusters presented the identification of different barcodes.

Table 6: Six indicators assessed for DNA barcoding.

| DNA barcodes | Average genetic distance | Identification efficiency | | Gap rate | Inter- to intraspecific variation | Barcoding gap | Total score |
		BLAST1	Nearest distances				
ITS2	8	12	8	8	8	4	48
ITS	6	28	22	0	0	6	62
*psb*A-*trn*H	6	26	18	0	2	2	54
*rbc*L	4	12	14	4	6	8	48
*mat*K	4	14	24	4	4	2	52
COI	2	6	10	6	0	6	30

*The total score of six parameters was set by 10, 30, 30, 10, 10, and 10 in order. Identification efficiency based on two methods was set by 30 score because of its importance for identification.

Conflict of Interests

Acknowledgments

References

[1] Y. Kuo, W. Tsai, S. Loke, T. Wu, and W. Chiou, "Astragalus membranaceus flavonoids (AMF) ameliorate chronic fatigue syndrome induced by food intake restriction plus forced swimming," *Journal of Ethnopharmacology*, vol. 122, no. 1, pp. 28–34, 2009.

[2] W. C. S. Cho and K. N. Leung, "*In vitro* and *in vivo* immunomodulating and immunorestorative effects of *Astragalus membranaceus*," *Journal of Ethnopharmacology*, vol. 113, no. 1, pp. 132–141, 2007.

[3] T. T. X. Dong, X. Q. Ma, C. Clarke et al., "Phylogeny of *Astragalus* in China: molecular evidence f rom the DNA sequences of 5S rRNA spacer, ITS, and 18S rRNA," *Journal of Agricultural and Food Chemistry*, vol. 51, no. 23, pp. 6709–6714, 2003.

[4] X. Ma, P. Tu, Y. Chen, T. Zhang, Y. Wei, and Y. Ito, "Preparative isolation and purification of two isoflavones from *Astragalus membranaceus* Bge. var. *mongholicus* (Bge.) Hsiao by high-speed counter-current chromatography," *Journal of Chromatography A*, vol. 992, no. 1-2, pp. 193–197, 2003.

[5] X. Ma, P. Tu, Y. Chen, T. Zhang, Y. Wei, and Y. Ito, "Preparative isolation and purification of isoflavan and pterocarpan glycosides from *Astragalus membranaceus* Bge. var. *mongholicus* (Bge.) Hsiao by high-speed counter-current chromatography," *Journal of Chromatography A*, vol. 1023, no. 2, pp. 311–315, 2004.

[6] P. Y. Yip and H. S. Kwan, "Molecular identification of Astragalus membranaceus at the species and locality levels," *Journal of Ethnopharmacology*, vol. 106, no. 2, pp. 222–229, 2006.

[7] Y. Z. Zhao, "Investigation the source and distribution of Radix Astragli," *Chinese Traditional and Herbal Drugs*, vol. 35, no. 10, pp. 1189–1190, 2004.

[8] Y. H. Zhang, L. M. Zhang, X. B. Liu et al., "Study on morphological and microscopic identification for different producing areas of Radix Astragali," *Journal of Chinese Medicinal Materials*, vol. 36, no. 10, pp. 1602–1604, 2013.

[9] L. Wei and F. T. Zeng, "Using thin-layer chromatography and ultra-violet spectroscopy to identify Radix Astragali and its adulterants," *Journal of Chinese Medicinal Materials*, vol. 16, no. 12, pp. 14–17, 1993.

[10] G. Li, H. Zhao, Y. Liu et al., "Study on Chinese herb astragalus membranceus by FTIR fingerprint," *Spectroscopy and Spectral Analysis*, vol. 30, no. 6, pp. 1493–1497, 2010.

[11] X. Q. Ma, Q. Shi, J. A. Duan, T. T. X. Dong, and K. W. K. Tsim, "Chemical analysis of Radix Astragali (Huangqi) in China: a comparison with its adulterants and seasonal variations," *Journal of Agricultural and Food Chemistry*, vol. 50, no. 17, pp. 4861–4866, 2002.

[12] H. J. Na, J. Y. Um, S. C. Kim et al., "Molecular discrimination of medicinal Astragali radix by RAPD analysis," *Immunopharmacology and Immunotoxicology*, vol. 26, no. 2, pp. 265–272, 2004.

[13] L. X. Duan, T. L. Chen, M. Li et al., "Use of the metabolomics approach to characterize chinese medicinal material Huangqi," *Molecular Plant*, vol. 5, no. 2, pp. 376–386, 2012.

[14] P. D. N. Hebert, A. Cywinska, S. L. Ball, and J. R. DeWaard, "Biological identifications through DNA barcodes," *Proceedings of the Royal Society B: Biological Sciences*, vol. 270, no. 1512, pp. 313–321, 2003.

[15] P. D. N. Hebert, E. H. Penton, J. M. Burns, D. H. Janzen, and W. Hallwachs, "Ten species in one: DNA barcoding reveals cryptic species in the neotropical skipper butterfly Astraptes fulgerator," *Proceedings of the National Academy of Sciences of the United States of America*, vol. 101, no. 41, pp. 14812–14817, 2004.

[16] S. H. Zheng, X. Jiang, L. B. Wu, Z. H. Wang, and L. F. Huang, "Chemical and genetic discrimination of cistanches herba based on UPLC-QTOF/MS and DNA barcoding," *PLoS ONE*, vol. 9, no. 5, Article ID e98061, 2014.

[17] L. F. Huang, S. H. Zheng, L. B. Wu, X. Jiang, and S. L. Chen, "Ecotypes of Cistanche deserticolabased on chemical component and molecular traits," *Scientia Sinica Vitae*, vol. 44, no. 3, pp. 318–328, 2014.

[18] X. Q. Ma, J. A. Duan, D. Y. Zhu, T. T. X. Dong, and K. W. K. Tsim, "Species identification of Radix *Astragali* (Huangqi) by DNA sequence of its 5S-rRNA spacer domain," *Phytochemistry*, vol. 54, no. 4, pp. 363–368, 2000.

[19] G. Chen, X. L. Wang, W. S. Wong, X. D. Liu, B. Xia, and N. Li, "Application of 3′ Untranslated Region (UTR) sequence-based amplified polymorphism analysis in the rapid authentication of Radix astragali," *Journal of Agricultural and Food Chemistry*, vol. 53, no. 22, pp. 8551–8556, 2005.

[20] J. Liu, H.-B. Chen, B.-L. Gou, Z.-Z. Zhao, Z.-T. Liang, and T. Yi, "Study of the relationship between genetics and geography in determining the quality of *Astragali* Radix," *Biological and Pharmaceutical Bulletin*, vol. 34, no. 9, pp. 1404–1412, 2011.

[21] Z. H. Cui, Y. Li, Q. J. Yuan, L. Zhou, and M. Li, "Molecular identification of Astragali Radix and its adulterants by ITS sequences," *China Journal of Chinese Materia Medica*, vol. 37, no. 24, pp. 3773–3776, 2012.

[22] T. Gao, H. Yao, X. Y. Ma, Y. J. Zhu, and J. Y. Song, "Identification of Astragalus plants in China using the region ITS2," *World Science and Technology/Modernization of Traditional Chinese Medicine and Materia Medica*, vol. 12, no. 2, pp. 222–227, 2010.

[23] H.-Y. Guo, W.-W. Wang, N. Yang et al., "DNA barcoding provides distinction between *Radix Astragali* and its adulterants," *Science China Life Sciences*, vol. 53, no. 8, pp. 992–999, 2010.

[24] CBOL Plant Working Group, "A DNA barcode for land plants," *Proceedings of the National Academy of Sciences of United States of America*, vol. 106, no. 31, pp. 12794–12797, 2009.

[25] S. L. Chen, H. Yao, J. P. Han et al., "Validation of the ITS2 region as a novel DNA barcode for identifying medicinal plant species," *PLoS ONE*, vol. 5, no. 1, Article ID e8613, 2010.

[26] W. J. Kress, K. J. Wurdack, E. A. Zimmer, L. A. Weigt, and D. H. Janzen, "Use of DNA barcodes to identify flowering plants," *Proceedings of the National Academy of Sciences of the United States of America*, vol. 102, no. 23, pp. 8369–8374, 2005.

[27] A. Keller, T. Schleicher, J. Schultz, T. Müller, T. Dandekar, and M. Wolf, "5.8S-28S rRNA interaction and HMM-based ITS2 annotation," *Gene*, vol. 430, no. 1-2, pp. 50–57, 2009.

[28] K. Tamura, G. Stecher, D. Peterson, A. Filipski, and S. Kumar, "MEGA6: molecular evoluationaay genetics analysis version 6.0," *Molecular Biology and Evolution*, vol. 30, no. 12, pp. 2725–2729, 2013.

[29] C. P. Meyer and G. Paulay, "DNA barcoding: error rates based on comprehensive sampling," *PLoS Biology*, vol. 3, no. 12, article e422, 2005.

[30] H. A. Ross, S. Murugan, and W. L. S. Li, "Testing the reliability of genetic methods of species identification via simulation," *Systematic Biology*, vol. 57, no. 2, pp. 216–230, 2008.

[31] D. A. Morrison, "Increasing the efficiency of searches for the maximum likelihood tree in a phylogenetic analysis of up to 150 nucleotide sequences," *Systematic Biology*, vol. 56, no. 6, pp. 988–1010, 2007.

[32] Y. P. Zhang, M. K. Nie, S. Y. Shi et al., "Integration of magnetic solid phase fishing and off-line two-dimensional high-performance liquid chromatographydiode array detectormass spectrometry for screening and identification of human serum albumin binders from Radix Astragali," *Food Chemistry*, vol. 146, no. 1, pp. 56–64, 2014.

[33] X. H. Liu, L. G. Zhao, J. Liang et al., "Component analysis and structure identification of active substances for anti-gastric ulcer effects in Radix *Astragali* by liquid chromatography and tandem mass spectrometry," *Journal of Chromatography B*, vol. 960, no. 1, pp. 43–51, 2014.

[34] C. Chu, H.-X. Cai, M.-T. Ren et al., "Characterization of novel astragaloside malonates from *Radix Astragali* by HPLC with ESI quadrupole TOF MS," *Journal of Separation Science*, vol. 33, no. 4-5, pp. 570–581, 2010.

[35] J. Fu, L. F. Huang, H. T. Zhang, S. H. Yang, and S. L. Chen, "Structural features of a polysaccharide from Astragalus membranaceus (Fisch.) Bge. var. mongholicus (Bge.) Hsiao," *Journal of Asian Natural Products Research*, vol. 15, no. 6, pp. 687–692, 2013.

[36] X. Huang, Y. Liu, F. Song, Z. Liu, and S. Liu, "Studies on principal components and antioxidant activity of different Radix Astragali samples using high-performance liquid chromatography/electrospray ionization multiple-stage tandem mass spectrometry," *Talanta*, vol. 78, no. 3, pp. 1090–1101, 2009.

[37] A. Nalbantsoy, T. Nesil, Ö. Yilmaz-Dilsiz, G. Aksu, S. Khan, and E. Bedir, "Evaluation of the immunomodulatory properties in mice and in vitro anti-inflammatory activity of cycloartane type saponins from Astragalus species," *Journal of Ethnopharmacology*, vol. 139, no. 2, pp. 574–581, 2012.

[38] W. L. Xiao, T. J. Motley, U. J. Unachukwu et al., "Chemical and genetic assessment of variability in commercial Radix Astragali (Astragalus spp.) by ion trap LC-MS and nuclear ribosomal DNA barcoding sequence analyses," *Journal of Agricultural and Food Chemistry*, vol. 59, no. 5, pp. 1548–1556, 2011.

Research Article

Rapid Identification of *Asteraceae* Plants with Improved RBF-ANN Classification Models Based on MOS Sensor E-Nose

Hui-Qin Zou,[1] Shuo Li,[2] Ying-Hua Huang,[1] Yong Liu,[3] Rudolf Bauer,[4] Lian Peng,[3] Ou Tao,[3] Su-Rong Yan,[3] and Yong-Hong Yan[3]

[1] *Library, Beijing University of Chinese Medicine, No. 11 Bei San Huan Dong Lu, Chaoyang District, Beijing 100029, China*

[2] *Beijing University of Posts and Telecommunications, No. 10 Xi Tu Cheng Lu, Haidian District, Beijing 100876, China*

[3] *School of Chinese Materia Medica, Beijing University of Chinese Medicine, No. 6 Wang Jing Zhong Huan Nan Lu, Chaoyang District, Beijing 100102, China*

[4] *Institute of Pharmaceutical Sciences, University of Graz, Universitaetsplatz 4, 8010 Graz, Austria*

Correspondence should be addressed to Hui-Qin Zou; zouhuiqin_bucm@sina.cn and Yong-Hong Yan; lxdyyh@yeah.net

Plants from *Asteraceae* family are widely used as herbal medicines and food ingredients, especially in Asian area. Therefore, authentication and quality control of these different *Asteraceae* plants are important for ensuring consumers' safety and efficacy. In recent decades, electronic nose (E-nose) has been studied as an alternative approach. In this paper, we aim to develop a novel discriminative model by improving radial basis function artificial neural network (RBF-ANN) classification model. Feature selection algorithms, including principal component analysis (PCA) and BestFirst + CfsSubsetEval (BC), were applied in the improvement of RBF-ANN models. Results illustrate that in the improved RBF-ANN models with lower dimension data classification accuracies (100%) remained the same as in the original model with higher-dimension data. It is the first time to introduce feature selection methods to get valuable information on how to attribute more relevant MOS sensors; namely, in this case, S1, S3, S4, S6, and S7 show better capability to distinguish these *Asteraceae* plants. This paper also gives insights to further research in this area, for instance, sensor array optimization and performance improvement of classification model.

1. Introduction

Chinese herbal medicines are getting more and more international attention based on their alternative treatment for some refractory diseases and chronic disorders. However, it appears in the medicinal materials markets that nowadays some medicines with low quality or even fake materials are sold. This phenomenon results in economic loss, poor clinical effects, and even poisoning. Therefore, the need for efficient and reliable identification and quality control of these herbal medicines is of crucial importance.

In recent years, lots of modern techniques are introduced into traditional Chinese medicine (TCM) analysis, including high performance liquid chromatography (HPLC), mass spectrometry (MS), nuclear magnetic resonance (NMR), and DNA genetic analysis [1]. The whole chemical profile of TCM could be expressed in different fingerprints which are used to identify original materials [2], especially combined with multivariate statistical analyses [3, 4]. As for the analyses of volatile components in TCM, gas chromatography (GC) and gas chromatography-mass spectrography (GC-MS) are the most popular ways to determine volatile components in TCM. However, these methods normally only detect one or more chemical compositions, and most of the given information reflects the fragments instead of the holistic state of the volatile components. Besides, they are time-consuming for complex sample pretreatment and no environmental protection.

Compared to them, metal oxide semiconductor sensors (MOS sensor) electronic nose (E-nose) is a simple, rapid,

and noninvasive technology with less sample amount and without organic reagents. The initial and unique chemical form of the volatile components in TCM could be reflected by their response to MOS sensor which can be used to identify different TCM [5, 6]. And the information could be fully collected for further analysis.

E-nose, which has already been applied in various fields in the past decades [7–10], is a very promising method for identifying different samples based on their different information of the responses between their volatile components and the sensors. In these studies, different kinds of data processing methods have been applied to construct the classification models such as probabilistic neural network (PNN) [11], Bayesian neural network (BNN) [12], multilayer perceptrons (MLP) [13], and radial basis function artificial neural network (RBF-ANN). Among them, RBF-ANN shows good performance for classification modeling [14].

Lin et al. [15] employed RBF-ANN to construct a classification model based on E-nose to successfully distinguish different kinds of *Apiaceae* plants. However, there are few studies on the improvement of RBF-ANN classification model combined with the selection and optimization of MOS sensor array. Daqi et al. proposed a type of modular RBF-ANN to improve its performance [16].

In this paper, we aim to develop a novel discriminative model by improving RBF-ANN classification model. Through applying feature selection algorithms, principal component analysis (PCA), and BestFirst + CfsSubsetEval (BC), the construction of networks in RBF-ANN models was simplified, maintaining the same high-quality discriminative ability. Based on feature screening, the redundant information in the original RBF-ANN model for identifying different *Asteraceae* plants was eliminated and more valuable information was retained. Furthermore, using these improved RBF-ANN models, five MOS sensors were selected to possess better capability to distinguish these eight species of *Asteraceae* plants, which are S1, S3, S4, S6, and S7.

2. Materials and Methods

2.1. Plant Materials. Eight different species of plants, all originating from *Asteraceae* family, were purchased from Beijing Tongrentang Co., Ltd. (Beijing, China) and identified by Professor Yong-Hong Yan in Beijing University of Chinese Medicine (Beijing, China). As shown in Table 1, samples were labeled as *Bai Zhu, Cang Zhu, Gong Ju, Ye Ju Hua, Ai Ye, Mu Xiang, E Bu Shi Cao,* and *Niu Bang Zi.*

2.2. E-Nose. E-nose (α-FOX3000, Alpha M.O.S., France) consists of 12 MOS sensors, a head space sampler, and a signal processing system. Twelve commercial metal oxide sensors are placed in two rectangular chambers, six per each. A list of all MOS sensors' information and their application is illustrated in Table 2. They are LY2/LG, LY2/G, LY2/AA, LY2/GH, LY2/gCTL, LY2/gCT, T30/1, P10/1, P10/2, P40/1, T70/2, and PA/2, respectively, numbered as S1, S2, S3, . . . , S12. The sensor response was expressed as the ratio of conductance (($G - G_0$)/G).

TABLE 1: *Asteraceae* plant as an herbal medicine.

Number	Label	Herbal name
1	*Bai Zhu*	Dried Rhizoma of *Atractylodes macrocephala* Koidz.
2	*Cang Zhu*	Dried Rhizoma of *Atractylodes lancea* (Thunb.) DC.
3	*Gong Ju*	Dried Flos of *Chrysanthemum morifolium* Ramat.
4	*Ye Ju Hua*	Dried Flos of *Chrysanthemum indicum* L.
5	*Ai Ye*	Dried Folium of *Artemisia argyi* Levl. et Vant.
6	*Mu Xiang*	Dried Radix of *Aucklandia lappa* Decne.
7	*E Bu Shi Cao*	Dried Herba of *Centipeda minima* (L.) A. Br. et Aschers.
8	*Niu Bang Zi*	Dried Fructus of *Arctium lappa* L.

Ground into small particles, 0.2 g of each sample was accurately weighed into a 10 mL septa-sealed bottle and loaded into the autosampler tray. After incubation with optimized parameters in the previous research (temperature is 30°C and time is 300 seconds), 2000 μL of headspace air was automatically injected into the E-nose system by a syringe and detected by MOS sensor array. The conductance ratio of each sensor changed during the measurement process. The measurement phase lasted for 120 s, which was enough for all the sensors to reach the stable values and return to the baseline. Signals were collected by the computer and the data acquisition cycle was 1 s.

Six repeated samples were prepared for each kind of plants and totally 48 measurements were performed by the dynamic headspace sampling procedure. The E-nose responses values of those plants were extracted and recorded by the computer. Then different kinds of RBF-ANN models were established to identify them.

2.3. Classification Model Improved RBF-ANN Combined with PCA and BC. In the field of mathematical modeling, a radial basis function network is an artificial neural network which uses radial basis functions as activation functions. Normally, it contains three layers: one input layer, one hidden layer (sometimes more than one), and one output layer. The output of the network is a linear combination of radial basis functions of the inputs and neuron parameters. One of the principal problems encountered in the RBF network modeling procedure is that more redundant or uncorrelated information in the input layer may increase the error rate or result in overfitting in the output layer. Hence, in order to solve the above problems, we employ two kinds of feature selection methods, namely, PCA and BC, to process the high-dimension data, eliminating redundant information and selecting the factors which contribute more valuable information to the final target: presenting a rapid and accurate method for identification of these eight species of *Asteraceae* plants.

Table 2: Main application of 12 MOS sensors in α-FOX3000 E-nose.

Number	Name	Main application
S1	LY2/LG	Oxidizing gas
S2	LY2/G	Ammonia/carbon monoxide
S3	LY2/AA	Ethanol
S4	LY2/GH	Ammonia/organic amine
S5	LY2/gCTL	Hydrogen sulfide
S6	LY2/gCT	Propane/butane
S7	T30/1	Organic solvents
S8	P10/1	Hydrocarbons
S9	P10/2	Methane
S10	P40/1	Fluorine
S11	T70/2	Aromatic compounds
S12	PA/2	Ethanol/ammonia/organic amine

PCA helps us to figure out which samples are different from the others and which principal components extracted from the original variances contribute more to this difference. Focus on dealing with those principal components with more important information is one way for us to reduce high dimension in data processing.

BC is a kind of feature extraction technologies, which can screen out the characteristic parameter vectors with high relevance to the classification and low relevance to the others. We can get an optimum set of MOS sensors for final identification based on BC.

As for the evaluation of the established models, 10-fold cross-validation method is applied to avoid the overfitting and get the classification accuracy. The classification results should not be considered if the classification accuracy was lower than 80%.

3. Results and Discussion

3.1. E-Nose Responses to the Volatile Components of Samples from Asteraceae Plants. When detecting the sensor response to a given sample, the response values are used as $R = (G - G_0)/G$, where R is the response, G_0 is the conductance of a sensor in the reference air, and G is the conductance of the sensor in the sample gas.

Figure 1 shows the typical responses of 12 MOS sensors with one sample of *Cang Zhu* (dried Rhizoma of *Atractylodes lancea* (Thunb.) DC.). Each line represents the signals of a *Cang Zhu* sample in one of the 12 MOS sensors. The horizontal axis is the time line, a total of 120 seconds; the vertical axis is the response value of the MOS sensor. The curves represent the resistance value of each sensor against time due to the electrovalve action when the volatile compounds reached the detection chamber. In the initial period, the response value of each sensor was low and then increased continuously and finally stabilized after a few seconds or minutes. In this study, 12 maximum response values of each sample from 12 MOS sensors were extracted and analyzed individually.

The repeatability of the established method was evaluated with six parallel tests of the samples. The relative standard deviation (RSD, $n = 6$) values of 12 MOS sensors were
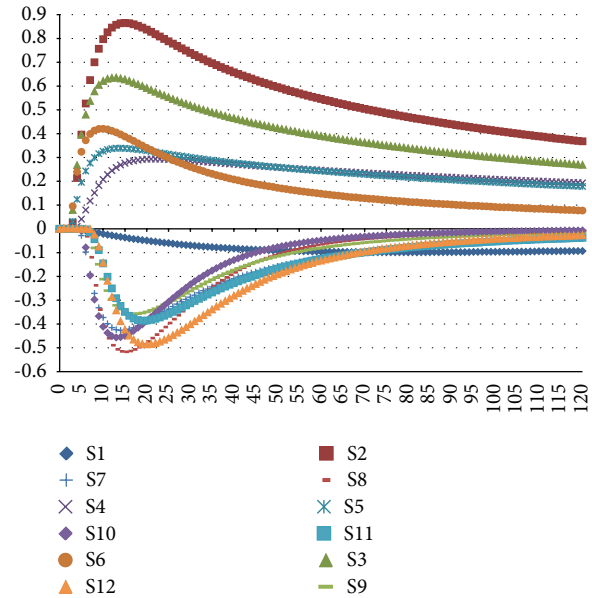
Figure 1: Typical responses of 12 MOSs measuring of a *Cang Zhu* sample.

calculated. The results were all less than 3%, proving a high repeatability of E-nose response.

3.2. RBF-ANN with Original Data from 12 MOS Sensors. Figure 2 shows the different contributions of 12 MOS sensors in the original RBF-ANN model for *Asteraceae* plants. Eight kinds of colors presented eight species of *Asteraceae* plants. Firstly, they are divided into different groups in each sensor. For example, they are four groups in the case of S1 but three groups in the case of S2. That means S1 contributes more valuable information to distinguish these eight species of *Asteraceae* plants into smaller groups. Secondly, the classification situation differs in every sensor. For example, the green samples and the light blue samples are considered as the same group and they could not be separated in the case of S1. However, in the case of S2, S3, S4, S7, S9, and S11, they are separated into different groups. Thirdly, some identification information is overlapped in some sensors. For example, S2 and S3 contain the same information which means, in this identification of *Asteraceae* plants, S2 and S3 have the similar contribution. According to these, it is certain that some of the sensors contain more valuable information for the identification but some of them resemble the others which should be eliminated for model simplification. Therefore, it shows us a potential way to improve the classification model on the basis of sensors screening and optimization.

Figure 3 shows the architecture of three layers of RBF-ANN for training and identification. The input layer in this network consists of 12 units and the identification result can be gained directly from this model. In this initial RBF-ANN model, input layer contains 12 units from 12 MOS sensors. All the original data of the input layer are imported into the hidden layer and then calculated by the RBF. Afterwards identification results are gained and the samples are divided
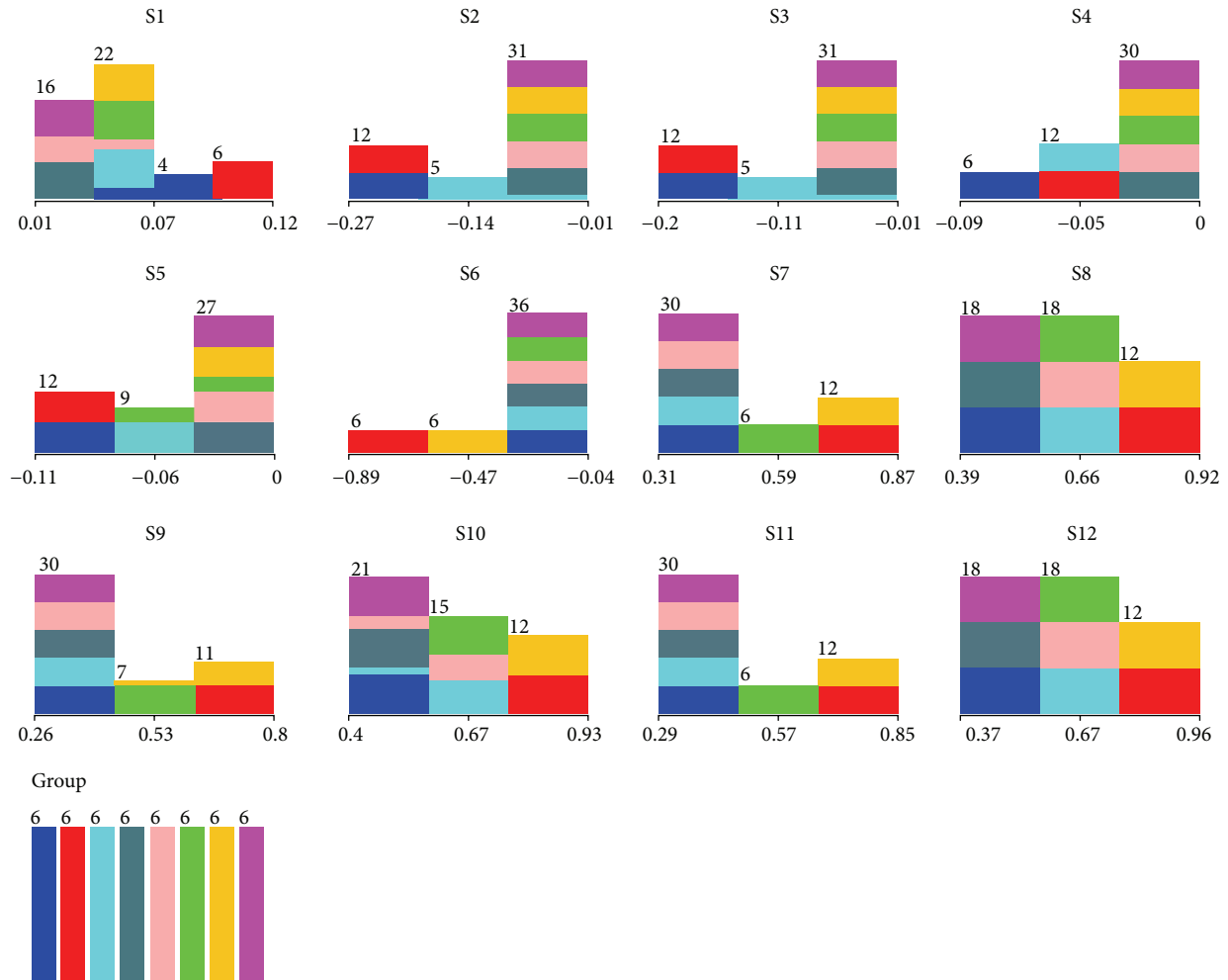
FIGURE 2: Different contributions of 12 MOS sensors in the original RBF-ANN model for *Asteraceae* plants identification.

into eight different groups. Figure 3 tells it is necessary to reduce the high-dimension data in the network so as to simplify the modeling process.

3.3. Comparison of Original and Improved RBF-ANN Models.

Based on PCA feature selection method, two main factors were selected and the factors with minimum weight were rejected.

Based on BC feature selection method, six MOS sensors (S1, S3, S4, S6, and S7) were screened out to contribute the most valuable information to identify these eight species of *Asteraceae* plants. Table 3 shows that the classification accuracies of three types of RBF-ANN models with 12, 2, and 5 units by 10-fold cross-validation are all 100%. That means the RBF-ANN still can achieve the identification goal by lower dimension data reduced by these two kinds of feature selection methods. Meanwhile, the sum of square error is decreased in the improved RBF-ANN models combined with PCA as well as with BC. Last but not least, it is suggested BC should be considered as a method for optimizing the set of sensor array. Further research on which type of sensor is more

sensitive and exclusive to volatile components in TCM should be carried on.

4. Conclusions

Lots of plants originating from the *Asteraceae* family are applied as Chinese herbs and beverage ingredients in Asian areas, particularly in China. However, they may be confused due to their similar odor, especially when they are ground into powder, losing the typical macroscopic characteristics. In this paper, E-nose was employed to extract and analyze the volatile components fingerprints of eight species of *Asteraceae* plants. Then RBF-ANN was applied to establish the classification model. Furthermore, two different kinds of feature selection methods, PCA and BC, were used to solve high-dimension data problem. Through PCA and BC, we have synthesized numerous criteria, eliminated information overlapping of the sample, and reduced the input dimensions of RBF network. And it is the first time to introduce feature selection methods to improve RBF-ANN classification model and get valuable information on how to attribute more relevant MOS sensors. In this paper, S1, S3, S4, S6, and S7

Hidden layer activation function: softmax
Output layer activation function: identity

—— Synaptic weight > 0
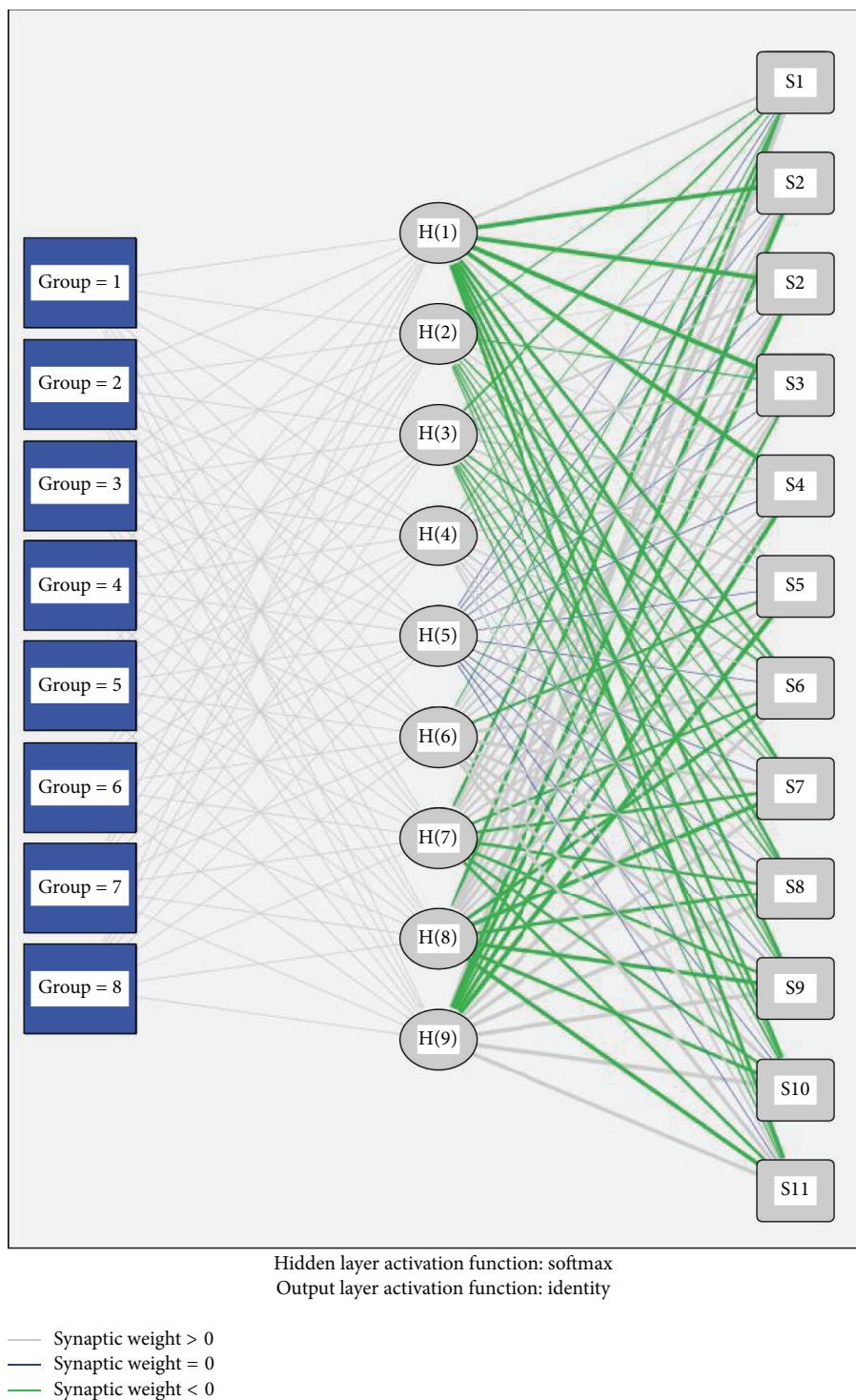—— Synaptic weight = 0
—— Synaptic weight < 0

FIGURE 3: Architecture of three layers of original RBF-ANN with 12 units in the input layer (codes stand for samples and S1~S12 stand for 12 MOS sensors).

show better capability to distinguish these eight species of *Asteraceae* plants.

In a word, this paper presents a rapid, accurate, and effective method to distinguish *Asteraceae* plants. Also it gives insights into further studies, for instance, to search some kinds of unique sensors which are more sensitive and exclusive to volatile components in TCM, to improve the identification ability of E-nose. Besides, screening sensors made by other novel materials would be also an interesting way to improve identification capability of E-nose [17].

TABLE 3: Comparison of three types of RBF-ANN with 12, 2, and 5 units.

Sum of square error	Training	Testing	Classification accuracy via 10-fold cross-validation
12 units RBF-ANN	0.939	0.320[a]	100%
2 units RBF-ANN	0.083	0.029[a]	100%
5 units RBF-ANN	0.522	0.207[a]	100%

Abbreviations

TCM:	Traditional Chinese medicine
E-nose:	Electronic nose
MOS:	Metal oxide semiconductor
PCA:	Principal component analysis
BC:	BestFirst + CfsSubsetEval
RBF-ANN:	Radial basis function artificial neural networks.

Conflict of Interests

The authors have no personal or financial conflict of interests associated with this work.

Authors' Contribution

Hui-Qin Zou and Shuo Li contributed equally to this work.

Acknowledgments

References

[1] Z. Z. Zhao, Z. T. Liang, and G. Ping, "Macroscopic identification of Chinese medicinal materials: traditional experiences and modern understanding," *Journal of Ethnopharmacology*, vol. 134, no. 3, pp. 556–564, 2011.

[2] J. Rong, R. Tilton, J. Shen et al., "Genome-wide biological response fingerprinting (BioReF) of the Chinese botanical formulation ISF-1 enables the selection of multiple marker genes as a potential metric for quality control," *Journal of Ethnopharmacology*, vol. 113, no. 1, pp. 35–44, 2007.

[3] Y. H. Lai, Y. N. Ni, and S. Kokot, "Discrimination of Rhizoma Corydalis from two sources by near-infrared spectroscopy supported by the wavelet transform and least-squares support vector machine methods," *Vibrational Spectroscopy*, vol. 56, no. 2, pp. 154–160, 2011.

[4] T. M. Zhang, Z. Zhao, X. Q. Fang et al., "Determining method, conditional factors, traits and applications of nonlinear chemical fingerprint by using dissipative components in samples," *Science China Chemistry*, vol. 55, no. 2, pp. 285–303, 2012.

[5] F. Röck, N. Barsan, and U. Weimar, "Electronic nose: current status and future trends," *Chemical Reviews*, vol. 108, no. 2, pp. 705–725, 2008.

[6] M. Peris and L. Escuder-Gilabert, "A 21st century technique for food control: electronic noses," *Analytica Chimica Acta*, vol. 638, no. 1, pp. 1–15, 2009.

[7] A. K. Deisingh, D. C. Stone, and M. Thompson, "Applications of electronic noses and tongues in food analysis," *International Journal of Food Science and Technology*, vol. 39, no. 6, pp. 587–604, 2004.

[8] A. H. Gómez, J. Wang, G. Hu, and A. G. Pereira, "Discrimination of storage shelf-life for mandarin by electronic nose technique," *LWT: Food Science and Technology*, vol. 40, no. 4, pp. 681–689, 2007.

[9] H. Yu and J. Wang, "Discrimination of LongJing green-tea grade by electronic nose," *Sensors and Actuators B: Chemical*, vol. 122, no. 1, pp. 134–140, 2007.

[10] S. Li, X. R. Li, G. L. Wang et al., "Rapid discrimination of Chinese red ginseng and Korean ginseng using an electronic nose coupled with chemometrics," *Journal of Pharmaceutical and Biomedical Analysis*, vol. 70, pp. 605–608, 2012.

[11] M. Ghasemi-Varnamkhasti, S. S. Mohtasebi, M. Siadat et al., "Aging fingerprint characterization of beer using electronic nose," *Sensors and Actuators, B: Chemical*, vol. 159, no. 1, pp. 51–59, 2011.

[12] C. Y. Li, P. Heinemann, and R. Sherry, "Neural network and Bayesian network fusion models to fuse electronic nose and surface acoustic wave sensor data for apple defect detection," *Sensors and Actuators B: Chemical*, vol. 125, no. 1, pp. 301–310, 2007.

[13] P. G. Micone and C. Guy, "Odour quantification by a sensor array: an application to landfill gas odours from two different municipal waste treatment works," *Sensors and Actuators B: Chemical*, vol. 120, no. 2, pp. 628–637, 2007.

[14] R. Dutta, A. Das, N. G. Stocks, and D. Morgan, "Stochastic resonance-based electronic nose: a novel way to classify bacteria," *Sensors and Actuators, B: Chemical*, vol. 115, no. 1, pp. 17–27, 2006.

[15] H. Lin, Y. Yan, T. Zhao et al., "Rapid discrimination of Apiaceae plants by electronic nose coupled with multivariate statistical analyses," *Journal of Pharmaceutical and Biomedical Analysis*, vol. 84, pp. 1–4, 2013.

[16] G. Daqi, W. Shuyan, and J. Yan, "An electronic nose and modular radial basis function network classifiers for recognizing multiple fragrant materials," *Sensors and Actuators B: Chemical*, vol. 97, no. 2-3, pp. 391–401, 2004.

[17] M. C. Mcalpine, H. Ahmad, D. Wang, and J. R. Heath, "Highly ordered nanowire arrays on plastic substrates for ultrasensitive flexible chemical sensors," *Nature Materials*, vol. 6, no. 5, pp. 379–384, 2007.

Research Article

Dynamics of *Panax ginseng* Rhizospheric Soil Microbial Community and Their Metabolic Function

Yong Li, YiXin Ying, and WanLong Ding

Institute of Medicinal Plant Development, Chinese Academy of Medical Sciences and Peking Union Medical College, No. 151 Malianwa North Road, Beijing 100193, China

Correspondence should be addressed to WanLong Ding; wlding@implad.ac.cn

The bacterial communities of 1- to 6-year ginseng rhizosphere soils were characterized by culture-independent approaches, random amplified polymorphic DNA (RAPD), and amplified ribosomal DNA restriction analysis (ARDRA). Culture-dependent method (Biolog) was used to investigate the metabolic function variance of microbe living in rhizosphere soil. Results showed that significant genetic and metabolic function variance were detected among soils, and, with the increasing of cultivating years, genetic diversity of bacterial communities in ginseng rhizosphere soil tended to be decreased. Also we found that *Verrucomicrobia*, *Acidobacteria*, and *Proteobacteria* were the dominants in rhizosphere soils, but, with the increasing of cultivating years, plant disease prevention or plant growth promoting bacteria, such as *Pseudomonas*, *Burkholderia*, and *Bacillus*, tended to be rare.

1. Introduction

Ginseng (*Panax ginseng* C.A. Meyer) is mainly cultivated in China, Korea, and Japan. It has been regarded as one of the most important remedies in oriental medicine for more than 1,000 years [1]. Nowadays, it is usually used as adaptogenic, antiaging health tonic, and so forth. As herbaceous perennial plant, ginseng requires at least 6 years of growth from sow to harvest. In China, after growing 2 or 3 years, ginseng usually is transplanted to another site until harvest. During the long growing process, soilborne diseases made a severe threat on the health of *P. ginseng* root.

Rhizosphere soil is defined as soil tightly adhering with plant root [2]. Plant releases a series of compounds through root into rhizosphere soil which provide plentiful nutrition to rhizosphere microbe [3]. On the other hand, rhizosphere bacteria play an important role in nutrient cycling, organic matter decomposition, and soil fertility maintaining [4]. Recently, though a few novel bacterial strains have been isolated from field plant ginseng ever [5–7] or from the interior of ginseng root [8, 9], most of the bacterial community in ginseng rhizosphere soil is still unknown yet.

In the present study, culture-independent methods, random amplified polymorphic DNA (RAPD), and amplified ribosomal DNA restriction analysis (ARDRA) were used to examine the bacterial community and dynamics of dominant bacterial species in ginseng rhizosphere soil during the growth of *P. ginseng*. Furthermore, Biolog EcoPlate was used to study the metabolic function variance of rhizosphere microbe. The aim of the present study was to reveal the dynamics of rhizosphere bacterial communities during the growth of *P. ginseng* by culture-dependent and culture-independent methods.

2. Experimental Section

2.1. Soil Collection and DNA Extraction. Rhizosphere soils of one- to six-year ginseng were sampled from Dafang (H: 570.8 m N: $42°26'03.2''$ E: $127°20'00.1''$) in Fusong county, Jilin Province, China, in January 2009. The soil is uniform with histosols soil according to the UN-FAO soil classification system. For each sample, soil tightly adhering on the surface of five healthy ginseng roots at the same field was collected. The genomic DNA of soil microbes was extracted immediately.

Genomic DNA was extracted from 0.5 g fresh soil using E.Z.N.A. Soil DNA Kit (OMEGA, USA) according to

the manufacturer's instructions. The successful extraction of genomic DNA was checked by 0.8% agarose gel electrophoresis with $1 \times$ TAE buffer (2 mol/L Tris-base, 50 mmol/L EDTA, and 1 mol/L acetic acid, pH 8.0).

2.2. RAPD Fingerprinting. Genetic diversity of microbes in ginseng rhizosphere soils was examined by RAPD method. Amplification was performed in a 25 μL volume containing 20 ng template DNA, 0.2 μmol/L primer, 100 μmol/L dNTP, $1 \times$ PCR buffer (10 mmol/L Tris-HCl, pH 8.0, 50 mmol/L KCl, 1.5 mmol/L MgCl$_2$), and 1 U Taq DNA polymerase. In total, 15 repetitive and polymorphic primers (OPH11, OPI4, OPJ1, OPJ4, OPJ7, OPR7, OPR8, OPR10, OPR11, OPR14, OPR17, OPS4, OPS10, OPT16, and OPT17) were used for RAPD analysis. Amplification was performed in a T Gradient 96 Thermal Cycler (Biometra) with cycling program that consisted of initial denaturation of 1 min at 94°C, followed by 40 cycles of 1 min denaturation at 94°C, 1 min annealing at 37°C, 1.5 min extension at 72°C, and a final extension at 72°C for 7 min.

Products amplified were separated on 1.2% agarose gels containing ethidium bromide, and reproducible, clear bands from 100 bp to 1500 bp were recorded. Fingerprinting profile was then converted to a two-dimensional binary matrix ("1" indicates presence of band; "0" indicates absence of band) and calculated using NTSYSpc version 2.10e software for clustering analysis [10]. The dendrogram was constructed using the unweighted pair group method (UPGMA). Nei's genetic diversity and Shannon's information index were calculated by population genetic analysis software Popgene version 1.32 (32-bit).

2.3. Amplified Ribosomal DNA Restriction Analysis (ARDRA). The bacterial community was analyzed by a cultivation-independent method. 16S ribosomal DNA of bacteria was amplified by a pair of universal primers 27f (5′-AGA GTT TGA TCM TGG CTC AG-3′) and 1492r (5′-TAC GGY TAC CTT GTT ACG ACT T-3′) [11, 12] in a T Gradient 96 Thermal Cycler. The successful amplification was checked by 1% agarose gel electrophoresis.

Target fragments were purified by Wizard PCR Preps DNA Purification System (Promega, USA), ligated with PMD-18T vector (TaKaRa), and then transferred into *E. coli* TOP10 competent cell according to the manufacturer's instructions. Aliquot (100 μL) of each transformation was spread on LB/ampicillin/IPTG/X-gal plates and incubated at 37°C for 16 h. For each sample, 192 white colonies were picked out, which were amplified by 27f and 1492r primer that the positive clones were confirmed through. Then, 10 μL target insert fragments (about 1,500 bp) were digested by 3 U restriction endonuclease Hinf I (TaKaRa) [13, 14] and Pst I (TaKaRa) [15] at 37°C for 2 h. Clones having the same restriction patterns were defined as an operational taxonomic unit (OTU).

Representative clones of unique ARDRA patterns were sequenced by automated DNA capillary sequencer 3730 (Applied Biosystems, USA). The partial sequences of 16S rRNA gene were blasted with known 16S rDNA sequences

in GenBank databases using nucleotide BLAST program (http://blast.ncbi.nlm.nih.gov/blast.cgi) [16]. The saturation of clones in the library was evaluated by rarefaction curves [17] calculated using the Analytic RarefactWin Version 1.3 (http://www.uga.edu/~strata/software/index.html) program [18].

2.4. Metabolic Characteristics of Soil Microbe. Soil metabolisms of soil microbial communities were characterized by community level physiological profiles (CLPP) using Biolog EcoPlate [19]. Ten grams of fresh soil was suspended in 90 mL of sterile 0.85% saline solution and shaken at 120 rpm for 30 min, and then suspensions were diluted 1,000-fold. Each well of a Biolog EcoPlate was inoculated with 150 μL diluents and incubated at 25°C in dark without agitation. The plates were scanned at wavelength of 590 nm by a Biolog reader on OmniLog Plus (BIOLOG Inc., Hayward, CA, USA) at a 24-hour interval for 168 h. Each soil sample using one plate with 31 carbon substrates is arranged in triplicate.

The average well color development (AWCD) was used to evaluate the general carbon substrates utilization ability [9, 20], where "A_i" is the absorption of ith well and "A_{A_1}" is the absorption of the "A_1" well following the incubation measured in terms of the optical density at wavelength of 590 nm (OD590). AWCD of each well was calculated using the following formula:

$$\text{AWCD} = \frac{\sum \left(A_i - A_{A_1} \right)}{31}. \tag{1}$$

The metabolic profile of microbial community includes the Shannon index (H') and the evenness index (E) [21, 22]. The diversity of microbial community was evaluated by the Shannon index (H') [23], calculated using the formula

$$H' = -\sum_{i=1}^{s} p_i \cdot \ln p_i, \tag{2}$$

where "p_i" is the principal color development of the "ith" well relative to the total color development, that is, $p_i = (C - R)/\sum(C - R)$, and "$s$" is the summation of absorption values of all wells in a Biolog EcoPlate. The evenness index was calculated using the formula $E = H'/\ln S$, where diversity "S" is the total number of carbon substrates utilized by microbial community in a given soil sample, and only the positive data, the optical density (OD) ≥ 0.2, was used to calculate "S." The AWCD value at 120 h was used to calculate the Shannon index (H'); SPSS 17.0 and SIMCA-P 11.5 Demo software were used for PCA analysis [24].

3. Results

3.1. RAPD Analysis. Bacterial diversity indices H' and I decreased in soil B compared to soil A but increased sharply in soil C. H' and I of soils D, E, and F were significantly lower than of soils A, B, and C. Soil D has the lowest indices, while soil C has the highest indices (Table 1).

Clustering results showed that, under the 0.58 coefficient threshold, 6 soil samples were divided into two groups. Group

TABLE 1: Bacterial diversity and metabolic function indices of ginseng rhizosphere soils.

Soil samples	Cultivating year	H'	I	Shannon diversity	Evenness
A	1	0.4782	0.6712	2.791	0.829
B	2	0.4357	0.6273	2.786	0.827
C	3	0.4880	0.6811	2.768	0.838
D	4	0.3519	0.5367	2.716	0.832
E	5	0.3866	0.5750	2.778	0.822
F	6	0.4142	0.6047	2.664	0.818

H' indicates Nei's gene diversity; I indicates Shannon's information index.
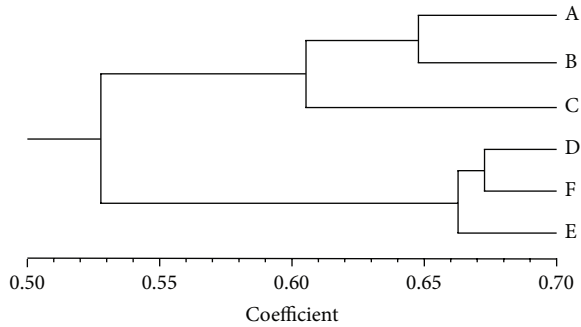
FIGURE 1: UPGMA dendrogram of six ginseng rhizosphere soils.

FIGURE 2: Rarefaction curves for bacterial OTUs, clustering at 97% rRNA gene similarity.

I included soils A, B, and C, while group II included soils D, E, and F. The highest similarity coefficient was detected between soils D and F (Figure 1).

3.2. ARDRA and Phylogenetic Analysis. In total, 167 OTUs were generated from 961 clones, in which 27, 27, 44, 16, 28, and 25 OTUs were identified in soils A, B, C, D, E, and F, respectively.

The saturation of OTUs analyzed was evaluated by rarefaction curves, which indicated that six clone libraries were near the saturated status (Figure 2). ARDRA analyzing results indicated that soil D has the lowest diversity (16 OTUs), whereas diversities of soil C (44 OTUs) were the highest.

Sequencing results indicated that *Verrucomicrobia*, *Acidobacteria*, and *Proteobacteria* were the dominants in six soils. Also, *Gemmatimonadetes*, *Planctomycetes*, *Firmicutes*, *Bacteroidetes*, *Actinobacteria*, *Gemmatimonadales*, and unclassified bacteria were identified in soils. *Proteobacteria* showed the most significant differences among 6 soils. *Firmicutes* are only present in soils A, B, and C. *Gemmatimonadales* are only present in soils C and E. *Bacteroidetes* are only present in soils A and C. α- and γ-*Proteobacteria* are present in 6 soils simultaneously. γ-*Proteobacteria* constitute a substantial proportion of clones (about 60%) in soil F. Except for soil F, β-*Proteobacteria* are present in another 5 soils. δ-*Proteobacteria* are present in soils except soils A and E. *Verrucomicrobia* are another major group present in 6 soils. *Actinobacteria* are present in soil F. Except for soils B and F, *Planctomycetes* are present in another 4 soils with a small proportion. Unclassified bacteria (about 8.5% of total) are detected in 6 soils. Of the 167 OTUs sequenced, 63.2% (607
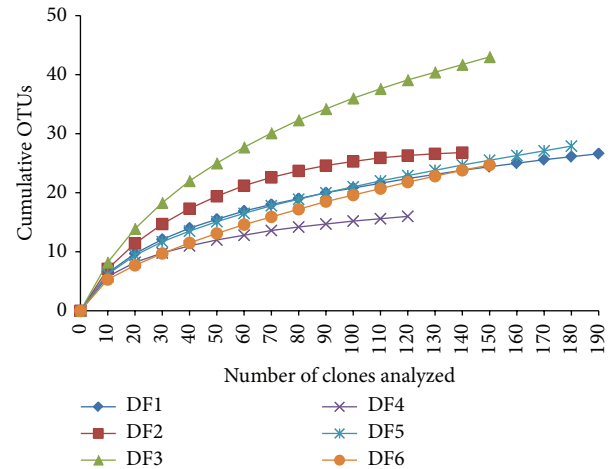
clones) had higher similarity to the 16S rDNA sequences of uncultured bacteria, and only 36.8% (354 clones) were most closely related to cultured isolates (Figure 3).

3.3. BIOLOG Analysis. As a universal indicator of metabolic activity, AWCD changes were shown in Figure 4. Obviously, the metabolic activity tended to be increasing along with incubation time. However, metabolic activity among soils showed significant differences. For example, soils D and F usually had the lowest AWCD, which indicated that their metabolic activity was the lowest.

According to the curve of AWCD versus the culturing time, the AWCD values in 120 h were used to describe the difference of soil microbial metabolic activity. In the present research, the order of metabolic activity based on AWCD was described as follows: soil D < soil F < soil A < soil C < soil E < soil B. The Shannon diversity ranged from 2.664 to 2.791; soil F has the lowest Shannon diversity and evenness indices (Table 1).

To show which types of the substrates were utilized and the intrinsic differences between microbial communities, principal component analysis was then performed to display the variance of microbial communities (Figure 5), which could clearly separate the soil samples according to the different age of ginseng. The first principal component (PC1) and the second principal component (PC2) contributed 58% and
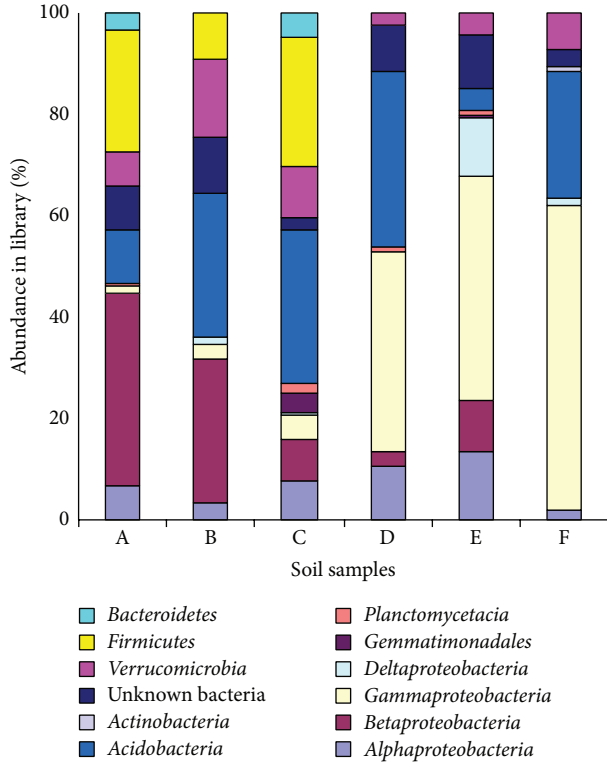
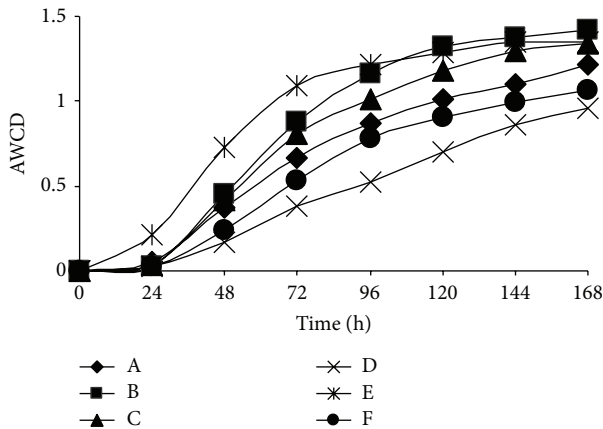FIGURE 3: Bacterial communities in ginseng rhizosphere soil.

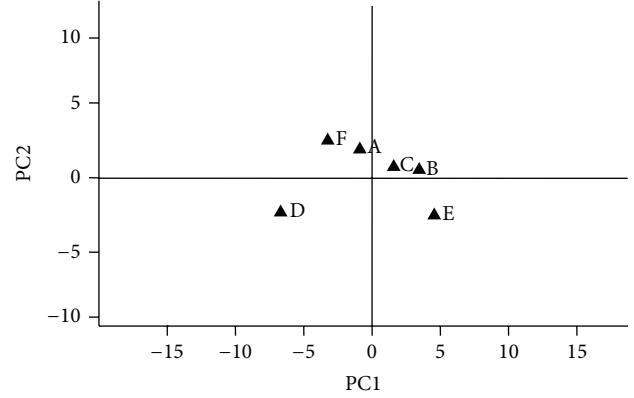FIGURE 4: Average well color development (AWCD) with incubation.

FIGURE 5: Principal component analysis (PCA) of Biolog EcoPlates data. Each solid triangle represents a soil sample.

TABLE 2: Substrates highly correlated with PC1 and PC2.

PC1	r
Carbohydrates	
I-Erythritol	0.895
Glycogen	0.835
D-Glucosaminic acid	0.859
D-Cellobiose	0.891
Amino acids	
L-Arginine	0.848
L-Phenylalanine	0.918
L-Threonine	0.838
Carboxylic acids	
Pyruvic acid methyl ester	0.873
y-Hydroxybutyric	0.930
Itaconic acid	0.959
a-Ketobutyric acid	0.907
Amines	
Putrescine	0.968
Phenolic	
2-Hydroxybenzoic acid	0.802
4-Hydroxybenzoic acid	0.905
Polymer	
a-Cyclodextrin	0.886
PC2	r
Amino acids	
L-Asparagine	0.805
Carbohydrates	
N-Acetyl-D-glucosamine	0.804

18% to the total variation, respectively. By substrate utilization patterns, soil samples were clearly divided into two groups: one with soil samples D, F, and A and the other with soils C, B, and E. The difference of C utilization patterns supported the fact that ginseng of different ages had significant influence on rhizosphere soil microbial community (Table 2).

The substrates with high correlation coefficients to PC1 and PC2 were shown in Table 2. It is illustrated that carboxylic acids and carbohydrates influence PC1 greatly, which were carbohydrates and amino acids for PC2.

4. Discussion

Culture-independent method was used to investigate the bacterial community; the dominant bacteria in ginseng rhizosphere soils were not the same as those found from a wide range of soils, such as pristine forest, grassland, and agricultural soils [25]. Such differences could likely be explained by different soil characteristics [26]. Root exudates

released by plant provide plenteous nutrition for rhizospheric microorganisms and had a great influence on the microbial community. So we deduced that ginseng is a herbaceous perennial plant growing at a special environment, and its exudates are different from others, which finally resulted in special bacterial community.

According to RAPD and ARDRA analysis, soil C has the highest diversity index. It was also found that bacterial diversity in rhizosphere soil of cotton increased from squaring period to flowering period [27]. The reason for this could be that young roots are known to excrete more organic material than older roots, which can result in different specific bacterial populations [28]. Among soils tested, soils D and F have the lowest diversity index. Further analysis indicated that carbon sources metabolic activity of two soils were also the lowest. Although the relationship between biological diversity and ecological function of soil bacterial community has not been fully understood, the decrease of microbial diversity will obviously result in the loss of some ecological function and finally make the ecological system unhealthy [29–31]. Actually, soils ever cultivated ginseng, which are traditionally called "old ginseng soil," such as soils D and F, which are not suitable for the growth of the next generation of ginseng. So we deduced that the decreased genetic diversity and reduced ecological function disorder made the soil unsuitable for ginseng growth further.

Rhizosphere is a unique environment, where pathogens and beneficial microbe have important influence on the growth and health of plants [32]. *Pseudomonas* and *Burkholderia* belong to *Proteobacteria*, and *Bacillus* belongs to *Firmicutes* which were reported to have antagonistic activity against soilborne pathogenic fungi, such as *Rhizoctonia*, *Sclerotinia*, *Verticillium*, and *Gaeumannomyces* [33–35]. In the present study, genera of *Pseudomonas*, *Burkholderia*, and *Bacillus* were found in soils A, B, C, and E. Actually, during the cultivation, 6-year-old ginseng is more easily infected by soilborne pathogenic fungi. So we deduced that the decrease of the *Pseudomonas*, *Burkholderia*, and *Bacillus* in rhizosphere soil may be a key cause that resulted in 6-year ginsengs being more easily infected by soilborne pathogens.

It is known that soil bacterial populations are influenced by a wide range of factors. Soil type, plant species, and cropping patterns are the factors that most affect the bacterial community structure in soil [8, 36]. In order to reduce interference from other factors and truly reflect the relationship between soil bacterial succession and continuous cropping with ginseng plants, several measures were used, including the uniformity of management of ginseng cultivation. Cluster analyses demonstrated that the soil bacterial assemblages obtained from the same cropping cycle were similar; genetic polymorphic analyses and carbon metabolic analyses also showed dynamic changes in bacterial populations with continuous ginseng cropping. It has been reported that soil microbial biomass and their structure were also significantly influenced by continuous cropping with the other grain crops or economic crops [37, 38]. These findings indicated that successional change in soil microbial communities with continuous cropping may be a common feature.

Conflict of Interests

The authors declare that there is no conflict of interests.

References

[1] W. Yu, B. Lee, S. Nam, D. Yang, and Y. Yun, "Modulating effects of Korean ginseng saponins on ovarian function immature rats," *Biological and Pharmaceutical Bulletin*, vol. 26, no. 11, pp. 1574–1580, 2003.

[2] A. D. Kent and E. W. Triplett, "Microbial communities and their interactions in soil and rhizosphere ecosystems," *Annual Review of Microbiology*, vol. 56, pp. 211–236, 2002.

[3] J. M. Whipps, "Microbial interactions and biocontrol in the rhizosphere," *Journal of Experimental Botany*, vol. 52, pp. 487–511, 2001.

[4] D. Atkinson and C. A. Watson, "The beneficial rhizosphere: a dynamic entity," *Applied Soil Ecology*, vol. 15, no. 2, pp. 99–104, 2000.

[5] W. Im, S. Kim, Q. Liu, J. Yang, S. Lee, and T. Yi, "*Nocardioides ginsengisegetis* sp. nov., isolated from soil of a ginseng field," *Journal of Microbiology*, vol. 48, no. 5, pp. 623–628, 2010.

[6] M. Lee, L. N. Ten, S. Baek, W. Im, Z. Aslam, and S. Lee, "*Paenibacillus ginsengisoli* sp. nov., a novel bacterium isolated from soil of a ginseng field in Pocheon province, South Korea," *Antonie van Leeuwenhoek, International Journal of General and Molecular Microbiology*, vol. 91, no. 2, pp. 127–135, 2007.

[7] H. Yi, S. Srinivasan, and M. K. Kim, "*Stenotrophomonas panacihumi* sp. nov., isolated from soil of a ginseng field," *Journal of Microbiology*, vol. 48, no. 1, pp. 30–35, 2010.

[8] P. Garbeva, J. A. Van Veen, and J. D. Van Elsas, "Microbial diversity in soil: selection of microbial populations by plant and soil type and implications for disease suppressiveness," *Annual Review of Phytopathology*, vol. 42, pp. 243–270, 2004.

[9] J. L. Garland, K. L. Cook, M. Johnson, R. Sumner, and N. Fields, "Density and composition of microorganisms during long-term (418 day) growth of potato using biologically reclaimed nutrients from inedible plant biomass," *Advances in Space Research*, vol. 20, no. 10, pp. 1931–1937, 1997.

[10] N. Ramesh Kumar, V. Thirumalai Arasu, and P. Gunasekaran, "Genotyping of antifungal compounds producing plant growth-promoting rhizobacteria, *Pseudomonas fluorescens*," *Current Science*, vol. 82, no. 12, pp. 1463–1466, 2002.

[11] G. Muyzer, E. C. De Waal, and A. G. Uitterlinden, "Profiling of complex microbial populations by denaturing gradient gel electrophoresis analysis of polymerase chain reaction-amplified genes coding for 16S rRNA," *Applied and Environmental Microbiology*, vol. 59, no. 3, pp. 695–700, 1993.

[12] W. G. Weisburg, S. M. Barns, D. A. Pelletier, and D. J. Lane, "16S ribosomal DNA amplification for phylogenetic study," *Journal of Bacteriology*, vol. 173, no. 2, pp. 697–703, 1991.

[13] J. Hunt, L. Boddy, P. F. Randerson, and H. J. Rogers, "An evaluation of 18S rDNA approaches for the study of fungal

diversity in grassland soils," *Microbial Ecology*, vol. 47, no. 4, pp. 385–395, 2004.

[14] S. Ntougias, N. Kavroulakis, K. K. Papadopoulou, C. Ehaliotis, and G. I. Zervakis, "Characterization of cultivated fungi isolated from grape marc wastes through the use of amplified rDNA restriction analysis and sequencing," *Journal of Microbiology*, vol. 48, no. 3, pp. 297–306, 2010.

[15] M. Scortichini, U. Marchesi, and P. Di Prospero, "Genetic relatedness among *Pseudomonas avellanae*, *P. syringae* pv. theae and P.s. pv. actinidiae, and their identification," *European Journal of Plant Pathology*, vol. 108, no. 3, pp. 269–278, 2002.

[16] S. F. Altschul, T. L. Madden, A. A. Schäffer et al., "Gapped BLAST and PSI-BLAST: a new generation of protein database search programs," *Nucleic Acids Research*, vol. 25, no. 17, pp. 3389–3402, 1997.

[17] K. Ravenschlag, K. Sahm, J. Pernthaler, and R. Amann, "High bacterial diversity in permanently cold marine sediments," *Applied and Environmental Microbiology*, vol. 65, no. 9, pp. 3982–3989, 1999.

[18] K. L. Heck, G. Van Belle, and D. Simberloff, "Explicit calculation of the rarefaction diversity measurement and the determination of sufficient sample size," *Ecology*, vol. 56, pp. 1459–1461, 1975.

[19] M. Schutter and R. Dick, "Shifts in substrate utilization potential and structure of soil microbial communities in response to carbon substrates," *Soil Biology and Biochemistry*, vol. 33, no. 11, pp. 1481–1491, 2001.

[20] J. L. Garland and A. L. Mills, "Classification and characterization of heterotrophic microbial communities on the basis of patterns of community-level sole-carbon-source utilization," *Applied and Environmental Microbiology*, vol. 57, no. 8, pp. 2351–2359, 1991.

[21] Z. Li, X. Wu, and B. Chen, "Changes in transformation of soil organic c and functional diversity of soil microbial community under different land uses," *Agricultural Sciences in China*, vol. 6, no. 10, pp. 1235–1245, 2007.

[22] J. C. Zak, M. R. Willig, D. L. Moorhead, and H. G. Wildman, "Functional diversity of microbial communities: a quantitative approach," *Soil Biology and Biochemistry*, vol. 26, no. 9, pp. 1101–1108, 1994.

[23] C. E. Shannon and W. Weaver, *The Mathematical Theory of Communication*, The University of Illinois Press, Urbana, Ill, USA, 1949.

[24] R. T. Vendan, Y. J. Yu, S. H. Lee, and Y. H. Rhee, "Diversity of endophytic bacteria in ginseng and their potential for plant growth promotion," *Journal of Microbiology*, vol. 48, no. 5, pp. 559–565, 2010.

[25] P. H. Janssen, "Identifying the dominant soil bacterial taxa in libraries of 16S rRNA and 16S rRNA genes," *Applied and Environmental Microbiology*, vol. 72, no. 3, pp. 1719–1728, 2006.

[26] L. Zhang and Z. Xu, "Assessing bacterial diversity in soil," *Journal of Soils and Sediments*, vol. 8, no. 6, pp. 379–388, 2008.

[27] Y. Zhang, B. H. Du, Z. G. Jin, Z. H. Li, H. N. Song, and Y. Q. Ding, "Analysis of bacterial communities in rhizosphere soil of healthy and diseased cotton (*Gossypium* sp.) at different plant growth stages," *Plant and Soil*, vol. 339, no. 1, pp. 447–455, 2011.

[28] E. A. Curl and B. Truelove, *The Rhizosphere*, Advanced Series in Agriculture Sciences, Springer, 1986.

[29] T. Anderson, "Microbial eco-physiological indicators to asses soil quality," *Agriculture, Ecosystems and Environment*, vol. 98, no. 1–3, pp. 285–293, 2003.

[30] L. Brussaard, P. C. de Ruiter, and G. G. Brown, "Soil biodiversity for agricultural sustainability," *Agriculture, Ecosystems and Environment*, vol. 121, no. 3, pp. 233–244, 2007.

[31] B. S. Griffiths, H. L. Kuan, K. Ritz, L. A. Glover, A. E. McCaig, and C. Fenwick, "The relationship between microbial community structure and functional stability, tested experimentally in an upland pasture soil," *Microbial Ecology*, vol. 47, no. 1, pp. 104–113, 2004.

[32] J. Lynch, *The Rhizosphere*, Wiley, London, UK, 1990.

[33] G. E. Harman, R. Petzoldt, A. Comis, and J. Chen, "Interactions between *Trichoderma harzianum* strain T22 and maize inbred line Mo17 and effects of these interactions on diseases caused by *Pythiuin ultimum* and *Colletotrichum graminicola*," *Phytopathology*, vol. 94, no. 2, pp. 147–153, 2004.

[34] J. M. Raaijmakers, T. C. Paulitz, C. Steinberg, C. Alabouvette, and Y. Moënne-Loccoz, "The rhizosphere: a playground and battlefield for soilborne pathogens and beneficial microorganisms," *Plant and Soil*, vol. 321, no. 1-2, pp. 341–361, 2009.

[35] J. Shi, X. Yuan, H. Lin, Y. Yang, and Z. Li, "Differences in soil properties and bacterial communities between the rhizosphere and bulk soil and among different production areas of the medicinal plant *Fritillaria thunbergii*," *International Journal of Molecular Sciences*, vol. 12, no. 6, pp. 3770–3785, 2011.

[36] G. Wieland, R. Neumann, and H. Backhaus, "Variation of microbial communities in soil, rhizosphere , and rhizoplane in response to crop species, soil type, and crop development," *Applied and Environmental Microbiology*, vol. 67, no. 12, pp. 5849–5854, 2001.

[37] H. Yao, X. Jiao, and F. Wu, "Effects of continuous cucumber cropping and alternative rotations under protected cultivation on soil microbial community diversity," *Plant and Soil*, vol. 284, no. 1-2, pp. 195–203, 2006.

[38] M. N. Chen, X. Li, Q. L. Yang et al., "Dynamic succession of soil bacterial community during continuous cropping of peanut (*Arachis hypogae*a L.)," *PLoS ONE*, vol. 9, Article ID e101355, 2014.

Research Article

Natural Resource Monitoring of *Rheum tanguticum* by Multilevel Remote Sensing

Caixiang Xie,[1] Jingyuan Song,[1] Fengmei Suo,[1] Xiwen Li,[1] Ying Li,[1] Hua Yu,[2] Xiaolan Xu,[1] Kun Luo,[1] Qiushi Li,[1] Tianyi Xin,[1] Meng Guan,[3] Xiuhai Xu,[3] Eiji Miki,[4] Osami Takeda,[4] and Shilin Chen[5]

[1] *Institute of Medicinal Plant Development, Chinese Academy of Medical Sciences, Beijing 100193, China*
[2] *Shandong Academy of Agriculture Sciences, Jinan 250100, China*
[3] *China Meheco Co., Ltd., Beijing 100061, China*
[4] *Botanical Raw Material Research Department, Tsumura & Co., Ibaraki 300-1192, Japan*
[5] *Institute of Chinese Materia Medica, China Academy of Chinese Medical Sciences, Beijing 100700, China*

Correspondence should be addressed to Shilin Chen; slchen@implad.ac.cn

Remote sensing has been extensively applied in agriculture for its objectiveness and promptness. However, few applications are available for monitoring natural medicinal plants. In the paper, a multilevel monitoring system, which includes satellite and aerial remote sensing, as well as ground investigation, was initially proposed to monitor natural *Rheum tanguticum* resource in Baihe Pasture, Zoige County, Sichuan Province. The amount of *R. tanguticum* from images is $M = S^* \rho$ and S is vegetation coverage obtained by satellite imaging, whereas ρ is *R. tanguticum* density obtained by low-altitude imaging. Only the *R. tanguticum* which coverages exceeded $1\,m^2$ could be recognized from the remote sensing image because of the 0.1 m resolution of the remote sensing image (called effective resource at that moment), and the results of ground investigation represented the amounts of *R. tanguticum* resource in all sizes (called the future resource). The data in paper showed that the present available amount of *R. tanguticum* accounted for 4% to 5% of the total quantity. The quantity information and the population structure of *R. tanguticum* in the Baihe Pasture were initially confirmed by this system. It is feasible to monitor the quantitative distribution for natural medicinal plants with scattered distribution.

1. Introduction

Remote sensing has been extensively applied in agriculture in recent years. This approach can provide objective, accurate, and timely information on the ecological environment of crops. Many remote sensing applications for medicinal plants are focused on cultivated medicinal plants. By contrast, natural medicinal plants are largely ignored because of their scattering distribution characteristic and small coverage area. A multilevel monitoring system, which includes satellites, aerial remote sensing, and ground investigation was proposed in this paper to monitor natural *Rheum tanguticum* in the Baihe Pasture, Zoige County, Sichuan Province, to determine the quantitative distribution and population structure of *R. tanguticum* in this region.

A number of studies indicate that domestic *R. tanguticum* are mainly distributed in temperate Asian zones, including the Greater Khingan Mountains, Taihang Mountains, Qinling Mountain, Daba Mountains, and Yunnan-Guizhou Plateau [1, 2]. *R. tanguticum* is a peculiar Chinese perennial herb that belongs to the Polygonaceae family. This herb mainly thrives in Southern Gansu Province, Northwest Sichuan Province, and Northeast Tibet. These areas are characterized by high altitudes and short frost-free periods. *R. tanguticum* grows slowly in these regions and has rich substances with good qualities. The popular "Xining Rheum" and "Quanshui
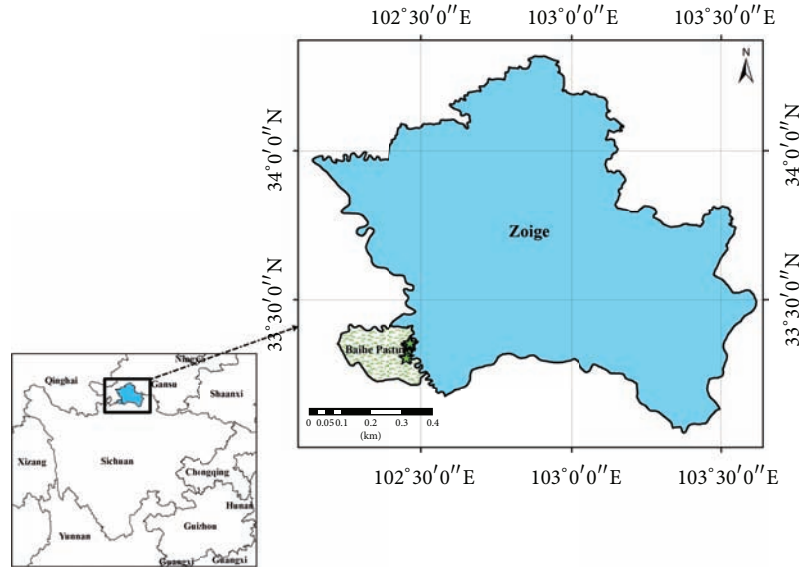
Figure 1: Baihe pasture location (means the fenced field).

Rheum" originated from these areas. Recent studies on *R. tanguticum* are mainly focused on ecological suitability, chemical analysis, and pharmacology [3–7]. The demand for *R. tanguticum* as an ingredient for Tibetan medicine, health products, and specialty food has gradually increased [8]. *R. tanguticum* in the Qinghai-Tibet Plateau proliferates slowly because of the cold climate and fragile ecological environment. Moreover, the unreasonable excavation of *R. tanguticum* leads to a significant reduction in the quantity of this resource and may even lead to desertification. Determining the updated status of the quantitative distribution and population structure of *R. tanguticum* is necessary for ecological protection and resource development [9]. Thus, the multilevel monitoring system was established to monitor the updated status of *R. tanguticum* [10–12]. Satellite remote sensing and low-altitude remote sensing were initially applied to monitor the quantitative distribution and population structure of natural *R. tanguticum* in the Baihe Pasture. The viability and effectiveness of the multilevel remote system were evaluated by ground-sampled surveys. This paper presented a new technical method and platform for monitoring wild and scattered medicinal plant resources.

2. Materials and Methods

2.1. Study Area. Zoige County ($102°8'$ to $103°39'$ E, $33°56'$ to $34°19'$ N), which is located in the northeastern margin of the Tibetan Plateau, belongs to the northernmost area of Aba, Sichuan Province. This area is bordered by 4 counties of Gansu Province (i.e., Maqu, Luqu, Zhuoni, and Diebu Counties) and Sichuan Province (i.e., Aba, Hongyuan, Songpan, and Jiuzhaigou Counties). Zoige County is an important region of the Northwest Sichuan Pasture and covers an area of $10,620 \, km^2$ with an altitude of 3,400 m to 3,900 m. Zoige County is located on a plateau with a cold, temperate, and humid monsoon climate with a relative humidity of 68%.

The average temperatures in January and July are −9.4 and $11.5°C$, respectively. The average annual temperature is $1.7°C$, and the highest and lowest temperatures are 25.4 and $−29.5°C$, respectively. The annual accumulated temperature higher than 10 is $718.4°C$. Annual sunshine duration, rainfall, evaporation, gale day, and dust day are 2,506.7 h, 543.2 mm to 761.6 mm, 1,188.24 mm, 11.2 d, and 0.6 d, respectively. Zoige County has abundant water resources and contains several main branches of the Yellow River upstream, including the Heihe, Baihe, and Jiasong Rivers. Zoige County receives significant sunshine and heat energy, thus contributing to its rich $8,084 \, km^2$ natural grasslands that contain various medicinal plants, including *Fritillaria*, *Cordyceps*, *Gentiana*, Rhubarb, *and Saussurea*. These plants amount to 121 families and 1,094 species. *Rheum palmatum*, *R. tangulicum* and *Rheum officinale* all have distribution in Sichuan Province, but only wild *R. tangulicum* scatters in the studied region, and the other two species are mainly cultivated in farmlands or around farmhouses. The studied region is shown in Figure 1. The studied region is located in Tangke Town, Zoige County, Aba Prefecture, and Sichuan Province with an altitude of 3,437 m and total area of $433 \, km^2$. Most areas of the Baihe Pasture are covered with natural grasslands, except for the 1,000 ha of crops.

2.2. Data Collection

Satellite Image. Landsat Thematic Mapper (TM) 5 image with a $0.45 \, \mu m$ to $2.35 \, \mu m$ spectrum range was used to determine the vegetation area in the Baihe Pasture. The image parameters were as follows: $N33°25'$ $E102°14'$ image center, blue B1 band, $0.45 \, \mu m$ to $0.52 \, \mu m$ spectrum range, and 30 m resolution; green B2 band, $0.52 \, \mu m$ to $0.60 \, \mu m$ spectrum range, and 30 m resolution; red B3 band, $0.63 \, \mu m$ to $0.69 \, \mu m$ spectrum range, and 30 m resolution; near-infrared B4 band, $0.76 \, \mu m$
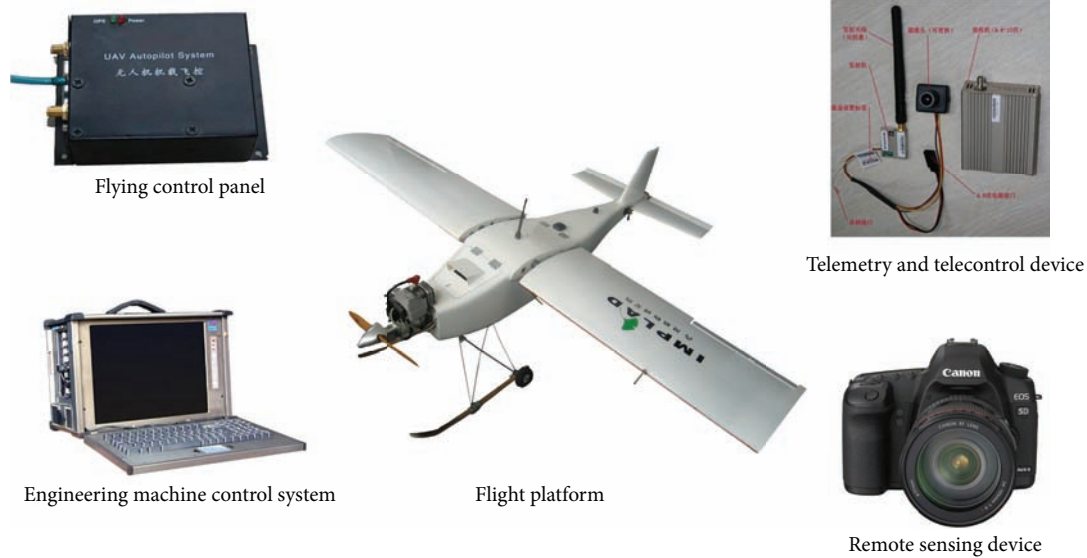
Figure 2: Low-altitude remote sensing system.

to 0.90 μm spectrum range, and 30 m resolution; short-wave infrared B5 band, 1.55 μm to 1.75 μm spectrum range, and 30 m resolution; thermal infrared B6 band, 10.4 μm to 12.5 μm spectrum range, and 120 m resolution; middle-infrared B7 band, 2.08 μm to 3.35 μm spectrum range, and 30 m resolution. TM imaging is suitable for large-scale object monitoring because of its moderate resolution and low cost. The TM5 image shot on 18 July 2008 was chosen in the monitoring of the Baihe Pasture vegetation based on the biological features of natural *R. tanguticum*.

The low-altitude remote sensing system consisted of a flight platform, digital camera, single-axis stabilized platform, and equipment control system (Figure 2). The flight platform is an unmanned aerial vehicle from the Institute of Medicinal Plant Development. The Canon 5D digital camera with a charge-coupled device array was adopted for data acquisition. The camera also has array pixels and a lens focal length of 4368 pixels × 2912 pixels and 35 mm, respectively. The 0.1 m resolution of the camera for aerial images was appropriate for the requirements of the survey goal based on the ground survey. The high-resolution aerial photography for wild *R. tanguticum* was initially conducted in the Baihe Pasture of Zoige County by the low-altitude remote sensing system.

Ground Survey. A total of 10 fenced zones with an area of 200 m × 200 m were selected for the *R. tanguticum* field survey. Four 10 m × 10 m plots were established in the 10 fenced zones based on the plot-setting principle. The ground survey for *R. tanguticum* was conducted separately in the fenced zones in July 2008, 2010, and 2011.

2.3. Study Method. The complete technical road map is summarized in Figure 3. First, the location and boundary of the Baihe Pasture in the satellite image were determined by using ArcGIS software based on the Landsat TM and Baihe Pasture map. Second, the interpretation keys of the vegetation zone

were established by normalized difference vegetation index (NDVI) analysis based on the Landsat TM image. Third, ground samples were designed based on the topography and geomorphology of the Baihe Pasture. The distribution density of *R. tanguticum* in vegetation was determined by using low-altitude images with 0.1 m resolutions. Finally, the amount of natural *R. tanguticum* resource was calculated based on the vegetation area from the satellite image and the *R. tanguticum* distribution density from low-altitude remote sensing. The results were compared and assessed with those of the ground survey.

3. Data Analysis

3.1. Image Processing. Bands 4, 3, and 2 in the TM image were fused to distinguish the vegetation and water. The Baihe Pasture boundary in the TM image was determined via the registration function by the feature points. Thus, the Baihe Pasture satellite image was detached from the original TM image. NDVI is an internationally accepted criterion for vegetation coverage level. Consider that NDVI = (NIR − R)/(NIR + R), where NIR denotes the near-infrared band reflectivity and R stands for red band reflectivity. An NDVI value in the range of zero to one generally refers to vegetation regions. The vegetation region of the Baihe Pasture was determined based on the NDVI analysis in Figure 4.

3.2. Object-Based Image Classification. High-spatial resolution images have limited spectral information but contain many spatial information of objects, such as size, shape, and topological information. The object-oriented approach classifies different objects based on spectral signature, shape, and contextual relationship. Homogeneous objects were initially formed by multiscale image segmentation. Thereafter, image classification was used to endow the objects with different semantic information based on size, spectrum, and shape
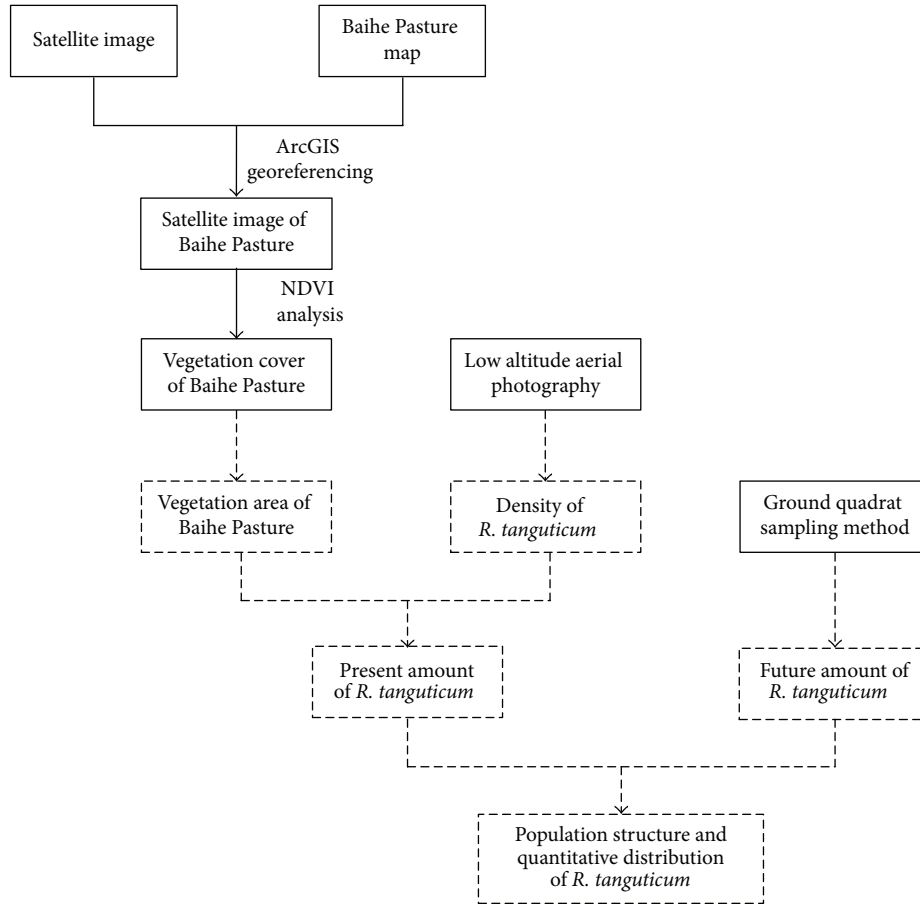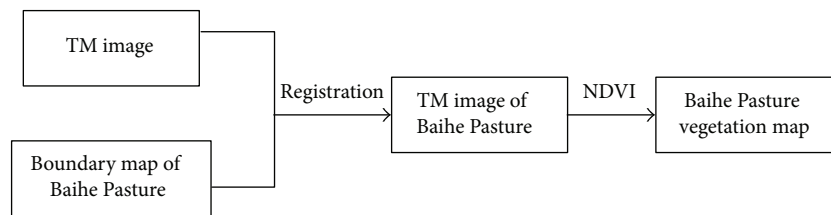
Figure 3: Overall technical route.

Figure 4: Image processing.

parameters. These objects were then used as a basis for the fuzzy classification of the image. The use of spectral, textural, and shape properties, as well as fuzzy thinking, might reduce uncertainty in the classification process. The results of the object-based image interpretation showed better integration levels than the pixel-based interpretation method [9, 13, 14], which is suitable for high-spatial resolution images.

4. Results

4.1. Biological and Community Characteristics of R. tanguticum. *R. tanguticum* is a perennial and tall herb that is resistant to cold but has zero endurance to high temperatures. This herb thrives in a cool and moist climate and is

mainly scattered in forests, scrubs, and meadows. Natural *R. tanguticum* plants in the Baihe Pasture can grow for approximately seven or eight years with a height of 1.5 m to 2.0 m and a corolla diameter of 2.4 mm to 3.7 mm. The blooming stage of *R. tanguticum* is from May to July. The ecology community type of *R. tanguticum* is alpine meadows with only an herb layer. The vegetation coverage of such alpine meadows is more than 95% and includes a small amount of cultivated barley. Figure 5 presents the community characteristics of *R. tanguticum*.

The accompanying plants of Rhubarb are mainly Ranunculaceae, Cyperaceae, Gramineae, Rosaceae, Compositae, Polygonaceae, Dipsacaceae, Leguminosae, Umbelliferae, Gentianaceae, Labiatae, Boraginaceae, Basidiomycetes, and

(a)

(b)

FIGURE 5: Community characteristics of wild *R. tanguticum*.

Cremanthodium

Morina nepalensis

Puffball

Pedicularis

Microula ovalifolia

Angelica

Lamiophlomis rotata

Anaphalis

Oxytropis
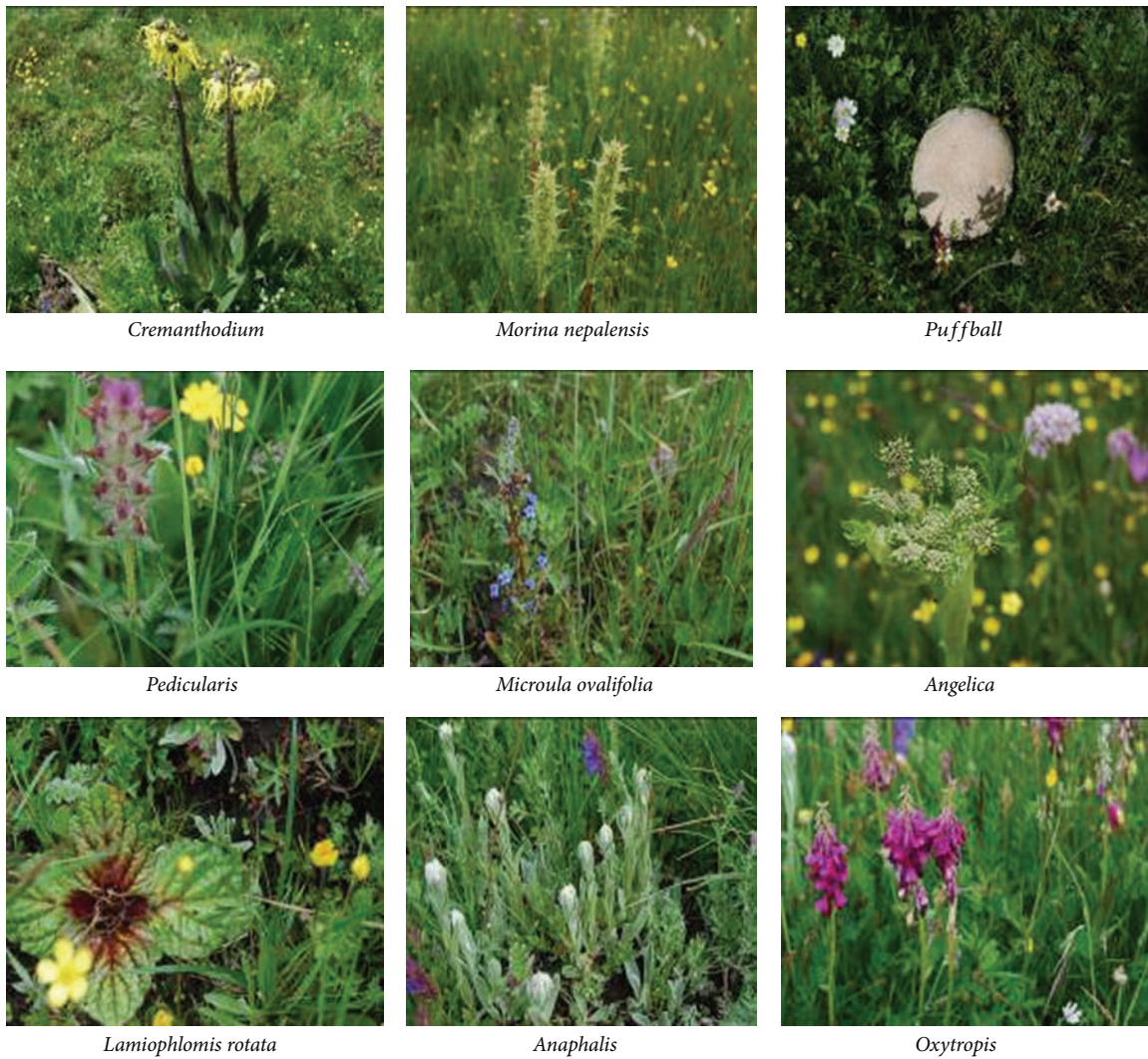
FIGURE 6: Accompanying plant picture of wild *R. tanguticum*.

others. Cyperaceae and Gramineae assume absolute superiority among these plants. Ranunculaceae, Compositae, and a few fungi compose the weed layer. Figure 6 and Table 1 show the vegetation type and accompanying plants of natural *R. tanguticum* in the Baihe Pasture, respectively.

4.2. Multilevel Remote Sensing Resource Monitoring for R. tanguticum. Based on NDVI anlysis, the pixel numbers of $0.1 < \text{NDVI} < 1$ and $\text{NDVI} < 0.1$ were 305,676 and 189,658, with each representing the vegetation and nonvegetation regions, respectively. Therefore, the vegetation area ratio (P),

Table 1: Accompanying plants of wild *R. tanguticum*.

Species name	Family	Genus	Remarks
Anaphalis flavescens.		*Anaphalis*	Weed layer
Aster tongolensis		*Aster*	Weed layer
Carpesium lipskyi		*Carpesium*	Weed layer
Ligularia virgaurea		*Saussurea*	Weed layer
Leontopodium longifolium	Asteraceae		Weed layer
Saussurea graminea		*Ligularia*	Weed layer
Saussurea superba		*Trollius*	Weed layer
Trollius ranunculoides		*Leontopodium*	Weed layer
Thlaspi arvense	Brassicaceae	*Thlaspi*	Weed layer
Blysmus sinocompressus			Dominant population
Kobresia pygmaea			Dominant population
Kobresia setchwanensis		*Kobresia*	Dominant population
Kobresia humilis	Cyperaceae		Dominant population
Kobresia tibetica			Dominant population
Kobresia kansuensis		*Blysmus*	Dominant population
Astragalus polycladus		*Gueldenstaedtia*	Weed layer
Gueldenstaedtia diversifolia	Fabaceae	*Oxytropis*	Weed layer
Oxytropis kansuensis			Weed layer
Oxytropis ochrocephala		*Astragalus*	Weed layer
Agrostis schneideri		*Elymus*	Dominant population
Cymbopogon distans		*Roegneria*	Dominant population
Deyeuxia scabrescens		*Festuca*	Dominant population
Deschampsia caespitosa		*Poa*	Dominant population
Elymus nutans			Dominant population
Festuca ovina		*Deyeuxia*	Dominant population
Heteropogon contortus		*Deschampsia*	Dominant population
Koeleria cristata	Gramineae	*Agrostis*	Dominant population
Miscanthus sinensis		*Koeleria*	Dominant population
Poa pachyantha		*Heteropogon*	Dominant population
Poa pratensis		*Cymbopogon*	Dominant population
Roegneria nutans		*Miscanthus*	Dominant population
Stipa capillacea			Weed layer
Stipa purpurea		*Stipa*	Weed layer
Stipa przewalskii			Weed layer
Geranium pylzowianum	Geraniaceae	*Geranium*	Weed layer
Polygonum taquetii	Polygonaceae	*Polygonum*	Weed layer
Polygonum viviparum			Weed layer
Fragaria orientalis		*Potentilla*	Weed layer
Potentilla anserina	Rosaceae		Weed layer
Potentilla griffithii		*Fragaria*	Weed layer
Anemone rivularis		*Ranunculus*	Weed layer
Ranunculus tanguticus	Ranunculaceae	Anemone	Weed layer
Trollius lilacinus		*Trollius*	Weed layer
Trollius ranunculoides			Weed layer
Galium verum	Rubiaceae	*Galium*	Weed layer
Stellera chamaejasme	Thymelaeaceae	*Stellera*	Weed layer
Viola biflora	Violaceae	*Viola*	Weed layer

TABLE 2: *R. tanguticum* number of ground sample investigation.

| Fences | Quadrats Year | | | | | | | | | | | |
| | 1 (10×10 m^2) | | | 2 (10×10 m^2) | | | 3 (10×10 m^2) | | | 4 (10×10 m^2) | | |
	2008	2010	2011	2008	2010	2011	2008	2010	2011	2008	2010	2011
I (200×200 m^2)	0	0	2	4	6	7	6	10	5	1	2	1
II (200×200 m^2)	2	6	1	1	2	0	3	5	0	4	8	2
III (150×150 m^2)	1	4	0	1	3	4	2	1	4	0	3	1
IV (200×200 m^2)	2	2	0	2	0	12	0	0	4	1	1	1
V (200×200 m^2)	3	5	1	3	6	1	3	3	6	5	8	6
VI (200×200 m^2)	10	18	0	3	4	5	1	2	5	1	0	4
VII (200×200 m^2)	4	7	1	4	5	5	6	10	3	3	1	4
VIII (200×200 m^2)	0	0	4	0	0	0	0	0	1	0	0	3
IX (200×200 m^2)	3	3	4	5	4	2	8	13	4	3	3	3
X (200×200 m^2)	2	3	3	2	1	4	2	1	4	3	2	5

area (M), and vegetation area (M_1) of the Baihe Pasture were $P = 305676/(305676 + 189658) = 62\%$, $M = (305676 + 189658) \times 30$ m $\times 30$ m $= 445$ km^2 (44,500 ha), and $M_1 = 445 \times 62\% = 276$ km^2 (27,600 ha), respectively. The results were consistent with the 43,333 ha provided by the Baihe Pasture. Therefore, remote sensing technology was feasible in monitoring the fields.

As a matter of experience, only *R. tanguticum* with more than 1 m^2 of coverage (called effective resource) could be interpreted from the image. Thus, the average density of available *R. tanguticum* could be calculated by the interpretation results of many low-altitude images. The effective resources of *R. tanguticum* in the entire Baihe Pasture were that the Baihe Pasture vegetation area multiplied by the average *R. tanguticum* density, which was equal to 350,000. Therefore, the amount of available natural *R. tanguticum* resources in the Baihe Pasture in 2008 was 350,000.

4.3. R. tanguticum Sample Investigation. Ten vegetation fences, each with an area of 200 m $\times$ 200 m, except for the third fence with 150 m $\times$ 150 m, were established in the Baihe Pasture, and there were four 10 m $\times$ 10 m quadrats in every fence. Ground survey work was conducted in July 2008, 2010, and 2011 in the above fences and quadrats (Table 2).

The ground survey results in 2008 indicated the existence of 2.6 *R. tanguticum* per 100 m^2; thus, the total amount of *R. tanguticum* in the Baihe Pasture was M_1(276 km^2) $\times$ 2.6/ 100 m$^2 = 718 \times 10^4$.

The ground survey results in 2010 indicated that the number of *R. tanguticum* in each fence was approximately 1,520, except for approximately 855 in the third fence. Thus, approximately 3.8 *R. tanguticum* per 100 m^2 existed, and the total amount of *R. tanguticum* was $1,049 \times 10^4$.

The results in 2011 indicated that the average number of *R. tanguticum* in each fence was approximately 1,220; the minimum amount was approximately 300 in the second fence, and the amount was approximately 1600 in the first, fourth, and sixth fences. The calculation result was 3.1 *R. tanguticum* per

100 m^2. Thus, the total amount of *R. tanguticum* in 2011 was 856×10^4.

Quantity variance existed in the total amount of *R. tanguticum* based on the results of different years because of operation errors and other factors. However, the total quantity of *R. tanguticum* was approximately 750×10^4 to $1,000 \times 10^4$. The current available amount and the future total amount of natural *R. tanguticum* resources in 2008 were, respectively, 35×10^4 and 718×10^4 based on the results of the multilevel remote sensing and ground survey. The population structure of natural *R. tanguticum*, that is, the available amount of *R. tanguticum*, comprised 4% to 5% of the total amount. Therefore, the safe digging quantity of *R. tanguticum* in the Baihe Pasture was 4% to 5% for the protection of natural resources.

5. Discussion

Remote sensing technology has become an important means of obtaining geographic environment information. This technology has remarkably extended and improved the ability of humans to recognize their surrounding environment. Technology innovation in remote sensing provides a new method and platform for surveying natural Chinese medicine resources

(1) Remote sensing has been extensively applied in agriculture in recent years [15–25]. Remote sensing technology can provide objective, accurate, and timely information on the ecological environment of crops and is an important data source for precision agriculture [26]. However, a significant difference exists in the resource distribution between agricultural and natural Chinese medicinal herbs. Artificially cultivated crops are characterized by large areas, centralized distributions, and regular shapes. Thus, these crops have significant image features that are easy to interpret. By contrast, natural Chinese medicinal herbs often exist in wide, inaccessible regions and are scattered in different vegetation communities. Thus, interpreting natural Chinese medicinal herbs from satellite images was difficult because of the lack of distinct image features. Multilevel remote sensing was initially

proposed to monitor the natural *R. tanguticum* in the Baihe Pasture. Based on the satellite image results, the Baihe Pasture area was $445\,\text{km}^2$ (44,500 ha), which was consistent with the 43,333 ha provided by the administrative department of the Baihe Pasture. The vegetation coverage in the Baihe Pasture was $276\,\text{km}^2$. *R. tanguticum* density was 2.6 to 3.8 per $100\,\text{m}^2$ based on the result of the multilevel remote sensing. Compared with the ground investigation, the multilevel remote sensing technology system was fast and convenient. Results indicated that the available amount of *R. tanguticum* comprised 4% to 5% of the total amount. The quantity information and population structure of *R. tanguticum* in the Baihe Pasture of Zoige County were initially confirmed by this multilevel monitoring system. This system was also successfully applied in monitoring *Ferula sinkiangensis* in the fourth survey of the Chinese medicine resources of Xinjiang.

(2) An object-oriented image-recognition method was initially adopted to extract *R. tanguticum* in low-altitude aerial images. Only *R. tanguticum* with coverage greater than $1\,\text{m}^2$ could be extracted from the low-altitude aerial image because of the spatial resolution limitations. Therefore, the amount of *R. tanguticum* obtained from multilevel remote sensing was the current available resources, whereas the results from the ground investigation were the total resources because all *R. tanguticum* sizes could be observed through ground surveys. The amount of *R. tanguticum* obtained from the ground survey represented the total available resource in three years to five years. The results from the two methods (remote sensing, ground survey) represented the present and the future amounts of *R. tanguticum*. Thus, the corresponding method should be selected to satisfy different demands and purposes.

(3) The optimum time for monitoring *R. tanguticum* through remote sensing was early July because *R. tanguticum* was in bloom and taller than the surrounding vegetation during this period. The ground survey results in three years indicated that the total quantity of *R. tanguticum* was approximately 750×10^4 to $1,000 \times 10^4$. The available amount of natural *R. tanguticum* resources was 35×10^4 in 2008 based on the results of the multilevel remote sensing. However, the total amount in 2008 was 718×10^4 based on the ground survey results. So, the safety digging quantity of *R. tanguticum* in the Baihe Pasture was 4% to 5% for the protection of natural resources.

We conclude that the use of low-altitude remote sensing technology to monitor the scattered distribution of natural medicinal plants was feasible. This study provided a new technical system for monitoring objects with scattered distributions.

Conflict of Interests

The authors declare that there is no conflict of interests regarding the publication of this paper.

Acknowledgments

References

[1] G. J. Xue, L. He, and X. Pan, "Development and utilization of research on Chinese Rhubarb," *China Natural Plant Resource*, pp. 1–5, 1995.

[2] Z. Q. Xie, "Ecogeographical distribution of the species from *Rheum* L., (Polygonaceae) in China," in *Proceedings of the 3rd Chinese National Symposim on Biodiversity Protection and Sustained Utilization*, pp. 230–238, 1998.

[3] H. Yu, C. Xie, J. Song, Y. Zhou, and S. Chen, "TCMGIS-II based prediction of medicinal plant distribution for conservation planning: a case study of *Rheum tanguticum*," *Chinese Medicine*, vol. 5, article 31, 2010.

[4] F. M. Suo, J. Y. Song, S. L. Chen et al., "AFLP analysis on genetic relationship among *Rheum tanguticum*, *Rheum palmatum*, and *Rheum officinale*," *Chinese Traditional and Herbal Drugs*, vol. 41, no. 2, pp. 292–296, 2010.

[5] Y. Liu, Q. Wang, M. Jiang, H. Li, M. Zou, and G. Bai, "Screening of effective components for inhibition of tyrosinase activity in rhubarb based on spectrum-efficiency-structure-activity relationship," *Chinese Traditional and Herbal Drugs*, vol. 43, no. 11, pp. 2120–2126, 2012.

[6] C. X. Xie, F. M. Suo, Y. Q. Zhou et al., "Quantitative study on ecological suitability of Chinese herbalmedicine based on GIS," *China Journal of Chinese Materia Medica*, vol. 36, no. 3, pp. 379–382, 2011.

[7] S. L. Chen, *Ecology Suitability Regionalization of Chinese Medical Plants*, Science Press, Beijing, China, 2011.

[8] J. P. Li, G. S. Chen, and X. F. Lu, "Status of *Rheum tanguticum* maxim. exbalf resources of Qinghai and countermeasures for protection," *Qinghai Prataculture*, vol. 16, pp. 38–42, 2007.

[9] J. F. Wang and S. T. Bao, "Application of object-oriented interpretation to information classification on remote sensing image," *Tropical Geography*, pp. 234–238, 2006.

[10] C. X. Xie, S. L. Chen, Y. Wang, Y. Q. Zhou, and Y. Li, "Some key problems of quantitative estimation in multilevel remote sensing monitoring system of plant medicinal materials," *China Journal of Chinese Materia Medica*, vol. 33, no. 3, pp. 326–329, 2008.

[11] C. X. Xie, S. L. Chen, and Z. J. Lin, "Application of Unmanned Aerial Vehicles to medical plants survey," *Modern Chinese Medicine*, vol. 9, pp. 4–6, 2007.

[12] Y. Q. Zhou, S. L. Chen, R. H. Zhao, C. X. Xie, and Y. Li, "Study on application of low altitude remote sensing to Chinese herb medicinal sustainable utilization," *China Journal of Chinese Materia Medica*, vol. 33, no. 8, pp. 977–979, 2008.

[13] J. Zeng, X. X. Li, and T. Wang, "Study on object-oriented extracting water from high resolution remote sensing image," *Jiangxi Science*, pp. 263–266, 2011.

[14] Q. L. Wang, *Study on Object-Oriented Remote Sensing Image Classification and Its Application*, Beijing Forestry University, 2008.

[15] T. Ahamed, L. Tian, Y. Zhang, and K. C. Ting, "A review of remote sensing methods for biomass feedstock production," *Biomass and Bioenergy*, vol. 35, no. 7, pp. 2455–2469, 2011.

[16] H. Xiang and L. Tian, "An automated stand-alone in-field remote sensing system (SIRSS) for in-season crop monitoring," *Computers and Electronics in Agriculture*, vol. 78, no. 1, pp. 1–8, 2011.

[17] Y. S. Zhang, R. Feng, R. P. Ji, P. Chen, S. Zhang, and J. Wu, "Application of remote sensing technology in crop chilling injury monitoring," in *Proceedings of the 4th International Conference on Genetic and Evolutionary Computing (ICGEC '10)*, pp. 375–378, Shenzhen, China, December 2010.

[18] M. Anbarashan and N. Parthasarathy, "Diversity and ecology of lianas in tropical dry evergreen forests on the Coromandel Coast of India under various disturbance regimes," *Flora: Morphology, Distribution, Functional Ecology of Plants*, vol. 208, no. 1, pp. 22–32, 2013.

[19] H. D. Musa and B. Shaib, "Integrated remote sensing approach to desertification monitoring in the crop-rangeland area of Yobe State," *Nigeria. Journal of Sustainable Development in Africa*, pp. 236–250, 2010.

[20] Q. Huang, L. Zhang, W. Wu, and D. Li, "MODIS-NDVI-based crop growth monitoring in China Agriculture Remote Sensing Monitoring System," in *Proceedings of the 2nd IITA International Conference on Geoscience and Remote Sensing (IITA-GRS '10)*, pp. 287–290, Qingdao, China, August 2010.

[21] J. E. Wasige, T. A. Groen, E. Smaling, and V. Jetten, "Monitoring basin-scale land cover changes in Kagera Basin of Lake Victoria using: ancillary data and remote sensing," *International Journal of Applied Earth Observation and Geoinformation*, vol. 21, no. 1, pp. 32–42, 2012.

[22] M. Yuping, W. Shili, Z. Li et al., "Monitoring winter wheat growth in North China by combining a crop model and remote sensing data," *International Journal of Applied Earth Observation and Geoinformation*, vol. 10, no. 4, pp. 426–437, 2008.

[23] F. Tao, M. Yokozawa, Z. Zhang, Y. Xu, and Y. Hayashi, "Remote sensing of crop production in China by production efficiency models: Models comparisons, estimates and uncertainties," *Ecological Modelling*, vol. 183, no. 4, pp. 385–396, 2005.

[24] D. B. Lobell, G. P. Asner, J. I. Ortiz-Monasterio, and T. L. Benning, "Remote sensing of regional crop production in the Yaqui Valley, Mexico: estimates and uncertainties," *Agriculture, Ecosystems and Environment*, vol. 94, no. 2, pp. 205–220, 2003.

[25] T. Ahamed, L. Tian, Y. Jiang, B. Zhao, H. Liu, and K. C. Ting, "Tower remote-sensing system for monitoring energy crops; image acquisition and geometric corrections," *Biosystems Engineering*, vol. 112, no. 2, pp. 93–107, 2012.

[26] A. Lausch, M. Pause, I. Merbach et al., "A new multiscale approach for monitoring vegetation using remote sensing-based indicators in laboratory, field, and landscape," *Environmental Monitoring and Assessment*, vol. 185, no. 2, pp. 1215–1235, 2013.